

**Development of Antisense Therapies for Facioscapulohumeral  
and Duchenne Muscular Dystrophy**

by

Kenji Rowel Q. Lim

A thesis submitted in partial fulfillment of the requirements for the degree of

Doctor of Philosophy

Medical Sciences – Medical Genetics  
University of Alberta

© Kenji Rowel Q. Lim, 2021

## Abstract

Facioscapulohumeral muscular dystrophy (FSHD) and Duchenne muscular dystrophy (DMD) are two of the most commonly inherited muscular disorders in the world. There is currently no cure for both of them. Antisense oligonucleotides (AOs) are short, synthetic, single-stranded nucleic acids that hybridize to target mRNAs via base-pairing. In doing so, AOs could inhibit gene expression or modulate splicing and serve as viable therapeutic options for genetic disorders. In this work, we aim to develop novel, effective AOs for treating FSHD and DMD.

FSHD is an autosomal dominant disorder caused by mutations inducing aberrant *double homeobox protein 4 (DUX4)* gene expression in skeletal muscle. When present in differentiated muscle, DUX4 is a cytotoxic protein that dysregulates pathways involved in cell death and muscle development, among others. Previous groups have attempted to reduce *DUX4* mRNA expression using steric-blocking AOs, but the efficacy of these therapeutics could be improved. Gapmers are a class of AOs that induce the degradation of their target mRNAs via the recruitment of RNase H, and may present a better alternative to *DUX4* knockdown. Here, we designed and evaluated the efficacy of gapmers with the locked nucleic acid (LNA) and 2'-*O*-methoxyethyl (2'-MOE) chemistries towards reducing *DUX4* expression. Using immortalized patient-derived muscle cells, we demonstrated that both gapmers could significantly knock down *DUX4* mRNA expression to nearly undetectable levels. We observed restorative transcriptomic effects, and treatment improved muscle fiber size *in vitro*. Local treatment with these gapmers also significantly reduced *DUX4* expression in an FSHD mouse model.

DMD is an X-linked recessive disorder primarily caused by large out-of-frame mutations in the dystrophin gene (*DMD*). Dystrophin loss weakens muscle cell membranes and predisposes muscles to degeneration upon use. AOs can skip out-of-frame exons in the *DMD* transcript,

restoring the reading frame as well as the production of truncated, partially functional dystrophin. This approach has met with much success, such that four exon skipping AOs have been approved by the U.S. Food and Drug Administration for DMD. However, efficacy could be improved, since most of these AOs only restored <2% dystrophin of healthy levels (versus the target 10%) in patients after 48-180 weeks of once-weekly treatment, and did not show convincing evidence of functional benefit. All these are also single-exon skipping AOs, and only treat <30% of all patients in total. Here, we first investigated the advantages of early exon skipping treatment using dystrophic dog neonates. As DMD is a progressive disorder, there is a strong rationale for early treatment, but its benefits are poorly understood. Early exon skipping was safe, and restored dystrophin to an average 2% of healthy levels in skeletal muscles after three systemic injections. Early treatment was most beneficial for respiratory muscles. Secondly, we developed an exons 45-55 skipping AO cocktail for DMD therapy. By targeting exons in a mutation hotspot of the *DMD* gene, exons 45-55 skipping could treat nearly half of all patients. We achieved exons 45-55 skipping and dystrophin restoration by targeting as few as 5 exons. Conjugating the novel cell-penetrating peptide DG9 to AOs in this cocktail led to dystrophin restoration upon local *in vivo* treatment. We also tested a DG9-conjugated AO for single-exon 51 skipping, and saw functional improvement upon systemic treatment of dystrophic mice.

Overall, we identified *DUX4*-targeting gapmers as potential candidates for further pre-clinical testing towards FSHD therapy. We also showed proof-of-concept that *DMD* exons 45-55 can be skipped with a minimized AO cocktail, and identified a peptide that could be conjugated to exon skipping AOs to improve their *in vivo* efficacy. Together with our findings regarding early exon skipping treatment, our work not only produced candidates for further pre-clinical testing but also helps inform the development of future exon skipping AOs for DMD therapy.

## Preface

Parts of Chapter 1 of this thesis were derived from a version of the following published review articles: (1) Lim, K. R. Q. & Yokota, T. *Front. Pharmacol.* **12**, 642858 (2021); (2) Lim, K. R. Q., Nguyen, Q. & Yokota, T. *Int. J. Mol. Sci.* **21**, 729 (2020); (3) Lim, K. R. Q., Maruyama, R. & Yokota, T. *Drug Des. Devel. Ther.* **11**, 533-545 (2017); (4) Lim, K. R. Q. & Yokota, T. In *Exon Skipping and Inclusion Therapies: Methods and Protocols* (eds. Yokota, T. & Maruyama, R.) 3-30 (Springer, 2018); (5) Lim, K. R. Q.\*, Yoon, C.\* & Yokota, T. *J. Pers. Med.* **8**, 38 (2018); (6) Lim, K. R. Q. & Yokota, T. Invention and early history of gapmers. In *Gapmers: Methods and Protocols* (eds. Yokota, T. & Maruyama, R.) 3-19 (Springer, 2020); and (7) Lim, K. R. Q.\*, Nguyen, Q.\* & Yokota, T. Genotype–Phenotype Correlations in Duchenne and Becker Muscular Dystrophy Patients from the Canadian Neuromuscular Disease Registry. *J. Pers. Med.* **10**, 241 (2020) (\*co-first). I was involved with concept formation, performed literature review or research, and wrote the manuscript for all articles, with assistance from Q. Nguyen or C. Yoon on (2), (5) and (7). R. Maruyama provided a figure for (3). T. Yokota was the supervisory author for all articles, and was involved with concept formation and manuscript composition.

A version of Chapter 2 of this thesis has been published as Lim, K.R.Q., Maruyama, R., Echigoya, Y., Nguyen, Q., Zhang, A., Khawaja, H., Sen Chandra, S., Jones, T., Jones, P., Chen, Y. & Yokota, T. *Proc. Natl. Acad. Sci.* **117**, 16509-16515 (2020). I was involved with concept formation, performed all experiments and data analysis using immortalized patient-derived cells, with the assistance of Q. Nguyen on quantitative real-time PCR and flow cytometry. Our collaborators A. Zhang, H. Khawaja, and S. Sen Chandra performed all experiments using mice. R. Maruyama and Y. Echigoya designed the antisense oligonucleotides. T. Jones and P. Jones

provided the mouse model for experiments. I wrote the entire manuscript, with the assistance of H. Khawaja, S. Sen Chandra, and Y. Chen for sections concerning mouse experiments. Y. Chen and T. Yokota were the supervisory authors for this article, and were involved with concept formation and manuscript composition. Animal experiments were approved by the Institutional Animal Care and Use Committee of the Children's Research Institute of the Children's National Health System, Washington, DC. Animal experiments were not conducted at the University of Alberta or by University of Alberta students and staff. Experiments on immortalized patient-derived cells were approved by the University of Alberta Health Research Ethics Board (study ID Pr00079871).

A version of Chapter 3 of this thesis has been published as Lim, K.R.Q., Bittel, A., Maruyama, R., Echigoya, Y., Nguyen, Q., Huang, Y., Dzierlega, K., Zhang, A., Chen, Y. & Yokota, T. *Mol. Ther.* **29**, 848-858 (2021). I was involved with concept formation, performed all experiments and data analysis using immortalized patient-derived cells, with the assistance of Q. Nguyen on flow cytometry, as well as Y. Huang and K. Dzierlega on cell culture. Our collaborators A. Bittel and A. Zhang performed all experiments using mice. I designed the antisense oligonucleotides for this study, based on the original design of R. Maruyama and Y. Echigoya. I wrote the entire manuscript, with the assistance of A. Bittel, A. Zhang, and Y. Chen for sections concerning mouse experiments. Y. Chen and T. Yokota were the supervisory authors for this article, and were involved with concept formation and manuscript composition. Animal experiments were approved by the Institutional Animal Care and Use Committee of the Children's Research Institute of the Children's National Health System, Washington, DC. Animal experiments were not conducted at the University of Alberta or by University of

Alberta students and staff. Experiments on immortalized patient-derived cells were approved by the University of Alberta Health Research Ethics Board (study ID Pr00079871).

A version of Chapter 4 of this thesis has been published as Lim, K. R. Q.\*, Echigoya, Y.\*, Nagata, T.\*, Kuraoka, M., Kobayashi, M., Aoki, Y., Partridge, T., Maruyama, R., Takeda, S., Yokota, T. *Mol. Ther.* **27**, 76-86 (2019) (\*co-first). Our collaborators T. Nagata, M. Kuraoka, M. Kobayashi, and Y. Aoki performed all direct work on animals, including injections, functional testing, euthanasia, and tissue/blood collection. I performed all experiments and data analysis using tissues obtained from the animals, with the assistance of Y. Echigoya on Western blotting and T. Yokota on immunofluorescence. Y. Echigoya also gave general advice throughout the study. Y. Aoki, R. Maruyama, S. Takeda, and T. Yokota supervised the study. T. Partridge, S. Takeda, and T. Yokota were involved with concept formation. I wrote the entire manuscript. S. Takeda was a supervisory author for this article. T. Yokota was also a supervisory author, and was involved with manuscript composition. Animal experiments were approved by the Ethics Committee for the Treatment of Laboratory Middle-Sized Animals of the National Center for Neurology and Psychiatry at Tokyo, Japan. Animal experiments were not conducted at the University of Alberta or by University of Alberta students and staff.

Chapter 5 of this thesis contains original work that I conducted in collaboration with S. Woo, D. Melo, Y. Huang, K. Dzierlega, T. Aslesh, R. R. Roshmi, M. N. A. Shah, and R. Maruyama at the Yokota laboratory (University of Alberta), with Y. Echigoya at Nihon University, and with H. Moulton at Oregon State University. I was involved with concept formation, performed all experiments and data analysis, with the assistance of S. Woo on animal work (injections, functional testing, tissue collection), D. Melo on preliminary experiments minimizing the exons 45-55 skipping cocktail in immortalized patient-derived cells, Y. Huang

and K. Dzierlega on molecular work for the exon 51 skipping single-dose study, as well as S. Woo, Y. Huang, T. Aslesh, R. R. Roshmi, and M. N. A. Shah on the quantification of histological images. The antisense oligonucleotides used were based on the original design of Y. Echigoya. R. Maruyama helped supervise the study. I wrote the entire manuscript, which we plan to submit to a journal for publication. T. Yokota will be the supervisory author for this article, and was involved with concept formation and manuscript composition. Animal experiments were reviewed and approved by the Animal Care and Use Committee at the University of Alberta Research Ethics Office, under study ID AUP00000365. Experiments on immortalized patient-derived cells were approved by the University of Alberta Health Research Ethics Board (study ID Pr00079871).

Permission was obtained from the respective journals, as necessary, to include content from the mentioned articles in this thesis.

“What is essential is invisible to the eye”

Antoine de Saint-Exupéry, *The Little Prince*

This thesis is dedicated to my parents, Kirk Lim and Rowena Lim,  
for all the little things and all the big things.

## Acknowledgments

To my supervisor, Dr. Toshifumi Yokota—thank you for accepting me into your research group and for giving me countless opportunities to develop as a scientist. I could not have been as productive, as successful, and as surrounded by wonderful people had it not been for the many doors you opened for me, beginning with that of 8-31 MSB.

To my committee members, Dr. Daniel Graf and Dr. Gavin Oudit—thank you for all our lively discussions and for all the times you helped me overcome my limits. I gained a deeper understanding of science thanks to you, and have learned much as a result.

To my many collaborators—thank you for making our work what it is today. I would like to especially thank Dr. Yoshitsugu Aoki and his team for warmly receiving me in Japan when I visited them to do research. I will always remember my time there, and all those chats over cups of green tea. Special thanks as well to Dr. Yi-Wen Chen and her team for all their support.

To my funding sources, the University of Alberta Faculty of Medicine and Dentistry, University of Alberta Department of Medical Genetics, Alberta Health Services, Stollery Children's Hospital Foundation (through the Women and Children's Health Research Institute), Canadian Institutes of Health Research, and Alberta Innovates—thank you for financially supporting me throughout my studies, and for giving me the time and resources needed so I could focus on my research and grow as a scientist.

To the members of the Yokota Lab I have been fortunate to meet—thank you for making my lab experience something I will always remember. To Yusuke, we may have only worked together briefly, but the things I learned from you during those times are things that have stayed with me to this very day. To Kana, Tejal, Kevin, Stanley, Saeed, and Ahad, thank you for the

friendship and for always lending an ear or a hand (or one bubble tea, with tapioca) when I need it. To all my amazing students, thank you for being amazing and for teaching me a lot of things.

To the Department of Medical Genetics faculty and staff—thank you for all the support and for answering all of my many questions. I would like to especially thank Dr. Sarah Hughes and Dr. Rachel Wevrick for being people I could go to whenever I had things I wanted to talk about. Thank you as well to Dr. Peter Kannu, for encouraging me to think outside the box.

To my fellow Medical Genetics students—thank you for making my time at the department fun. I am very happy to have met all of you, and hope we could get the chance to play board games again in the future.

To my friends here and on the other side of the globe—thank you for everything, and by that I mean everything. Thank you most especially to Quynh, for always being supportive, for always understanding me, for always helping me back up when life takes me down, and for being a best friend to me since the first day we met. Thank you to my friends in high school (C.U.) and in university (MBB 2014), for staying connected with me despite the distance. I enjoy all our conversations, and cannot wait to see all of you in person again someday.

And of course to my dearest family—thank you for all your love and support. To my parents, Kirk and Rowena, and to my siblings, Kamei, Kobin, Kenzo, and Kimi, I am thankful every day for all of you and will love you forever and ever and ever. This is for you.

Kenji Rowel Q. Lim

Edmonton, AB

April 2021

# Table of Contents

<b>Abstract</b>	<b>ii</b>
<b>Preface</b>	<b>iv</b>
<b>Acknowledgments</b>	<b>ix</b>
<b>Table of Contents</b>	<b>xi</b>
<b>List of Tables</b>	<b>xvii</b>
<b>List of Figures</b>	<b>xviii</b>
<b>List of Abbreviations</b>	<b>xxi</b>
<b>Chapter 1 Introduction</b>	<b>1</b>
<i>1.1. General overview</i>	2
<i>1.2. Facioscapulohumeral muscular dystrophy</i>	3
1.2.1. Overview	3
1.2.2. <i>DUX4</i> expression and FSHD	5
1.2.3. <i>DUX4</i> in skeletal muscle signalling, growth, and development	8
1.2.4. Oligonucleotide therapies for FSHD	12
1.2.5. Alternative genetic therapies for FSHD	19
<i>1.3. Duchenne muscular dystrophy</i>	22
1.3.1. Overview	22
1.3.2. Dystrophin protein: structure and function	25
1.3.3. Exon skipping development for DMD	28
1.3.4. Exon skipping in humans	34
	<b>xi</b>

1.3.5. Alternative genetic therapies for DMD	36
<i>1.4. Study Objectives</i>	40
<b>Chapter 2 Inhibition of <i>DUX4</i> expression with antisense LNA gapmers as a therapy for facioscapulohumeral muscular dystrophy</b>	<b>42</b>
<i>2.1. Abstract</i>	43
<i>2.2. Introduction</i>	43
<i>2.3. Results</i>	46
2.3.1. LNA gapmers effectively knock down DUX4 expression in vitro	46
2.3.2. LNA4 decreases the expression of FSHD-associated genes	51
2.3.3. Effects of LNA gapmer treatment on myogenic fusion and apoptosis	57
2.3.4. Minimal potential off-target toxicity with LNA gapmer treatment in silico, in vitro	61
2.3.5. In vivo uptake and efficacy of LNA4	63
<i>2.4. Discussion</i>	65
<i>2.5. Methods</i>	69
2.5.1. Animals	69
2.5.2. Antisense oligonucleotides	69
2.5.3. Cell culture	70
2.5.4. AO transfection	71
2.5.5. RNA extraction from cells and qPCR	71
2.5.6. RNA sequencing	73
2.5.7. Myogenic fusion index and hypotrophy phenotype analysis	73
2.5.8. Apoptosis assessment by flow cytometry	75
2.5.10. In vivo delivery of LNA gapmers	76

2.5.11. RNA secondary structure analysis	77
2.5.12. Statistical analysis	77
<b>Chapter 3 <i>DUX4</i> Transcript Knockdown with Antisense 2'-O-Methoxyethyl Gapmers for the Treatment of Facioscapulohumeral Muscular Dystrophy</b>	<b>78</b>
3.1. <i>Abstract</i>	79
3.2. <i>Introduction</i>	79
3.3. <i>Results</i>	81
3.3.1. Designed 2'-MOE gapmers effectively knock down DUX4 transcript expression	81
3.3.2 A subset of transcriptome-level alterations were restored with 2'-MOE gapmer treatment	84
3.3.3. Improvements in cellular phenotypes upon 2'-MOE gapmer treatment	91
3.3.4. Off-target effect analysis of 2'-MOE gapmer treatment	94
3.3.5. 2'-MOE gapmer treatment reduces DUX4 expression in an FSHD mouse model	96
3.4. <i>Discussion</i>	98
3.5. <i>Methods</i>	102
3.5.1. Antisense oligonucleotides, cell culture	102
3.5.2. Transfection for gapmer screen	104
3.5.3. RNA extraction and qPCR	104
3.5.4. RNA sequencing and bioinformatics	106
3.5.5. Cellular phenotype analysis	107
3.5.6. Western blotting	108
3.5.7. Searching for potential off-target genes	109
3.5.8. In vivo delivery of 2'-MOE gapmers	109

3.5.9. Statistical analysis	110
<b>Chapter 4 Efficacy of Multi-exon Skipping Treatment in Duchenne Muscular Dystrophy</b>	
<b>Dog Model Neonates</b>	<b>111</b>
4.1. Abstract	112
4.2. Introduction	112
4.3. Results	114
4.3.1. Early exon skipping treatment leads to variable improvements across skeletal muscles	114
4.3.2. Treatment-related dystrophin rescue is not detectable in cardiac muscle regardless of early-age PMO administration	123
4.3.3. PMO serum clearance and muscle uptake in treated neonatal dystrophic dogs	126
4.3.4. Functional testing of treated neonatal CXMD <sub>J</sub> dogs	128
4.3.5. Early treatment with exon skipping PMOs is not associated with detectable toxicity in blood tests	128
4.4. Discussion	131
4.5. Methods	136
4.5.1. Animals	136
4.5.2. Intravenous PMO treatment and sample collection	136
4.5.3. Functional assessment	137
4.5.4. Exon skipping efficiency determination	137
4.5.5. Western blot analysis of dystrophin rescue	138
4.5.6. Immunohistochemistry	139
4.5.7. Histology	139

4.5.8. Blood tests	140
4.5.9. ELISA	140
4.5.10. Statistical analysis	141
<b>Chapter 5 Development of DG9 Peptide-Conjugated Single- and Multi-exon Skipping Antisense Oligonucleotides for the Treatment of Duchenne Muscular Dystrophy</b>	<b>142</b>
<i>5.1. Abstract</i>	<i>143</i>
<i>5.2. Introduction</i>	<i>143</i>
<i>5.3. Results</i>	<i>147</i>
5.3.1. Minimizing the exons 45-55 skipping cocktail	147
5.3.2. Minimized exon skipping cocktails effectively skip exons 45-55 in various patient cells	151
5.3.3. Single intravenous treatment with DG9-PMO induces higher dystrophin production than unconjugated PMO in the skeletal muscles and the heart	152
5.3.4. Repeated intravenous treatment with DG9-PMO improves dystrophin production, muscle function, and fiber size in dystrophic mice	156
5.3.5. Local treatment with the DG9-conjugated minimized exons 45-55 skipping cocktail induces successful skipping and dystrophin production	161
<i>5.4. Discussion</i>	<i>163</i>
<i>5.5. Methods</i>	<i>167</i>
5.5.1. Cell culture	167
5.5.2. PMO transfection	167
5.5.3. Animals and treatments	168
5.5.4. Functional testing	169

5.5.5. RT-PCR and exon skipping evaluation	170
5.5.6. Western blot	171
5.5.7. Dystrophin immunofluorescence	172
5.5.8. Histology	173
5.5.9. Statistical Analysis	174
<b>Chapter 6 Conclusions and future directions</b>	<b>175</b>
<i>6.1. Developing an antisense therapy for FSHD</i>	<i>176</i>
<i>6.2. Developing an antisense therapy for DMD</i>	<i>178</i>
<b>Bibliography</b>	<b>182</b>

## List of Tables

Table 1.1. Global prevalence estimates of selected muscular dystrophies from meta-analysis studies. ....	2
Table 1.2. Summary of results from pre-clinical studies on AOs for <i>DUX4</i> knockdown. ....	16
Table 2.1. Characteristics of the LNA gapmers used in this study. ....	48
Table 2.2. Significantly up-/down-regulated genes* comprising the FSHD signature. ....	53
Table 2.3. FSHD signature genes with expression values significantly restored to healthy levels after LNA4 treatment <i>in vitro</i> . ....	56
Table 2.4. Potential off-targets of LNA gapmers 1, 4, and 6 as identified by GGGenome. ....	61
Table 2.5. Primer sequences used in this study. ....	72
Table 3.1. Characteristics of designed 2'-MOE gapmers against the <i>DUX4</i> transcript. ....	83
Table 3.2. Information on the 94 FSHD signature genes obtained from RNA sequencing analysis. ....	87
Table 3.3. Validation of some FSHD signature genes from RNA sequencing analysis. ....	90
Table 3.4. Potential off-target transcripts of the 2'-MOE gapmers, as determined by GGGenome ....	94
Table 3.5. Characteristics of the immortalized human muscle cells used in this study. ....	103
Table 3.6. Primers used for qPCR evaluation of gene expression in this study. ....	105
Table 4.1. Comprehensive list of dogs used in the study. ....	117
Table 5.1. List of PMO sequences used for exons 45-55 skipping. ....	148
Table 5.2. List of primers and sequences used in this study. ....	170

## List of Figures

Figure 1.1. Activation of <i>DUX4</i> expression in FSHD. ....	6
Figure 1.2. <i>DUX4</i> signalling in FSHD-affected skeletal muscle.....	9
Figure 1.3. Antisense oligonucleotide mechanisms of action.....	13
Figure 1.4. Antisense oligonucleotide (AO) chemistries.....	14
Figure 1.5. Overview of <i>DUX4</i> regions that have been targeted by oligonucleotide therapies....	17
Figure 1.6. Dystrophin-associated glycoprotein complex and dystrophin isoforms. ....	23
Figure 1.7. Dystrophin protein domains. ....	24
Figure 1.8. Eteplirsen is an exon skipping therapeutic. ....	30
Figure 2.1. <i>DUX4</i> mRNA expression levels in the course of muscle differentiation <i>in vitro</i> . ....	48
Figure 2.2. LNA gapmer screen and evaluation of knockdown efficacy by qPCR.....	49
Figure 2.3. Predicted <i>DUX4</i> exon 3 pre-mRNA secondary structure.....	50
Figure 2.4. RNA sequencing analysis of LNA gapmer therapeutic efficacy.....	52
Figure 2.5. Alternative comparison for RNA sequencing analysis of LNA gapmer therapeutic efficacy.....	55
Figure 2.6. Effect of LNA gapmer treatment on <i>in vitro</i> muscle cell fusion and apoptosis. ....	58
Figure 2.7. Flow cytometry evaluation of <i>in vitro</i> apoptosis.....	60
Figure 2.8. Evaluation of potential LNA gapmer off-target effect. ....	62
Figure 2.9. <i>In vivo</i> uptake and efficacy of LNA gapmers. ....	64
Figure 3.1. <i>DUX4</i> knockdown efficacy evaluation of designed 2'-MOE gapmers.....	83
Figure 3.2. RNA sequencing analysis of 2'-MOE gapmer-treated muscle cells.....	85
Figure 3.3. qPCR analysis of <i>TRIM48</i> , <i>TRIM64B</i> , and <i>PRAMEF4/5/9/11</i> expression. ....	90
Figure 3.4. <i>In vitro</i> muscle cell phenotypes after 2'-MOE gapmer treatment.....	92

Figure 3.5. Western blot analysis of myosin heavy chain protein levels.....	93
Figure 3.6. Off-target effect evaluation upon 2'-MOE gapmer treatment.....	95
Figure 3.7. <i>In vivo</i> efficacy of MOE3 gapmer treatment in <i>FLEXDUX4</i> mice.....	97
Figure 4.1. Overview of experimental design.....	116
Figure 4.2. Effects of early exon skipping treatment on dystrophin production in CXMD <sub>J</sub> skeletal muscles.....	118
Figure 4.3. Dystrophin Western blot results for other treated CXMD <sub>J</sub> neonatal dogs. ....	119
Figure 4.4. Representative immunohistochemistry images of skeletal muscles from 8603MA, stained using DYS1.....	121
Figure 4.5. Histopathological improvements in PMO-treated neonatal CXMD <sub>J</sub> skeletal muscles. .....	122
Figure 4.6. Effects of early exon skipping treatment on dystrophin production in CXMD <sub>J</sub> cardiac muscles.....	124
Figure 4.7. Representative immunohistochemistry images of cardiac muscles detected with DYS2.....	125
Figure 4.8. ELISA-based quantification of PMOs in serum and muscle.....	127
Figure 4.9. Functional testing of CXMD <sub>J</sub> dogs. ....	129
Figure 4.10. Analysis of serum biomarkers from weekly blood tests in neonatal dogs. ....	130
Figure 5.1. Testing minimized exons 45-55 skipping cocktails in immortalized patient myotubes. .....	149
Figure 5.2. Preliminary testing of minimized exons 45-55 skipping cocktails. ....	150
Figure 5.3. Single-dose exon 51 skipping treatment with DG9-PMO.....	154
Figure 5.4. Histological data from single-dose exon 51 skipping treatment with DG9-PMO. ..	155

Figure 5.5. Repeated-dose exon 51 skipping treatment with DG9-PMO.....	157
Figure 5.6. Functional and histological data from repeated-dose exon 51 skipping treatment with DG9-PMO.....	159
Figure 5.7. Liver and kidney histology from single- and repeated-dose exon 51 skipping treatment studies. ....	160
Figure 5.8. Local treatment with the minimized “block” DG9-PMO exons 45-55 skipping cocktail.....	162

## List of Abbreviations

2'-MOE	2'- <i>O</i> -methoxyethyl
2'-O-Me	2'- <i>O</i> -methyl
2'-OMePS	phosphorothioated 2'- <i>O</i> -methyl
6MWT	6-minute walk test
AAV	adeno-associated virus
aFSDH	atrophic FSDH
ALB	serum albumin
ALP	alkaline phosphatase
ALT	alanine aminotransferase
AO	antisense oligonucleotide
AP	anterior papillary muscle
AQP4	aquaporin 4
AST	aspartate aminotransferase
BCA	bicinchoninic acid
BF	biceps femoris
BIC	biceps brachii
BMD	Becker muscular dystrophy
BUN	blood urea nitrogen
Cas9	CRISPR-associated protein 9
cDNA	complementary DNA
cEt	constrained ethyl
CK	creatine kinase

CNF	centrally nucleated fiber
CRE	creatinine
CRISPR	clustered regularly interspaced short palindromic repeats
CXMD <sub>J</sub>	canine X-linked muscular dystrophy in Japan
DAGC	dystrophin-associated glycoprotein complex
DAPI	4',6-diamidino-2-phenylindole
dCas9	catalytically-deficient Cas9
dFSHD	disorganized FSHD
DIA	diaphragm
DMD	Duchenne muscular dystrophy
DMEM	Dulbecco's modified Eagle medium
DNA	deoxyribonucleic acid
DUX4	double homeobox protein 4
e.p.	electroporation
ECU	extensor carpi ulnaris
EDL	extensor digitorum longus
EDTA	ethylenediamine tetra-acetic acid
ELISA	enzyme-linked immunosorbent assay
ESC	embryonic stem cell
ESOP	esophagus
Ex	exon
FBS	fetal bovine serum
FDA	U.S. Food and Drug Administration

FITC	fluorescein isothiocyanate
FSHD	Facioscapulohumeral muscular dystrophy
GAS	gastrocnemius
GGT	gamma-glutamyl transferase
GRA	gracilis major
gRNA	guide RNA
HDR	homology-directed repair
HE	hematoxylin-eosin
HEPES	4-(2-hydroxyethyl)-1-piperazineethanesulfonic acid
i.m.	intramuscular
i.p.	intraperitoneal
IC	intercostal muscles
IMEP	intramuscular injection and electroporation of naked plasmid DNA
KOSR	KnockOut serum replacement
LDH	lactate dehydrogenase
LNA	locked nucleic acid
LV	left ventricle
MFI	myogenic fusion index
MHC/MyHC	myosin heavy chain
miRNA	microRNA
NHEJ	non-homologous end-joining
NMJ	neuromuscular junction
nNOS	neuronal nitric oxide synthase

NSAA	North Star Ambulatory Assessment
ORF	open reading frame
PAS	polyadenylation signal
PBS	phosphate-buffered saline
PBST	PBS with 0.05% Tween 20
PBSTX	PBS with 0.1% Triton X-100
PCR	polymerase chain reaction
PEV	posterior external left ventricle
PMO	phosphorodiamidate morpholino oligomer
PNA	peptide nucleic acid
PP	posterior papillary muscles
PPMO	peptide-conjugated PMO
PVDF	polyvinylidene fluoride
PW	posterior wall of the left ventricle
qPCR	quantitative real-time PCR
QUA	quadriceps
RIPA	radioimmunoprecipitation assay
RNA	ribonucleic acid
RNAi	RNA interference
RNase H	ribonuclease H
ROS	reactive oxygen species
RT-PCR	reverse transcription PCR
RTK	receptor tyrosine kinase

RV	right ventricle
SA	splice acceptor
SC	sternocleidomastoid
SDS	sodium dodecyl sulfate
SDS-PAGE	SDS-polyacrylamide gel electrophoresis
SG	sarcoglycan
siRNA	small interfering RNA
SL	left side of the interventricular septum
SOL	soleus
SR	right side of the interventricular septum
SSPN	sarcospan
SYN	syntrophin
TA	tibialis anterior
TBIL	total bilirubin
tcDNA	tricyclo DNA
TP	total protein
UTR	untranslated region
$\alpha$ -DB	$\alpha$ -dystrobrevin
$\alpha$ -DG	$\alpha$ -dystroglycan
$\beta$ -DG	$\beta$ -dystroglycan
$\beta$ -tub	$\beta$ -tubulin
$\beta$ 2-AR	$\beta$ 2-adrenergic receptor

## Chapter 1 Introduction

Parts of Chapter 1 were derived from a version of the following published articles:

Lim, K. R. Q. & Yokota, T. Genetic approaches for the treatment of facioscapulohumeral muscular dystrophy. *Front. Pharmacol.* **12**, 642858 (2021). – Sections 1.2.1, 1.2.2, 1.2.4, 1.2.5

Lim, K. R. Q., Nguyen, Q. & Yokota, T. DUX4 signalling in the pathogenesis of facioscapulohumeral muscular dystrophy. *Int. J. Mol. Sci.* **21**, 729 (2020). – Section 1.2.3

Lim, K. R. Q., Maruyama, R. & Yokota, T. Eteplirsen in the treatment of Duchenne muscular dystrophy. *Drug Des. Devel. Ther.* **11**, 533-545 (2017); originally published by Dove Medical Press – Sections 1.3.1, 1.3.3

Lim, K. R. Q. & Yokota, T. Invention and early history of exon skipping and splice modulation. In *Exon Skipping and Inclusion Therapies: Methods and Protocols* (eds. Yokota, T. & Maruyama, R.) 3-30 (Springer, 2018); reprinted/adapted by permission from Springer Nature Customer Service Centre GmbH – Sections 1.3.3, 1.3.4

Lim, K. R. Q.\*, Yoon, C.\* & Yokota, T. Applications of CRISPR/Cas9 for the treatment of Duchenne muscular dystrophy. *J. Pers. Med.* **8**, 38 (2018). (\*co-first) – Section 1.3.5

Lim, K. R. Q. & Yokota, T. Invention and early history of gapmers. In *Gapmers: Methods and Protocols* (eds. Yokota, T. & Maruyama, R.) 3-19 (Springer, 2020); reprinted/adapted by permission from Springer Nature Customer Service Centre GmbH – Figure 1.3

Lim, K. R. Q., Nguyen, Q. & Yokota, T. Genotype–Phenotype Correlations in Duchenne and Becker Muscular Dystrophy Patients from the Canadian Neuromuscular Disease Registry. *J. Pers. Med.* **10**, 241 (2020). – Figure 1.7

## 1.1. General overview

The muscular dystrophies are a group of inherited disorders that, although heterogeneous in many aspects, are characterized by progressive muscle deterioration.<sup>1</sup> Patient muscle biopsies show typical dystrophic histopathology, including necrosis, fibrosis, fat replacement, inflammatory infiltration, and morphologically abnormal muscle fiber shape and size. Global prevalence estimates for some of the more common muscular dystrophies are shown in **Table 1.1**. The prevalence of Duchenne muscular dystrophy (DMD) is low in the general population, likely due to patients dying at younger ages. It is in fact quite high in specific populations at 19.8 (95% confidence interval: 16.6-23.6) per 100,000 live male births and 7.1 (5.0-10.1) per 100,000 males according to a recent study.<sup>2</sup> Thus, it is considered the most common form of muscular dystrophy worldwide. This is followed by myotonic dystrophy and facioscapulohumeral muscular dystrophy (FSHD) as the second and third most common muscular dystrophies, respectively. Also, in comparison to DMD, the global prevalence of its mild counterpart Becker muscular dystrophy (BMD) is at 1.53 (0.26-8.94) per 100,000 males.<sup>3</sup> It is important to note that these estimates are variable across studies, and exhibit wide regional differences.

**Table 1.1. Global prevalence estimates of selected muscular dystrophies from meta-analysis studies.**

<b>Muscular dystrophy</b>	<b>Prevalence (95% CI)*</b>	<b>Reference</b>
Duchenne muscular dystrophy	2.8 (1.6-4.6)	Crisafulli et al. 2020 <sup>2</sup>
Myotonic dystrophy	8.26 (4.99-13.68)	Mah et al. 2016 <sup>4</sup>
Facioscapulohumeral muscular dystrophy	3.95 (2.89-5.40)	Mah et al. 2016 <sup>4</sup>
Limb girdle muscular dystrophy	1.63 (0.94-2.81)	Mah et al. 2016 <sup>4</sup>
Congenital muscular dystrophy	0.99 (0.62-1.57)	Mah et al. 2016 <sup>4</sup>
Emery-Dreifuss muscular dystrophy	0.39 (0.12-1.30)	Mah et al. 2016 <sup>4</sup>

\*per 100,000 in the general population; CI, confidence interval.

Antisense oligonucleotide (AO) therapies were developed for two inherited muscular dystrophies in this thesis: FSHD and DMD. We discuss here the characteristics of FSHD and DMD, the state of genetic therapy development for each (focusing on AOs), and the objectives of this thesis. It is hypothesized that targeted AO therapies could be developed to post-transcriptionally “correct” genetic events or mutations that cause FSHD and DMD, respectively, and will lead to an amelioration of disease-associated phenotypes at the molecular, cellular, and/or functional levels as applicable.

## **1.2. Facioscapulohumeral muscular dystrophy**

### **1.2.1. Overview**

FSHD is an autosomal dominant disorder that affects 1 in 8,000-22,000 people in the world and is the third most common inherited muscular dystrophy.<sup>5</sup> It presents as a progressive, distinctively asymmetric weakening of muscles in the face, shoulders, and upper limbs. Muscles in other regions may become affected with age; around 20% of patients become wheelchair-bound.<sup>6</sup> Extramuscular symptoms are uncommon, with a few patients experiencing restrictive lung disease, cardiac conduction abnormalities, hearing loss, or retinal vasculopathy.<sup>7-12</sup> Age of onset and disease severity are both widely variable in FSHD.<sup>5,13</sup> Intriguingly, 4-21% of patients who manifest symptoms before the age of 5 almost all follow a more severe and rapid course of the disease.<sup>14,15</sup> There is no available cure for FSHD. Patients are currently managed for their symptoms at best.

While the genetic mechanisms leading to FSHD are diverse and complex, these all result in aberrant expression of the *double homeobox protein 4 (DUX4)* gene in skeletal muscle. *DUX4* has roles in early embryonic development, where it appears to be essential for zygotic gene

activation.<sup>16,17</sup> Under healthy conditions, *DUX4* is epigenetically silenced after the 4-cell stage in humans and kept as such in all developed tissues but the testis<sup>18</sup> and thymus.<sup>19</sup> This repression is compromised in patients with FSHD, allowing for the synthesis of the DUX4 transcription factor whose activities in skeletal muscle induce potent cytotoxicity by dysregulating pathways involved in cell death, oxidative stress, and muscle development, among others.<sup>7,20</sup>

Various approaches are being explored to treat FSHD. Pharmacological treatments have been evaluated mostly with the aim of improving muscular symptoms, and include the use of prednisone,  $\beta$ 2 receptor agonists, myostatin inhibitors, and antioxidants, among others. Unfortunately, these generally offered little to no therapeutic benefit based on results from clinical trials.<sup>21,22</sup> Intramuscular transplantation of myoblasts or mesoangioblasts (perivascular myogenic stem cells) from unaffected muscles of FSHD patients into immunodeficient mice revealed that these could integrate with recipient muscle fibers fairly well.<sup>23,24</sup> However, follow-up studies examining the benefits of such cell-based therapies on FSHD muscle pathology or function are currently unavailable and so their potential for treating FSHD remains uncertain.

In response to developing a more targeted form of treatment, reducing muscle-specific *DUX4* expression and DUX4-mediated toxicity have become attractive goals for FSHD therapy.<sup>25-27</sup> Indeed, a number of genetic methods have been employed to achieve one or both of these, including oligonucleotide-based strategies to knockdown *DUX4* transcript levels or reduce DUX4 protein activity, and genome editing to correct FSHD-associated mutations. The pre-clinical development of these strategies and others has shown much promise, and identifies possible candidates for clinical trials. Compared to pharmaceutical and cell-based interventions, genetic treatments target the root cause of the disease (i.e., *DUX4*) and are thus expected to lead to more effective or far-reaching therapeutic effects.

### 1.2.2. *DUX4* expression and FSHD

Much of the complexity associated with FSHD genetics comes from the curious location of *DUX4* in the genome. The *DUX4* gene is part of the D4Z4 macrosatellite repeat array at chromosome 4q35, which is typically 11-100 repeats long in healthy individuals.<sup>28,29</sup> There is a homologous D4Z4 repeat array at chromosome 10q26, but mutations in this region have not been linked to FSHD.<sup>29-31</sup> Each D4Z4 repeat contains the first two exons of *DUX4*, with the entire open reading frame of the gene in exon 1 (**Figure 1.1**).<sup>28</sup> *DUX4* has other exons downstream of the array; the full-length isoform that contributes to FSHD pathology ends at exon 3.<sup>18,32</sup> Only exons from the last D4Z4 repeat contribute to the *DUX4* mRNA, and a polyadenylation signal (PAS) at exon 3 is required to stabilize the pathogenic *DUX4* transcript, a feature that is only present in the disease-permissive 4qA haplotype.<sup>29,33,34</sup> Finally, the 4q35 D4Z4 repeat array is normally hypermethylated, which keeps the *DUX4* gene repressed in most adult tissues.<sup>35</sup> Two mechanisms activate *DUX4* expression in FSHD: D4Z4 repeat array contraction, and mutations in genes coding for epigenetic regulators (**Figure 1.1**). These cause approximately 95% (FSHD1) and 5% (FSHD2) of cases, respectively.<sup>5</sup> Despite vast differences in their underlying genetics, FSHD1 and FSHD2 are clinically indistinguishable, implying that aberrant *DUX4* expression is the key genetic event leading to FSHD pathogenesis.

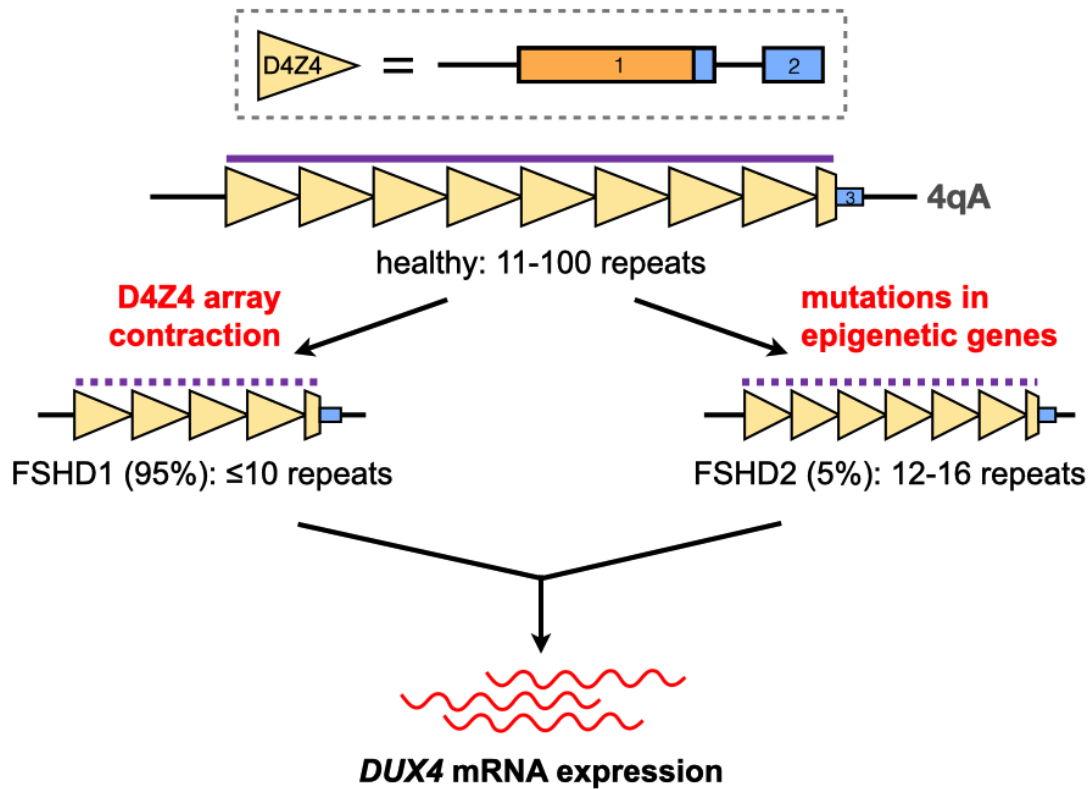


**Figure 1.1. Activation of *DUX4* expression in FSHD.** The *DUX4* gene is located in the D4Z4 macrosatellite repeat array at chromosome 4q35. Each D4Z4 repeat (yellow triangles) contains *DUX4* exons 1 and 2 (solid boxes; orange, open reading frame); exon 3 is found downstream of the last repeat in the array. The D4Z4 array is normally 11-100 repeats long and hypermethylated (purple line) in healthy individuals. Contractions of this array or mutations in genes coding for epigenetic regulators, in the 4qA haplotype, disrupt the silencing of *DUX4* (dotted purple line) and lead to its aberrant expression in skeletal muscle.

Figure from: Lim, K. R. Q. & Yokota, T. Genetic approaches for the treatment of facioscapulohumeral muscular dystrophy. *Front. Pharmacol.* **12**, 642858 (2021).

In FSHD1, contraction of the 4qA D4Z4 array to  $\leq 10$  repeats activates *DUX4* expression by increasing chromatin accessibility and promoting DNA hypomethylation in the region.<sup>36,37</sup> It was previously thought that individuals with  $\leq 10$  D4Z4 repeats in one 4qA chromosome form a homogeneous FSHD1 population, but it is now known that this is not the case. Clinical variability is high in individuals with 7-10 D4Z4 repeats, with most cases ranging from mild to asymptomatic.<sup>38,39</sup> This spread of phenotypes is attributed to inter-individual differences in D4Z4 methylation, indicating that factors other than array contraction may be more important in determining disease penetrance within this repeat range.<sup>38,40</sup> Conversely, penetrance is more complete in individuals with 1-6 D4Z4 repeats. Disease severity is also roughly inversely correlated with repeat count in these patients, e.g. those with the severe early-onset form of FSHD typically have 1-3 D4Z4 repeats.<sup>39,41,42</sup> Considering the 1-10 D4Z4 repeat range, it appears that the lower the number of repeats present, the less contribution factors other than contraction size have in influencing the FSHD1 phenotype.

Unlike in FSHD1, moderately-sized D4Z4 arrays are observed in FSHD2. On average, FSHD2 patients have 12-16 D4Z4 repeat units on at least one 4qA chromosome, which is at the shorter end of the range that characterizes the general population.<sup>32,43</sup> However, at our current level of understanding, D4Z4 array size has little to do with FSHD2 development. Instead, the majority of FSHD2 patients (~80%) carry mutations in *SMCHD1*, which codes for a protein involved in maintaining repressive chromatin architecture;<sup>44</sup> others have mutations in *DNMT3B* or *LRIF1*, which code for a DNA methyltransferase or an interactor of SMCHD1, respectively.<sup>45,46</sup> These mutations lead to D4Z4 hypomethylation independent of D4Z4 array size, creating a permissive environment for *DUX4* expression on the 4qA chromosome. One study showed that the extent of D4Z4 hypomethylation correlated with disease severity in

FSHD2, at least for *SMCHD1* mutation carriers.<sup>38</sup> Because of their role in D4Z4 methylation, *SMCHD1* and *DNMT3B* are also genetic modifiers for FSHD1, leading to cases with characteristics of both FSHD1 and FSHD2.<sup>45,47–49</sup>

### 1.2.3. DUX4 in skeletal muscle signalling, growth, and development

In 1999, Gabriëls et al. discovered that the D4Z4 repeat unit contained the sequence for a putative protein that contained two homeobox domains, which was the DUX4 transcription factor.<sup>28</sup> They further determined by *in vitro* reporter assays that part of the sequence preceding the *DUX4* open reading frame (ORF) in the D4Z4 repeat had promoter activity. Endogenous *DUX4* expression is extremely low however (we now know only 1/1000 myoblast or 1/200 myotube nuclei in patient primary cells are DUX4-positive by immunofluorescence).<sup>50</sup> This led to difficulties in detecting *DUX4* expression from patient samples, preventing inquiry into whether or not DUX4 was a key player in FSHD pathogenesis. Improvements in the knowledge of the *DUX4* gene, technique, and reagent availability eventually confirmed the presence of *DUX4* mRNA and protein in FSHD primary muscle cells<sup>20</sup> nearly a decade later, strengthening the link between muscle-specific *DUX4* expression and FSHD.

DUX4 has since been implicated as being involved in cell death, oxidative stress, muscle differentiation and growth, epigenetic regulation, and in regulating a number of other signalling pathways in skeletal muscle. While most of these investigations were launched to try and explain the mechanism behind DUX4-mediated cytotoxicity, they have also been instrumental in helping us understand the basic biology of FSHD. **Figure 1.2** shows a simplified overview of the various signalling pathways in skeletal muscle that are regulated by the DUX4 transcription factor.

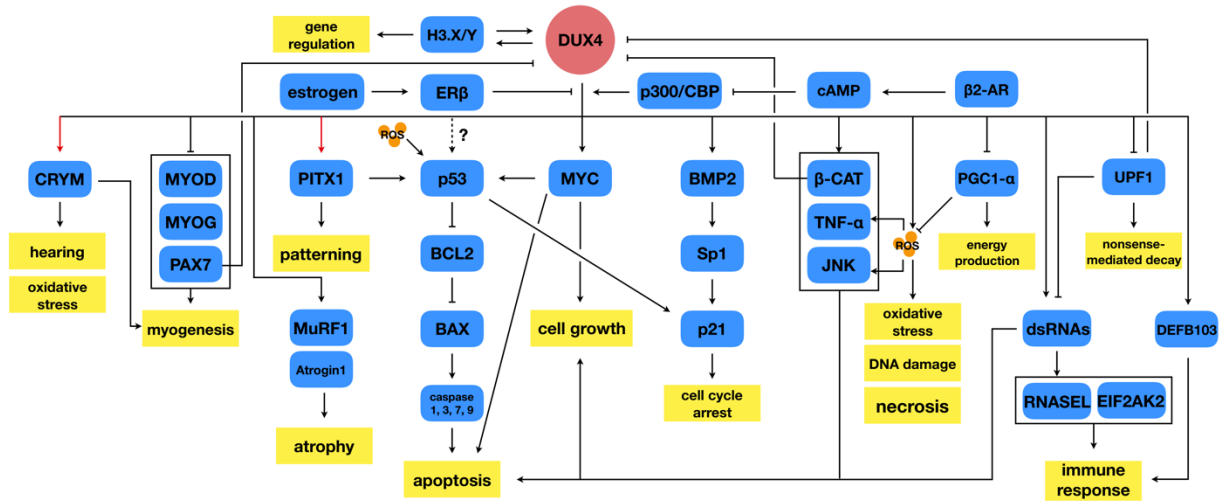


**Figure 1.2. Signalling pathways regulated by DUX4 in FSHD-affected skeletal muscle.** A simplified overview of the various regulatory activities of DUX4 discussed in this section is depicted. Red arrows indicate a confirmed direct downstream DUX4 transcriptional target. Abbreviation: ROS, reactive oxygen species.

Figure from: Lim, K. R. Q., Nguyen, Q. & Yokota, T. DUX4 signalling in the pathogenesis of facioscapulohumeral muscular dystrophy. *Int. J. Mol. Sci.* **21**, 729 (2020).

The degeneration of skeletal muscle in FSHD suggests that DUX4 may be initiating cell death pathways. Indeed, Kowaljew et al. (2007) found that overexpression of *DUX4 in vitro* resulted in significant cell death that was accompanied by significant increases in released lactate dehydrogenase into the medium, emerin redistribution, and caspase 3/7 activity.<sup>51</sup> Flow cytometry revealed an increased proportion of annexin V-positive cells when *DUX4* was transfected. Together, these findings point out a possible role for DUX4 in apoptosis.

Wallace et al. (2011) injected wild-type mice intramuscularly with adeno-associated viral (AAV) vectors containing the *DUX4* gene and collected samples for testing on a quantitative real-time PCR array for apoptosis-associated genes.<sup>52</sup> A third of the significantly up-regulated genes were involved in the p53 pathway, which is primarily known for regulating intrinsic or mitochondrial apoptosis.<sup>53,54</sup> Chemical inhibition of p53 pathway members (p53, caspase-1, and Bax) significantly decreased DUX4-mediated caspase-3/7 activation *in vitro* in *DUX4*-transfected HEK293 cells, a finding corroborated by a later study using different inhibitors.<sup>55</sup> Finally, *p53* knockout mice injected intramuscularly with AAV-*DUX4* had transduced muscles that were histologically normal,<sup>52</sup> suggesting that *DUX4*-induced cell death depends on the p53 pathway. This dependence of *DUX4* toxicity on p53 is contested, however.<sup>56-58</sup> Aside from p53, *DUX4* up-regulates Wnt/ $\beta$ -catenin signalling, as well as the expression of *CDKN1A*, *MYC*, and double-stranded RNAs, all of which lead to increased apoptosis.<sup>56,57,59,60</sup>

*DUX4* expression has also been demonstrated to downregulate genes involved in myogenesis, such as those coding for MyoD, myogenin, desmin, and Pax7; *Myf5* expression levels, on the other hand, were increased by DUX4.<sup>57</sup> Low levels of *DUX4* expression decreased muscle differentiation *in vitro*, as confirmed by a reduction in MyHC-positive fibers.<sup>57,61</sup> This *DUX4*-induced suppression of myogenic genes is found in both murine and human *in vitro*

models.<sup>57,61,62</sup> Furthermore, *DUX4* decreased myogenic gene expression in satellite cells, which not only reduced their proliferation but also impaired the differentiation and fusion of myotubes derived from them.<sup>62</sup> Transcriptomic analysis revealed that *DUX4* created an overall less-differentiated state of gene expression in myoblasts<sup>62</sup>, agreeing with the above observations.

Other genes implicated in myogenesis are affected by *DUX4*. In addition to the above, *DUX4* activates the expression of the muscle-specific E3 ubiquitin ligases Atrogin1 (or MAFbx) and MuRF1, which are involved in protein degradation and muscle atrophy.<sup>63</sup>  $\beta$ 2-adrenergic receptor ( $\beta$ 2-AR) signalling has been associated with regulating the expression of these two genes. Treatment of FSHD patient-derived muscle cells with  $\beta$ 2 agonists considerably inhibited *DUX4* expression and antagonized its effects<sup>64</sup>—Atrogin1 and MuRF1 may likely be involved in mediating the amelioration observed here. *DUX4* also directly binds the promoter of *CRYM*, upregulating its expression and increasing the levels of its protein product *in vitro*.<sup>63</sup> *CRYM* (or  $\mu$ -crystallin) is an NADPH-dependent thyroid-hormone binding protein that regulates the metabolic plasticity and contractility of skeletal muscles.<sup>65</sup> *CRYM* is also expressed in the cochlea and vestibule of the inner ear. Mutations in *CRYM* have been found to cause hearing loss,<sup>66</sup> potentially explaining the occurrence of this phenotype in some FSHD patients. Finally, *DUX4* induces the expression of the *RET* receptor tyrosine kinase (RTK) gene, which promotes the proliferation of satellite cell-derived myoblasts and maintains them in an undifferentiated state.<sup>67</sup> Treatment with sunitinib, an RTK inhibitor, inhibited Ret signalling and rescued differentiation in both mouse myoblasts expressing *DUX4* and FSHD patient-derived myoblasts.

The pathways described here represent but a mere fraction of *DUX4*-mediated signalling. Advances in transcriptomic and proteomic methods have accelerated our ability to identify global changes in gene expression, and we are extremely fortunate that the FSHD field has been

taking advantage of such technologies. Studies have implicated DUX4 in a myriad of pathways in the context of skeletal muscle: RNA metabolism and splicing;<sup>68–70</sup> protein translation and homeostasis;<sup>68,69,71</sup> sarcomeric organization;<sup>68</sup> germline and stem cell development;<sup>62,72</sup> extracellular and intracellular transport;<sup>69,70</sup> stress response;<sup>69</sup> cell polarity, adhesion, and migration;<sup>70</sup> and extracellular matrix signalling,<sup>70</sup> to name just a few.

#### 1.2.4. Oligonucleotide therapies for FSHD

Depending on their structure and chemistry, oligonucleotides can cause the inhibition of *DUX4* expression in a variety of ways. One of the most extensively tested for FSHD are AOs, single-stranded nucleic acid analogues that can bind target mRNA sequences by Watson-Crick base-pairing. There are two kinds of promising AOs that can mediate a reduction in gene expression (**Figure 1.3**). The first are those that interfere with mRNA splicing and processing.<sup>73</sup> These AOs act as steric blockers, preventing factors from accessing critical sequences in the mRNA such as splice sites, and are usually phosphorodiamidate morpholino oligomers (PMOs) or phosphorothioated 2'-O-methyl RNAs (2'-OMePS) (**Figure 1.4**). Besides knocking down gene expression, such AOs have also been used as splice modulation therapies, e.g. exon skipping for DMD.<sup>73</sup> The second are those that reduce gene expression by inducing target mRNA degradation.<sup>74</sup> The AOs in this group are gapmers, fully phosphorothioated oligonucleotides that have a central DNA stretch flanked by bases of modified chemistry, e.g. locked nucleic acids (LNA) or 2'-O-methoxyethyl RNAs (2'-MOE) (**Figure 1.4**). When a gapmer binds its target mRNA, a DNA/RNA hybrid is created in the middle of the AO that is recognized by ribonuclease H, which proceeds to bind the hybrid and cleave its RNA portion.

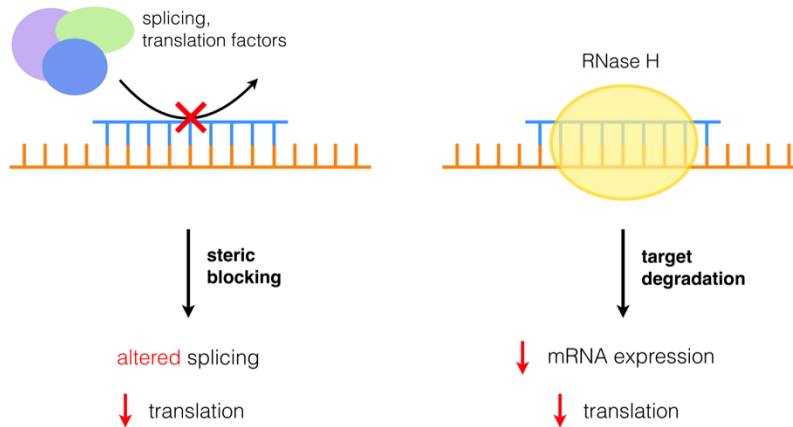


**Figure 1.3. Antisense oligonucleotide mechanisms of action.** Antisense oligonucleotides (blue) act on their target RNAs (orange) by one of two mechanisms: steric blocking of splicing and translation factors (left) or target degradation by recruiting and inducing ribonuclease H/RNase H activity (right). In the context of gene knockdown, use of both will inhibit protein synthesis

Reprinted/adapted by permission from Springer Nature Customer Service Centre GmbH: Springer, Invention and early history of gapmers by Lim, K. R. Q. & Yokota, T. In *Gapmers: Methods and Protocols* (eds. Yokota, T. & Maruyama, R.) 3-19. © 2020.

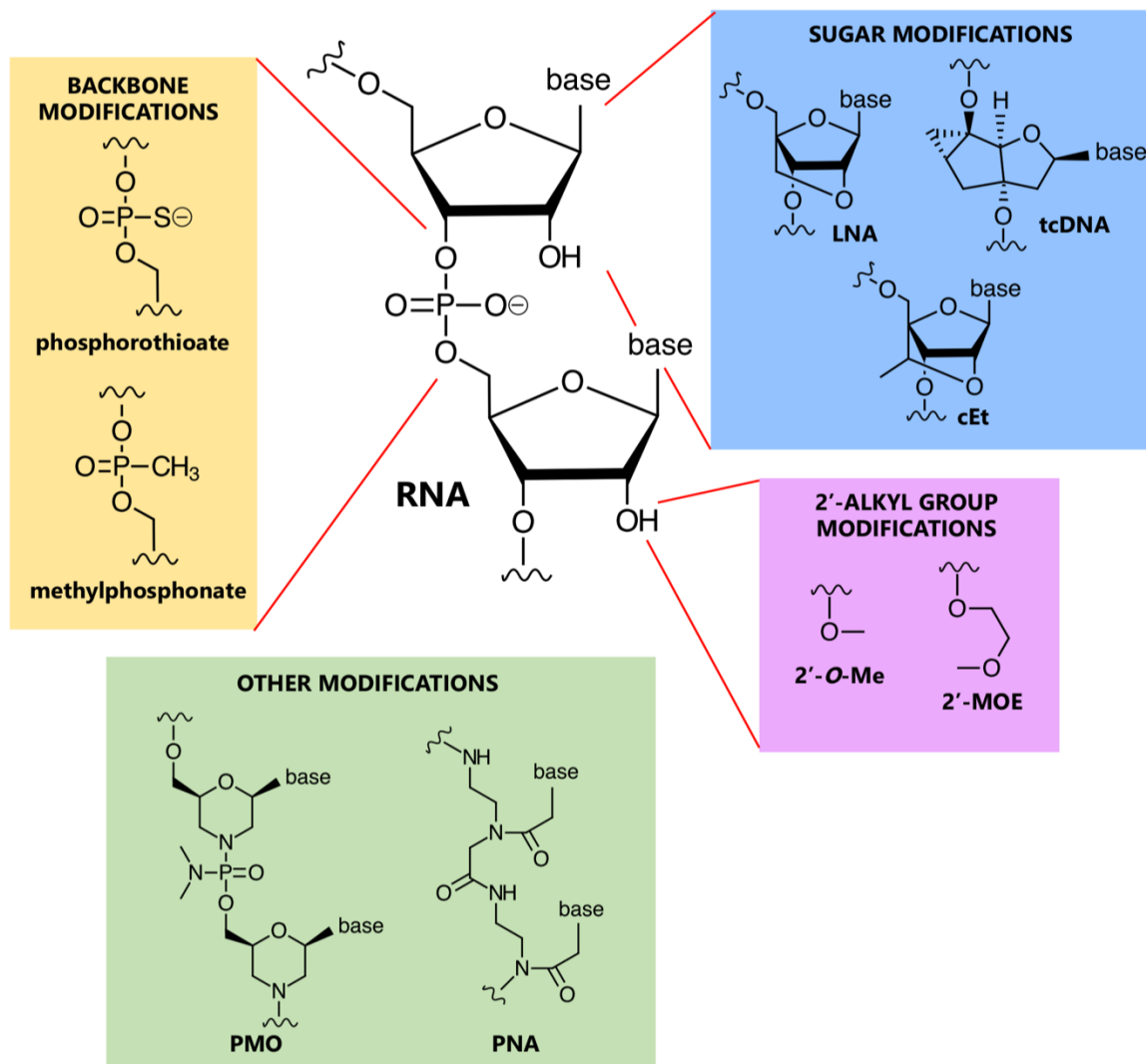


**Figure 1.4. Antisense oligonucleotide (AO) chemistries.** Through the years, various chemical modifications to the original RNA structure have been made in an effort to improve the efficacy of AO therapy. Modifications can generally be classified into those of the backbone, sugar, or the 2'-alkyl group of RNA. There are also other modifications which involve altering one or more of these components. Note that modifications can be combined when designing AOs, e.g. the 2'-O-Me modification is usually combined with the phosphorothioate backbone modification. Abbreviations: LNA, locked nucleic acid; tcDNA, tricyclo-DNA; cEt, constrained ethyl nucleic acid; 2'-O-Me, 2'-O-methyl RNA; 2'-MOE, 2'-O-(2-methoxyethyl) RNA; PMO, phosphorodiamidate morpholino oligomer; PNA, peptide nucleic acid.

Reprinted/adapted by permission from Springer Nature Customer Service Centre GmbH: Springer, Invention and early history of exon skipping and splice modulation by Lim, K. R. Q. & Yokota, T. In *Exon Skipping and Inclusion Therapies: Methods and Protocols* (eds. Yokota, T. & Maruyama, R.) 3-30. © 2018.

AOs of both kinds have successfully inhibited *DUX4* expression in patient-derived cells and FSHD mouse models (**Table 1.2**). The gapmer AOs were developed in studies that are part of this thesis (Chapters 2 and 3), and will be described in their respective sections. PMOs and 2'-OMePS AOs targeting splice acceptor sites for *DUX4* exons 2 and 3 (**Figure 1.5**) gave 30-90% *DUX4* mRNA knockdown (at 10 and 50 nM tested doses) in myotubes from treated primary patient myoblasts.<sup>63,75</sup> Corresponding reductions in *DUX4* downstream target gene expression and *DUX4*-positive nuclei, as well as improvements in muscle cell morphology, were observed. AOs targeting the exon 3 splice acceptor site were particularly more effective, one of which was tested in mice as a vivo-PMO.<sup>75,76</sup> Vivo-PMOs are PMOs that have been covalently linked to an octaguanidine dendrimer for improving uptake in tissues.<sup>77</sup> Mice transduced with *DUX4* constructs at the tibialis anterior (TA) were intramuscularly (i.m.) injected at the same muscle with 10 µg of the vivo-PMO, which led to 30-fold lower *DUX4* expression than the control vivo-PMO-treated leg by semi-quantitative RT-PCR, 10 days after treatment.<sup>75</sup> Histopathological improvements were observed in another study using the same AO.<sup>76</sup> PMOs have also been used to target the PAS in exon 3 (**Figure 1.5**), which knocked down *DUX4* transcript expression in immortalized patient-derived myotubes by 25-52% at a 50 nM dose<sup>78</sup> and in a xenograft FSHD mouse model by nearly 100% with a 20-µg injection.<sup>79</sup> Reduced expression of *DUX4* downstream target genes, transcriptomic-level restoration, and loss of *DUX4*-positive nuclei were observed *in vitro*; treatment showed no significant improvements in muscle cell fusion, however. While promising, the *DUX4* knockdown levels of steric-blocking AOs could be improved. Nearly complete *DUX4* knockdown should ideally be achieved, given that only small amounts of *DUX4* expression are necessary to drive the phenotypes observed in FSHD patients.<sup>50</sup>

**Table 1.2. Summary of results from pre-clinical studies on AOs for *DUX4* knockdown.**

Study	Chemistry	<i>DUX4</i> target	Model	<i>DUX4</i> knockdown (dose)	Other results
Vanderplanck et al. 2011 <sup>63</sup>	2'-OMePS	Ex2 SA, Ex3 SA	Primary FSHD myoblasts, differentiated post-treatment	30% (ex2 SA, 50 nM), 50% (ex3 SA, 10 nM)	Reduced TP53 levels, <i>TRIM43</i> expression
Marsollier et al. 2016 <sup>78</sup>	PMO	Ex3 PAS, down-stream elements	Immortalized FSHD myotubes	25-52% (50 nM)	Reduced <i>DUX4</i> downstream gene expression; fusion not affected
Chen et al. 2016 <sup>79</sup>	PMO	Ex2 SA, Ex3 PAS	Primary FSHD myotubes	Not assessed	Reduced <i>DUX4</i> <sup>+</sup> nuclei, <i>DUX4</i> downstream gene expression (only for PAS PMOs); transcriptomic improvements
		Ex3 PAS	FSHD xenograft mice, 1x e.p. into xenograft, evaluated 2 wks post-treatment	~100% (20 µg)	Reduced <i>DUX4</i> downstream gene expression
Anseau et al. 2017 <sup>75</sup>	2'-OMePS	Ex2 SA, Ex3 SA	Primary aFSHD and dFSHD myoblasts, differentiated post-treatment	~90% (ex2 SA, 50 nM; ex3 SA, 10 nM)	Reduced <i>DUX4</i> <sup>+</sup> nuclei; saw improvements in size (in aFSHD but not dFSHD myotubes)
	vivo-PMO	Ex3 SA	AAV- <i>DUX4</i> mice, 1x i.m. TA, evaluated 10 d post-treatment	30-fold lower than control vivo-PMO	None
Derenne et al. 2020 <sup>76</sup>	vivo-PMO	Ex3 SA	<i>DUX4</i> IMEP mice, 1x i.p., evaluated 1 wk post-treatment	Not assessed	2.5-fold decrease in histological lesion compared to non-treated
Lim et al. 2020 (Chapter 2 of this thesis)	LNA gapmer	Ex1, Ex3	Immortalized FSHD myotubes	~100% (100 nM)	Reduced <i>DUX4</i> downstream gene expression; partial transcriptomic restoration; improved muscle cell fusion/size
		Ex3	<i>FLExDUX4</i> mice, 3x i.m., evaluated 1 or 7 d post-treatment	84% (1 d, 20 µg/i.m.), 70% (7 d, 20 µg/i.m.)	Gapmer uptake observed in and between muscle fibers
Lim et al. 2021 (Chapter 3 of this thesis)	2'-MOE gapmer	Ex3	Immortalized FSHD myotubes	~100% (100 nM)	Reduced <i>DUX4</i> downstream gene expression; partial transcriptomic restoration; improved muscle cell fusion/size
		Ex3	<i>FLExDUX4</i> mice, 3x i.m., evaluated 1 d post-treatment	~65% (20 µg/i.m.)	None

Abbreviations: 2'-OMePS, phosphorothioated 2'-O-methyl RNAs; PMO, phosphorodiamidate morpholino oligomer; LNA, locked nucleic acid; 2'-MOE, 2'-O-methoxyethyl; Ex, exon; SA, splice acceptor; PAS, polyadenylation signal; e.p., electroporation; i.m., intramuscular injection; i.p., intraperitoneal injection; TA, tibialis anterior; AAV, adeno-associated virus; IMEP, intramuscular injection and electroporation of naked plasmid DNA; aFSHD, atrophic FSHD myotubes; dFSHD, disorganized FSHD myotubes

Table from: Lim, K. R. Q. & Yokota, T. Genetic approaches for the treatment of facioscapulohumeral muscular dystrophy. *Front. Pharmacol.* **12**, 642858 (2021).

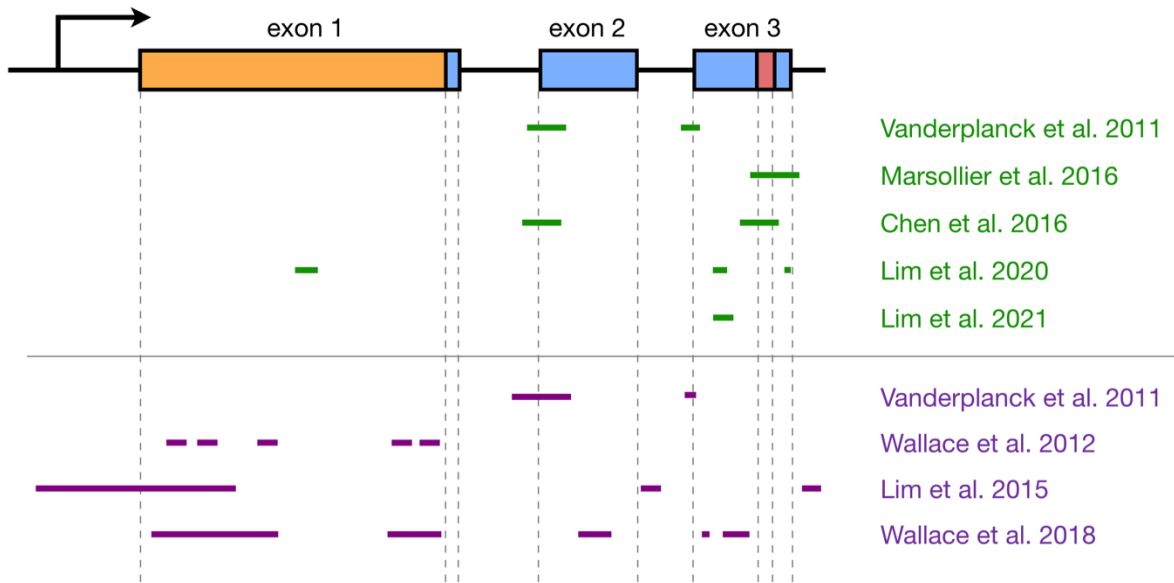


**Figure 1.5. Overview of *DUX4* regions that have been targeted by oligonucleotide therapies.** The structure of the *DUX4* gene is shown at the top (arrow indicates promoter region; boxes, exons; lines, introns; orange, open reading frame; red, polyadenylation signal), and the regions that have been targeted by antisense oligonucleotides (green) or RNA interference (purple) are shown at the bottom. Approximate locations are shown, and the figure is not to scale. Note that Anseau et al. (2017) used the same oligonucleotides as Vanderplanck et al. (2011). *DUX4* structure was based on information from Ensembl, transcript ID ENST00000569241.5.

Figure modified from: Genetic approaches for the treatment of facioscapulohumeral muscular dystrophy. *Front. Pharmacol.* **12**, 642858 (2021).

Another class of oligonucleotide therapy is RNA interference (RNAi), which makes use of small interfering RNAs (siRNAs) or microRNAs (miRNAs). Unlike AOs, siRNAs and miRNAs require association with effector proteins to reduce target gene expression. siRNAs targeting *DUX4* promoter elements or exons (**Figure 1.5**) knocked down *DUX4* transcript levels by 50-90% *in vitro*, with corresponding restorative effects on *DUX4* downstream targets.<sup>63,80</sup> Interestingly, siRNAs against the promoter likely inhibited *DUX4* expression through epigenetic silencing at the DNA level, since 2'-MOE gapmers against the same region did not affect *DUX4* transcript levels.<sup>80,81</sup> Meanwhile, one group screened a large number of miRNAs (**Figure 1.5**) and found two targeting exon 1 (mi1155, mi405) to knock down *DUX4* expression the best at >75% in *DUX4*-luciferase reporter cells.<sup>82,83</sup> Treatment of *DUX4*-transduced mice (i.m., TA) with  $3 \times 10^{10}$  adeno-associated viruses (AAVs) carrying mi405 constructs reduced *DUX4* mRNA expression by 64%, and *DUX4* protein levels by 90%.<sup>82</sup> Histopathology was improved with this miRNA, but not with mi1155 that instead showed signs of overt toxicity.<sup>83</sup>

Oligonucleotides can also be designed to target the *DUX4* protein. Double-stranded DNA decoys containing the *DUX4* binding motif have recently been developed to sequester and prevent *DUX4* from activating its downstream targets.<sup>84</sup> Indeed, the expression levels of *DUX4* downstream targets *ZSCAN4* and *TRIM43* were knocked down by 39-91% in primary patient myotubes upon treatment with these decoys. The DNA decoys were also tested in AAV-*DUX4* mice, where administration either by intramuscular electroporation or AAV delivery led to decreased expression of *Tm7sf4*, another *DUX4* downstream target. On a related note, single-stranded DNA aptamers have recently been developed with high, preferential affinity to the *DUX4* DNA-binding domain.<sup>85</sup> However, these aptamers have yet to be tested for their therapeutic potential. Developing oligonucleotides for targets other than *DUX4* may be useful as

well. For instance, *PITX1* is a direct transcriptional target of DUX4 whose overexpression induces an FSHD-like dystrophic phenotype in mice.<sup>20,86</sup> Intravenous injection of AOs against *Pitx1* in *Pitx1*-transgenic mice improved grip strength and decreased muscle pathology.<sup>87</sup> *FRG1* is another direct transcriptional target of *DUX4*, whose knockdown by RNAi reversed dystrophic histopathology and improved treadmill performance in *FRG1*-overexpressing mice.<sup>88,89</sup> It would be interesting to see if similar effects could be observed if these strategies were used to treat *DUX4*-overexpressing mouse models such as *FLExDUX4*,<sup>90</sup> the doxycycline-inducible iDUX4pA,<sup>91,92</sup> or the tamoxifen-inducible TIC-DUX4.<sup>93</sup>

### **1.2.5. Alternative genetic therapies for FSHD**

The bacterial defense system based on clustered regularly interspaced short palindromic repeats (CRISPR) has been adapted and developed to become perhaps one of the most revolutionary tools for targeted genome editing to date. In its most common configuration, CRISPR has two basic components: an endonuclease for cleaving DNA (the CRISPR-associated or Cas protein), and an RNA molecule that associates with this enzyme and tells it where in the genome to cut (the guide RNA or gRNA).<sup>94,95</sup> The gRNA is designed complementary to the target DNA site, which additionally has to have a protospacer-adjacent motif sequence nearby to facilitate Cas binding.<sup>96,97</sup> Upon binding of the gRNA-Cas complex, a double-stranded break is introduced into the target DNA. This break is subsequently resolved by non-homologous end joining (NHEJ) or homology-directed repair (HDR), which create random insertions/deletions or precise edits at the site, respectively, and form the basis of CRISPR-based genome editing.

CRISPR has been previously used to correct an FSHD2-associated *SMCHD1* mutation, a missense variant in intron 34 that introduced an out-of-frame 53-bp pseudoexon in the final

transcript.<sup>98</sup> CRISPR/Cas9 with gRNAs against the intronic sequences flanking this pseudoexon restored the *SMCHD1* reading frame and increased wild-type *SMCHD1* expression in primary and immortalized patient myotubes, resulting in reduced *DUX4* mRNA expression. It has been suggested that CRISPR be used to edit the permissive 4qA to the restrictive 4qB haplotype,<sup>27</sup> but attempts on realizing this approach have not yet been reported in the literature. In addition to genome editing, CRISPR can also be used for the targeted modulation of gene expression. Using a catalytically-deficient version of Cas9 (dCas9) fused to a KRAB transcriptional repressor, together with gRNAs against the *DUX4* promoter or exon 1, one group achieved ~45% *DUX4* knockdown in myotubes differentiated from treated primary patient myoblasts.<sup>99</sup> A trend towards increased chromatin repression of the *DUX4* gene at the contracted locus was observed. When dCas9-KRAB was used with gRNAs solely targeting *DUX4* exon 3 or various regions within/upstream of the D4Z4 repeat sequence, no significant *DUX4* knockdown was observed. The same group used dCas9-KRAB to inhibit the expression of other genes—*BRD2*, *BAZ1A*, *KDM4C*, and *SMARCA5*—which led to about 40-60% *DUX4* knockdown in primary patient myotubes.<sup>100</sup> These genes code for epigenetic regulators, and were previously identified from an RNAi screen as candidates whose knockdown lowered *DUX4* transcript levels without negatively impacting the expression of genes involved in muscle development or homeostasis. On a related note, CRISPR/Cas9 has itself been employed for a genome-wide knockout screen to search for genes whose loss-of-function was protective against *DUX4* cytotoxicity.<sup>101</sup> Hypoxia signaling pathway members were identified as the most promising candidates, in accordance with the role of oxidative stress in *DUX4*-mediated pathogenesis.<sup>7,102,103</sup>

Another interesting approach is to use other proteins to compete with *DUX4* activity. *DUX4-s* is a short isoform of *DUX4* that contains only the first 159 N-terminal amino acids of

the protein, spanning both homeodomains.<sup>104</sup> It is non-pathogenic, and its expression has been detected in both healthy and FSHD skeletal muscle.<sup>18,104,105</sup> Since DUX4-s shares the exact same homeodomains as full-length DUX4, it is thought that overexpression of the former will prevent the latter from binding its usual genomic targets. Indeed, co-injection of *DUX4-s* and full-length *DUX4* mRNA at a 20:1 ratio into fertilized zebrafish eggs decreased embryo mortality rates to ~10%, improved musculature, and led to 70% of embryos having an overall normal phenotype.<sup>106</sup> In contrast, eggs injected with only full-length *DUX4* mRNA had an embryo mortality rate of ~40%, and less than 20% of resulting embryos were phenotypically wild-type. As the physiological functions of DUX4-s are unknown, more research into this area may help further develop this approach as an FSHD therapy. The DUX4 homeodomains are also highly similar and functionally interchangeable with those of PAX7.<sup>107</sup> Overexpression of *Pax7* or its homolog *Pax3* considerably improved viability in *DUX4*-inducible C2C12 cells.<sup>57</sup> This rescue was diminished in a dose-dependent manner when *DUX4* expression was induced at higher levels, indicating that Pax7 or Pax3 may be exerting their effects via competition with the DUX4 protein. Although promising, pre-clinical testing of DUX4-s and PAX7/3 in FSHD mouse models have yet to be performed.

Developing treatments to alleviate FSHD symptoms may be beneficial as well. For instance, AAV delivery of a follistatin gene construct into TIC-DUX4 FSHD model mice (i.m.) increased mass and improved strength in injected muscles.<sup>93</sup> Follistatin is an inhibitor of myostatin, which in turn is a known inhibitor of muscle growth.<sup>108</sup> It is important to note though that follistatin did not reverse DUX4-induced histopathology in treated mice, suggesting that treatments directed at secondary pathological features of FSHD are probably not curative and may be more useful when administered in conjunction with *DUX4*-targeting genetic therapies.

## 1.3. Duchenne muscular dystrophy

### 1.3.1. Overview

DMD is a fatal X-linked recessive neuromuscular disorder characterized by progressive muscle weakening and wasting.<sup>109</sup> It affects ~1 in 3500-5000 males born worldwide.<sup>110,111</sup> The disorder progresses rapidly, with boys losing ambulation by 12 years of age or earlier; death often occurs within the twenties, usually due to respiratory or cardiac complications.<sup>112,113</sup> DMD is caused by mutations in the *DMD* gene coding for dystrophin,<sup>109,114</sup> a membrane-associated protein that links cytoskeletal actin in muscle fibers with the surrounding extracellular matrix by forming a network with sarcolemmal glycoproteins (otherwise known as the dystrophin-associated glycoprotein complex or DAGC) (**Figure 1.6a**).<sup>115-117</sup> This linkage strengthens muscle structure during stressful contraction/relaxation cycles<sup>118</sup>; recent studies, however, indicate that dystrophin also has non-mechanical roles.<sup>119</sup> Dystrophin has four domains: an N-terminal domain for actin-binding; a rod domain mainly for structural flexibility; a cysteine-rich domain for facilitating protein-protein interactions; and a C-terminal domain for binding DAGC proteins at the sarcolemma (**Figure 1.7**).<sup>117,120</sup> Dystrophin loss predisposes muscle fibers to mechanical damage, leading to muscle degeneration.

*DMD* is considered the longest gene in humans, spanning 2.4 Mb in chromosomal region Xp21 with 79 exons and producing a 14 kb transcript.<sup>121,122</sup> Due to its length, it is highly susceptible to mutations. Furthermore, certain regions of *DMD* are mutation hotspots.<sup>123,124</sup> Approximately 60% of DMD cases are due to deletions of at least one exon in *DMD*,<sup>112,120</sup> ~6% to duplications,<sup>125</sup> and the rest to small mutations. In most cases, these disrupt the *DMD* reading frame or introduce a premature stop codon, both of which cease dystrophin production.

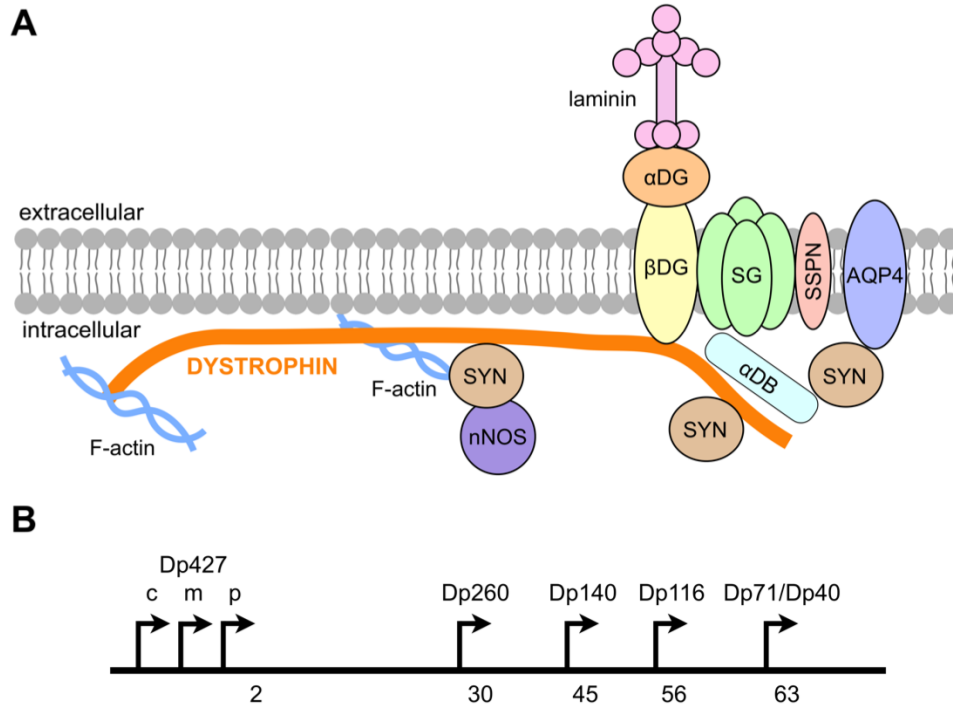


**Figure 1.6. Dystrophin-associated glycoprotein complex and dystrophin isoforms.** (A) A schematic showing the dystrophin-associated glycoprotein complex. (B) Approximate locations of dystrophin isoform promoters are shown, relative to exon numbers of the full-length Dp427m isoform. Abbreviations: SYN, syntrophin; nNOS, neuronal nitric oxide synthase;  $\beta$ -DG,  $\beta$ -dystroglycan;  $\alpha$ -DG,  $\alpha$ -dystroglycan; SG, sarcoglycan complex; SSPN, sarcospan; AQP4, aquaporin 4;  $\alpha$ -DB,  $\alpha$ -dystrobrevin.

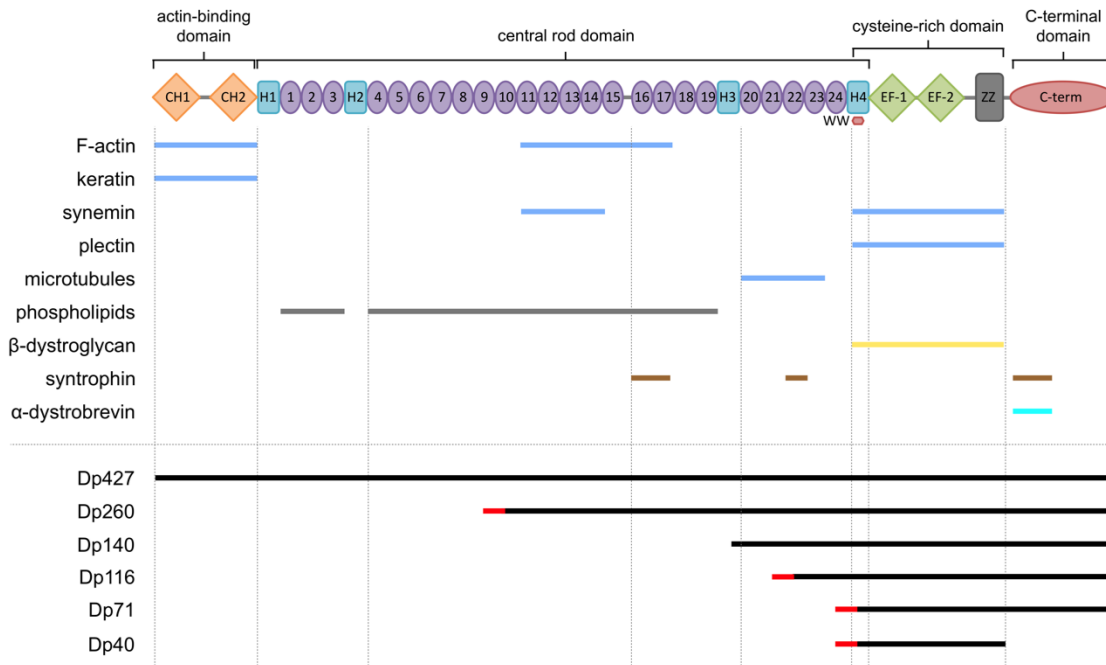


**Figure 1.7. Dystrophin protein domains.** The structure of the dystrophin protein is shown at the top, with the major domains and sub-domains labeled. The approximate binding sites for various proteins interacting with dystrophin are shown below, as well as the portions of the dystrophin protein that belong to its various isoforms (red, indicates use of an alternative N-terminus that is not in the full-length Dp427 isoform).

Dystrophin protein structure modified from: Lim, K. R. Q., Nguyen, Q. & Yokota, T. Genotype–Phenotype Correlations in Duchenne and Becker Muscular Dystrophy Patients from the Canadian Neuromuscular Disease Registry. *J. Pers. Med.* **10**, 241 (2020).

Protein-binding site information adapted from: Duan, D. *et al.* Duchenne muscular dystrophy. *Nat. Rev. Dis. Primers* **7**, 13 (2021) and the eDystrophin website, “Binding domains” tab (<http://edystrophin.genouest.org/index.php?page=knowledge&box=domain>, accessed April 29, 2021)

At present, most practices for DMD treatment are palliative at best, aimed at managing problems with ambulation, respiration, and cardiac health that are typical of DMD.<sup>112,113</sup> Of these, corticosteroid treatment was found to be the overall most effective option for patients. Improved muscular strength, prolonged ambulation, and better respiratory function were observed in patients treated with the corticosteroids prednisolone/prednisone or deflazacort in separate long-term clinical trials.<sup>126,127</sup> However, these improvements were temporary—disease progression was only delayed—and treatment was associated with a number of side effects (eg weight gain, bone fractures, cataracts).

There is thus a push towards the development of curative therapies for DMD. To date, a number of cell- and gene-based strategies have been explored, with varying degrees of success.<sup>113,120</sup> Cell-based strategies involve transplantation of healthy myoblasts into patients, and as such are handicapped by issues of immune rejection, and poor systemic delivery and viability of transplanted cells. In contrast, therapies targeting the genetic cause of DMD have shown much more progress in clinical trials. One such strategy is exon skipping, which attempts to correct defective *DMD* transcripts through the use of nucleic acid-based drugs.<sup>128,129</sup> This approach has spurred the development of numerous pharmaceuticals, including four recently approved for DMD therapy by the U.S. Food and Drug Administration (FDA). These are eteplirsen (Sarepta), golodirsen (Sarepta), viltolarsen (NS Pharma), and casimersen (Sarepta), which together could treat roughly 30%<sup>130</sup> of all DMD patients.

### **1.3.2. Dystrophin protein: structure and function**

In its full-length form, dystrophin is a 427-kDa protein that consists of four major domains: an N-terminal actin-binding domain, a central rod domain, a cysteine-rich domain, and

a C-terminal domain (**Figures 1.6a, 1.7**).<sup>117,131</sup> The N-terminal domain contains two calponin homology domains that enable binding to F-actin and the intermediate filament cyokeratin 19.<sup>132-134</sup> These help establish connections between dystrophin, the cytoskeleton, and the contractile apparatus in muscle cells. The central rod domain serves as a flexible bridge between the N- and C-terminal domains, fulfilling the function of dystrophin in linking the intracellular cytoskeleton to the extracellular matrix.<sup>135</sup> It consists of 24 spectrin-like repeats, each having a triple-helix structure. These repeats are divided across the domain by 4 hinges. Similar to the N-terminus, the rod domain possesses an actin-binding domain.<sup>136</sup> Aside from F-actin, the central rod binds other cytoskeletal proteins such as synemin<sup>137</sup> and microtubules<sup>138</sup>—these associations serve not only to strengthen the intracellular connections of dystrophin but also to help with cytoskeletal organization.<sup>131</sup> The central rod can additionally bind phospholipids along its structure, which help localize dystrophin to the membrane.<sup>139-141</sup> Previously, the central rod domain was also thought to contain a binding site at repeats 16-17 for neuronal nitric oxide synthase (nNOS), an enzyme that participates in regulating muscle contraction and metabolism.<sup>142</sup> More recent work has revealed that this is not the case. Rather,  $\alpha$ 1-syntrophin instead bound to repeats 16-17, which then recruited nNOS to the membrane.<sup>143</sup> The same group further discovered a binding site for  $\beta$ 1- and  $\beta$ 2-syntrophin on repeat 22. Studies of patient mutations have shown that parts of the central rod domain may be dispensable for overall dystrophin function, and have informed the design of exon skipping therapies as well as of abbreviated versions of dystrophin (i.e., micro-dystrophins) for gene therapy.

The cysteine-rich domain is composed of subdomains that facilitate protein-binding: WW, two EF-hands, and ZZ.<sup>144,145</sup> Through these sites, the cysteine-rich domain is bound by cytoskeletal proteins (synemin, plectin),<sup>137,146</sup> ankyrin (localizes dystrophin to the membrane),<sup>147</sup>

and the transmembrane  $\beta$ -dystroglycan protein.<sup>144,148,149</sup>  $\beta$ -dystroglycan in particular is primarily responsible for connecting the DAGC to the extracellular matrix, via  $\alpha$ -dystroglycan and laminin (**Figure 1.6a**).<sup>117,131</sup>  $\beta$ -dystroglycan also mediates connections with the various sarcoglycans ( $\alpha$ ,  $\beta$ ,  $\gamma$ ,  $\delta$ ) that, in turn, associate with sarcospan—all together, these lend structural integrity to the DAGC.<sup>117,131</sup> Moreover, the EF-hand and ZZ domain structures can potentially be altered by  $\text{Ca}^{2+}$  and  $\text{Zn}^{2+}$  ions, respectively, indicating possible routes of regulation.<sup>145,150</sup> Finally, the C-terminal domain has coiled-coil motifs that allow binding to the intracellular syntrophins ( $\alpha 1$ ,  $\beta 1$ ,  $\beta 2$ ) and  $\alpha$ -dystrobrevin.<sup>151,152</sup> The  $\alpha 1$ -syntrophin that binds to the C-terminus is not responsible for nNOS recruitment.<sup>143</sup> However, it is involved in recruiting aquaporin 4, ion channels, and other transporters to the proximity of the DAGC.<sup>153,154</sup> On the other hand, since the C-terminus of  $\alpha$ -dystrobrevin contains coiled-coil motifs homologous to those in the C-terminus of dystrophin, it follows that  $\alpha$ -dystrobrevin is also capable of binding syntrophins.<sup>151,152</sup>  $\alpha$ -dystrobrevin also binds to the sarcoglycans in the sarcolemma,<sup>155</sup> further adding to the compactness of the DAGC.

By facilitating interactions with the proteins above, dystrophin serves as the foundation for the DAGC. In doing so, not only does dystrophin maintain the structural integrity of the sarcolemma, but it also allows for the formation of a signaling complex at the membrane. Dystrophin, dystroglycans, sarcoglycans, sarcospan, syntrophins and dystrobrevin are all known to bind a number of signaling proteins.<sup>153</sup> Thus, dystrophin and the DAGC have a host of non-mechanical roles, which include regulating recovery from muscle fatigue, cachexia, ion homeostasis, vasodilation/vasoconstriction, neuromuscular junction formation, and even cognitive function.<sup>119,153,156</sup>

At this point, it is important to mention that many isoforms of dystrophin exist. The description provided here mostly applies to the full-length, muscle-specific isoform. There are eight main isoforms identified, transcribed from alternative promoters across the *DMD* gene: Dp427c, Dp427m, Dp427p, Dp260, Dp140, Dp116, Dp71, and Dp40 (**Figure 1.6b**). They are named according to the molecular weight (in kDa) of the dystrophin protein they produce and vary in length as well as tissue expression (**Figure 1.7**). Dp427c, Dp427m, and Dp427p have all the domains of full-length dystrophin and differ only at the first few amino acids of the N-terminus (owing to usage of alternative first exons). These are distinguished by where they are predominantly expressed—Dp427c in cortical neurons,<sup>157</sup> Dp427m in the muscle, and Dp427p in cerebellar Purkinje cells.<sup>158</sup> Dp260, Dp140, and Dp116 contain varying lengths of the distal rod domain as well as the full cysteine-rich and C-terminal domains. They are primarily expressed in the retina,<sup>159</sup> central nervous system/kidney,<sup>160</sup> and Schwann cells in peripheral nerves,<sup>161</sup> respectively. Dp71 and Dp40 share the same promoter, but whereas Dp71 has both the cysteine-rich and C-terminal domains of full-length dystrophin, Dp40 only has the cysteine-rich domain. This is because Dp40 uses an alternative 3'-UTR site.<sup>162,163</sup> Both Dp71 and Dp40 are ubiquitously expressed dystrophin isoforms.<sup>162,164</sup> The functions of all these other isoforms have not yet been fully elucidated, and are an area of active investigation.

### **1.3.3. Exon skipping development for DMD**

Not all *DMD* deletions result in out-of-frame mutations; some lead to in-frame mutations, generating variants able to produce functional albeit truncated versions of dystrophin. This kind of deletion occurs in patients with BMD, a milder dystrophinopathy compared to DMD.<sup>165</sup> The genetic difference between DMD and BMD presents an important observation: the nature of the deletion determines the severity of the disorder. This led to the realization that making a deletion

less harmful by turning an out-of-frame to an in-frame mutation should alter the DMD phenotype to that of the less severe BMD. Based on patient databases, this approach should be applicable to 90% of *DMD* mutations.<sup>166–168</sup>

It is with this underlying principle that exon skipping was developed as a therapeutic strategy for DMD. In this approach, the translational reading frame of a gene is restored using AOs to interfere with pre-mRNA splicing (**Figure 1.8**).<sup>128,169</sup> AOs are employed to bind target complementary sequences in the pre-mRNA, which influence the splicing machinery to exclude an exon (or exons) from the final transcript. The potential of exon skipping as a therapy for DMD was further strengthened by observations that DMD patients and animal models can have dystrophin-positive muscle fibers despite having a loss-of-function *DMD* mutation.<sup>170,171</sup> These fibers, called revertant fibers, were surprisingly found to have in-frame *DMD* transcripts that were thought to arise as a result of spontaneous exon skipping events;<sup>172,173</sup> their occurrence is linked with age, *DMD* mutation type, and genetic background.<sup>174,175</sup> These instances show that it is possible to generate dystrophin from *DMD* transcripts that have undergone exon skipping.

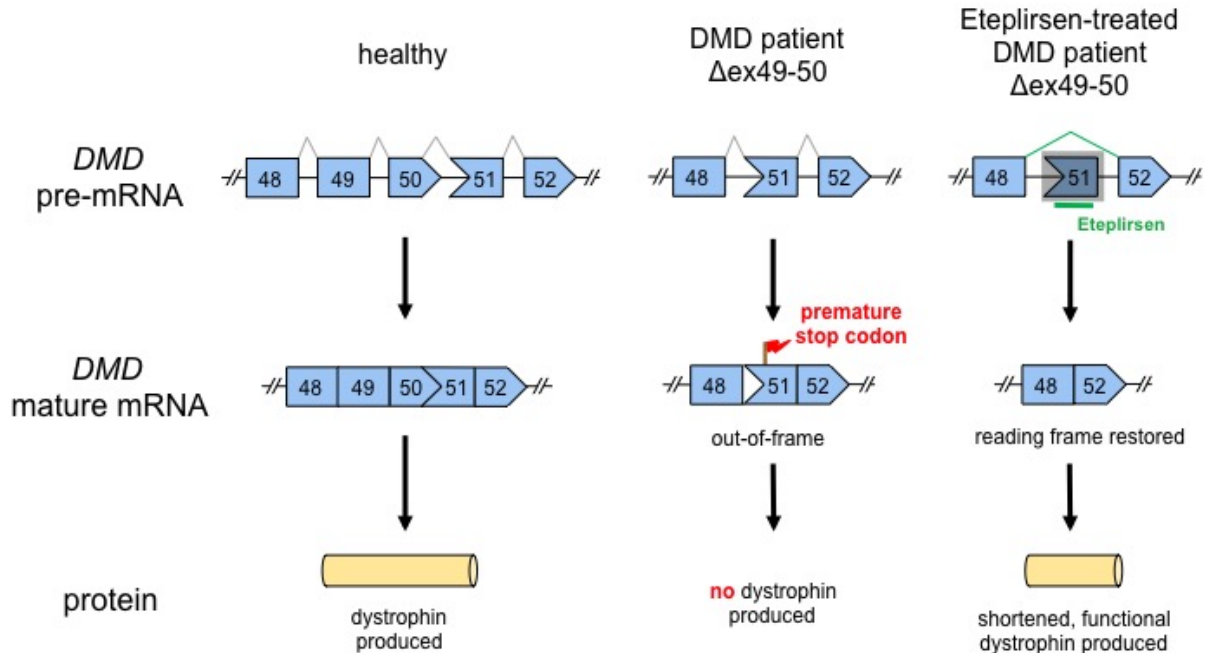


**Figure 1.8. Eteplirsen is an exon skipping therapeutic.** Eteplirsen (green bar) specifically recognizes exon 51 of the *DMD* gene. Upon binding, it influences the splicing machinery to skip exon 51 from the mature mRNA transcript. This restores the reading frame of *DMD*, allowing for successful translation of a shortened but functional dystrophin protein. Shown above is a case where eteplirsen is used to treat a DMD patient with a deletion spanning exons 49 and 50—this creates an out-of-frame frameshift that introduces a premature stop codon and results in non-production of dystrophin.

Figure from: Lim, K. R. Q., Maruyama, R. & Yokota, T. Eteplirsen in the treatment of Duchenne muscular dystrophy. *Drug Des. Devel. Ther.* **11**, 533-545 (2017).

Two early independent studies showed that exon skipping was feasible in *mdx* mouse muscle cells *in vitro*. The *mdx* mouse is a widely used animal model for DMD. It harbors a spontaneous nonsense mutation in exon 23 of the *Dmd* gene, which renders the mouse incapable of producing dystrophin.<sup>176</sup> Exon 23 skipping is sufficient to restore the *Dmd* reading frame. In the first of these studies, by Dunckley et al. (1998), transfection of a 2'-OMePS AO (**Figure 1.4**) against the intron 22 3' splice site interestingly led to the in-frame skipping of multiple exons from exon 23 to 29.<sup>177</sup> On the other hand, Wilton et al. (1999) found that a 2'-OMePS AO against the intron 23 5' splice site produced an in-frame exon 23-skipped transcript in a dose-dependent manner.<sup>178</sup> Both studies confirmed that exon skipping was sequence-specific. Besides broadening the applicability of exon skipping, these studies showed that one could also target splice sites to induce exon skipping, not just exonic splicing enhancers.

*DMD* exon skipping was then shown for the first time to restore dystrophin protein levels in primary DMD patient-derived muscle cells with an exon 45 deletion by van Deutekom et al. (2001). Treatment of patient-derived myotubes with various 2'-OMePS AOs complementary to the exon 46 exonic splicing enhancer resulted in the skipping of this exon.<sup>179</sup> Dystrophin production and correct localization in cells were confirmed by immunostaining. Shortly after the release of this study, Takeshima et al. (2001) published an essentially similar paper, showing that exon skipping was possible in exon 19-deleted patient cells.<sup>180</sup> Successful *DMD* exon skipping was subsequently demonstrated in numerous patient cells of different mutation backgrounds.<sup>181–</sup><sup>185</sup> Notably in two of these, by Aartsma-Rus et al. in 2004 and 2007, it was shown that multi-exon skipping was possible<sup>182</sup> and that exon skipping can treat duplications,<sup>185</sup> respectively, further increasing the applicability of the approach to more DMD mutation types.

At around the same time as exon skipping was first being applied to patient cells, studies on exon skipping *in vivo* were being done. The first report of this was by Mann et al. (2001) in *mdx* mice. Intramuscular injections of a 2'-OMePS AO targeting the intron 23 5' splice site, in complex with cationic lipids, led to dystrophin rescue as observed by immunostaining and Western blotting.<sup>186</sup> Additionally, the localization of  $\gamma$ -sarcoglycan, a dystrophin-associated protein, was restored in muscle cell membranes after treatment. A similar study by Lu et al. (2003), using a more optimized version of the AO and administering it with F127 block copolymer to enhance delivery, even showed that treated *mdx* mice can exhibit some physiological improvement post-treatment.<sup>187</sup>

The same group also reported the first use of the PMO chemistry for *in vivo* exon skipping of *Dmd*. PMOs are highly stable, nuclease-resistant, exhibit minimal off-target effects, bind their targets with high affinity and do not activate RNase H (**Figure 1.4**).<sup>188,189</sup> They are also charge-neutral, which makes them less susceptible to activating immune responses but also renders them difficult to deliver into cells.<sup>169,190</sup> In their 2003 study, Gebiski et al. showed that leashed PMOs (PMOs annealed to complementary anionic oligonucleotides to improve delivery) administered intramuscularly against the intron 23 5' splice site effectively induced exon 23 skipping and restored dystrophin production in *mdx* mice.<sup>191</sup> They even observed the skipped transcript two weeks post-injection, an effect they did not observe with 2'-OMePS AOs.

Other studies on the efficacy of locally administered exon skipping AOs were soon reported.<sup>192,193</sup> However, as DMD affects body-wide muscles, the feasibility of administering AOs systemically would have to be determined before testing in patients. Lu et al. (2005) reported that intravenous injections of their donor splice site 2'-OMePS AO in complex with F127 variably restored dystrophin expression in a wide range of skeletal muscles in *mdx* mice.<sup>194</sup>

Three intravenous injections of the AO rescued 1-5% of normal dystrophin levels and restored proper localization of dystrophin-associated proteins to the muscle membrane without any safety concerns. Treatment was not beneficial for cardiac muscles, however, which did not differ from the non-treated controls. Better results were obtained by Alter et al. (2006) when exon 23-skipping morpholino AOs were intravenously administered seven times weekly in *mdx* mice, with at least 50% of normal dystrophin levels observed.<sup>195</sup> Cardiac muscle remained unresponsive to treatment, which is unfortunate since cardiomyopathy is a leading cause of death among DMD patients.<sup>112</sup>

*In vivo* studies were eventually conducted in dog models of DMD. Such models were deemed more useful for translational research because these had phenotypes that better resembled those found in DMD patients.<sup>196</sup> The first such study was by Yokota et al. in 2009, where they used the canine X-linked muscular dystrophy in Japan (CXMD<sub>J</sub>) model. CXMD<sub>J</sub> dogs have an acceptor splice site point mutation in intron 6, which leads to the out-of-frame skipping of exon 7.<sup>197</sup> In the study, CXMD<sub>J</sub> dogs were either intramuscularly or intravenously treated with a 3-PMO cocktail that induces the in-frame skipping of exons 6 to 8.<sup>198</sup> Intramuscularly treated muscles showed 61-83% exon skipping efficiency two weeks post-injection, which led to around 25-50% dystrophin protein restoration. Different regimens of systemic treatment resulted in variable levels of dystrophin restoration across muscles, with as much as 50% of normal levels observed in one dog; cardiac muscle showed minimal response to treatment. Functional improvements of treated dogs compared to non-treated controls in terms of clinical grading scores and performance in the 15-m run test were also observed. Treatment showed no signs of toxicity. Yokota et al. also tried using 2'-OMePS AOs, but found PMOs to be more effective. While *in vitro* studies showing the feasibility of exon skipping in DMD dog

muscle cells were reported as early as 2006,<sup>199</sup> this was its first demonstration in dogs *in vivo*. Furthermore, this was also the first demonstration of multi-exon skipping in an *in vivo* model.

#### **1.3.4. Exon skipping in humans**

The first demonstration of exon skipping in a patient was in 2006 by Takeshima et al. In the study, they administered 0.5 mg/kg of a PS DNA AO as an intravenous infusion (four times weekly) to a 10 year-old patient with an out-of-frame *DMD* exon 20 deletion.<sup>200</sup> They used an AO complementary to the ESE in exon 19 to skip it, which would result in an in-frame transcript. Approximately 6% skipping was observed in a biceps sample from the patient a week after the last infusion. Weak dystrophin expression, as well as the re-localization of dystrophin-associated proteins at the membrane, was identified by immunostaining. Treatment was considered safe, with no adverse effects.

Two years later in 2008, results from a proof-of-concept clinical trial by a group affiliated with Prosensa (now BioMarin) would be reported in which *DMD* patients with amenable mutations were treated with an exon 51-skipping drug.<sup>201</sup> The drug, a 2'-OMePS AO called PRO051 or more commonly known as drisapersen, was administered intramuscularly into the tibialis anterior muscle to four *DMD* patients at a 0.8 mg dose; biopsies were obtained a month later. No serious treatment-related adverse effects were found. Exon 51 skipping was observed in all patients (levels not quantified), with no evidence of aberrant splicing due to treatment. Dystrophin rescue was strikingly good as determined by immunostaining. Western blot quantification revealed that ~3-12% of normal dystrophin levels were found across patients. While it seemed promising in the initial study, drisapersen was rejected by the FDA in the first part of 2016 due to reasons concerning safety and lack of convincing evidence on efficacy.<sup>202</sup>

Clinical trials for other exon skipping drugs for DMD treatment would soon undergo development. In September 2016, the exon 51-skipping PMO eteplirsen (brand name, Exondys 51) received conditional accelerated approval from the FDA, making it the first FDA-approved drug for DMD patients.<sup>203,204</sup> Despite being well-tolerated, the claimed efficacy of eteplirsen is under controversy, especially since it only led up to ~0.93% dystrophin rescue after 180 weeks of intravenous treatment with 30 or 50 mg/kg/week doses in a clinical trial.<sup>202,203,205</sup> Furthermore, eteplirsen was observed to only at most delay disease progression in terms of ambulatory ability as measured by the 6-minute walk test (6MWT).<sup>206</sup> In fact, 3 years into a clinical trial, 2 out of 12 patients lost ambulation. Although it was argued that this was a considerable improvement compared to historical controls (where 6 out of 13 patients lost ambulation in the same period of time), the action of eteplirsen still cannot be deemed sufficient to satisfy the clinical endpoint of the trial, as also concluded by the FDA.<sup>205</sup> As such, the FDA is requiring additional evidence of clinical utility in a phase III trial before eteplirsen can be granted full approval.

The accelerated, conditional approval by the FDA of three exon skipping PMOs for DMD would soon follow: golodirsen (brand name, Vyondys 53) in 2019, viltolarsen (brand name, Viltepso) in 2020, and casimersen (brand name, Amondys 45) in 2021. All are administered as intravenous infusions. Golodirsen skips *DMD* exon 53, and significantly increased dystrophin levels in patients to 1.019% of healthy levels from 0.095% at baseline after 48 weeks of treatment in a phase I/II trial.<sup>207</sup> In this trial, patients initially received varying weekly doses of golodirsen (4 to 30 mg/kg/week) for 12 weeks, after which all patients were given 30 mg/kg/week of golodirsen. Functional improvement with golodirsen treatment has not been demonstrated. Viltolarsen also skips *DMD* exon 53, and appears to be more efficacious. In a phase I/II trial in Japan, dystrophin protein reached an average 1.92% and 5.21% of normal

levels after treatment with 40 and 80 mg/kg/week of viltolarsen for 24 weeks, respectively.<sup>208</sup> Baseline dystrophin levels were at 1.13% and 0.41% of normal, respectively. Viltolarsen was similarly tested in a phase II North American trial, where it restored an average 5.7% and 5.9% dystrophin of normal levels from baseline (0.3% and 0.6%) after treatment at 40 and 80 mg/kg/week doses for 24 weeks.<sup>209</sup> Encouragingly, combined timed function test results from both treatment groups revealed significant improvement at the 13- and 25-week time-points. On the other hand, casimersen skips *DMD* exon 45. Results from an ongoing phase III trial where patients have been treated with 30 mg/kg/week of casimersen for 48 weeks revealed an average 1.736% dystrophin of normal levels compared to 0.925% at baseline.<sup>210</sup> Functional improvement has not been demonstrated.

Each of these exon skipping PMOs can treat 8-13% of DMD patients.<sup>130</sup> Overall, the efficacy of exon skipping PMOs in patients can certainly be improved. Observations from BMD patients show that at least 10% dystrophin of normal levels are predicted to lead to clinical benefit.<sup>211</sup> Studies from mouse models indicate that even as low as 3% dystrophin of normal levels may be beneficial.<sup>212</sup> However, three of these approved exon skipping PMOs have only been able to restore <2% dystrophin of normal levels after extended treatment. Functional benefit has also not been convincingly demonstrated by these therapies at present, with some not having any results from muscle performance tests. Results from ongoing trials should help shed light on the future of these PMOs as effective therapies for DMD.

### **1.3.5. Alternative genetic therapies for DMD**

Besides exon skipping, the suppression of nonsense point mutations is another post-transcriptional genetic therapy that has been developed for DMD. The approach uses small

molecule compounds to promote readthrough of premature termination codons, allowing for dystrophin translation.<sup>213</sup> Perhaps the most successful in this class of therapies is ataluren (brand name, Translarna; PTC Therapeutics). Ataluren, or (3-(5-(2-fluorophenyl)-1,2,4-oxadiazol-3-yl)-benzoic acid, was conditionally approved for DMD therapy by the European Medicines Agency in 2014. A phase IIa trial showed that treatment with daily total doses of 16, 40, and 80 mg/kg ataluren for nearly a month restored dystrophin production to 12.3%, 8.4%, and 14.7% of normal levels on average, respectively.<sup>214</sup> Succeeding phase IIb and phase III trials evaluated the effects of daily 40 mg/kg ataluren on patient muscle function.<sup>215,216</sup> Unfortunately, these studies generally found non-significant improvement in the 6MWT compared to placebo at 48 weeks. Dystrophin restoration levels were not evaluated in these latter two trials, but their measurement may help contextualize the observed results. Gentamicin, an aminoglycoside antibiotic, has also been tested as a nonsense suppression therapy for DMD but studies have been largely discontinued owing to its toxicity.<sup>213</sup> Other small molecules are constantly being considered for nonsense suppression in DMD, as identified by various high throughput screens.<sup>217</sup>

CRISPR strategies have also been developed to correct *DMD* mutations at the DNA level. In the context of DMD, CRISPR can conventionally be used in three different strategies. Firstly, if a single gRNA is used to target cleavage at or near a premature stop codon in a mutant or frameshifted *DMD* exon, indel formation by NHEJ can eliminate the stop codon and/or restore the reading frame back to the normal configuration (NHEJ reframing). Secondly, if a single gRNA is used to target cleavage at or near splicing sequences in *DMD* exons or introns, indels can disrupt these sites and allow for skipping of an out-of-frame exon to occur (classical exon skipping). And finally, if at least two gRNAs are used to target cleavage in separate exons or

introns, deletions of one or more exons can be achieved to restore the *DMD* reading frame (direct exon skipping).

Aside from these strategies, CRISPR has also been used for editing single bases to correct *DMD* point mutations as well as for upregulating the expression of utrophin. Utrophin is a homolog of dystrophin that is expressed in the myotendinous and neuromuscular junctions (NMJ) of adult skeletal muscles.<sup>218,219</sup> During fetal development, utrophin is localized at the sarcolemma of muscle cells, where it functions similarly as dystrophin in stabilizing the membrane.<sup>220</sup> It is eventually replaced later in development by dystrophin, at which point utrophin can no longer be found at the sarcolemma except at the neuromuscular junction. Because of its structural and functional similarity to dystrophin, various groups are attempting to upregulate or reactivate its expression in dystrophic muscle cells with the expectation that it can act as a dystrophin substitute.<sup>221</sup>

We have previously written comprehensive reviews on the pre-clinical work evaluating the potential of CRISPR for DMD therapy, and direct interested readers there for further information.<sup>222,223</sup> Generally speaking, CRISPR has been quite successful in restoring dystrophin production *in vivo*, in both the skeletal muscles and the heart. Muscle and cardiac function appear to be improved by CRISPR therapy, but more studies are needed to cement this finding. The safety concerns associated with CRISPR also have to be addressed moving forward, e.g. off-target effects and Cas9 immunogenicity.

The use of abbreviated dystrophin constructs called micro-dystrophins has also been investigated for DMD gene therapy, overcoming previous limitations in packaging the full-length *DMD* cDNA for viral delivery.<sup>224,225</sup> Treatment with micro-dystrophins is not mutation-specific, and would in theory be applicable to all DMD patients unlike exon skipping, nonsense

suppression, and CRISPR therapies. Micro-dystrophin structures are largely informed by genotype-phenotype correlation studies in patients, and have been further refined through a wealth of pre-clinical experience. Numerous animal studies have demonstrated that treatment with AAV-packaged micro-dystrophins could ameliorate dystrophic pathology and improve muscle/heart function.<sup>224,225</sup> Based on these promising results, four micro-dystrophins have now reached human clinical trials: SGT-001 (Solid Biosciences), PF-06939926 (Pfizer), SRP-9001 (Sarepta), and GNT 0004 (Genethon, Sarepta). All these lack the dystrophin C-terminal domain, and contain varying components of the rod domain. SGT-001 is in a phase I/II trial with two single-dose treatment cohorts, each with three patients. The trial is ongoing, but interim results at 90 days post-administration of  $2 \times 10^{14}$  vg/kg SGT-001 showed about 5%, 8%, and 17.5% micro-dystrophin levels of normal dystrophin in three patients.<sup>226</sup> PF-06939926 has recently started a phase III trial in late 2020, following successful results from their phase Ib trial.<sup>227</sup> The phase Ib trial showed that single-dose treatment with  $1 \times 10^{14}$  vg/kg and  $3 \times 10^{14}$  vg/kg PF-06939926 led to average micro-dystrophin levels of 24% and 51.6% of normal dystrophin 12 months later.<sup>228</sup> Significant improvement in North Star Ambulatory Assessment (NSAA) scores was found in the combined low- and high-dose patient group. Results from the phase II trial of SRP-9001 revealed that it met its primary biological endpoint (micro-dystrophin expression) but not its primary functional endpoint (NSAA score improvement) after 48 weeks of treatment; further study is ongoing.<sup>229</sup> Dosing for the phase I/II/III trial of GNT 0004 has recently commenced, in April 2021.<sup>230</sup>

As in FSHD, there are also genetic therapies that focus more on ameliorating the symptoms associated with DMD. These include micro-utrophin delivery,<sup>231,232</sup> *GALGT2* delivery for utrophin upregulation,<sup>233</sup> follistatin delivery for improved muscle growth,<sup>234</sup> and *SERCA2a*

delivery for restoring calcium homeostasis,<sup>235</sup> among others. However, these are also probably not curative and will serve more to enhance the efficacy of genetic therapies for DMD.

#### 1.4. Study Objectives

The general objectives of this thesis are to develop novel, effective antisense therapies for FSHD and DMD. In **Chapters 2 and 3**, we describe the development of *DUX4*-targeting LNA and 2'-MOE gapmers as potential therapies for FSHD. Antisense therapies for FSHD have so far only used steric blocking AOs, which do not directly degrade target *DUX4* transcripts. Gapmer AOs on the other hand induce target mRNA degradation through the recruitment of RNase H. Based on this mechanism of action, we hypothesized that gapmers would lead to more potent *DUX4* knockdown *in vitro* and *in vivo*. We investigate the efficacy of such *DUX4*-targeting gapmers in immortalized FSHD patient-derived muscle cells and in an FSHD mouse model.

**Chapters 4 and 5** are concerned with developing and improving exon skipping approaches for DMD therapy. In **Chapter 4**, we evaluate outcomes from treating dystrophic dog neonates with a multi-exon skipping PMO cocktail that targets *dystrophin* exons 6-8. The canine model we used has a point mutation in *dystrophin* intron 6, which leads to the out-of-frame skipping of exon 7. Exons 6-8 skipping corrects the reading frame in this model, thereby restoring dystrophin production. DMD is a progressive, childhood-onset disorder—while there is strong rationale for early treatment with exon skipping therapies, the exact benefits of this are largely unknown. This study was done to investigate the advantages of early systemic exon skipping therapy, using a large animal model of DMD.

Finally, in **Chapter 5**, we outline the development of a minimized, peptide-conjugated exons 45-55 skipping PMO cocktail for DMD treatment. The FDA-approved exon skipping

therapies for DMD all target single exons. Thus, each of them could treat only a highly specific subset of mutations; the exon 51-skipping eteplirsen is applicable to the most number of patients, at ~13% of the DMD population. Skipping multiple exons could increase applicability to more mutations. Exons 45-55 skipping in particular could treat all patients amenable to treatment by the four approved exon skipping PMOs and more, covering nearly half of all patients. In this study, we generate a PMO cocktail capable of skipping *DMD* exons 45-55 by targeting as few as 5 exons in immortalized patient-derived cells and a humanized mouse model of DMD. Since PMOs exhibit limited efficacy *in vivo*, we also tested if conjugating PMOs to the novel cell-penetrating peptide DG9 could improve skipping activity in skeletal and cardiac muscles. We investigate the efficacy of these DG9-PMOs in both single-exon skipping (exon 51) and multi-exon skipping (exons 45-55) formats, using humanized dystrophic mice.

## **Chapter 2 Inhibition of *DUX4* expression with antisense LNA gapmers as a therapy for facioscapulohumeral muscular dystrophy**

Chapter 2 was derived from the following published article:

Lim, K.R.Q., Maruyama, R., Echigoya, Y., Nguyen, Q., Zhang, A., Khawaja, H., Sen Chandra, S., Jones, T., Jones, P., Chen, Y. & Yokota, T. Inhibition of *DUX4* expression with antisense LNA gapmers as a therapy for facioscapulohumeral muscular dystrophy. *Proc. Natl. Acad. Sci.* **117**, 16509-16515 (2020).

## 2.1. Abstract

Facioscapulohumeral muscular dystrophy (FSHD), characterized by progressive muscle weakness and deterioration, is genetically linked to aberrant expression of *DUX4* in muscle. *DUX4*, in its full-length form, is cytotoxic in non-germline tissues. Here, we designed locked nucleic acid (LNA) gapmer antisense oligonucleotides (AOs) to knock down *DUX4* in immortalized FSHD myoblasts and the *FLEXDUX4* FSHD mouse model. Using a screening method capable of reliably evaluating the knockdown efficiency of LNA gapmers against endogenous *DUX4* mRNA *in vitro*, we demonstrate that several designed LNA gapmers selectively and effectively reduced *DUX4* expression with nearly complete knockdown. We also found, for the first time, potential functional benefits of AOs on muscle fusion and structure *in vitro*. Finally, we show that one of the LNA gapmers was taken up and induced effective silencing of *DUX4* upon local treatment *in vivo*. The LNA gapmers developed here will help facilitate the development of FSHD therapies.

## 2.2. Introduction

FSHD is an autosomal dominant disorder characterized by progressive, asymmetric muscle weakness beginning at the face, shoulders, and upper limbs, which spreads to the lower regions of the body with age.<sup>5</sup> It is the third most common muscular dystrophy, with ~1:8000-1:22000 people affected worldwide.<sup>5</sup> Age of onset is variable, ranging from birth to adulthood. Patients with the rare infantile form of FSHD, presenting symptoms before 5 years of age, follow a more severe and rapid course of the disease.<sup>14</sup> At present, FSHD is incurable.

The majority of FSHD patients (~95%, FSHD1) have a contraction of the D4Z4 repeat array in chromosome 4q35, which is typically 11-100 D4Z4 units long in healthy individuals.<sup>5,236</sup>

FSHD1 was thought to be caused by having 10 or fewer D4Z4 repeats in the array, however, recent evidence indicates that factors other than contraction size determine whether one will manifest the disorder. For instance, individuals with 7-10 D4Z4 units exhibit wide clinical variability, with some remaining asymptomatic.<sup>38</sup> In this case, factors influencing D4Z4 array methylation play a larger role in disease penetrance. This is unlike in those having <7 D4Z4 units, for whom the degree of contraction primarily determines array de-methylation and disease severity.<sup>38</sup> Each D4Z4 repeat contains the first two exons of the double homeobox protein 4 (*DUX4*) gene, with its third (and final) exon located immediately downstream of the array.<sup>28,29,75</sup> There are several *DUX4* isoforms;<sup>18</sup> we refer to the full-length pathogenic one here unless otherwise stated. The D4Z4 array is normally hypermethylated in the course of development. Studies show that the contraction relaxes the chromatin and de-methylates DNA in this region, resulting in aberrant *DUX4* expression in skeletal muscle.<sup>37</sup> In other patients (~5%, FSHD2), the D4Z4 array is shorter in comparison to the average array size in the general population, with an average of 12-16 D4Z4 units observed.<sup>32,43</sup> The more important determinant in FSHD2 however is the presence of mutations in the genes of epigenetic regulators that similarly lead to D4Z4 array de-methylation.<sup>5,37</sup> In both cases FSHD only develops when chromosome 4 is of certain permissive A haplotypes, in which exon 3 has a polyadenylation signal (PAS) required for *DUX4* mRNA stability.<sup>29</sup>

The aberrant expression of *DUX4* in skeletal muscle is thought to cause FSHD, and thus serves as an attractive therapeutic target. *DUX4* encodes a transcription factor that activates pathways involved in muscle degeneration and apoptosis, events observed in patient muscles.<sup>51,63</sup> *DUX4* also inhibits myogenic differentiation and increases the sensitivity of muscle cells to oxidative stress.<sup>57,237</sup> Several studies have demonstrated the feasibility of using AOs to reduce

*DUX4* expression. Phosphorodiamidate morpholino oligomer (PMO) AOs against the PAS, interfering with its recognition, knocked down the expression of *DUX4* and its downstream targets in immortalized and primary FSHD muscle cells.<sup>78,79</sup> Approximately 25-50% *DUX4* knockdown was observed by RT-PCR in one study, where 50 nM of each of these PMOs were transfected.<sup>78</sup> Electroporation of one PAS-targeting PMO into mice with FSHD patient biopsy xenografts led to ~100% *DUX4* knockdown and a reduction in downstream gene expression in the transplanted muscle.<sup>79</sup>

Another strategy uses AOs to disrupt proper *DUX4* mRNA splicing. Phosphorothioated 2'-*O*-methyl RNA AOs against splice sites in *DUX4* exons 2 and 3 reduced *DUX4* expression by ~30-50% and significantly prevented atrophy in primary FSHD myotubes.<sup>63,75</sup> The *in vivo* efficacy of an exon 3 splice site-targeting vivo-PMO was also tested in mice with recombinant adeno-associated virus (AAV)-mediated *DUX4* expression. Intramuscular (i.m.) injection of the AO into the tibialis anterior (TA) reduced *DUX4* expression by ~30-fold compared to control AO-injected mice.<sup>75</sup>

While the above studies are promising, there remains a need to more effectively knock down *DUX4* expression and screen for AOs against *DUX4*. AO chemistries are available that directly degrade target mRNA, and not passively act via mRNA processing interference. One example would be LNA gapmers, which consist of a central segment of DNA flanked by short LNA stretches. LNA gapmers bind targets by sequence complementarity, producing a DNA/RNA hybrid that is cleaved by RNase H, leading to gene knockdown.<sup>169</sup> Having enhanced stability, specificity, and potency at low doses, LNA gapmers are expected to more effectively reduce *DUX4* expression than previously used chemistries.

In this work, we sought to develop LNA gapmer AOs for the treatment of FSHD. We designed LNA gapmers targeting the *DUX4* transcript and screened them for efficacy using immortalized FSHD patient-derived muscle cells. We use a method capable of reliably detecting changes in endogenous *DUX4* expression post-treatment that should be useful for future AO and drug screening efforts, given that endogenous *DUX4* detection *in vitro* has proven difficult due to its low expression.<sup>50</sup> We then proceeded to determine the *in vivo* uptake and efficacy of a selected LNA gapmer from this screen using the recently developed *FLExDUX4* FSHD mouse model.<sup>90</sup> Ours is the first study reporting the use of this model for *DUX4* AO testing. *FLExDUX4* mice naturally express low amounts of *DUX4* without suffering from severe disease phenotypes. This makes them a useful model for *in vivo* screening, especially since they develop no embryonic lethality despite the toxicity of *DUX4*, an issue that has immensely hampered the use of FSHD animal models in the past.<sup>238</sup>

## 2.3. Results

### 2.3.1. LNA gapmers effectively knock down *DUX4* expression *in vitro*

To induce *DUX4* mRNA expression to detectable levels *in vitro* in immortalized patient-derived muscle fibers, KOSR-supplemented medium was used for differentiation.<sup>239</sup> *DUX4* expression significantly increased with differentiation (**Figure 2.1**). At 13 days post-differentiation, *DUX4* expression was on average ~20 times greater than at 4 days post-differentiation. Since no further increase in *DUX4* expression was detected past this 13-day mark, we screened our LNA gapmers (**Table 2.1, Figure 2.2a**) by transfecting them at 100 nM into myotubes during this time (**Figure 2.2b**). We chose to mainly target *DUX4* exon 3, which is specifically associated with the pathogenic *DUX4* transcript. We also avoided the PAS, given its

similarity to other such sequences in the genome. All gapmers significantly reduced *DUX4* expression in vitro (n=3, p<0.05), demonstrating ~100% knockdown of the transcript on average (**Figure 2.2c**). Corresponding decreases in expression of *ZSCAN4*, *TRIM43*, and *MBD3L2*—known activated downstream targets of DUX4—were also observed (**Figure 2.2d**). Considering gapmers against exon 3, efficacy appeared to correlate with the openness of the target site secondary structure (**Figure 2.3**). Based on these results, three gapmers were selected for further analysis: LNA1, LNA4, and LNA6.

Dose-dependent activity was displayed by these gapmers in vitro, with significant *DUX4* knockdown at ~90% achievable at a ten-fold lower dose of 10 nM (n=6, p<0.005) (**Figure 2.2e**). No significant reduction in *DUX4* expression was observed at the 1 nM dose. Corresponding dose-dependent decreases in DUX4 target gene expression were similarly observed (**Figure 2.2f**). When cells were transfected with the gapmers at 4 days post-differentiation, we observed significant knockdown of *DUX4* (n=5, p<0.005), *ZSCAN4*, *TRIM43*, and *MBD3L2* (n=6, p<0.0005) by LNA1, LNA4, and LNA6 at 14 days post-differentiation (**Figure 2.2g**). The downstream genes, in particular, had lower levels of expression than observed previously (**Figure 2.2d**) indicating that DUX4 protein levels were most likely reduced by treatment.

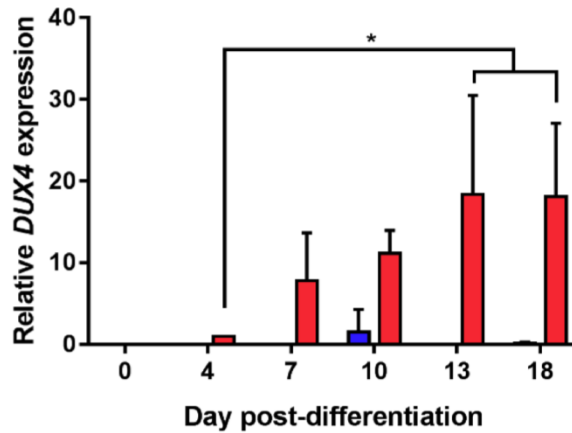


**Figure 2.1. *DUX4* mRNA expression levels in the course of muscle differentiation *in vitro*.** *DUX4* expression was evaluated at various times post-differentiation of healthy FSHD-unaffected (blue) or FSHD patient-derived (red) immortalized muscle cells. Error bars: S.D. (n = 3). \* $p < 0.05$ , one-way ANOVA with Tukey's post hoc test.

**Table 2.1. Characteristics of the LNA gapmers used in this study.**

ID	Sequence* (5' to 3')	Length (nt)	Target <i>DUX4</i> exon	GC content (%)
LNA1	<b>AGCGTCGGAAGGTGG</b>	15	3	66.7
LNA2	<b>ATAGGATCCACAGGGA</b>	16	3	50.0
LNA3	<b>AGATCCCCTCTGCC</b>	14	1	64.3
LNA4	<b>CAGCGTCGGAAGGTG</b>	15	3	66.7
LNA5	<b>ACAGCGTCGGAAGGTG</b>	16	3	62.5
LNA6	<b>GACAGCGTCGGAAGGT</b>	16	3	62.5
LNA7	<b>AGACAGCGTCGGAAGG</b>	16	3	62.5

\*All sequences are fully phosphorothioated; **bold** indicates LNA, non-bold indicates DNA.

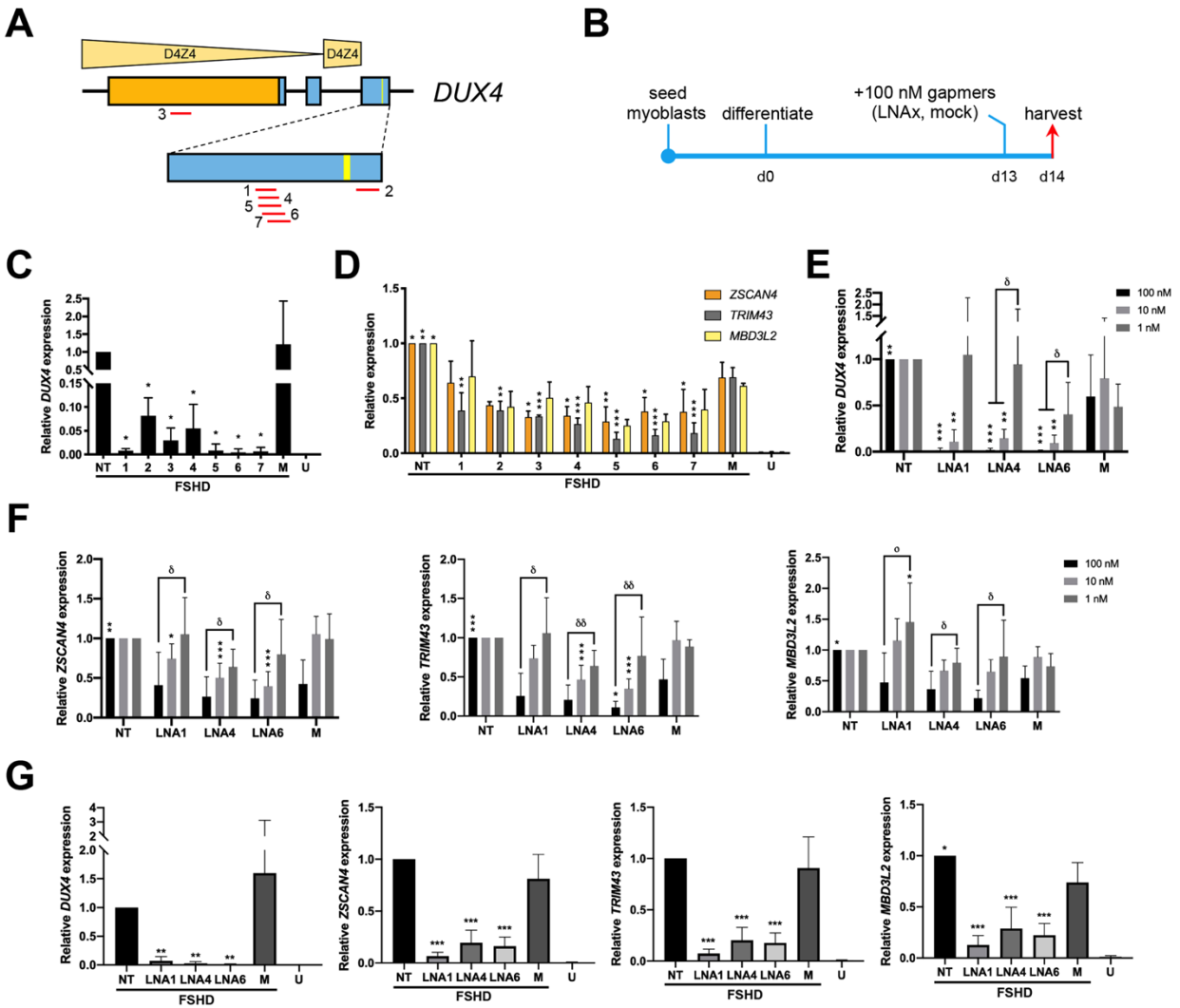


**Figure 2.2. LNA gapmer screen and evaluation of knockdown efficacy by qPCR.** (A) LNA gapmers (red lines) were designed across *DUX4*. The relative positions of the distal D4Z4 units are shown. Exons, boxes; open reading frame, orange; exon 3 PAS, yellow line. (B) Culture schedule for the LNA gapmer screen. Days post-differentiation are indicated. (C) *DUX4* expression post-treatment with 100 nM of the various gapmers, indicated by numbers. (D) *ZSCAN4*, *TRIM43*, and *MBD3L2* expression post-treatment with 100 nM gapmers. For (C) and (D), U = unaffected/healthy control. (E, F) LNA1, LNA4, LNA6, and the mock gapmer were transfected at 100, 10, or 1 nM following (B). Expression of (E) *DUX4* and (F) *ZSCAN4*, *TRIM43*, and *MBD3L2* after these treatments is shown. (G) *DUX4* and the expression of its downstream targets 10 days after treatment with 100 nM gapmers at 4 days post-differentiation. Error bars: S.D. (n=3 for C, D and healthy controls in G; n=5-6 for E, F, and treatment groups in G). \* $p < 0.05$ , \*\* $p < 0.005$ , \*\*\* $p < 0.0005$ , one-way ANOVA with Dunnett's test versus mock (M),  $\delta p < 0.05$ ,  $\delta\delta p < 0.005$ , one-way ANOVA with Tukey's test.

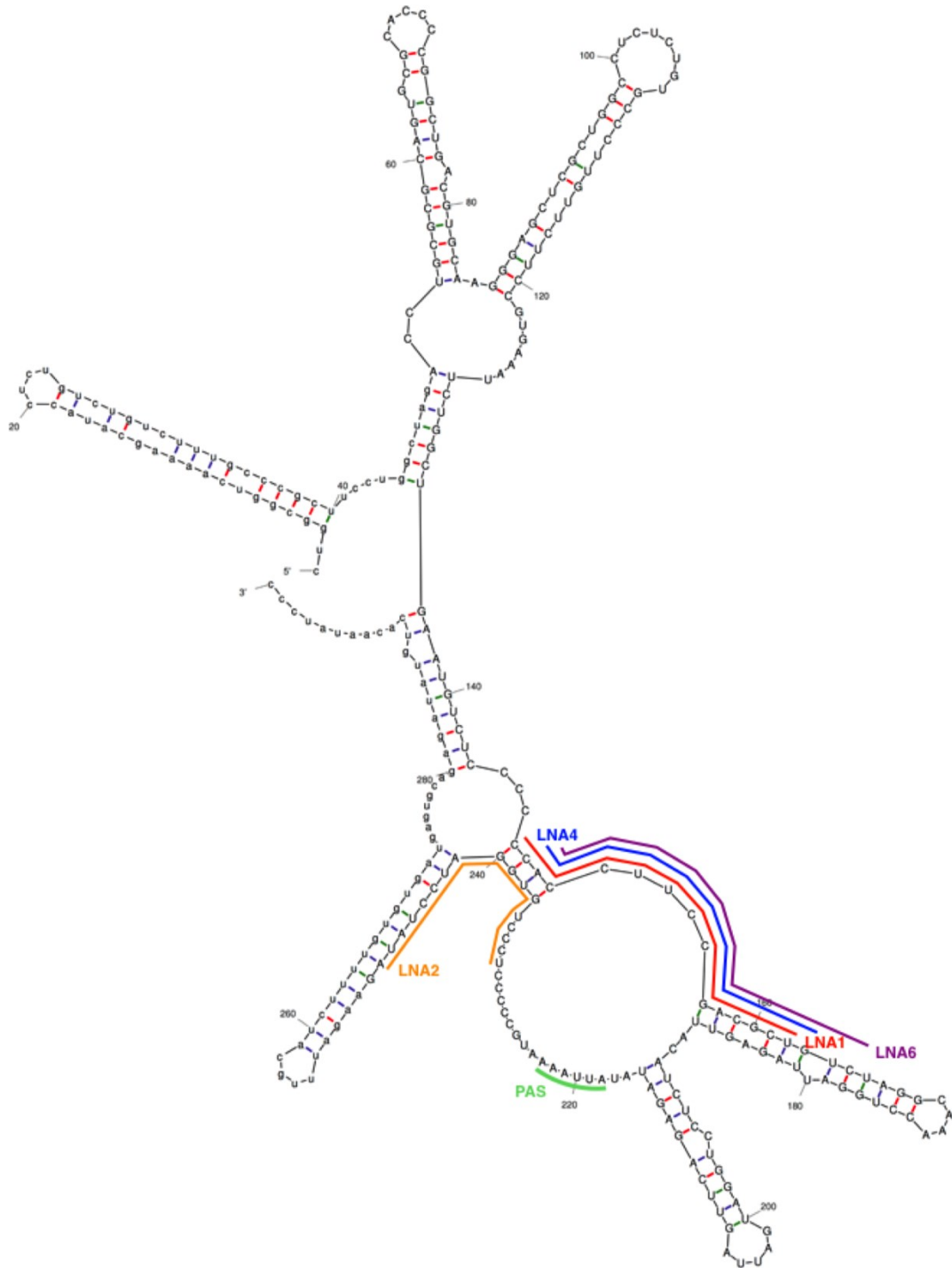


**Figure 2.3. Predicted *DUX4* exon 3 pre-mRNA secondary structure.** The locations of four LNA gapmers (LNA1, LNA2, LNA4, and LNA6) are mapped on the folded structure shown for *DUX4* exon 3. The PAS sequence is indicated as well.

### 2.3.2. LNA4 decreases the expression of FSHD-associated genes

RNA sequencing was conducted to evaluate the in vitro therapeutic efficacy of 100 nM LNA4 treatment on a more global scale. Approximately 30 million reads per sample were obtained, mapping to ~93-96% of the genome. With the healthy control as reference, we identified 877 genes whose expression was significantly affected (i.e., at least a 2-fold increase/decrease in expression,  $p < 0.05$ ) in immortalized FSHD patient-derived cells. To extract a subset of these genes that are associated with FSHD, we compared our dataset with that of Rickard et al. (2015).<sup>70</sup> Rickard et al. used FSHD patient-derived primary myoblasts carrying a DUX4-responsive fluorescent reporter that were differentiated and sorted by flow cytometry to obtain a pool of myocytes currently or recently expressing DUX4, which were then used as samples for RNA sequencing. We decided to use this dataset as it had the most similar cell culture conditions to ours, in particular with the use of KOSR for differentiation. The comparison revealed 91 overlapping genes between the lists of significantly affected genes of the two studies (**Figure 2.4a**). These were considered our FSHD signature genes: 86 significantly up-regulated and 5 significantly down-regulated genes (**Table 2.2**). When the fold change values obtained by the two different RNA sequencing experiments were plotted for each gene, we found that the majority of genes were regulated in the same direction (**Figure 2.4b**), validating use of the signature.

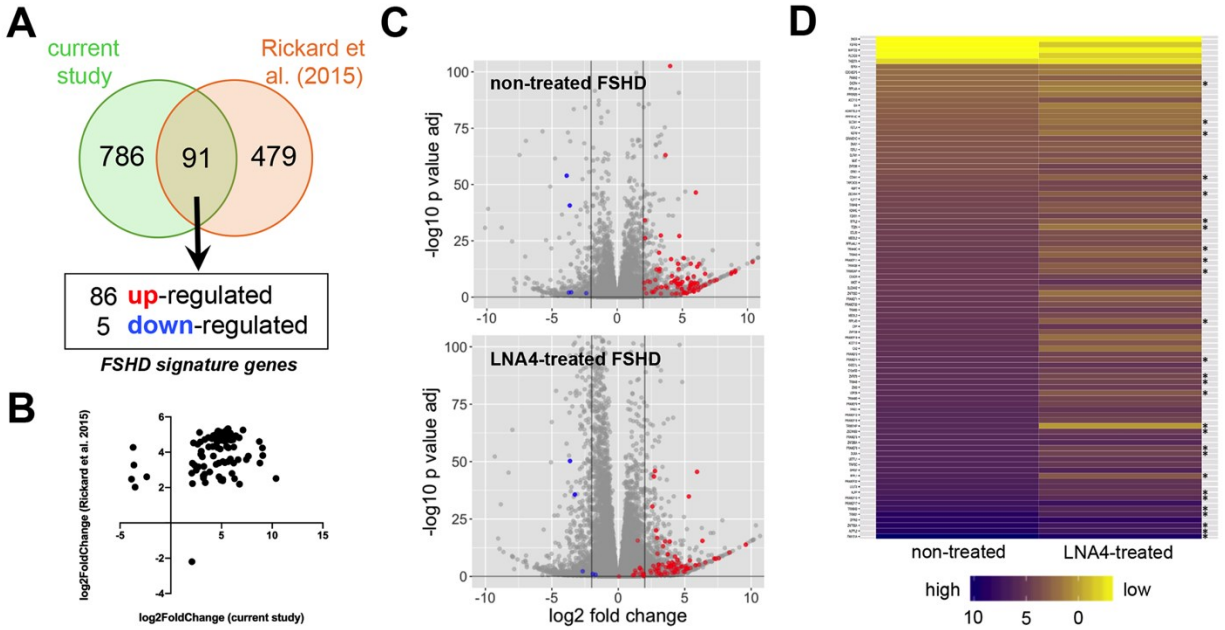


**Figure 2.4. RNA sequencing analysis of LNA gapmer therapeutic efficacy.** (A) FSHD signature genes were determined via comparison with the Rickard et al. (2015) dataset. For the current study, clonal immortalized healthy control and FSHD patient-derived myotube populations were compared. (B) 2D plot of  $\log_2(\text{Fold Change})$  values between the present study and Rickard et al., with a  $\log_2(\text{Fold Change})$  cut-off of  $+2/-2$  for the significantly affected genes of both datasets. (C) Volcano plots of RNA sequencing data from non-treated and LNA4-treated myotubes, with the FSHD-unaaffected control as reference. The 91 FSHD signature genes are marked (red: up-regulated, blue: down-regulated in FSHD); gray vertical lines indicate 2-fold  $\log_2(\text{Fold Change})$  values in either direction. (D) Heat map displaying expression changes for the 91 FSHD signature genes after LNA4 treatment, with the FSHD-unaaffected control as reference. High expression is indicated by more purple shades (n=3 independent experiments per condition).

**Table 2.2. Significantly up-/down-regulated genes\* comprising the FSHD signature.**

Gene name	log <sub>2</sub> Fold Change	Adjusted p-value	Gene name	log <sub>2</sub> Fold Change	Adjusted p-value	Gene name	log <sub>2</sub> Fold Change	Adjusted p-value
<i>FAM151A</i>	10.387	2.20E-16	<i>KHDC1L</i>	5.51	0.000149	<i>ZSCAN4</i>	4.065	2.64E-103
<i>ALPPL2</i>	9.07	1.68E-12	<i>PRAMEF4</i>	5.434	3.14E-09	<i>RBP7</i>	3.841	7.75E-05
<i>ZNF705A</i>	9.038	7.96E-12	<i>PRAMEF2</i>	5.399	6.40E-09	<i>TRPC5OS</i>	3.734	1.57E-05
<i>DPPA3</i>	8.794	1.00E-11	<i>CA2</i>	5.342	0.0122	<i>CCNA1</i>	3.704	9.22E-64
<i>TRIM51</i>	8.737	4.42E-11	<i>ACOT12</i>	5.338	0.0192	<i>GRIK1</i>	3.4	3.65E-05
<i>TRIM64B</i>	7.648	2.09E-08	<i>PRAMEF19</i>	5.144	0.0133	<i>ZNF296</i>	3.354	0.0285
<i>PRAMEF17</i>	7.461	5.29E-08	<i>ZNF728</i>	5.143	0.00696	<i>MIAT</i>	3.349	4.44E-28
<i>PRAMEF10</i>	7.13	1.39E-07	<i>CFP</i>	5.13	0.0137	<i>OLFM1</i>	3.265	3.18E-13
<i>ALPP</i>	6.779	3.89E-06	<i>RFPL4B</i>	5.114	5.08E-18	<i>F2RL1</i>	3.232	3.20E-12
<i>LEUTX</i>	6.749	4.43E-11	<i>MBD3L3</i>	5.005	1.83E-07	<i>SNAI1</i>	3.21	1.92E-20
<i>PRAMEF22</i>	6.643	7.61E-06	<i>TRIM60</i>	4.962	0.000174	<i>GRAMD1C</i>	3.117	6.27E-05
<i>RFPL1</i>	6.416	4.08E-05	<i>PRAMEF20</i>	4.943	0.00034	<i>NEFM</i>	3.008	4.95E-13
<i>GPR37</i>	6.299	1.60E-15	<i>PRAMEF1</i>	4.888	1.99E-06	<i>FSTL4</i>	2.959	0.000387
<i>TFAP2C</i>	6.219	0.000682	<i>ZNF705D</i>	4.875	0.0476	<i>SLC3A1</i>	2.926	2.56E-08
<i>UBTFL1</i>	6.209	2.63E-05	<i>SLC34A2</i>	4.79	1.29E-06	<i>PPP1R14C</i>	2.838	0.00432
<i>DUXA</i>	6.149	7.13E-07	<i>AMOT</i>	4.766	7.33E-28	<i>ADAMTSL3</i>	2.725	0.00788
<i>PRAMEF6</i>	6.137	3.11E-14	<i>CXADR</i>	4.736	9.92E-07	<i>ID4</i>	2.648	0.00383
<i>ZNF280A</i>	6.036	3.76E-47	<i>TRIM53AP</i>	4.722	3.75E-13	<i>ADCY10</i>	2.522	1.92E-07
<i>PRAMEF5</i>	5.98	7.38E-05	<i>TRIM43B</i>	4.673	2.25E-06	<i>PPP2R2B</i>	2.355	8.57E-08
<i>ZSCAN5B</i>	5.941	4.90E-07	<i>PRAMEF11</i>	4.672	1.71E-15	<i>RFPL4A</i>	2.242	0.0221
<i>TRIM51HP</i>	5.891	0.00355	<i>TRIM43</i>	4.641	3.92E-05	<i>CXCR4</i>	2.136	8.18E-35
<i>PRAMEF16</i>	5.887	0.000427	<i>TRIM49C</i>	4.623	6.41E-09	<i>PNMA2</i>	2.134	7.21E-27
<i>PRAMEF12</i>	5.874	6.28E-10	<i>RFPL4AL1</i>	4.584	0.0198	<i>CDC42EP5</i>	2.086	0.00018
<i>TPRX1</i>	5.874	2.37E-06	<i>MBD3L2</i>	4.557	6.31E-07	<i>RIPK4</i>	2.075	4.80E-07
<i>PRAMEF9</i>	5.797	0.00164	<i>CCL20</i>	4.475	0.0416	<i>THSD7A</i>	-2.369	0.0181
<i>TRIM49B</i>	5.687	2.75E-07	<i>TC2N</i>	4.423	4.96E-08	<i>PLCXD3</i>	-3.521	0.00723
<i>USP29</i>	5.653	3.63E-05	<i>RFPL2</i>	4.389	8.36E-08	<i>MAP7D2</i>	-3.636	2.17E-41
<i>ZIM3</i>	5.646	2.63E-06	<i>FOXR1</i>	4.204	0.0383	<i>FGFR3</i>	-3.715	0.0103
<i>TRIM49</i>	5.645	1.51E-15	<i>KDM4E</i>	4.202	4.80E-10	<i>DNER</i>	-3.873	1.25E-54
<i>ZNF679</i>	5.59	7.37E-06	<i>TRIM48</i>	4.152	3.66E-07			
<i>C12orf50</i>	5.587	0.00264	<i>KLF17</i>	4.135	1.39E-17			

\*versus the healthy FSHD-unaffected control

The 91 FSHD signature genes were marked on volcano plots of the RNA sequencing data from non-treated FSHD and LNA4-treated FSHD muscle cells, with the unaffected control as reference (**Figure 2.4c**). Upon treatment with LNA4, there is an overall observable shift in the position of the marked genes towards the center of the plot, indicating restoration of expression to levels found in FSHD-unaffected muscle cells. This is similarly depicted using a heat map showing changes in expression for each of the 91 FSHD signature genes post-treatment (**Figure 2.4d**). We found that the expression of the downstream DUX4 target gene *ZSCAN4* was significantly decreased post-treatment compared to non-treated controls ( $p < 0.05$ ). Of the 86 up-regulated FSHD signature genes, 27 had significantly reduced expression after treatment with LNA4 ( $p < 0.05$ ) compared to the non-treated FSHD muscle cells. Expression levels of the 5 down-regulated FSHD signature genes were not significantly affected by the treatment. To further validate our results, we performed a similar analysis using the dataset of Geng et al. (2012), who performed microarray analysis on *DUX4*-transduced healthy primary myoblasts.<sup>72</sup> Our comparison revealed 50 overlapping significantly affected genes ( $p < 0.05$ ), 47 up-regulated and 3 down-regulated, the majority of which were similarly regulated between the two studies (**Figures 2.5a,b**). Of the 47 up-regulated genes, 16 had significantly decreased expression post-treatment while of the 3 down-regulated genes, 2 had significantly increased expression post-treatment ( $p < 0.05$ ) (**Figures 2.5c,d**). Overall, 39 common FSHD signature genes were identified from both comparisons (our study versus Rickard et al. and Geng et al.), consisting of 1 down- and 38 up-regulated genes (**Figure 2.5e**). The common down-regulated gene, *FGFR3*, was not significantly affected by LNA4 treatment. However, 15 of the common up-regulated signature genes had significantly decreased expression post-treatment ( $p < 0.05$ ) (**Table 2.3**).

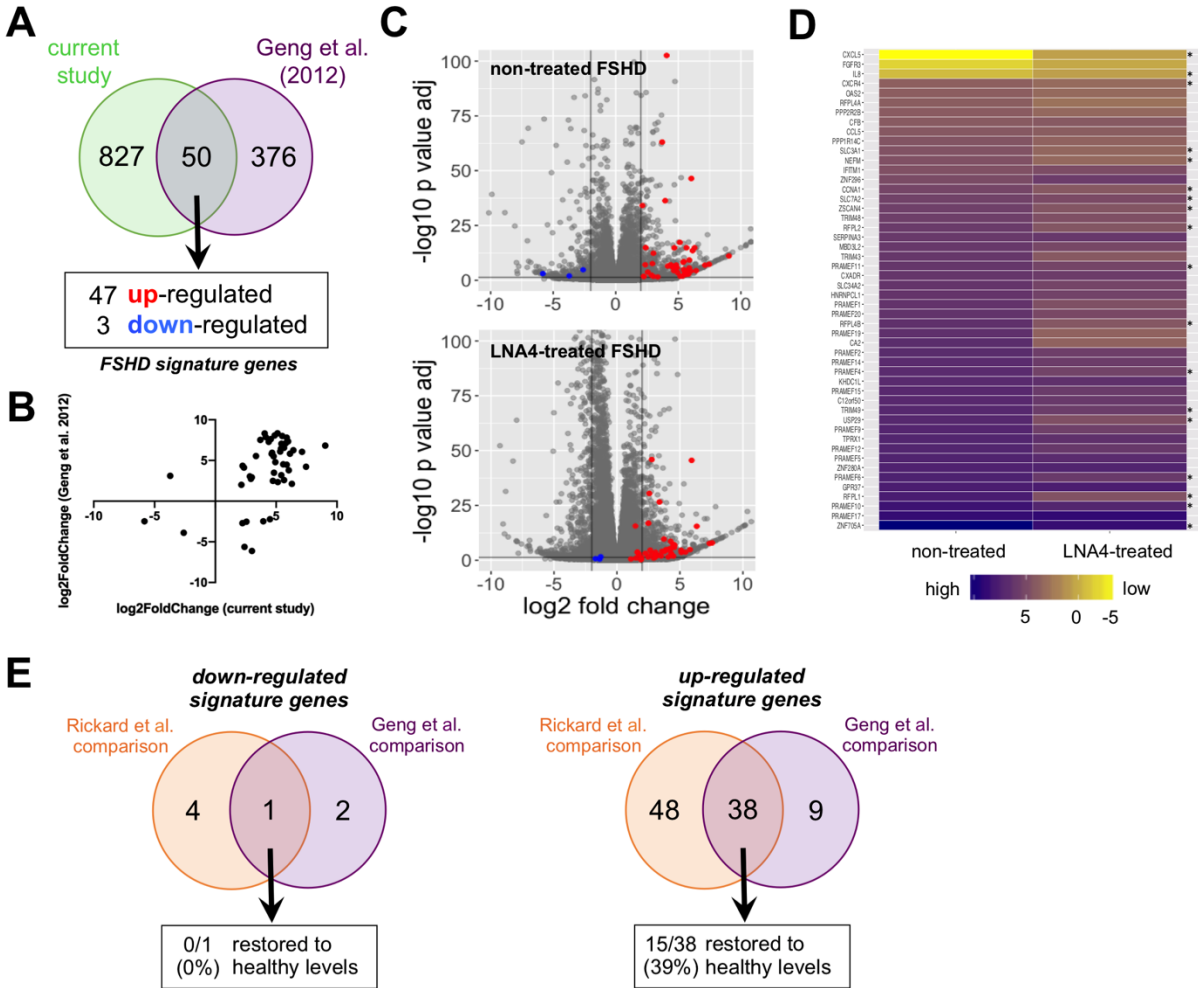


**Figure 2.5. Alternative comparison for RNA sequencing analysis of LNA gapmer therapeutic efficacy.** (A) FSHD signature genes were similarly determined following comparison with the dataset of Geng et al. (2012). (B) 2D plot of the  $\log_2(\text{Fold Change})$  values between the present study and Geng et al. (2012), with a  $\log_2(\text{FoldChange})$  cut-off of  $+2/-2$  for the significantly affected genes of both datasets. (C) Volcano plots of RNA sequencing data from non-treated and LNA4-treated immortalized FSHD patient-derived muscle fibers, with healthy FSHD-unaffected control muscle fibers as reference. The 50 FSHD signature genes are marked (red: up-regulated, blue: down-regulated in FSHD); gray vertical lines indicate two-fold  $\log_2$ fold change values in either direction. (D) Heat map displaying expression changes for the 50 FSHD signature genes after treatment with LNA4, with the healthy FSHD-unaffected control as reference. High expression is indicated by a more purple shade, and genes with expression values significantly restored to healthy levels are indicated by an asterisk ( $n = 3$ ). (E) Overlaps in the down- and up-regulated FSHD signature genes obtained from the two comparisons are shown. The numbers of overlapping genes whose expression values were significantly restored to healthy levels after LNA4 treatment are indicated.

**Table 2.3. FSHD signature genes with expression values significantly restored to healthy levels after LNA4 treatment *in vitro*.**

Gene name	Up/Down-regulated in FSHD?	log <sub>2</sub> Fold Change*	Adjusted p-value*	Rickard et al. comparison**	Geng et al. comparison**
<i>TC2N</i>	up	-2.784	6.61E-06	O	X
<i>TRIM49C</i>	up	-1.692	0.00225	O	X
<i>TRIM53AP</i>	up	-1.686	0.000234	O	X
<i>ZNF679</i>	up	-1.584	0.0125	O	X
<i>TRIM51HP</i>	up	-5.838	0.00289	O	X
<i>ZSCAN5B</i>	up	-1.134	0.0164	O	X
<i>DUXA</i>	up	-1.739	0.00466	O	X
<i>ALPP</i>	up	-1.697	0.0436	O	X
<i>TRIM64B</i>	up	-1.567	0.00712	O	X
<i>TRIM51</i>	up	-2.182	5.20E-06	O	X
<i>ALPPL2</i>	up	-1.836	8.39E-08	O	X
<i>FAM151A</i>	up	-0.79	0.0069	O	X
<i>CXCR4</i>	up	-0.67	2.30E-05	O	O
<i>SLC3A1</i>	up	-1.177	0.0148	O	O
<i>NEFM</i>	up	-1.38	0.000635	O	O
<i>CCNA1</i>	up	-1.134	2.60E-07	O	O
<i>ZSCAN4</i>	up	-1.301	7.11E-18	O	O
<i>RFPL2</i>	up	-1.646	0.0235	O	O
<i>PRAMEF11</i>	up	-0.941	0.039	O	O
<i>RFPL4B</i>	up	-2.472	5.65E-09	O	O
<i>PRAMEF4</i>	up	-1.522	0.00625	O	O
<i>TRIM49</i>	up	-1.379	0.000363	O	O
<i>USP29</i>	up	-2.592	0.00295	O	O
<i>PRAMEF6</i>	up	-1.691	1.18E-07	O	O
<i>RFPL1</i>	up	-3.502	0.00305	O	O
<i>PRAMEF10</i>	up	-1.326	0.00883	O	O
<i>ZNF705A</i>	up	-1.688	0.000274	O	O
<i>SLC7A2</i>	up	-0.575	0.0212	X	O
<i>CXCL5</i>	down	4.455	0.0146	X	O
<i>IL8</i>	down	1.319	0.0474	X	O

\*versus the non-treated FSHD-affected control

\*\*"O" denotes inclusion in the gene set obtained from the comparison of our RNA sequencing data with the indicated study (Rickard et al. or Geng et al.); "X" denotes that the gene is not part of this comparison set.

### 2.3.3. Effects of LNA gapmer treatment on myogenic fusion and apoptosis

DUX4 negatively regulates MYOD, which is involved in establishing and ensuring proper muscle differentiation.<sup>62</sup> A manifestation of this DUX4-induced differentiation defect is the impaired fusion of myoblasts into muscle fibers in FSHD. We observed a significant decrease in myogenic fusion in immortalized FSHD-patient-derived muscle cells compared to FSHD-unaaffected controls (**Figures 2.6a,b**). Treatment with LNA6 significantly increased the myogenic fusion index of FSHD myotubes compared to the mock-treated group by ~56% (n=6, p<0.005), whereas no significant improvement was observed with LNA1 and LNA4. As FSHD patient-derived myotubes have been found to display hypotrophy in vitro,<sup>240</sup> we decided to quantify myotube diameters in our different treatment groups. LNA-treated muscle fibers displayed an observable shift towards larger diameters that were characteristic of healthy myotubes (**Figure 2.6c**). FSHD patient-derived myotubes treated with LNA1, LNA4, or LNA6 had significantly increased myotube diameters at 16-20  $\mu\text{m}$  on average compared to the mock-treated control, which had an average myotube diameter of 14.8  $\mu\text{m}$  (n=3, p<0.05 for LNA4 and p<0.0005 for LNA1, LNA6) (**Figure 2.6d**).

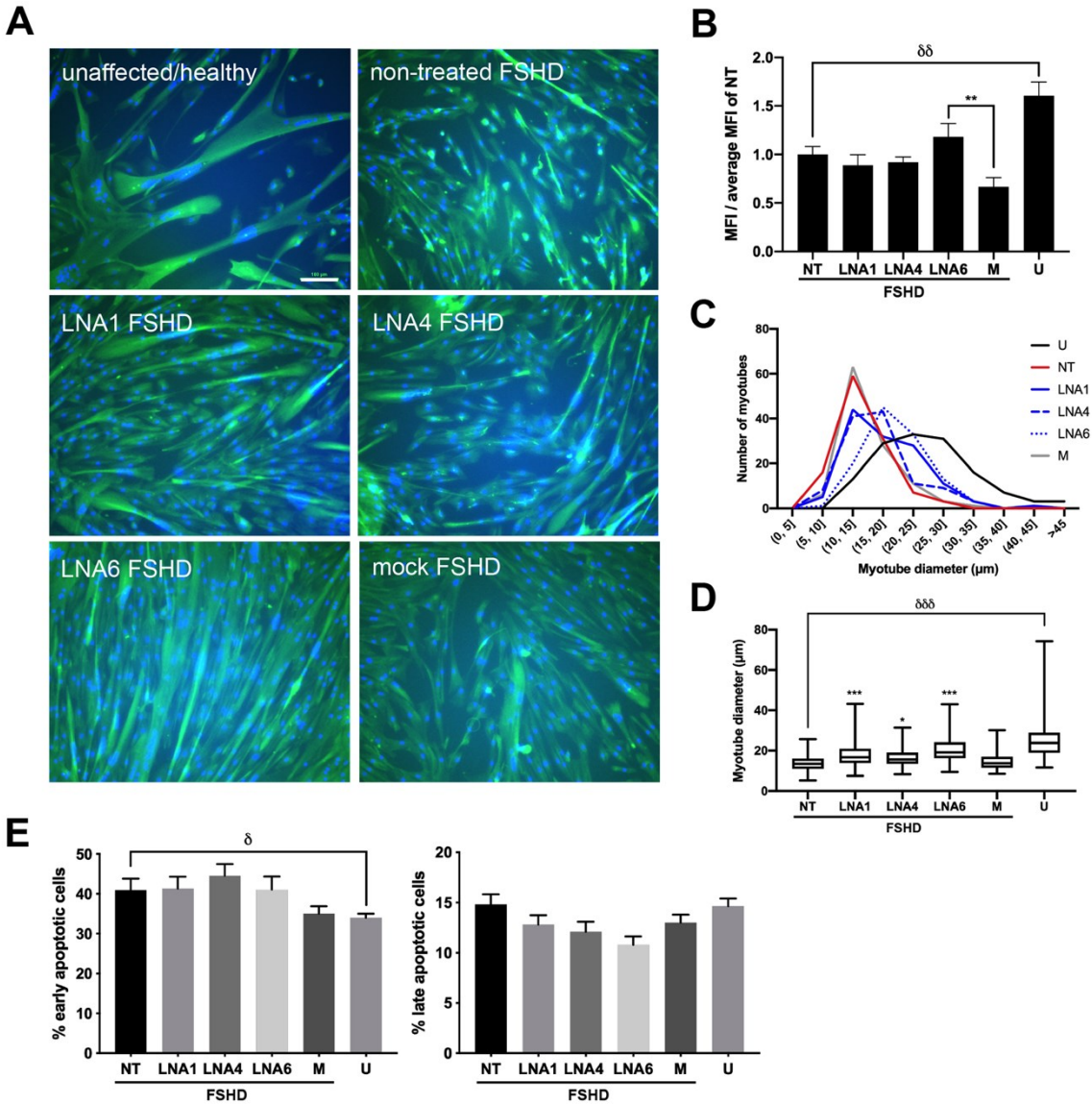


**Figure 2.6. Effect of LNA gapmer treatment on *in vitro* muscle cell fusion and apoptosis.**

(A) Representative images of immunostained immortalized healthy control and FSHD patient-derived cells with and without treatment using various LNA gapmers at 10 nM. Nuclei, blue; desmin, green. Scale bar = 100  $\mu\text{m}$ . (B) Quantification of myogenic fusion indices (MFIs) from immunostaining images. MFI values were divided by the average MFI of the non-treated (NT) groups to eliminate batch effect. Error bars: S.E.M. ( $n=6$ ). (C) Frequency distribution of muscle fiber diameters in the different conditions. (D) Quantification of the diameters in (C). The central line marks the median, the box covers the 25<sup>th</sup>-75<sup>th</sup> percentiles, and the whiskers represent the range. ( $n=3$ ) (E) Flow cytometry-based (Annexin V/propidium iodide) quantification of early and late apoptotic cells from immortalized healthy FSHD-unaffected control and FSHD patient-derived cells before and after 10 nM LNA gapmer treatment. For (B) and (E), error bars: S.E.M. ( $n=6$ ). \* $p<0.05$ , \*\* $p<0.005$ , \*\*\* $p<0.0005$ , one-way ANOVA with Dunnett's test versus the mock (M),  $\delta p<0.05$ ,  $\delta\delta p<0.005$ ,  $\delta\delta\delta p<0.0005$ , unpaired two-tailed  $t$ -test. U = unaffected/healthy control.

Transfection of *DUX4* constructs has also been reported to induce apoptosis *in vitro*.<sup>51,62</sup> We found that treatment with LNA1, LNA4, and LNA6 at 13 days post-differentiation did not significantly affect early apoptotic cell numbers, either upon evaluation at 1 or 5 days after transfection using an Annexin V/propidium iodide-based flow cytometry assay (**Figures 2.6e, 2.7**). No significant differences in late apoptotic cell populations were observed across treatments and between non-treated and FSHD-unaffected controls at 14 days post-differentiation (**Figure 2.6e**), whereas late apoptosis was interestingly significantly increased in FSHD-unaffected controls at 18 days post-differentiation (**Figure 2.7b**).

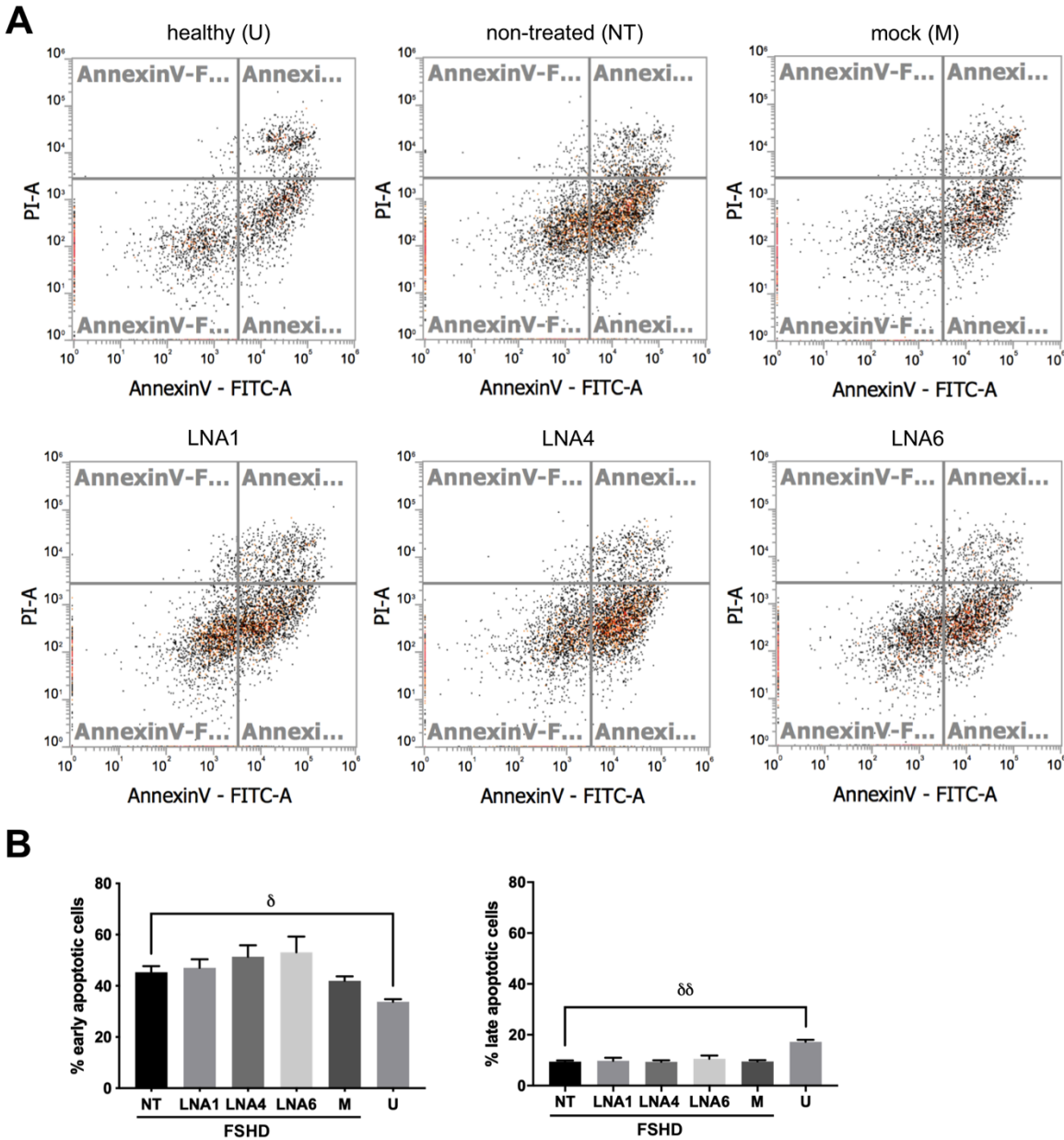


**Figure 2.7. Flow cytometry evaluation of *in vitro* apoptosis.** Healthy FSHD-unaffected control immortalized myotubes (U), non-treated (NT), LNA gapmer-treated, and mock-treated (M) immortalized FSHD patient-derived myotubes were harvested and stained with fluorochrome-conjugated Annexin V and propidium iodide to assess apoptotic condition by flow cytometry. (A) Representative plots are shown for when the cells were transfected with gapmers at 13 days post-differentiation and then evaluated for apoptosis the following day. The top-left quadrant represents late apoptotic cells, the bottom-right represents early apoptotic cells, and the bottom-left represents live cells. (B) Percentage of early and late apoptotic cells from immortalized healthy control and non-treated (NT) or gapmer-treated (transfected at 13 days post-differentiation) FSHD patient-derived cells at 18 days post-differentiation. Error bars: S.E.M. (n = 3).  $\delta p < 0.05$ ,  $\delta\delta p < 0.005$ , unpaired two-tailed *t*-test.

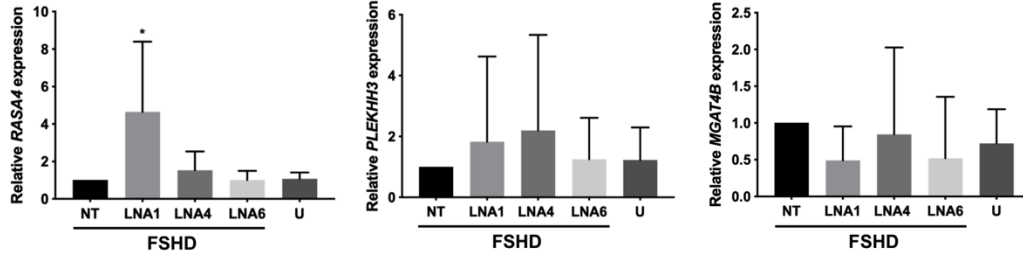
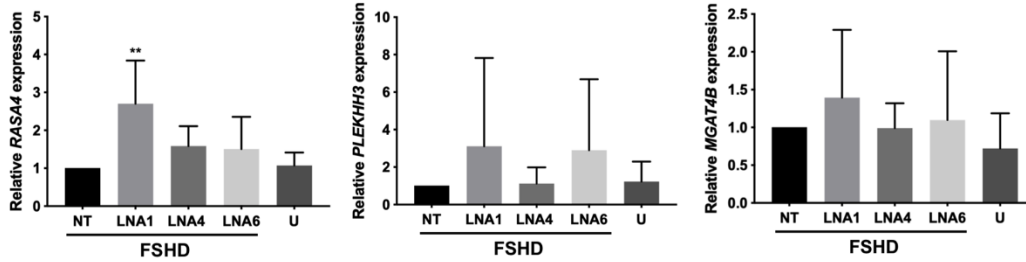
### 2.3.4. Minimal potential off-target toxicity with LNA gapmer treatment *in silico*, *in vitro*

To assess off-target effects resulting from LNA gapmer treatment *in vitro*, a list of potential targets with sequences having at least 1 base mismatch to the *DUX4* target sequence was compiled (Table 2.4). Of the listed genes, three have detectable expression in muscle: *RASA4*, *PLEKHH3*, and *MGAT4B*. At both the 100 nM and 10 nM doses, *PLEKHH3* and *MGAT4B* expression levels were not affected by LNA gapmer treatment (Figure 2.8). On the contrary, *RASA4* expression was significantly increased at both doses upon treatment by LNA1 (n=5, p<0.05 at 100 nM and p<0.005 at 10 nM), which does not constitute a direct off-target knockdown effect by the LNA gapmer.

**Table 2.4. Potential off-targets of LNA gapmers 1, 4, and 6 as identified by GGGenome.**

Gene	Transcript variant/s	Sequence showing mismatch*	# mismatches with LNA gapmer		
			LNA1	LNA4	LNA6
<i>DUX4</i>	n/a	CCACCTTCCGACGCTGTC	0	0	0
<i>GALNT14</i>	4	CCACCTTCGGACGCTGAC	1	1	2
<i>RASA4/4B</i>	1, 2	CCACCTTCC-ACGCTGTG	1	1	2
<i>CHD5</i>	n/a	CCACCTTCCGAGCTCCT	1	2	4
<i>PLEKHH3</i>	1, 2, 3	GCACCTTCCGAC-CTGGG	2	1	3
<i>MGAT4B</i>	1	GCACCTTCCTGACGCTGCT	2	1	3
<i>LINC01561</i>	n/a	ACACCTTCCGACACTGGG	2	1	3
<i>POLR2J4</i>	n/a	CCACCTTCC-ACGCTGTG	1	1	2

\*Red indicates mispairing, green indicates additional/missing base compared to reference *DUX4*

**A****B**

**Figure 2.8. Evaluation of potential LNA gapmer off-target effect.** LNA gapmer treatment effect on the expression of potential off-target genes *RASA4*, *PLEKHH3*, and *MGAT4B* was evaluated by qPCR. Expression of these genes was examined at the (A) 100 nM and (B) 10 nM transfected LNA gapmer dose. Error bars: S.D. (n = 5). \* $p < 0.05$ , \*\* $p < 0.005$ , one-way ANOVA with Dunnett's test versus non-treated (NT). U = unaffected/healthy control.

### 2.3.5. In vivo uptake and efficacy of LNA4

*FLEXDUX4* mice leak *DUX4* at a very low level, similar to amounts found in human FSHD myoblasts. At this level, no *DUX4* downstream genes are induced and no overt pathologies are reported.<sup>90</sup> To visualize LNA after *in vivo* delivery, we injected 20 µg of fluorescein-tagged LNA4 gapmers into the TA muscles of *FLEXDUX4* mice. Two *FLEXDUX4* mice received i.m. injections of phosphate buffered saline (PBS) instead. Fluorescence imaging showed no positive signal in the PBS-injected TA (**Figure 2.9a**), whereas TAs that received LNA4 showed fluorescent signals in the muscles. The signals can be clearly seen in the interstitial space (**Figure 2.9b**) and within muscle fibers (**Figure 2.9c**).

To determine if the LNA4 that significantly suppressed *DUX4* expression in FSHD patient myoblasts was also effective *in vivo*, *FLEXDUX4* mice were given either three i.m. injections of 20 µg LNA4 or three injections of LNA gapmer control with a non-specific, scrambled sequence every other day. Both groups received i.m. injections of LNA gapmers in one TA and of PBS in the contralateral TA. *DUX4* mRNA expression was reduced by 84% upon treatment with LNA4 compared to the PBS-injected contralateral TA one day after the last injection (**Figure 2.9d**). Injections of the scrambled control did not have a significant effect on *DUX4* mRNA expression (**Figure 2.9d**). We then repeated the experiment, but this time instead of collecting muscles one day after the last injection, we collected them 7 days post-injection. Our results showed a significant 70% knockdown of *DUX4* mRNA (n=5, p<0.05) in the muscles (**Figure 2.9e**). Thus, LNA4 significantly reduced *DUX4* expression in the skeletal muscles of *FLEXDUX4* mice, and the effect lasted for at least 7 days post-injection.

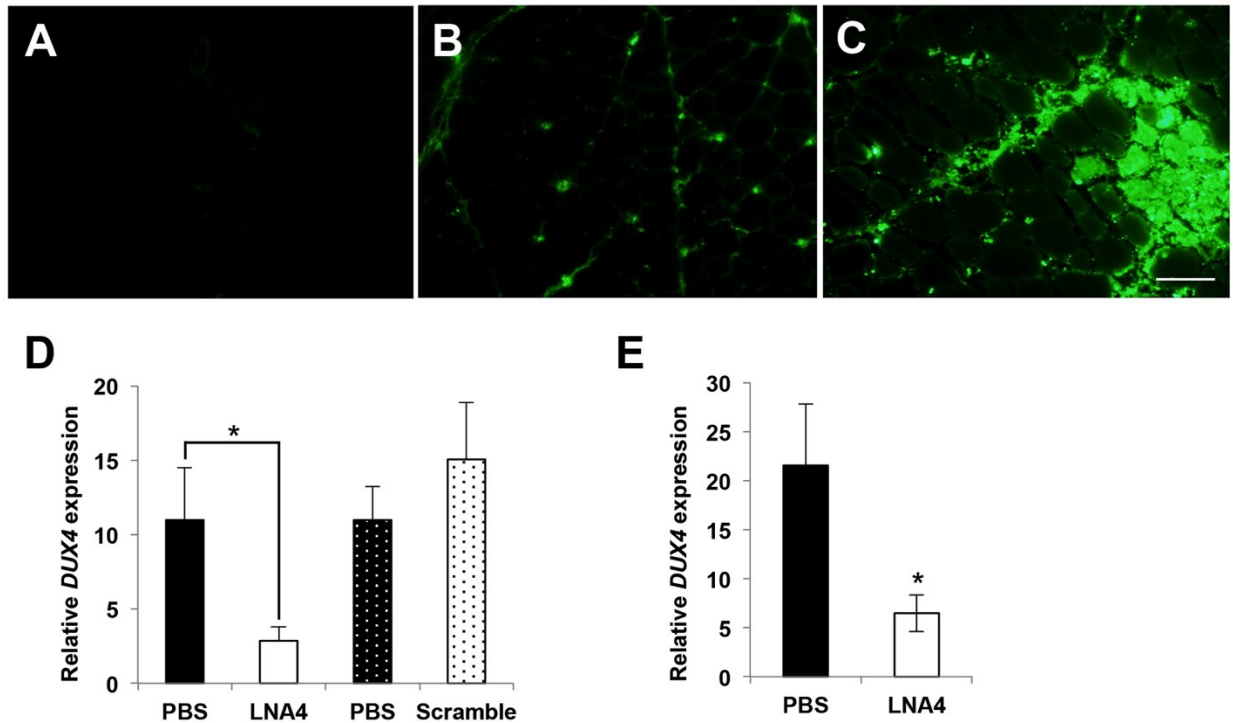


**Figure 2.9. *In vivo* uptake and efficacy of LNA gapmers.** (A-C) *FLEXDUX4* mice were injected with single 20  $\mu$ l injection volumes of PBS in the left TA (A) and 20  $\mu$ g fluorescently-tagged LNA4 (green) in the right TA (B and C). Muscles were collected one day later. The image in (B) depicts muscle tissue away from the injection site, while (C) shows the injection site. (n=2). Scale bar = 100  $\mu$ m. (D) Intramuscular injections of 20  $\mu$ g LNA4 in TA muscles (one leg with LNA, contralateral leg with PBS; solid and hashed bars indicate leg pairs) of *FLEXDUX4* mice every other day for a total of 3 injections showed knockdown of *DUX4* mRNA by qPCR one day after the last injection. No knockdown was observed when a scrambled LNA gapmer control was injected. (n=5 each) (E) *DUX4* transcript expression was evaluated 7 days after intramuscular injections of LNA4 in the TA. Significant *DUX4* knockdown was observed. Error bars: S.E.M. (n=5 each). \* $p$ <0.05, paired *t*-test.

## 2.4. Discussion

Our study shows the potential of using LNA gapmers for FSHD therapy through *DUX4* transcript knockdown. Gapmers are gaining traction in therapeutic development, with a number approved by the U.S. Food and Drug Administration (FDA) or in clinical trials.<sup>241</sup> One of the earliest successes is mipomersen (Kynamro; Ionis, Genzyme), a 2'-*O*-methoxyethyl (2'-MOE) gapmer targeting apolipoprotein B-100 that has been approved by the FDA for familial hypercholesterolemia treatment in 2013.<sup>241,242</sup> In 2018 the FDA approved another 2'-MOE gapmer, inotersen (Tegsedi; Ionis, Akcea), for treating hereditary transthyretin amyloidosis-associated polyneuropathy.<sup>241,243</sup> Gapmers have been tested for Huntington's disease, familial chylomicronemia, familial partial lipodystrophy, and various cancers.<sup>241,244</sup> Available results from these, particularly for Huntington's disease, are encouraging. To our knowledge, only three LNA gapmers (Enzon) have been evaluated in clinical trials thus far, for treating certain cancers. However, studies on these have all been discontinued, likely due to concerns related to safety and/or efficacy. The potential of LNA gapmers for therapy remains to be seen, particularly for neuromuscular disorders.

Aside from showing nearly complete reduction of *DUX4* transcript levels (**Figure 2.2c**) and likely a decrease of DUX4 protein levels (**Figures 2.2d,f,g**) in immortalized FSHD-patient derived myotubes, we demonstrated significant knockdown of *DUX4* mRNA in a muscle of an FSHD mouse model by local injections (**Figures 2.9d,e**). We also provided evidence of safety against potential off-target effects identified by a short input sequence-optimized search engine (**Figure 2.8**).

Previous studies have mostly used PMOs to interfere with PAS recognition or *DUX4* pre-mRNA splicing.<sup>63,75,78,79</sup> While these are viable strategies to knockdown *DUX4* expression,

certain limitations to efficacy are imposed by the PMO chemistry. PMOs are charge-neutral AOs proven safe and stable *in vivo*.<sup>73</sup> Despite their promising efficacy *in vitro*, PMOs display poor uptake into target tissues *in vivo* and are rapidly cleared from circulation, with an elimination half-life of less than 4 hr.<sup>245</sup> In contrast, LNA gapmers have a longer half-life, reaching up to 15 hr,<sup>246</sup> and their negatively-charged backbone likely allows better recognition by cell surface receptors, leading to more effective internalization.<sup>247</sup> This is supported by our study in which we observed good LNA gapmer uptake into injected muscles (**Figure 2.9c**). In addition, LNA gapmers are stable, have a stronger affinity to RNA, and have higher RNase H-mediated cleavage activity than 2'-*O*-methyl or phosphorothioated DNA AOs.<sup>246</sup> This allows for LNA gapmers to be administered at lower doses and yet retain appreciable potency. Whereas transfection of LNA gapmers at 100 nM knocked down *DUX4* to nearly undetectable levels (**Figure 2.2c**), transfection at a 10-fold lower dose still led to significant *DUX4* knockdown, strikingly by ~90% lower than non-treated controls on average (**Figure 2.2e**). This is more efficient than in previous studies, which used PMOs at higher concentrations (50-150 nM) and achieving at most 50% knockdown.<sup>63,78</sup> Finally, knocking down *DUX4* through RNase H-mediated degradation offers more assurance of efficacy rather than blocking PAS or splice sites. For instance, alternative PAS sequences are potentially available to *DUX4*,<sup>248</sup> and the introduction of splice-switching AOs can trigger the use of alternative splice sites.

We also introduce a pipeline for reliably screening *DUX4*-targeting AOs for FSHD treatment. One challenge working with *DUX4* is its low expression in FSHD muscle, with only 1/1000 myoblasts and 1/200 myotube nuclei expressing *DUX4* in primary cultures from FSHD muscle.<sup>18,50</sup> Conventional techniques such as RT-PCR and Western blot used previously<sup>63,78</sup> are limited in their ability to detect *DUX4*, and may not provide consistent, sufficiently quantitative

results. Here, we use a cell culture procedure to induce endogenous *DUX4* mRNA expression in immortalized patient-derived myotubes for AO screening.<sup>239</sup> This allowed for qPCR-based detection of *DUX4* at high sensitivity (**Figure 2.1**) and helped distinguish among our LNA gapmers based on efficacy (**Figure 2.2c**). Such an *in vitro* system would be simpler than one involving transfection of *DUX4*-containing vectors, which requires lengthy optimization and dealing with the inherent variability in transfection efficiencies across cells. Furthermore, we introduce the use of the *FLExDUX4* FSHD mouse model<sup>90</sup> for the *in vivo* testing of AOs (**Figure 2.9**). This model expresses *DUX4* transcripts at levels sufficient for qPCR detection even without induction of the inserted *DUX4* transgene.<sup>90</sup> Together, the *in vitro* and *in vivo* methods used here provide a valuable system for screening AOs and other drugs for FSHD therapy.

LNA gapmers targeting sites upstream of the PAS in exon 3 were determined most efficacious (**Figures 2.2a,c**). In the context of exon 3, *DUX4* knockdown efficacy appears to correlate with the predicted RNA folding conformation at the target site (**Figure 2.3**). LNA2, whose target site adopts an open conformation at only one end, exhibited lower efficacy than LNA1 and LNA4-7, whose target sites were open in the middle (**Figure 2.2c**). This is despite both groups of LNA gapmers being complementary to similar numbers of target bases in open regions. We believe this is because recruitment of RNase H occurs in the central DNA/RNA hybrid region of the LNA gapmer-target RNA complex; an open conformation in that region likely facilitates RNase H binding and activity. This stresses the need for the proper *in silico* design and screening of AOs prior to testing in cellular and animal models. In our previous work on PMOs for exon skipping in DMD,<sup>249</sup> we showed that certain features between AOs and their target sequences (e.g. binding energy, GC content) can be used to create a predictive tool to

determine which sites would lead to the highest levels of exon skipping when targeted. Perhaps the same logic can be applied for LNA gapmers in the selection of target sites for future studies.

We observed significant improvements in muscle cell fusion and fiber diameters upon treatment compared to non-treated controls (**Figures 2.6a-d**). Impaired fusion as a result of DUX4 has been demonstrated using transfection studies *in vitro*<sup>250</sup> and in some patient muscle samples.<sup>237</sup> Our result is encouraging, as it shows that LNA gapmer treatment is beneficial both in reversing the molecular effects of DUX4 mis-expression (**Figure 2.4**) and, for the first time to our knowledge, in ameliorating pathological *in vitro* phenotypes. Unlike for fusion, we did not find a significant effect of treatment on apoptosis (**Figures 2.6e, 2.7b**). It is likely that more time is required post-treatment to observe therapeutic effects on this phenotype. Furthermore, our data suggest that, using our culture system, at 14 days post-differentiation immortalized FSHD patient-derived myotubes are only still beginning to undergo the early phases of apoptosis, and are yet to exhibit differences in the number of late apoptotic cells observed (**Figure 2.6e**). However, it is encouraging to note that LNA gapmer treatment did not induce apoptosis, adding favorably to the safety of this treatment.

In conclusion, using immortalized FSHD patient-derived muscle cells and the *FLEXDUX4* FSHD mouse model, we were able to show that our designed LNA gapmers can significantly and selectively knock down *DUX4* expression in muscle. Effects on muscle structure and function, as well as an evaluation of the pharmacokinetic properties of LNA gapmers *in vivo*, remain to be determined with a systemic treatment study. This will complement our findings *in vitro*, which show a limited albeit promising view of the potential of our designed LNA gapmers for therapy. Additionally, we outline the use of a consistent, reliable method for screening *DUX4*-targeting AOs *in vitro* and *in vivo*. Taken together, we expect the promising

therapeutic we have developed and the AO screening method used in this study to facilitate progress in the field towards the production of viable treatments for FSHD.

## **2.5. Methods**

### **2.5.1. Animals**

Animal care and use were approved by the Institutional Animal Care and Use Committee of the Children's Research Institute of Children's National Health System, Washington DC. All animal procedures were carried out in accordance with approved guidelines. The mice were maintained in a facility accredited by the Association for Assessment and Accreditation of Laboratory Animal Care International. For visualizing LNA uptake into muscles, two male hemizygous seven-week-old *FLEXDUX4* mice were used. For testing the therapeutic efficacy of LNAs, fifteen male hemizygous adult *FLEXDUX4* mice were used. Animals were anesthetized with isoflurane inhalation to perform intramuscular injections, and were euthanized following CO<sub>2</sub> inhalation by cervical dislocation according to standard protocols.

### **2.5.2. Antisense oligonucleotides**

Seven different LNA gapmers against *DUX4* were designed (**Table 2.1**) and synthesized by Exiqon and Eurogentec for *in vitro* and *in vivo* studies, respectively. Their approximate target sites along the *DUX4* mRNA are illustrated in **Figure 2.2a**. One LNA gapmer (LNA3) was designed to target the *DUX4* open reading frame in exon 1, while the remaining ones targeted the 3'-UTR region in exon 3; none of the gapmers targeted the PAS sequence. Gapmers were designed to have 14-16 nucleotides in length, with the first and last three bases having the LNA chemistry and the backbone fully phosphorothioated. Target site GC content was also taken into

account. Lab-designed mock and scrambled LNA gapmers, synthesized by Exiqon and Eurogentec respectively for *in vitro* and *in vivo* experiments, were also used for experiments.

### 2.5.3. Cell culture

Immortalized FSHD patient-derived myoblasts were kindly provided by the Wellstone Program of the University of Massachusetts Medical School, MA, USA. Specifically, two cell lines were used: WS229 (FSHD-affected) and WS234 (FSHD-unaffected). Both originated from biceps-sourced primary myoblast cultures that were immortalized through the stable integration of a *CDK4/hTERT* cassette.<sup>251</sup> The individuals from whom the WS229 (male, age 66 years at biopsy, early adult onset of FSHD) and WS234 (female, age 60 at biopsy) lines were sourced are from the same family and are siblings. EcoRI/BlnI allele sizes and 4q haplotypes for WS229 and WS234 are >112kb(4qB)/28kb(4qA) and >145kb(4qB)/107kb(4qB), respectively.

Cells were grown in medium containing 15% fetal bovine serum (FBS) (Sigma), 2.5 ng/ml recombinant human hepatocyte growth factor (EMD Millipore), 10 ng/ml recombinant human fibroblast growth factor (BioPioneer), and 0.055 µg/ml dexamethasone in basal medium (BM). The BM consisted of 20% Medium 199 (Life Technologies), 0.03 µg/ml ZnSO<sub>4</sub>, and 1.4 µg/ml Vitamin B12 in DMEM (Life Technologies) with 2.5% penicillin-streptomycin (Life Technologies). For differentiation, the growth medium was replaced with the following once a confluence of 80-90% was reached: BM supplemented with 15% KnockOut Serum Replacement (KOSR) (Life Technologies), 10 µg/ml insulin (Sigma), and 100 µg/ml human apo-transferrin (R&D Systems). Cells were cultured at 37°C and 5% CO<sub>2</sub> for the entire study.

#### **2.5.4. AO transfection**

For transfection,  $4 \times 10^5$  WS229 cells were seeded onto each well of a gelatin-coated 6-well plate, grown, and then differentiated as described in the previous section (**Figure 2.2b**). *DUX4*-targeting LNA gapmers were transfected into myotubes 13 days post-differentiation with Lipofectamine® RNAiMAX (Life Technologies) according to manufacturer's instructions, except for the following modifications: 2% of RNAiMAX in OptiMEM (Life Technologies) was used for the initial dilution of the reagent, and differentiation medium was added at the last step such that it comprised 80% of the final transfection medium. LNA gapmers were transfected at a final concentration of either 1, 10, or 100 nM. To serve as negative controls, WS229 cells were either transfected with a mock LNA gapmer at the respective dose or subjected to the transfection procedure but with no AO added. Non-transfected WS234 cells were also prepared as an additional negative control. Cells were harvested the following day for RNA collection.

#### **2.5.5. RNA extraction from cells and qPCR**

Total RNA was extracted from cells using the RNeasy® Mini Kit (Qiagen), following the manufacturer's instructions with on-column DNase treatment (RNase-free DNase set, Qiagen). From this, 1400 ng was used for cDNA synthesis with SuperScript IV Reverse Transcriptase (Life Technologies) as directed by the manufacturer, using 0.5 µg of oligo(dT)<sub>12-18</sub> (Life Technologies) as primer and having a final reaction volume of 20 µl.

The synthesized cDNA was then used as a template for qPCR using the QuantStudio 3 Real-Time PCR System (Applied Biosystems). For *DUX4* and *GAPDH*, the SsoAdvanced™ Universal SYBR® Green Supermix (Bio-rad) was used, with forward and reverse primers added

to achieve final concentrations of 0.4  $\mu$ M each. Primer sequences are listed in **Table 2.5**. Gene expression was normalized against *GAPDH*.

Pre-designed TaqMan™ Gene Expression assays (Thermo Fisher) were used for qPCR-based detection of the *DUX4* downstream target genes *ZSCAN4* (Hs00537549\_m1), *TRIM43* (Hs00299174\_m1, and *MBD3L2* (Hs00544743\_m1). Reactions were prepared using these assays, the TaqMan™ Fast Advanced Master Mix (Thermo Fisher), and the synthesized cDNA using amounts recommended by the manufacturer. Expression values of all downstream target genes were normalized against *GAPDH* as well. For both SYBR and TaqMan reactions, the default “Fast” cycling program of the qPCR machine was used, 1) 95°C, 20 s, 2) 40 cycles of 95°C, 1 s then 60°C, 20 s; for SYBR reactions, there was an additional step for melt curve construction.

**Table 2.5. Primer sequences used in this study.**

<b>Gene</b>	<b>Forward (F) and reverse (R) primers, 5' to 3'</b>
<i>DUX4</i>	F: CCCAGGTACCAGCAGACC R: TCCAGGAGATGTA ACTCTAATCCA
<i>GAPDH</i>	F: GCAAATTCCATGGCACCGT R: AGGGATCTCGCTCCTGGAA
<i>RASA4</i>	F: CCCATCATCAACAAGGTGTTTG R: GGAGCACCCCTACATCCTTAAC
<i>PLEKHH3</i>	F: AGAGCTGGGAGGAGACTT R: GTACAGCCAACCTTTCACAAC
<i>MGAT4B</i>	F: GAGTCAGGTGGAGGACCAAA R: CGTAGTAGATGCCTTTGGACTG

### 2.5.6. RNA sequencing

Healthy FSHD-unaffected control, non-treated and LNA4-treated immortalized FSHD patient-derived cells were grown and differentiated as described in the *Cell culture* section, following the timeline indicated in **Figure 2.2b**. In the case of the LNA4-treated cells, transfection was done as described in Section 2.5.4, with 100 nM of LNA4 provided. Samples were prepared from three independent experiments for each condition. Total RNA was extracted via the RNeasy® Mini Kit (Qiagen), using the manufacturer's instructions with on-column DNase treatment (RNase-free DNase set, Qiagen). RNA samples were processed at the New York Genome Center (New York, NY) for high output RNA sequencing using the HiSeq 2500 system (Illumina).

Reads were aligned with STAR (version 2.4.0c),<sup>252</sup> and genes annotated in Gencode v18 were quantified with featureCounts (v1.4.3-p1).<sup>253</sup> Normalization and differential expression were done with the Bioconductor package DESeq2.<sup>254</sup> Downstream analysis and visualization of data were conducted using R (version 3.5.0). RNA sequencing data is publicly available from the SRA portal of NCBI under accession number PRJNA606474. We thank Dr. Juan Jovel, bioinformatics lead at the University of Alberta Faculty of Medicine and Dentistry The Applied Genomics Core, for their technical assistance and support for data analysis.

### 2.5.7. Myogenic fusion index and hypotrophy phenotype analysis

WS229 and WS234 cells were seeded onto gelatin-coated 24-well plates ( $2.5 \times 10^4$  cells/well), grown, and differentiated as described above. Once the cells reached 4 days post-differentiation, LNA gapmers were transfected overnight with Lipofectamine® RNAiMAX as described, at a final dose of 10 nM. Three days after transfection, cells were used for

immunocytochemistry. Following aspiration of the culture medium, cells were fixed for 5 min with 4% paraformaldehyde, washed briefly with PBS, and then incubated for 5 min in PBS with 0.5% Triton X-100. Cells were then blocked with 20% FBS (Sigma) in PBS for 1 hr, after which they were incubated in 1:200 rabbit polyclonal anti-desmin antibody (Abcam), diluted in the blocking solution, for 1 hr for visualization of muscle cells. After this, cells were subjected to three 5-min PBS washes and subsequently incubated in 1:100 Alexa594 goat anti-rabbit IgG (H+L) secondary antibody (Life Technologies) for 1 hr. Cells were once again subjected to three 5-min PBS washes and finally mounted with SlowFade Gold Antifade Mountant with DAPI (Life Technologies). All steps were conducted at room temperature; stained cells were kept at 4°C until analysis. Visualization was done using a Nikon Eclipse TE 2000-U fluorescence microscope.

The myogenic fusion index (MFI) was calculated by dividing the number of nuclei in myotubes, considered as having at least two nuclei sharing the same cytoplasm, by the total number of nuclei in an image and multiplying by 100 to arrive at a percentage value. Nuclei were counted by personnel blinded to the experimental conditions. Around 966 nuclei on average were counted (range: 548 – 1,400) for each replicate, per condition using Image J (NIH). The average MFI from three random fields of view were used for fusion index calculation for each replicate.

Myotube diameters were obtained using the measurement tool of Image J (NIH), by taking the average of three measured diameters across each myotube, and performing the measurement for at least 7-15 myotubes in a given field of view. Diameters were measured at the widest points across myotubes and away from branches or areas of overlap with other myotubes. At most 15 randomly selected myotubes were used for quantification; if less than 15 myotubes

were present in a given field of view, then all myotubes were considered for quantification. Around 40 myotubes on average were measured (range: 25-45) for each replicate, per condition.

### **2.5.8. Apoptosis assessment by flow cytometry**

WS229 and WS234 cells were seeded onto gelatin-coated 24-well plates ( $5 \times 10^4$  cells/well), grown, and differentiated as described above. At 13 days post-differentiation, LNA gapmers were transfected with Lipofectamine® RNAiMAX as previously described, at a final dose of 10 nM. The next day, cells were harvested by trypsinization, washed twice with PBS, and prepared for apoptosis evaluation via flow cytometry using the eBioscience™ Annexin V Apoptosis Detection Kit FITC (Thermo Fisher). Briefly, cells were washed once with 1x Binding Buffer and incubated in a 100  $\mu$ l solution containing 5  $\mu$ l each of fluorochrome-conjugated Annexin V and propidium iodide (PI) in 1x Binding Buffer. The mixture was incubated for 15 min at room temperature, and then cells were analyzed using Attune NxT (Life Technologies). Early apoptotic cells are Annexin-(+) and PI(-), late apoptotic cells are Annexin-(+) and PI(+). We thank Dr. Aja Rieger, Manager of the University of Alberta Faculty of Medicine and Dentistry Flow Cytometry Facility, for their technical assistance and support for this experiment.

### **2.5.9. Off-target effect evaluation**

Potential off-targets were found using GGGenome (<https://gggenome.dbcls.jp/>), which works similarly to BLAST except it is more optimized for searching databases with short sequence inputs.<sup>255</sup> Using the sequences of LNA1, LNA4, and LNA6, complementary targets with at least 1 mismatch were searched in the RefSeq human RNA release 90 (Sep 2018) database. Top hits were compiled in **Table 2.4**. No results were found with 1 mismatch for

LNA6. Three potential off-target genes, *RASA4*, *PLEKHH3*, and *MGAT4B*, were chosen for further analysis as the others were not expressed at detectable levels in muscle. Expression levels of *RASA4*, *PLEKHH3*, and *MGAT4B* were evaluated by qPCR, using SYBR as outlined in the Section 2.5.5, with primers in **Table 2.5**.

#### **2.5.10. In vivo delivery of LNA gapmers**

To visualize fluorescein-tagged gapmers, a 20- $\mu$ l injection containing 20  $\mu$ g of LNA4 in PBS was delivered intramuscularly (i.m.) to the tibialis anterior (TA) muscle in one of the legs of *FLEXDUX4* mice (n = 2). Twenty-four hours after the injection, TAs were collected and snap frozen in isopentane cooled in liquid nitrogen. The frozen tissues were kept at -80°C until further processing. For visualization of fluorescein-tagged gapmers, 8  $\mu$ m TA sections were prepared using a cryotome and visualized under a fluorescence microscope (Olympus BX61, 20X).

To determine the *in vivo* efficacy of LNA gapmer treatment, *FLEXDUX4* mice were randomly assigned to either the treatment or mock groups. For the treatment group, the *FLEXDUX4* mice (n = 5) received a 20- $\mu$ l injection containing 20  $\mu$ g of LNA4 in PBS via i.m. injections in the TA muscles of one of the legs. The injections were given every other day for a total of three i.m. injections. The TA muscles of the other legs received PBS as the control. Another five *FLEXDUX4* mice received mock LNA in one TA muscle and PBS in the contralateral TA muscle. Tissues were harvested from mice 24 hours or 7 days after the final injection. RNAs were isolated from both TA muscles and cDNA was prepared and used for SYBR-based qRT-PCR detection of *DUX4* as described previously.<sup>239</sup> Expression was normalized to *Gapdh*.<sup>256</sup>

### **2.5.11. RNA secondary structure analysis**

The Mfold RNA Folding web server (<http://unafold.rna.albany.edu/?q=mfold/RNA-Folding-Form>)<sup>257</sup> hosted by The RNA Institute, College of Arts and Sciences, State University of New York at Albany was used to determine the predicted secondary structure of *DUX4* exon 3. The *DUX4* exon 3 sequence with 50 bases of upstream (intron 2) and downstream sequences was used as input, and the pre-mRNA was folded using default parameters. The predicted folded structure with the most negative  $\Delta G$  value was used for this study.

### **2.5.12. Statistical analysis**

All statistical tests were conducted using GraphPad Prism 7 (GraphPad Software). For *in vitro* work, one-way ANOVA with post-hoc Tukey's or Dunnett's multiple comparisons test, or an unpaired two-tailed *t*-test was conducted as appropriate. For *in vivo* work, a paired *t*-test was conducted to determine the statistical significance of *DUX4* knockdown.

### **Chapter 3 *DUX4* Transcript Knockdown with Antisense 2'-O-Methoxyethyl Gapmers for the Treatment of Facioscapulohumeral Muscular Dystrophy**

Chapter 3 was derived from the following published article:

Lim, K.R.Q., Bittel, A., Maruyama, R., Echigoya, Y., Nguyen, Q., Huang, Y., Dzierlega, K., Zhang, A., Chen, Y. & Yokota, T. *DUX4* transcript knockdown with antisense 2'-O-methoxyethyl gapmers for the treatment of facioscapulohumeral muscular dystrophy. *Mol. Ther.* **29**, 848-858 (2021).

### 3.1. Abstract

Facioscapulohumeral muscular dystrophy (FSHD) is an autosomal dominant disorder characterized by a progressive, asymmetric weakening of muscles, starting with those in the upper body. It is caused by aberrant expression of the *double homeobox protein 4* gene (*DUX4*) in skeletal muscle. FSHD is currently incurable. We propose to develop a therapy for FSHD using antisense 2'-*O*-methoxyethyl (2'-MOE) gapmers, to knock down *DUX4* mRNA expression. Using immortalized patient-derived muscle cells and local intramuscular injections in the *FLExDUX4* FSHD mouse model, we showed that our designed 2'-MOE gapmers significantly reduced *DUX4* transcript levels *in vitro* and *in vivo*, respectively. Furthermore, *in vitro*, we observed significantly reduced expression of *DUX4*-activated downstream targets, restoration of FSHD signature genes by RNA sequencing, significant improvements in myotube morphology, and minimal off-target activity. This work facilitates the development of a promising candidate therapy for FSHD, and lays down the foundation for *in vivo* systemic treatment studies.

### 3.2. Introduction

FSHD is the third most common form of muscular dystrophy in the world, with 1:8,000 to 1:22,000 people affected globally.<sup>5,258</sup> FSHD is a disabling, autosomal dominant disorder primarily characterized by progressive muscle weakness that begins in the face, shoulders, and upper limbs, followed by the lower extremities.<sup>5</sup> Muscle involvement in FSHD is distinctly asymmetric, with disease severity varying across individuals. Around 15-20% of patients are wheelchair-bound.<sup>6</sup> In certain cases, often in early-onset FSHD, patients present with additional extra-muscular features, e.g. hearing loss, retinal vasculopathy, and cognitive impairment.<sup>14,15,259</sup>

Surgery and physical therapy, among others, are available to help manage symptoms and improve patient quality of life.<sup>260</sup> However, these approaches do not treat FSHD itself, and the disease remains incurable at present.

FSHD is caused by mutations promoting aberrant expression of the *double homeobox protein 4* gene (*DUX4*) in skeletal muscle. On chromosome 4q35, there is a macrosatellite array of 3.3-kb D4Z4 repeats that is typically 11-100 units long in healthy individuals. Each D4Z4 unit contains the first two exons of the *DUX4* gene.<sup>28</sup> Its third and final exon is found immediately after the most distal unit of the array and possesses a functional polyadenylation signal (PAS) only in the 4qA haplotype.<sup>29</sup> The presence of the PAS is required for successful *DUX4* transcription. In most tissues including skeletal muscle, the D4Z4 array is normally hypermethylated after early embryonic development, silencing *DUX4* expression.<sup>35,37</sup> However, in FSHD, D4Z4 methylation is reduced either through contraction of the array, mutations in genes coding for epigenetic regulators, or a combination of both.<sup>5,29,32,37,38</sup> It is now known that strict cut-offs of 4q35 D4Z4 array length (i.e.,  $\leq 10$  units) do not satisfactorily explain penetrance of the FSHD phenotype. For instance, individuals with less than 10 repeat units in this array can be asymptomatic.<sup>38</sup> While further study of the underlying genetics in this disease is warranted, it remains that these culminate in the de-repression of *DUX4*, which produces the *DUX4* transcription factor whose downstream activities are thought to cause FSHD.<sup>7</sup>

Given its central role in FSHD, reducing *DUX4* expression has been the focus of a number of therapies being developed for the disease. This was mostly achieved through the use of antisense oligonucleotides (AOs), such as those of the phosphorodiamidate morpholino oligomer (PMO) and 2'-*O*-methyl RNA (2'-OMe) chemistries. PMOs and 2'-OMe AOs were previously designed to target the *DUX4* PAS<sup>78,79</sup> or its splice sites,<sup>63,75</sup> respectively. Both

resulted in up to 50% reduced *DUX4* transcript levels *in vitro*, as well as considerable decreases in *DUX4* expression *in vivo* in xenograft and *DUX4*-transduced mouse models. More effective *DUX4* knockdown is desirable, however, since it is known that low levels of *DUX4* expression are sufficient to drive pathological changes in skeletal muscle.<sup>50</sup> Compared to PMOs and 2'-OMe AOs, which passively knock down gene expression by interfering with *DUX4* transcript maturation, use of antisense gapmers may prove more effective owing to their ability to actively induce the degradation of target mRNA transcripts via RNase H.

In the present study we therefore aimed to explore the efficacy of antisense gapmers for *DUX4* knockdown, specifically those with the 2'-MOE modification. The 2'-MOE chemistry has proven to be favorable for therapeutic AO development, with its enhanced resistance to nucleases, increased target binding affinity and specificity, as well as with four 2'-MOE-based antisense oligonucleotides already having received approval in the United States and/or the European Union.<sup>241,261–263</sup> We designed 2'-MOE gapmers against mRNA in the coding region of *DUX4* and evaluated their efficacy and specificity using immortalized FSHD patient-derived muscle cells as an *in vitro* model. We then test these gapmers *in vivo* via local intramuscular treatment in *FLEXDUX4* FSHD model mice.<sup>90</sup> Overall, we show that our 2'-MOE gapmers are potent agents of *DUX4* transcript knockdown, and serve as promising clinical trial candidates for FSHD therapy.

### **3.3. Results**

#### **3.3.1. Designed 2'-MOE gapmers effectively knock down *DUX4* transcript expression**

Three 2'-MOE gapmers were designed and tested for their potential to knockdown *DUX4* transcript levels (**Figure 3.1a, Table 3.1**). The 2'-MOE gapmers were transfected at 100 nM into

immortalized FSHD patient-derived muscle cells at 13 days post-differentiation, and cells were collected the following day for analysis. Quantitative real-time RT-PCR (qPCR) expression analysis revealed that all three 2'-MOE gapmers significantly reduced *DUX4* transcript levels almost completely (n=3,  $p<0.005$ ) (**Figure 3.1b**). No significant differences in knockdown efficacy were observed between the gapmers. Significant knockdown of the expression of *DUX4* downstream transcriptional targets *ZSCAN4*, *TRIM43*, and *MBD3L2* was observed for MOE2 and MOE3 (n=3,  $p<0.05$ ) (**Figure 3.1c**). Transfection of lower doses of the 2'-MOE gapmers led to significant *DUX4* transcript knockdown at the 10 nM but not the 1 nM dose (n=3,  $p<0.005$ ) (**Figure 3.1d**). Up to ~70% reduction in *DUX4* levels on average were observed upon treatment with 10 nM of the 2'-MOE gapmers. *ZSCAN4*, *TRIM43*, and *MBD3L2* expression levels were not affected at the 10 nM and 1 nM transfected doses of any of the 2'-MOE gapmers, however. Interestingly, treatment with lower doses of some of the 2'-MOE gapmers led to variably increased expression of *DUX4* and its downstream target genes compared to the non-treated control, particularly at the 1 nM transfected concentration (**Figure 3.1d**). Overall, these results show that the designed 2'-MOE gapmers could knock down *DUX4* transcript levels with high efficacy *in vitro*, even at reduced doses.

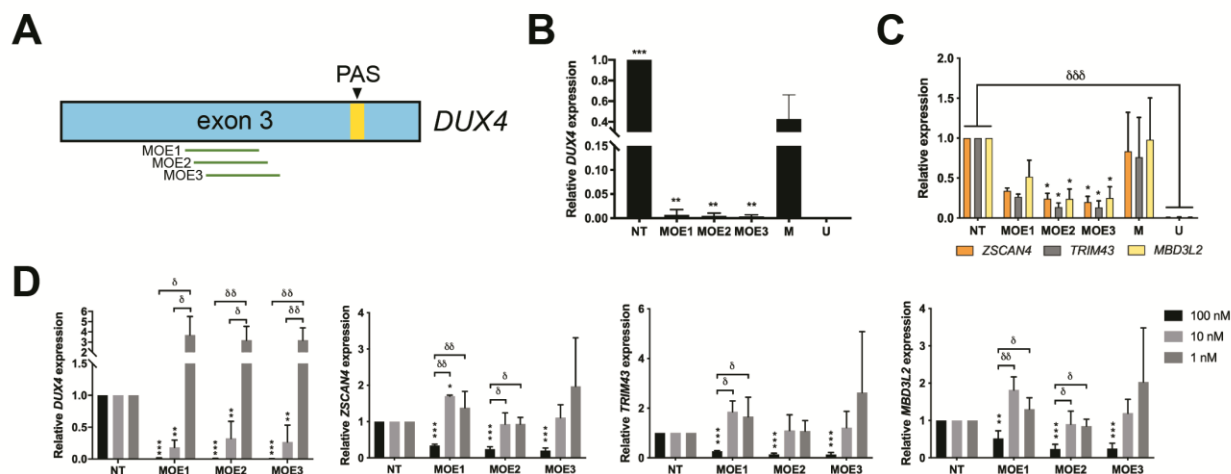


**Figure 3.1. *DUX4* knockdown efficacy evaluation of designed 2'-MOE gapmers.** (A) Scheme showing the approximate locations targeted by our 2'-MOE gapmers on *DUX4* exon 3. PAS, polyadenylation signal. Transcript levels of (B) *DUX4* and (C) *ZSCAN4*, *TRIM43*, and *MBD3L2* were evaluated by qPCR after overnight treatment of immortalized FSHD patient-derived myotubes with 100 nM of the 2'-MOE gapmers at 13 days post-differentiation. \* $p < 0.05$ , \*\* $p < 0.005$ , \*\*\* $p < 0.0005$  vs mock (M), one-way ANOVA with Dunnett's test.  $\delta\delta\delta$   $p < 0.0005$ , unpaired, two-tailed  $t$ -test. (D) Transcript levels of these same four genes after treatment with 100 nM, 10 nM, or 1 nM of the 2'-MOE gapmers, following similar culture conditions. NT, non-treated; U, FSHD-unaffected/healthy. Error bars: S.D.,  $n = 3$  independent experiments. \*\* $p < 0.005$ , \*\*\* $p < 0.0005$  vs NT, one-way ANOVA with Dunnett's test.  $\delta$   $p < 0.05$ ,  $\delta\delta$   $p < 0.005$ , one-way ANOVA with Tukey's test.

**Table 3.1. Characteristics of designed 2'-MOE gapmers against the *DUX4* transcript.**

ID	Sequence* (5' to 3')	Length (nt)	Target <i>DUX4</i> exon	GC content (%)
MOE1	<b>TAGACAGCGTCGGAAGGTGG</b>	20	3	60.0
MOE2	<b>CTAGACAGCGTCGGAAGGTG</b>	20	3	60.0
MOE3	<b>CCTAGACAGCGTCGGAAGGT</b>	20	3	60.0

\*fully phosphorothioated, bold indicates 2'-MOE nucleotides, non-bold indicates DNA

### 3.3.2 A subset of transcriptome-level alterations were restored with 2'-MOE gapmer treatment

To obtain a better idea of the restorative effects of 2'-MOE gapmer treatment at the transcriptomic level, we performed RNA sequencing analysis on total RNA extracts from immortalized healthy control myotubes and patient-derived myotubes that were either treated or not with MOE3. MOE3 was chosen since it induced the greatest reduction in *DUX4* transcript expression in our initial screen (**Figure 3.1b**). For the treatment, cells were transfected with 100 nM MOE3 at 13 days post-differentiation and harvested the following day, similar to what we did in the initial 2'-MOE gapmer screen. To obtain a list of transcripts linked to *DUX4* expression we compared our dataset to that of Rickard et al. (2015),<sup>70</sup> who performed RNA sequencing on extracts from flow cytometry-sorted *DUX4* reporter-positive primary FSHD patient myotubes and who used similar cell culture conditions as we did in this study. We initially obtained 96 overlapping transcripts with that of the Rickard et al. dataset, but excluded 2 since parameters for these were not present in all pair-wise comparisons across our groups (**Figure 3.2a**). This led us to an FSHD signature of 94 transcripts whose expression levels were significantly affected by *DUX4* expression ( $n=3$ ,  $p<0.05$ ) that consisted of 69 up-regulated and 25 down-regulated transcripts, representing 55 and 18 genes, respectively. A comparison of the expression levels obtained for these transcripts between our study and that of Rickard et al. revealed that the majority of genes had a similar direction of dysregulation (up/down) in both datasets (**Figure 3.2b**).

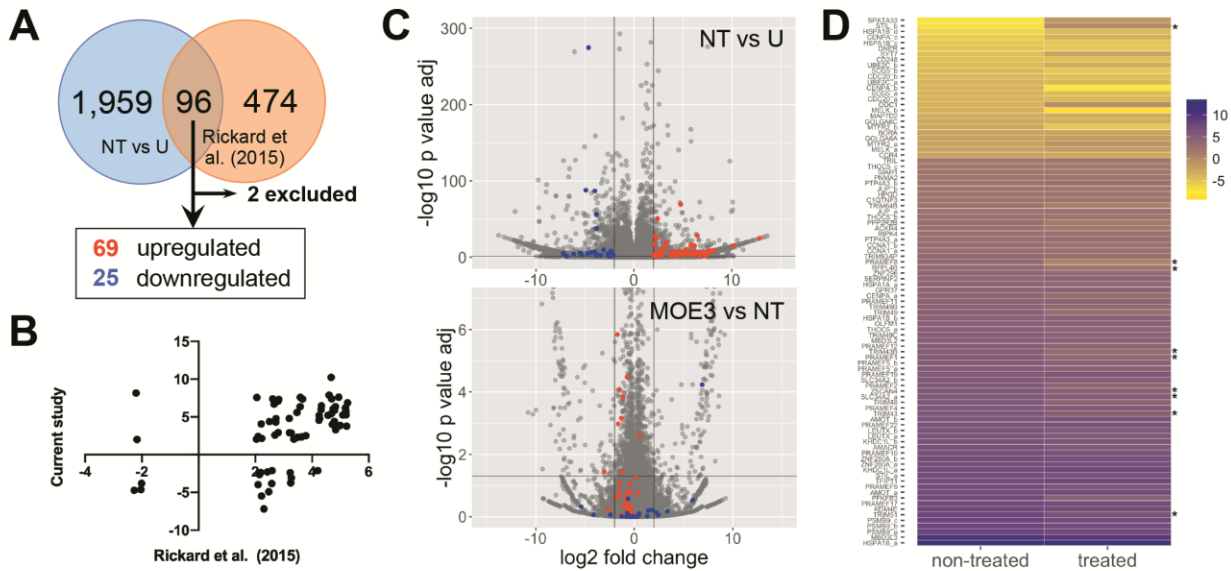


**Figure 3.2. RNA sequencing analysis of 2'-MOE gapmer-treated muscle cells.** (A) FSHD signature transcripts from comparison with the RNA sequencing results of Rickard et al. (2015), who used DUX4 reporter-positive primary FSHD patient myotubes. NT, non-treated; U, FSHD-unaaffected/healthy. (B) Plot of  $\log_2(\text{Fold Change})$  values (cut-off  $\pm 2$ ) for unique genes in the current study versus values obtained by Rickard et al. (2015). For genes with multiple transcripts in our dataset, the transcript with the least adjusted  $p$ -value was used to represent the gene. (C) Volcano plot visualizations of RNA sequencing results from our dataset. Comparisons are indicated in the upper-right, with the second listed sample as the reference. FSHD signature transcripts are shown as colored dots: up-regulated (red) and down-regulated (blue). The horizontal line represents the cut-off adjusted  $p$ -value of 0.05, and the vertical lines represent  $\log_2(\text{Fold Change})$  values of  $\pm 2$ . (D) Heat map visualization of the expression levels of the 94 FSHD signature transcripts before and after treatment with 100 nM MOE3. Expression levels are colored from high to low with purple to yellow shades, respectively. Asterisks indicate transcripts significantly restored ( $p < 0.05$ ) to healthy levels.  $n=3$  independent experiments.

We found that MOE3 treatment restored the expression of some FSHD signature transcripts to healthy levels (**Figures 3.2c,d**). Specifically, MOE3 significantly restored the expression of 8/69 (12%) up-regulated FSHD transcripts and 1/25 (4%) down-regulated transcripts (n=3,  $p<0.05$ ), all corresponding to unique genes (**Table 3.2**). Of the significantly restored up-regulated transcripts, 2 were validated by qPCR (*ZSCAN4* and *TRIM43*, **Figure 3.1c**); an additional 4 up-regulated transcripts (*MBD3L2*, *TRIM48*, *TRIM64B*, *PRAMEF4/5/9/11*) which showed non-significant restoration in RNA sequencing were demonstrated to have significantly reduced expression post-treatment by qPCR (**Figures 3.1c, 3.3; Table 3.3**).

**Table 3.2. Information on the 94 FSHD signature genes obtained from RNA sequencing analysis.**

Gene*	Transcript ID	Non-treated FSHD vs Healthy**			Treated FSHD vs Non-treated FSHD**		
		log2FC	adj. p-value	up/down?	log2FC	adj. p-value	significantly restored by treatment?
<i>HSPA1B a</i>	ENST00000391555	12.81	1.60E-25	up	0.18	0.05558362	No
<i>MBD3L3</i>	ENST00000333843	10.23	6.80E-16	up	-0.66	0.150525844	No
<i>PSMB9 a</i>	ENST00000453059	8.16	1.31E-09	up	-0.79	0.320090145	No
<i>PSMB9 b</i>	ENST00000434471	8.16	1.31E-09	up	-0.79	0.320090145	No
<i>PSMB9 c</i>	ENST00000427870	8.16	1.31E-09	up	-0.79	0.320090145	No
<i>TRIM51</i>	ENST00000449290	7.89	6.11E-09	up	-1.18	0.036749033	Yes
<i>KDM4E</i>	ENST00000450979	7.61	2.42E-08	up	-0.51	0.670007042	No
<i>PRAMEF17</i>	ENST00000376098	7.59	4.53E-08	up	-0.12	0.990219585	No
<i>PFKFB3</i>	ENST00000536985	7.58	4.68E-07	up	-2.63	0.58814826	No
<i>AMOT a</i>	ENST00000371959	7.38	2.26E-06	up	-0.13	0.992445062	No
<i>PRAMEF9</i>	ENST00000415919	7.38	6.87E-07	up	-1.12	0.457011498	No
<i>TFIP11</i>	ENST00000619735	7.37	0.011892526	up	0.49	0.983196789	No
<i>STIL a</i>	ENST00000337817	7.30	0.012435153	up	-0.61	0.982576204	No
<i>KHDCIL a</i>	ENST00000471312	7.12	8.45E-07	up	0.48	0.781306098	No
<i>ZNF280A a</i>	ENST00000302097	7.09	6.64E-07	up	-0.05	0.995731523	No
<i>ZNF280A b</i>	ENST00000620282	7.09	6.64E-07	up	-0.05	0.995731523	No
<i>PRAMEF10</i>	ENST00000235347	6.87	4.31E-06	up	-0.36	0.943642771	No
<i>AMACR</i>	ENST00000506639	6.71	0.034837731	up	-0.85	0.978289808	No
<i>KHDCIL b</i>	ENST00000370388	6.48	3.58E-29	up	-0.20	0.821838147	No
<i>LEUX a</i>	ENST00000396841	6.36	1.06E-07	up	-0.65	0.30504829	No
<i>LEUX b</i>	ENST00000629267	6.36	1.06E-07	up	-0.65	0.30504829	No
<i>PRAMEF22</i>	ENST00000616664	6.36	3.43E-05	up	0.14	0.991303373	No
<i>AMOT b</i>	ENST00000304758	6.21	6.02E-05	up	0.18	0.987440238	No
<i>TRIM43</i>	ENST00000272395	6.19	1.02E-15	up	-1.31	0.00068713	Yes
<i>PRAMEF4</i>	ENST00000235349	6.05	2.74E-05	up	-0.50	0.768132302	No
<i>TRIM48</i>	ENST00000417545	5.96	0.000173991	up	-1.72	0.249308715	No
<i>SLC34A2 a</i>	ENST00000382051	5.88	4.53E-17	up	-0.73	3.34E-05	Yes
<i>ZSCAN4</i>	ENST00000612521	5.86	5.07E-16	up	-1.15	0.00014191	Yes
<i>PRAMEF2</i>	ENST00000240189	5.76	1.04E-06	up	-1.52	0.133552181	No
<i>SLC34A2 b</i>	ENST00000513204	5.75	3.45E-06	up	-0.44	0.747265402	No
<i>PRAMEF19</i>	ENST00000376101	5.60	0.000249056	up	0.25	0.982576204	No
<i>PRAMEF5 a</i>	ENST00000622421	5.45	1.85E-08	up	-0.73	0.475006079	No
<i>PRAMEF5 b</i>	ENST00000621481	5.45	1.85E-08	up	-0.73	0.475006079	No
<i>PRAMEF1</i>	ENST00000332296	5.36	1.14E-07	up	-1.51	8.51E-05	Yes
<i>TRIM43B</i>	ENST00000432468	5.28	3.97E-11	up	-1.64	0.001063378	Yes
<i>PRAMEF12</i>	ENST00000357726	5.26	5.65E-07	up	-0.80	0.345957318	No
<i>MBD3L2</i>	ENST00000381393	5.21	4.98E-10	up	-0.37	0.576811781	No

**Table 3.2. (cont'd.)**

Gene*	Transcript ID	Non-treated FSHD vs Healthy**			Treated FSHD vs Non-treated FSHD**		
		log2FC	adj. p-value	up/down?	log2FC	adj. p-value	significantly restored by treatment?
<i>TRIM49C</i>	ENST00000448984	5.21	0.000369479	up	-0.56	0.876161011	No
<i>THOC5 a</i>	ENST00000488052	5.18	8.26E-07	up	-0.69	0.495486875	No
<i>OLFM1</i>	ENST00000252854	4.81	8.15E-05	up	0.12	0.988946093	No
<i>HSPA1B b</i>	ENST00000391548	4.78	4.55E-70	up	-0.02	0.991152883	No
<i>TRIM49</i>	ENST00000329758	4.78	0.000403045	up	-1.55	0.187848853	No
<i>TRIM49B</i>	ENST00000332682	4.56	1.13E-07	up	-0.73	0.30431758	No
<i>PRAMEF11</i>	ENST00000619922	4.40	0.010586296	up	-0.13	0.992833412	No
<i>CENPA a</i>	ENST00000475662	4.40	0.000326357	up	-1.17	0.84823361	No
<i>GPR37</i>	ENST00000303921	4.39	1.19E-08	up	0.14	0.981222213	No
<i>HSPA1A a</i>	ENST00000441618	4.31	0.000662654	up	-0.39	0.18443152	No
<i>SERPINF2</i>	ENST00000382061	4.07	6.14E-05	up	0.38	0.891316067	No
<i>ZNF296</i>	ENST00000303809	4.02	0.004702231	up	-0.35	0.969612411	No
<i>RFPL4B</i>	ENST00000441065	3.87	8.47E-08	up	-1.72	1.44E-06	Yes
<i>PRAMEF8</i>	ENST00000357367	3.78	0.019759829	up	-3.05	0.035391996	Yes
<i>TRIM53AP</i>	ENST00000532014	3.75	0.001015777	up	-0.70	0.597602437	No
<i>CCNA1 a</i>	ENST00000255465	3.31	3.94E-19	up	-0.37	0.463772143	No
<i>CCNA1 b</i>	ENST00000625767	3.27	2.05E-16	up	-0.45	0.09064676	No
<i>PTP4A3 a</i>	ENST00000520105	2.99	3.12E-13	up	0.43	0.166532775	No
<i>RIPK4</i>	ENST00000332512	2.93	6.86E-10	up	-0.03	0.995355899	No
<i>ACKR4</i>	ENST00000249887	2.90	0.000808967	up	-0.89	0.226235022	No
<i>PPP2R2B</i>	ENST00000394411	2.87	0.004828947	up	-1.23	0.845669111	No
<i>THOC5 b</i>	ENST00000484924	2.78	3.42E-05	up	-0.35	0.909720201	No
<i>JUP a</i>	ENST00000449889	2.59	3.54E-07	up	0.21	0.957590214	No
<i>TRIM64B</i>	ENST00000329862	2.51	0.02102623	up	-1.45	0.077007169	No
<i>CIQTNF3</i>	ENST00000231338	2.41	3.24E-51	up	-0.12	0.916619331	No
<i>HPGD</i>	ENST00000296522	2.37	0.04900649	up	0.12	0.992774603	No
<i>JUP b</i>	ENST00000591690	2.30	8.74E-07	up	0.00	0.999964077	No
<i>PTP4A3 b</i>	ENST00000521578	2.29	2.12E-25	up	0.58	0.002408606	No
<i>PNMA2</i>	ENST00000522362	2.15	1.87E-28	up	0.03	0.991303373	No
<i>SLAH1</i>	ENST00000356721	2.06	0.004347022	up	0.05	0.99534489	No
<i>THOC5 c</i>	ENST00000443089	2.05	1.24E-17	up	-0.20	0.772030789	No
<i>TRIL</i>	ENST00000539664	2.01	0.001074742	up	0.04	0.994199094	No
<i>CCR4</i>	ENST00000330953	-2.11	0.005067901	down	-0.53	0.971783714	No
<i>MELK a</i>	ENST00000298048	-2.12	0.000252848	down	0.40	0.94825751	No
<i>MTFR2 a</i>	ENST00000420702	-2.28	0.010004786	down	1.43	0.630429768	No
<i>GOLGA6A</i>	ENST00000290438	-2.34	5.35E-09	down	0.50	0.791090752	No
<i>BORA</i>	ENST00000377815	-2.38	0.009935466	down	0.05	0.999371732	No

**Table 3.2. (cont'd.)**

Gene*	Transcript ID	Non-treated FSHD vs Healthy**			Treated FSHD vs Non-treated FSHD**		
		log2FC	adj. p-value	up/down?	log2FC	adj. p-value	significantly restored by treatment?
<i>MTFR2 b</i>	ENST00000451457	-2.56	0.036193589	down	-2.42	0.866364671	No
<i>GOLGA6C</i>	ENST00000300576	-2.63	3.60E-05	down	-0.79	0.98271602	No
<i>MAP7D2</i>	ENST00000379643	-3.08	2.21E-10	down	0.14	0.992774603	No
<i>MELK b</i>	ENST00000626154	-3.38	0.003594245	down	-5.38	0.478787787	No
<i>ODC1</i>	ENST00000446285	-3.74	0.0101774	down	3.37	0.667785883	No
<i>CDC20 a</i>	ENST00000372462	-3.75	0.000246158	down	-0.34	0.992833412	No
<i>SCG5 a</i>	ENST00000475752	-3.81	2.45E-38	down	-0.71	0.776061124	No
<i>CENPA b</i>	ENST00000233505	-3.83	0.012455446	down	-4.13	0.862519595	No
<i>UBE2C a</i>	ENST00000356455	-3.83	5.08E-57	down	-0.24	0.944545174	No
<i>CDC20 b</i>	ENST00000310955	-3.98	1.25E-87	down	-0.63	0.263401187	No
<i>SCG5 b</i>	ENST00000498607	-3.99	1.17E-07	down	-1.28	0.967200594	No
<i>UBE2C b</i>	ENST00000372568	-4.33	5.29E-07	down	1.31	0.943676285	No
<i>CD248</i>	ENST00000311330	-4.62	2.42E-275	down	-0.08	0.987440238	No
<i>SYT7</i>	ENST00000542836	-4.71	1.31E-05	down	2.44	0.868797513	No
<i>DNER</i>	ENST00000341772	-4.91	1.32E-88	down	-0.11	0.991213343	No
<i>HSPA1B c</i>	ENST00000445736	-5.32	0.002037533	down	0.24	0.997320359	No
<i>CENPA c</i>	ENST00000335756	-5.48	2.08E-06	down	2.20	0.716243485	No
<i>HSPA1B d</i>	ENST00000450744	-6.14	5.68E-05	down	1.80	0.6047912	No
<i>STIL b</i>	ENST00000447475	-6.84	0.025544257	down	6.90	5.84E-05	Yes
<i>SPATA33</i>	ENST00000579310	-7.19	7.01E-06	down	5.94	0.294771871	No

\*letters after the underscore are arbitrary identifiers of different transcripts from the same gene

\*\*this group served as reference for the comparison

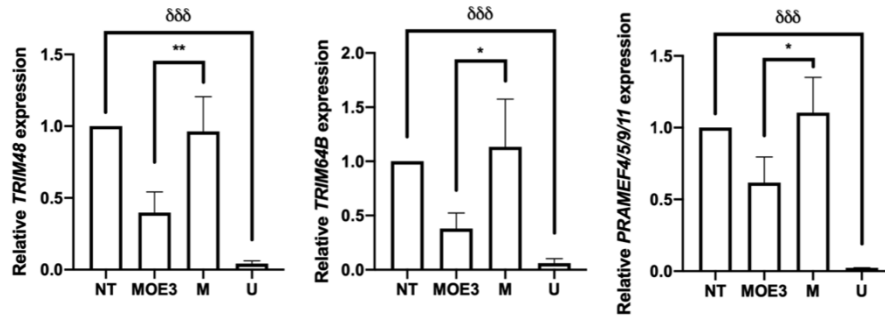


**Figure 3.3. qPCR analysis of *TRIM48*, *TRIM64B*, and *PRAMEF4/5/9/11* expression.** Relative expression levels of *TRIM48*, *TRIM64B*, and *PRAMEF4/5/9/11*, all significantly up-regulated FSHD-associated genes identified from our RNA sequencing analysis, were found to be significantly reduced by MOE3 treatment compared to mock gapmer-treated (M) controls. NT, non-treated; U, FSHD-unaffected/healthy. Error bars: S.D., n=3. \* $p < 0.05$ , \*\* $p < 0.005$  vs M, one-way ANOVA with Dunnett's test.  $\delta\delta\delta p < 0.0005$ , unpaired, two-tailed  $t$ -test.

**Table 3.3. Validation of some FSHD signature genes from RNA sequencing analysis.**

Transcript	Status in FSHD	Significantly restored by treatment in RNA-seq?	Validated by qPCR? (status, figure)
<i>TRIM51</i>	up-regulated	yes	not validated
<i>TRIM43</i>	up-regulated	yes	yes (restored, Fig. 1C)
<i>SLC34A2_a</i>	up-regulated	yes	not validated
<i>ZSCAN4</i>	up-regulated	yes	yes (restored, Fig. 1C)
<i>PRAMEF1</i>	up-regulated	yes	not validated
<i>TRIM43B</i>	up-regulated	yes	not validated
<i>RFPL4B</i>	up-regulated	yes	not validated
<i>PRAMEF8</i>	up-regulated	yes	not validated
<i>MBD3L2</i>	up-regulated	no	yes (restored, Fig. 1C)
<i>TRIM48</i>	up-regulated	no	yes (restored, Fig. S1)
<i>TRIM64B</i>	up-regulated	no	yes (restored, Fig. S1)
<i>PRAMEF4/5/9/11</i>	up-regulated	no	yes (restored, Fig. S1)
<i>STIL_b</i>	down-regulated	yes	not validated

### 3.3.3. Improvements in cellular phenotypes upon 2'-MOE gapmer treatment

Myotube fusion and size are two phenotypes negatively affected by aberrant *DUX4* expression and signaling in skeletal muscle.<sup>7,237,240</sup> We sought to determine if 2'-MOE gapmer treatment could promote increased muscle fusion and decreased hypotrophic characteristics *in vitro*. Qualitatively, immunocytochemistry showed that immortalized FSHD patient-derived muscle cells treated with 10 nM of the 2'-MOE gapmers had larger, extensive myotubes with more nuclei than the non-treated or mock gapmer-treated controls (**Figure 3.4a**). All 2'-MOE gapmer-treated muscle cells had significantly increased myogenic fusion indices (MFIs), reaching up to 55% higher MFIs on average than the mock control (n=3,  $p<0.05$ ) (**Figure 3.4b**). No significant MFI differences were observed across the gapmer-treated groups. Myotube diameters were also significantly increased by the treatment (n=3,  $p<0.0005$ ), shifting the frequency distribution peak from 15-20  $\mu\text{m}$  to 20-25  $\mu\text{m}$ , similar to that of the healthy control (**Figures 3.4c,d**). Once again, no significant differences in myotube diameters were observed between gapmer-treated groups. Moreover, Western blot analysis revealed that myosin heavy chain protein levels were observably but non-significantly increased by treatment with 100 nM of MOE3 compared to mock-treated controls (n=3,  $p=0.0828$ ) (**Figure 3.5**). On the other hand, we saw no effect of 10 nM 2'-MOE gapmer treatment on muscle cell apoptosis, another *in vitro* phenotype that characterizes FSHD (**Figure 3.4e**).<sup>7,51</sup>

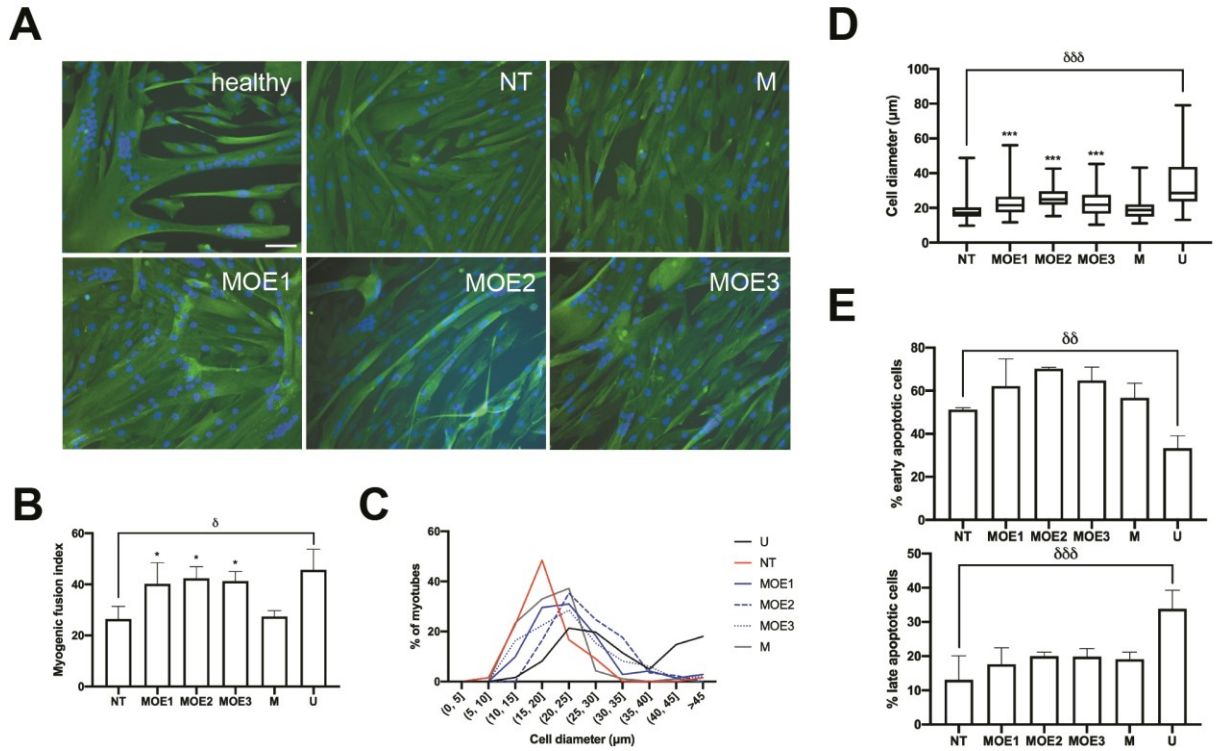


**Figure 3.4. *In vitro* muscle cell phenotypes after 2'-MOE gapmer treatment.** (A) Representative immunocytochemistry images of healthy immortalized control myotubes, and non-treated (NT), mock 2'-MOE gapmer-treated (M), and *DUX4*-specific MOE gapmer-treated (MOE1, MOE2, MOE3) immortalized FSHD patient-derived myotubes stained for nuclei (blue) and desmin (green). In this case, patient-derived myotubes were transfected with 10 nM of the various 2'-MOE gapmers at 4 days post-differentiation and then stained 3 days later. Scale bar: 100  $\mu\text{m}$ . (B) Myogenic fusion index quantification for the various treatment groups. (C) Frequency distribution of myotube diameters across the different treatment groups.  $n=3$  independent experiments; 382 nuclei and 26 myotubes on average for each replicate, per condition were counted for quantification of MFI and muscle cell diameters, respectively. (D) Individual myotube diameters from (C) were plotted. (E) Early and late apoptotic cell populations in immortalized FSHD patient-derived myotubes treated with 10 nM of the various 2'-MOE gapmers at 13 days post-differentiation were quantified by Annexin V/propidium iodide-based flow cytometry 1 day later. U, FSHD-affected/healthy. For (B) and (E), error bars: S.D.,  $n=3$  independent experiments. For (D), the box represents  $P_{25}$ - $P_{75}$  with the central line marking the median, and the whiskers represent the range;  $n=3$ . \* $p<0.05$ , \*\*\* $p<0.0005$  vs M, one-way ANOVA with Dunnett's test.  $\delta$   $p<0.05$ ,  $\delta\delta$   $p<0.005$ ,  $\delta\delta\delta$   $p<0.0005$ , unpaired, two-tailed  $t$ -test.

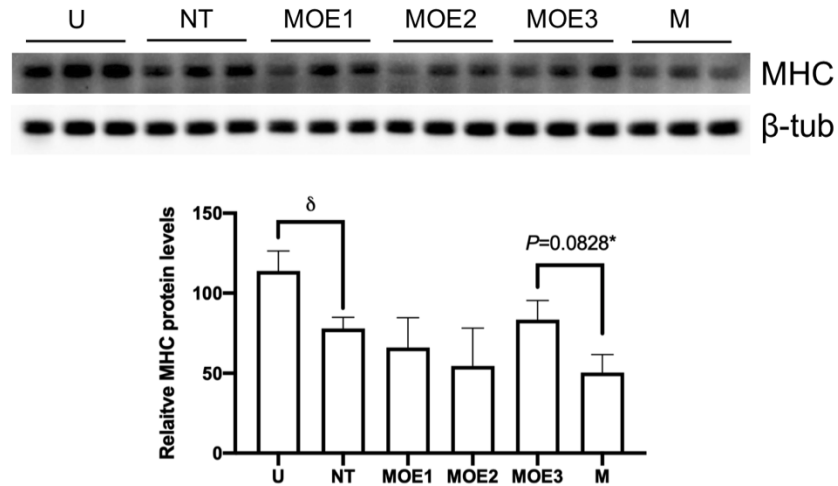


**Figure 3.5. Western blot analysis of myosin heavy chain protein levels.** Myosin heavy chain (MHC) protein levels were detected via Western blot, with  $\beta$ -tubulin ( $\beta$ -tub) as the loading control. Protein samples (12  $\mu$ g) were extracted from healthy WS234 myotubes (U), non-treated FSHD WS229 myotubes (NT), 2'-MOE gapmer-treated WS229 myotubes (MOE1-MOE3), and mock 2'-MOE gapmer-treated WS229 myotubes (M). Top: image of the visualized Western blot, bottom: quantification of MHC protein levels normalized to  $\beta$ -tub and calculated relative to one replicate from the healthy myotube samples. Error bars: S.D., n=3. \*one-way ANOVA with Dunnett's test vs M.  $\delta$   $p < 0.05$ , unpaired, two-tailed  $t$ -test.

### 3.3.4. Off-target effect analysis of 2'-MOE gapmer treatment

Using GGGenome, we compiled a list of sequences from other genes sharing the highest degree of similarity possible to the *DUX4* target sequence of our 2'-MOE gapmers (**Table 3.4**). In part due to the length of the 2'-MOE gapmers, the closest sequences we could find were those having at least a 3-bp mismatch to the targeted *DUX4* sequence. We examined whether the expression levels of these genes were knocked down upon 100 nM 2'-MOE gapmer treatment in immortalized FSHD patient-derived cells. Upon further testing, only *BANF1*, *SSR4*, *FARP1*, and *ZBTB7B* had detectable expression in FSHD patient-derived myotubes. Treatment with the 2'-MOE gapmers did not significantly reduce the transcript levels of these genes, except for *BANF1*, which was significantly knocked down by MOE1 and MOE2 (n=3,  $p<0.05$  and  $p<0.005$ , respectively) (**Figures 3.6a-d**). MOE1 treatment also significantly increased the expression of *ZBTB7B* (n=3,  $p<0.005$ ). However, by the nature of the change, this is not considered a direct off-target effect resulting from gapmer-mediated knockdown. Importantly, we note that the expression levels of all four potential off-target genes were not affected by MOE3.

**Table 3.4. Potential off-target transcripts of the 2'-MOE gapmers, as determined by GGGenome**

Gene	Transcript variant/s	Sequence showing mismatch	# mismatches to 2'-MOE gapmer target sequence		
			MOE1	MOE2	MOE3
<i>DUX4</i>	n/a	CCACCTTCCGACGCTGTCTAGG	0	0	0
<i>GALNT14</i>	4	CCACCTTCC <b>GG</b> ACGCTG <b>ACT</b> -GG	3	3	3
<i>FOXH1</i>	n/a	CC-CCT <b>GCCC</b> ACGCTGTCT <b>ACC</b>	3	4	5
<i>SSR4</i>	1-4	CCA-CTTCT <b>TG</b> ACGCTGTC- <b>ATT</b>	3	4	5
<i>ZBTB7B</i>	1-5	<b>AC</b> ACCTTCC <b>GCCTCTCT</b> CTAG <b>C</b>	4	3	4
<i>TSPEAR-ASI</i>	n/a	CCACCT <b>GCCGA</b> -GCTGTC- <b>AGC</b>	3	3	4
<i>FARP1</i>	1,3	<b>TC</b> ACCTT <b>T</b> CCGA-GCTGTCT- <b>GT</b>	4	3	4
<i>BANF1</i>	1,2	<b>GTA</b> -CTTCC <b>GG</b> CGCTGTCT <b>CGG</b>	5	4	3

\*bold indicates mispairing, dash/underline indicates indels versus the *DUX4* target sequence

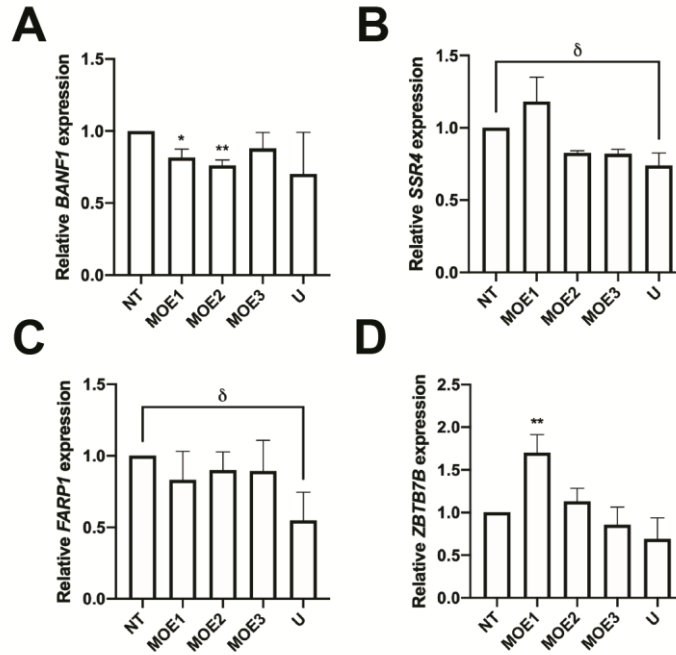


**Figure 3.6. Off-target effect evaluation upon 2'-MOE gapper treatment.** Immortalized patient-derived myotubes transfected with 100 nM of MOE1, MOE2, or MOE3 (numbered) at 13 days post-differentiation were harvested a day later and used for qPCR expression analysis of (A) *BANF1*, (B) *SSR4*, (C) *FARP1*, and (D) *ZBTB7B*. NT, non-treated; U, FSHD- unaffected/healthy. Error bars: S.D., n=3 independent experiments. \* $p < 0.05$ , \*\* $p < 0.005$  vs NT, one-way ANOVA with Dunnett's test.  $\delta$   $p < 0.05$ , unpaired, two-tailed  $t$ -test.

### 3.3.5. 2'-MOE gapmer treatment reduces DUX4 expression in an FSHD mouse model

*FLEXDUX4* mice carry a floxed human full-length *DUX4* transgene, and express very low levels of *DUX4* transcript even without Cre-mediated induction.<sup>90</sup> To determine the *in vivo* efficacy of local 2'-MOE gapmer treatment, we treated adult hemizygous *FLEXDUX4* mice with 20 µg i.m. injections of MOE3 to the tibialis anterior (TA) every other day for six days. MOE3 was chosen given its increased capacity to reduce *DUX4* transcript expression as previously mentioned, and also from its favorable performance in the off-target effect analysis. For each mouse, MOE3 was injected in one of the legs while vehicle (phosphate-buffered saline or PBS) was injected in the other. qPCR was performed to determine *DUX4* expression levels a day after the third injection; as the low level of *DUX4* expression in *FLEXDUX4* mice is not sufficient to induce *DUX4* downstream genes,<sup>90</sup> we were not able to evaluate for their expression in this experiment. Our results showed that injection of MOE3 into the TA of *FLEXDUX4* mice significantly reduced *DUX4* mRNA expression compared to the contralateral limb that only received a PBS injection (n=5,  $p<0.05$ ) (**Figure 3.7**). Similar injection of a scrambled 2'-MOE gapmer control did not have an effect on *DUX4* mRNA expression in *FLEXDUX4* mice; MOE3 significantly knocked down *DUX4* transcript levels compared to the scrambled control (n=5 MOE3-treated mice, n=3 scrambled gapmer-treated mice,  $p<0.05$ ).

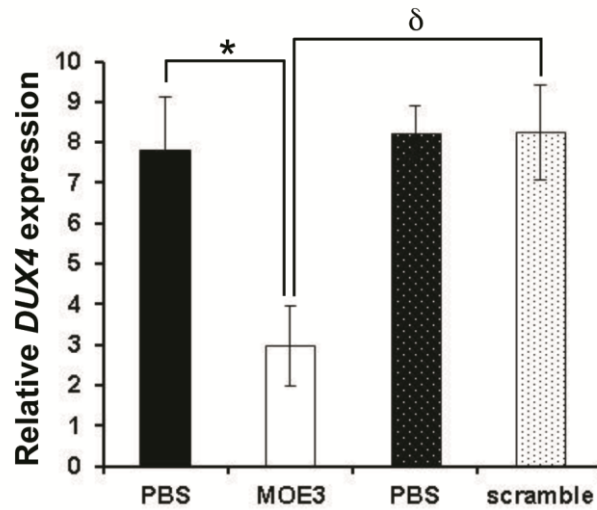


**Figure 3.7. *In vivo* efficacy of MOE3 gapmer treatment in *FLEXDUX4* mice.** Intramuscular injections of 20  $\mu$ g MOE3 to the TA muscles (one leg with MOE3 and the contralateral leg with PBS) every other day for a total of 3 injections showed knockdown of *DUX4* mRNA by qPCR one day after the last injection. No knockdown was observed when a 2'-MOE gapmer control with a scrambled sequence was injected instead. Bars with similar patterns (block or hashed) indicate leg pairs. Error bars: S.E.M.  $n=5$  for MOE3/PBS mice and  $n=3$  for scrambled 2'-MOE/PBS mice.  $*p<0.05$ , paired, two-tailed *t*-test.  $\delta p<0.05$ , unpaired, two-tailed *t*-test.

### 3.4. Discussion

Since initial demonstrations of their effective knockdown abilities *in vitro*,<sup>264,265</sup> 2'-MOE gapmers have proceeded to become one of the most successful AO chemistries in clinical development. Two AO gapmers have been given U.S. Food and Drug Administration (FDA) approval thus far, mipomersen (Kynamro, Ionis) for familial hypercholesterolemia and inotersen (Tegsedi, Akcea) for hereditary transthyretin amyloidosis, both of which are of the 2'-MOE chemistry.<sup>241,243,266</sup> A third, volanesorsen (Waylivra, Akcea), has received conditional marketing authorization at the European Union for the treatment of familial chylomicronemia syndrome.<sup>262</sup> Volanesorsen is currently under review for its second attempt at obtaining FDA approval. Although not a gapmer, there is the FDA-approved nusinersen (Spinraza, Biogen) for spinal muscular atrophy treatment, an AO composed entirely of 2'-MOE nucleotides.<sup>267,268</sup> There are also many 2'-MOE gapmers under clinical and pre-clinical development, e.g. for Huntington's disease, amyotrophic lateral sclerosis, Alzheimer's disease, among others.<sup>261</sup> Furthermore, 2'-MOE gapmers have favorable safety and pharmacokinetic profiles *in vivo*. Integrated assessments of 2'-MOE gapmer toxicity in non-human primates and human subjects found no safety concerns for liver and kidney function; cases of thrombocytopenia and complement activation were observed, however these were limited to animal models and not humans.<sup>269,270</sup> These AOs are stable *in vivo*, display broad tissue distribution, and have an elimination half-life of 2-4 weeks across tissues and species,<sup>270</sup> indicating the possibility of reduced patient administrations. With such a proven track record, in this study we sought to adapt the use of these 2'-MOE gapmers for the treatment of FSHD by targeting *DUX4* transcript knockdown.

We successfully demonstrated that our designed 2'-MOE gapmers could significantly reduce *DUX4* expression in immortalized patient-derived differentiated muscle fibers (**Figure**

**3.1b)** and in the *FLEXDUX4* FSHD mouse model (**Figure 3.7**). At the highest *in vitro* tested dose of 100 nM, we observed corresponding reductions in the expression of DUX4 downstream target genes *ZSCAN4*, *TRIM43*, and *MBD3L2* (**Figure 3.1c**). MOE3 was particularly effective among the three *DUX4*-targeting 2'-MOE gapmers. Notably, the extent of *DUX4* knockdown achieved here was comparably better than what was previously observed with PMO or 2'-OMe AOs, supporting the notion that a direct, RNase H-mediated approach to transcript knockdown is more effective at reducing gene expression than an indirect approach that relies on steric blocking AOs. We also showed that 2'-MOE treatment did not significantly reduce the expression of three out of four potential off-target genes (**Figures 3.6b-d**). However, we did observe significantly decreased *BANFI* expression upon treatment with MOE1 and MOE2 (**Figure 3.6a**). *BANFI* codes for a DNA-binding protein with roles in cell cycle progression, chromatin organization, and early development.<sup>271,272</sup> It has been reported that *BANFI* is important for mouse and human embryonic stem cell (ESC) self-renewal, with *BANFI* knockdown leading to their decreased survival and cloning efficiency.<sup>272</sup> In mouse ESCs, this also led to decreased pluripotent gene expression and increased differentiation. Since DUX4 is known to up-regulate genes associated with stem cells, as well as in generating an overall less-differentiated gene expression signature in skeletal muscle,<sup>62,273</sup> there is the possibility that *BANFI* is a downstream DUX4 target. As such, its decreased expression may have been an indirect result of *DUX4* knockdown, but this remains to be proven.

We further confirmed the potential restorative effects of 100 nM MOE3 treatment at the transcriptomic level by RNA sequencing analysis (**Figure 3.2**). Aside from confirming the significant reduction of *ZSCAN4* and *TRIM43* expression ( $p < 0.05$ ), we found that MOE3 treatment significantly decreased the expression of *TRIM43B*, *TRIM51*, *TRIM64B*, *PRAMEF1*,

and *PRAMEFB* (Figures 3.2d, 3.3; Tables 3.2, 3.3), which belong to gene families known to be up-regulated by *DUX4*.<sup>7,274</sup> We also observed a significant reduction in *SLC34A2* and *RFPL4B* expression, which have both been associated with FSHD;<sup>275,276</sup> *SLC34A2* in particular has been recently reported as an FSHD protein biomarker.<sup>276</sup> The roles of all these genes in FSHD pathogenesis are yet to be determined, however. On another note, while *DUX4* downstream target expression was reduced at the 100 nM gapmer dose, this was not the case at the 10 nM dose despite significant knockdown of *DUX4* transcript expression at this condition (Figure 3.1d). Increased 2'-MOE gapmer doses are recommended, as the level of *DUX4* knockdown at 10 nM may not have been sufficient to generate observable downstream effects. This once again stresses the need to achieve complete *DUX4* knockdown as much as possible, since any remaining low levels of *DUX4* expression<sup>50</sup> may be enough to maintain the dysregulated transcriptomic landscape seen in FSHD muscle. This scale-up of dose should be achievable in vivo, as 2'-MOE gapmers are non-toxic even at higher doses in humans—up to 475 mg in one study by subcutaneous or intravenous administration<sup>269</sup>—and a repeated dosing regimen can be easily established. On another note, we interestingly observed increased expression of *DUX4* and its downstream target genes upon treatment with some 2'-MOE gapmers at lower doses. We are not certain why this occurs—however, this phenomenon has also been observed in a previous report that instead treated primary FSHD patient-derived muscle fibers with *DUX4*-targeting PMOs.<sup>79</sup> In this study, expression levels of the downstream target genes *ZSCAN4*, *TRIM43*, and *MBD3L2* were evaluated as well, and were increased after treatment with 10  $\mu$ M of certain PMOs. As there are numerous differences between this work and ours, e.g. cell culture schedule, antisense chemistry employed and transfection dose used, a direct comparison to identify potential reasons for this increased expression post-treatment is not possible. However, these

observations provide valuable insight into considerations for future antisense therapy development, particularly concerning treatment dose, to minimize or prevent the occurrence of such off-target effects.

DUX4 orchestrates a large number of abnormal signaling events in skeletal muscle, whose cumulative effects give rise to FSHD.<sup>7</sup> One critically affected pathway is muscle development, with DUX4 down-regulating genes for Pax7, MyoD, and myogenin, among others.<sup>57</sup> As a result, FSHD myoblasts exhibit defects in fusion and differentiation, giving rise to abnormal or deformed myotube morphologies.<sup>237,240</sup> Treatment with *DUX4*-targeting 2'-MOE gapmers led to significant improvements in FSHD patient-derived muscle cell fusion, differentiation, and growth (**Figures 3.4a-d, 3.5**). In particular, treatment brought a large proportion of muscle fibers to over 20  $\mu\text{m}$  in diameter, a size threshold below which characterized hypotrophic-type FSHD patient myotubes in a previous study.<sup>237</sup> It is interesting to note that at a 10 nM transfected 2'-MOE dose, phenotypic improvements in muscle cell morphology were observed but not apoptosis (**Figure 3.4e**). This may be partly explained by the knowledge that DUX4 dysregulates far more pathways contributing to apoptosis than those involved in muscle development.<sup>7</sup> As we previously observed for low 2'-MOE gapmer doses on *in vitro* DUX4 downstream target gene expression (**Figure 3.1d**), even higher doses than those tested in this study may be required to achieve observable effects on apoptosis.

Finally, it is encouraging that we observed significant *DUX4* transcript reduction with three 20- $\mu\text{g}$  i.m. injections of MOE3 in *FLEXDUX4* mice (**Figure 3.7**), supporting the knockdown efficacy of our 2'-MOE gapmers not only *in vitro* but also *in vivo*. Practically, this supports the potential of i.m. injections for the muscle-specific treatment of FSHD, given how the disease exhibits asymmetric involvement of muscle groups.<sup>5</sup> Furthermore, this promising

proof-of-concept result sets the stage for future experiments, particularly evaluation of the therapeutic efficacy of our 2'-MOE gapmers upon systemic treatment. It would be beneficial to test these gapmers in Cre-induced *FLEXDUX4* mice,<sup>90</sup> to examine whether 2'-MOE gapmer treatment can restore DUX4-mediated downstream gene expression to normal levels and rescue FSHD phenotypes. For instance, a recent study presented that *FLEXDUX4* mice crossed to *ACTA1-Mer-cre-Mer* (*ACTA1-MCM*; with a skeletal muscle-specific and tamoxifen-inducible promoter) mice produce bi-transgenic animals showing FSHD-like phenotypes, e.g. with significantly decreased skeletal muscle function.<sup>277</sup> As disease severity can be modulated in these mice, this would be an interesting potential model for further testing of our 2'-MOE gapmers. In summary, we were able to design *DUX4*-targeting 2'-MOE gapmers that could effectively reduce *DUX4* transcript expression *in vitro* and *in vivo*, with improvements in some cellular phenotypes. Future work will evaluate the therapeutic efficacy and safety of these gapmers when administered systemically in a more severe FSHD animal model, to further assess their potential as candidate FSHD therapeutics.

### **3.5. Methods**

#### **3.5.1. Antisense oligonucleotides, cell culture**

Our group designed three 2'-MOE gapmers (MOE1-3) with target sequences on *DUX4* exon 3, before the PAS (**Figure 3.1a**). Target sites were chosen based on GC content and the mRNA secondary structure at the region. All gapmers were 20-bp long, fully phosphorothioated, consisted of a central 10-bp DNA segment flanked by 5-bp of 2'-MOE-modified nucleotides on each side, and synthesized by Eurogentec (Belgium). Gapmer sequences and characteristics are summarized in **Table 3.1**.

Cell culture was performed using immortalized WS229 FSHD patient-derived and WS234 healthy control myoblasts obtained in kind from the University of Massachusetts Medical School (MA, USA) Wellstone Program. Cells were derived from biceps biopsies of siblings and immortalized via stable *CDK4/hTERT* cassette integration<sup>251</sup> (**Table 3.5**). For growing cells, a growth medium was prepared with 15% fetal bovine serum (FBS) (Sigma, St. Louis, MO), 0.055 µg/ml dexamethasone, 2.5 ng/ml recombinant human hepatocyte growth factor (EMD Millipore, Burlington, MA), and 10 ng/ml recombinant human fibroblast growth factor (BioPioneer, San Diego, CA) in basal medium (BM; 20% Medium 199 [Life Technologies, Carlsbad, CA], 0.03 µg/ml ZnSO<sub>4</sub>, 1.4 µg/ml vitamin B12, and 2.5% penicillin-streptomycin in DMEM [Life Technologies]). For differentiation, the following was prepared: 15% KnockOut Serum Replacement (KOSR; Life Technologies),<sup>239</sup> 10 µg/ml insulin (Sigma), and 100 µg/ml human apo-transferrin (R&D Systems, Minneapolis, MN) in BM. All cells were cultured at 37°C and 5% CO<sub>2</sub>.

**Table 3.5. Characteristics of the immortalized human muscle cells used in this study.**

<b>Cell ID</b>	<b>Disease Status</b>	<b>Sex</b>	<b>Age at biopsy</b>	<b>EcoRI/BlnI allele size (4q haplotype)</b>
WS229	FSHD	Male	66 y/o	>112 kb (B) / 28 kb (A)
WS234	Healthy	Female	60 y/o	>145 kb (B) / 107 kb (B)

### 3.5.2. Transfection for gapmer screen

For AO transfection,  $4 \times 10^5$  WS229 or WS234 cells/well were seeded onto 6-well plates and differentiated the following day. Gapmers against *DUX4* or a mock 2'-MOE gapmer were prepared at 100 nM, 10 nM, and 1 nM doses in 2% Lipofectamine® RNAiMAX (Life Technologies) in OptiMEM (Life Technologies) following manufacturer's instructions. The transfection mixture was then diluted with differentiation medium at a 1:5 ratio, after which the final mixture was given to WS229 cells at 13 days post-differentiation. WS229 cells were also subjected to transfection but without any gapmer as non-treated control. Cells were transfected overnight and harvested the following day.

### 3.5.3. RNA extraction and qPCR

Total cell RNA extracts were obtained using the RNeasy® Mini Kit (Qiagen, Germany) with on-column DNase treatment, following the manufacturer's instructions. For cDNA synthesis, SuperScript IV Reverse Transcriptase (Life Technologies) was used following the manufacturer's instructions with 1400 ng RNA extract and 0.5  $\mu$ g of oligo(dT)<sub>12-18</sub> primer (Life Technologies). Using this cDNA, quantitative real-time PCR (qPCR) was then performed with the QuantStudio 3 Real-Time PCR system (Applied Biosystems, Foster City, CA) to evaluate transcript expression of the following genes: *DUX4*, *GAPDH*, *ZSCAN4*, *TRIM43*, *MBD3L2*, *TRIM48*, *TRIM64B*, *PRAMEF4/5/9/11*, *BANF1*, *SSR4*, *FARP1*, and *ZBTB7B*. Probe-based TaqMan™ Gene Expression assays (Thermo Fisher, Waltham, MA; reference numbers in parentheses) with the TaqMan™ Fast Advanced Master Mix (Thermo Fisher) were used for *ZSCAN4* (Hs00537549\_m1), *TRIM43* (Hs00299174\_m1), *MBD3L2* (Hs00544743\_m1), and *TRIM64B* (Hs04194067\_mH) expression analysis. For the other genes, a SYBR-based system

was used, with SsoAdvanced™ Universal SYBR® Green Supermix (Bio-rad, Hercules, CA). Primers were designed for these genes and are listed in **Table 3.6**. The default Fast cycling program corresponding to the detection system was used for qPCR: 1) 95°C, 20 s, and 2) 40 cycles of 95°C, 1 s then 60°C, 20 s. Expression levels were normalized to those of *GAPDH* and determined using the  $\Delta\Delta C_t$  method.

**Table 3.6. Primers used for qPCR evaluation of gene expression in this study.**

<b>Gene</b>	<b>Forward (F) and Reverse (R) primers, 5' to 3'</b>
<i>DUX4</i>	F: CCCAGGTACCAGCAGACC R: TCCAGGAGATGTA ACTCTAATCCA
<i>GAPDH</i>	F: GCAAATTCATGGCACC GT R: AGGGATCTCGCTCCTGGAA
<i>BANF1</i>	F: TGACAAGGCCTATGTTGTCC R: CACAAGTGTCTTTCAGCCATTC
<i>SSR4</i>	F: GCAGGCACCTATGAGGTTAG R: CTCGTTATTCCTCTGAGCCTTC
<i>FARP1</i>	F: GACTGCCGAGCCGCTTT R: TCTTGAGTTCGTGCAGCTTCTG
<i>ZBTB7B</i>	F: AA ACTGCCTCGCCACAT R: CAGCTTGTCGTTCCCTGGT
<i>TRIM48</i>	F: TATGGAGAGGAGGGACTCTTTAG R: CTACATGGTTGGTAGGTCTTGG
<i>PRAMEF4/5/9/11</i>	F: CCAGAGCAGAAGAAGGAGATTG R: TGGCCTTCGAGGAAAGAAAC

#### 3.5.4. RNA sequencing and bioinformatics

Total RNA was extracted from WS234, non-treated WS229 myotubes, and MOE3-treated WS229 myotubes as described in Section 3.5.3. WS229 myotubes were treated with the MOE3 gapmer as in Section 3.5.2. RNA quality was determined using an Agilent 2000 bioanalyzer instrument (Agilent, Santa Clara, CA) and a high-sensitivity RNA chip (Agilent). Total RNA was quantified using Qubit 2.0 and an RNA high-sensitivity Assay Kit (Invitrogen, Carlsbad, CA). RNAseq libraries were constructed from 100 ng of total RNA with the NEBNext Ultra II Directional RNA Library Prep Kit for Illumina (NEB, Ipswich, MA), according to the manufacturer's instructions. Briefly, polyadenylated mRNA was enriched with dT oligos conjugated to paramagnetic beads. Enriched mRNA was chemically fragmented, end-repaired, A-tailed and ligated to sequencing linkers. Linker sequences were used as binding sites to incorporate indexed sequencing adapters by 12 cycles of PCR. Libraries were inspected using a High-Sensitivity DNA bioanalyzer chip (Agilent) and the DNA was quantified using a High-Sensitivity DNA Qubit assay (Invitrogen). Indexed libraries were pooled to a final concentration of 4 nM and were finally sequenced at a 10 pM concentration using a MiSeq instrument (Illumina, San Diego, CA), with a 75 cycles paired-end protocol that included on-instrument de-multiplexing.

Sequences were inspected with fastqc and bases with quality (Q) scores lower than 30 were trimmed with fastq-mcf. Pseudo-alignment of sequences against the GRCH38 version of the human cDNA database from the Ensembl database was conducted with Kallisto, using 100 bootstraps and bias correction.<sup>278</sup> Transcripts that accumulated an average of at least 10 reads were subjected to statistical analysis. Differential expression analysis of RNAseq data were conducted using negative binomial generalized linear models with the DESeq2 R package.<sup>254</sup>

Plots were generated with in-house R scripts. RNA sequencing datasets are available at the NCBI SRA portal, accession number PRJNA629563. We thank Dr. Juan Jovel from the University of Alberta Faculty of Medicine and Dentistry The Applied Genomics Core for their technical assistance and support for this experiment.

### **3.5.5. Cellular phenotype analysis**

For immunocytochemistry, WS229 cells in 24-well plates seeded at  $2.5 \times 10^4$  cells/well were transfected as indicated in Section 3.5.2 with 10 nM of 2'-MOE gapmers at 4 days post-differentiation (overnight transfection). Cells at 7 days post-differentiation or 3 days post-transfection were fixed for 5 min with 4% paraformaldehyde, incubated for 5 min with 0.5% Triton X-100 in phosphate-buffered saline (PBS), and blocked for 1 hr with 20% fetal bovine serum (FBS) in PBS. Cells were then stained for desmin (1:200 rabbit polyclonal antibody [Abcam, United Kingdom] for 1 hr, followed by three 5-min PBS washes, and then 1:100 Alexa594 goat anti-rabbit IgG (H+L) [Life Technologies]), given three final 5-min PBS washes, and mounted with SlowFade Gold Antifade Mountant with DAPI (Life Technologies). The Nikon Eclipse TE 2000-U fluorescence microscope was used for visualization. Myogenic fusion index (MFI) determination and cell diameter measurements were done blinded using Image J (NIH), from three randomly chosen fields of view for each replicate, per condition. For MFI calculation, the number of nuclei in myotubes was divided by the total number of nuclei in a given field of view, and then multiplied by 100 to get a percentage value. Approximately 382 nuclei on average were counted per replicate, per condition (range: 69–541). Myotube diameters were taken as the average of the three widest measurements across the length of a myotube, avoiding locations near branch points or overlaps between myotubes. Approximately 26

myotubes on average were counted per replicate, per condition (range: 15–36). For purposes of quantification, we considered a myotube as a cell with at least two nuclei having the same cytoplasm. For apoptosis analysis, WS229 cells in 24-well plates seeded at  $5 \times 10^4$  cells/well were transfected as above with 10 nM of 2'-MOE gapmers at 13 days post-differentiation. Apoptosis was then assessed by flow cytometry with the eBioscience™ Annexin V Apoptosis Detection Kit FITC (Thermo Fisher). WS234 cells were grown alongside WS229 cells and subjected to similar procedures to serve as a control. We thank Dr. Aja Rieger, Manager of the University of Alberta Faculty of Medicine and Dentistry Flow Cytometry Facility, for their technical assistance with flow cytometry.

### **3.5.6. Western blotting**

WS229 and WS234 cells were seeded and differentiated in 6-well plates as described in Section 3.5.1. Transfection with 100 nM of either MOE1, MOE2, MOE3, or mock 2'-MOE gapmers to WS229 myotubes was done as in Section 3.5.2, with transfection performed at 4 days post-differentiation (overnight). Total protein was extracted from cells at 7 days post-differentiation or 3 days post-transfection using RIPA buffer (Sigma) with cOmplete™, Mini, EDTA-free protease inhibitor cocktail (Sigma); protein was quantified using the Pierce™ BCA Protein Assay kit (Thermo Fisher). For SDS-PAGE, 12 µg of protein extracts were loaded and run on a NuPAGE™ 4-12% Bis-Tris gel (Thermo Fisher) at 150 V for 70 min. Semi-dry transfer onto a PVDF membrane (Millipore) was then performed at 20 V for 30 min. Blocking was done overnight at 4°C using 5% skim milk in PBS with 0.05% Tween 20 (PBST). The next day, the membrane was cut and incubated in primary antibodies against myosin heavy chain (MF20, 1:800 in blocking solution, Developmental Studies Hybridoma Bank, Iowa City, IA) or  $\beta$ -tubulin

(ab6046, 1:5,000 in PBST, Abcam) for 1 hr at room temperature, followed by three 10-min PBST washes. Membranes were then incubated in 1:10,000 of the corresponding HRP-conjugated secondary antibody (anti-mouse IgG H+L for the myosin heavy chain antibody, and anti-rabbit IgG H+L for the  $\beta$ -tubulin antibody; Invitrogen) in PBST for 1 hr at room temperature, followed again by three 10-min PBST washes. Bands were visualized using the Amersham ECL Select detection kit (GE Healthcare, Chicago, IL). Myosin heavy chain protein levels were determined based on band intensities normalized to those of  $\beta$ -tubulin, and calculated relative to the normalized band intensity of one of the three WS234 replicates.

### 3.5.7. Searching for potential off-target genes

The GGGenome search engine (<https://gggenome.dbcls.jp/>) was used to find targets with highly similar sequences to those recognized by the various *DUX4*-targeting 2'-MOE gapmers.<sup>255</sup> The RefSeq human RNA release 80 (Jan 2017) database was used for the search. The top hits are shown in **Table 3.4**. Only *BANF1*, *SSR4*, *FARP1*, and *ZBTB7B* were found to have detectable expression by qPCR in our *in vitro* system, and so we focused on these for off-target analysis.

### 3.5.8. In vivo delivery of 2'-MOE gapmers

Experiments involving animals were approved by the Institutional Animal Care and Use Committee at the Children's National Health System, Washington, DC, USA. To examine the effect of 2'-MOE gapmer treatment on *DUX4* expression, five adult hemizygous *FLEXDUX4* mice (3 male, 2 female; 2-3 months old) received three intramuscular (i.m.) injections of MOE3 (20  $\mu$ g dissolved in PBS, for a final 20  $\mu$ l volume) to the tibialis anterior (TA) muscle over six

days, one injection every other day. The contralateral TA of each mouse was injected with PBS (20  $\mu$ L) as a control. In addition, three adult male hemizygous *FLEXDUX4* mice were similarly injected i.m. (TA) with a scrambled 2'-MOE gapmer control following the same dose and treatment schedule; contralateral TAs were injected with PBS as before. Twenty-four hours after the final injection, mice were euthanized by CO<sub>2</sub> asphyxiation with cervical dislocation and TAs were dissected, cleaned of connective tissue, snap-frozen in dry ice-cooled isopentane, and stored at  $-80^{\circ}\text{C}$  for further analysis. For *DUX4* expression analysis, qPCR was performed as previously described.<sup>86,239</sup> Briefly, RNA was extracted using Trizol (Ambion, Austin, TX) and cleaned up using the RNeasy® Plus Mini Kit (Qiagen). cDNA was synthesized from 2  $\mu$ g of total RNA using SuperScript IV Reverse Transcriptase (Life Technologies) and oligo(dT)<sub>12-18</sub> primers. *Gapdh* was used as an internal control, and relative gene expression was analyzed using the  $\Delta\Delta\text{Ct}$  method.

### **3.5.9. Statistical analysis**

Statistical analyses for all data besides those from RNA sequencing were done with GraphPad Prism 7 (GraphPad Software). One-way ANOVAs with post-hoc Tukey's or Dunnett's test, or unpaired two-tailed *t*-tests were used as needed.

## **Chapter 4 Efficacy of Multi-exon Skipping Treatment in Duchenne Muscular Dystrophy Dog Model Neonates**

Chapter 4 was derived from the following published article:

Lim, K. R. Q.\*, Echigoya, Y.\*, Nagata, T.\*, Kuraoka, M., Kobayashi, M., Aoki, Y., Partridge, T., Maruyama, R., Takeda, S., Yokota, T. Efficacy of multi-exon skipping treatment in Duchenne muscular dystrophy dog model neonates. *Mol. Ther.* **27**, 76-86 (2019). (\*co-first)

## 4.1. Abstract

Duchenne muscular dystrophy (DMD) is caused by mutations in *DMD*, which codes for dystrophin. Because the progressive and irreversible degeneration of muscle occurs from childhood, earlier therapy is required to prevent dystrophic progression. Exon skipping by antisense oligonucleotides called phosphorodiamidate morpholino oligomers (PMOs), which restores the *DMD* reading frame and dystrophin expression, is a promising candidate for use in neonatal patients, yet the potential remains unclear. Here, we investigate the systemic efficacy and safety of *early* exon skipping in dystrophic dog neonates. Intravenous treatment of canine X-linked muscular dystrophy in Japan dogs with a 4-PMO cocktail resulted in ~3-27% in-frame exon 6-9 skipping and dystrophin restoration across skeletal muscles up to 14% of healthy levels. Histopathology was ameliorated with the reduction of fibrosis/necrosis area and centrally nucleated fibers, significantly in the diaphragm. Treatment induced cardiac multi-exon skipping, though dystrophin rescue was not detected. Functionally, treatment led to significant improvement in the standing test. Toxicity was not observed from blood tests. This is the first study to demonstrate successful multi-exon skipping treatment and significant functional improvement in neonatal dystrophic dogs. Early treatment was most beneficial for respiratory muscles, with implications for addressing pulmonary malfunction in patients.

## 4.2. Introduction

DMD is a lethal X-linked recessive disorder affecting ~1:3000-1:6000 boys globally.<sup>111</sup> Symptoms begin at ~3-5 years old, with lower body muscle weakness. This rapidly progresses, leading to body-wide muscle degeneration.<sup>112,279</sup> Patients are typically wheelchair-bound before their teens, with scoliosis developing after. Cardiorespiratory complications then manifest, often

causing death within the third decade of life.<sup>112,279</sup> In DMD, irreversible pathogenesis occurs before observable physical signs appear. Newborns with DMD show elevated creatine kinase (CK) levels in blood tests.<sup>112</sup> Thus, there is a clear need for DMD patients to receive therapeutic interventions as soon as a diagnosis is reached.

DMD is caused by out-of-frame mutations in the gene for dystrophin (*DMD*), a protein maintaining muscle membrane integrity.<sup>115,117,120</sup> Therapies aim to restore dystrophin amounts to functionally-beneficial levels in muscle.<sup>113,120</sup> One approach is exon skipping, which uses short, synthetic antisense oligonucleotides (AOs) to restore the *DMD* reading frame by excluding out-of-frame exons from the final transcript. This strategy is based on the observation that in-frame *DMD* deletions give milder patient phenotypes (Becker muscular dystrophy or BMD).<sup>165,166</sup> Exon skipping produces truncated, partially functional dystrophin, which has shown promise in a number of animal studies.<sup>186,187,191,194,198</sup> Skipping individual exons can treat ~70% of patients with amenable deletions; skipping multiple exons can treat ~90% of this population.<sup>280</sup> Efforts are thus directed at developing multi-exon skipping cocktails, given their increased applicability.<sup>281</sup>

The U.S. Food and Drug Administration (FDA) granted accelerated approval to eteplirsen, a *DMD* exon 51-skipping PMO by Sarepta, for DMD treatment in 2016.<sup>204</sup> Eteplirsen only rescued <1% dystrophin of healthy levels after 180 weeks of treatment and did not satisfactorily improve ambulation as of yet.<sup>203</sup> Prior to eteplirsen's approval, the FDA rejected another exon 51-skipping AO—drisapersen (BioMarin)—for reasons of poor safety and efficacy.<sup>282</sup> More recently, results from a trial on another PMO by Sarepta called golodirsen, which skips exon 53, showed a mean dystrophin rescue of ~1% of healthy levels 48 weeks post-treatment.<sup>283</sup> Thus, while the efficacy of exon skipping PMOs in the pre-clinical setting is well

established,<sup>284</sup> their performance in clinical trials can be improved. Given the nature of DMD, early administration of exon skipping PMOs may improve efficacy. Earlier treatment with corticosteroids and cardioprotective agents (DMD standards-of-care) better-preserved motor and cardiac function, respectively, in patients and dystrophic mice<sup>285–288</sup>—thus, better outcomes could result from earlier exon skipping.

Here, we tested the efficacy and safety of multi-exon skipping using canine X-linked muscular dystrophy in Japan (CXMD<sub>J</sub>) neonates. CXMD<sub>J</sub> has a point mutation in the *dystrophin* intron 6 splice acceptor, which leads to the out-of-frame skipping of exon 7.<sup>197</sup> These dogs produce no dystrophin, and closely phenocopy DMD patients.<sup>196</sup> To rescue the reading frame, at least two exons, 6 and 8, need to be skipped. We previously reported a 3-PMO exon 6-8-skipping cocktail significantly rescuing dystrophin production and remarkably improving muscle function in 2-5-month-old CXMD<sub>J</sub> dogs.<sup>198</sup> Adding another exon 8-skipping PMO further improved efficacy *in vitro*.<sup>289</sup> This new cocktail has been tested locally<sup>290</sup> but not systemically *in vivo*. Here, we intravenously treated neonatal CXMD<sub>J</sub> dogs with this 4-PMO cocktail and analyzed its efficacy, safety, and uptake. Early treatment was non-toxic and induced body-wide exon skipping in skeletal muscles, restoring functional dystrophin levels and improving standing test performance; among muscles, treatment was most beneficial for the diaphragm.

## 4.3. Results

### 4.3.1. Early exon skipping treatment leads to variable improvements across skeletal muscles

Intravenous treatment of neonatal CXMD<sub>J</sub> dogs with the 4-PMO cocktail, consisting of Ex6A, Ex6B, Ex8A, and Ex8G (**Figure 4.1; Table 4.1**), induced body-wide exon skipping in

skeletal muscles. The cocktail was administered thrice intravenously every other week, with treatment initiated at 1 week of age. Exon 6-9 skipped transcripts were observed in all examined skeletal muscles by RT-PCR, with skipping efficiencies ranging from ~3-27% (**Figure 4.2a**). Exon 9 was spontaneously skipped due to the nature of *dystrophin* splicing, with the resulting product still in-frame.<sup>291</sup> Exon skipping efficiency was widely variable across muscles, with it significantly increased in the tibialis anterior, gracilis major, and diaphragm compared to non-treated controls, in which little to no exon skipping was observed.

Quantitative analysis by Western blotting revealed that early treatment with the 4-PMO cocktail rescued dystrophin synthesis in all analyzed skeletal muscles (**Figures 4.2b, 4.3**). An antibody against the dystrophin rod domain was used (DYS1), ensuring the detection of full-length (Dp427 with exons 6-9 skipped) protein. The extent of dystrophin rescue roughly correlated with the exon skipping efficiency observed in a particular muscle (**Figures 4.2a,b**). Dystrophin rescue was likewise variable across skeletal muscles. The highest levels of rescue were found in the diaphragm, reaching up to 14% of wild-type levels. The mean rescue in the diaphragm was observably higher in treated compared to non-treated dogs. Dystrophin restoration varied among individual treated dogs, with 10504MA responding particularly well to the treatment and giving the highest amounts of dystrophin rescue observed (**Figures 4.2b, 4.3**). Other dogs showed at most 2% dystrophin of wild-type levels post-treatment.

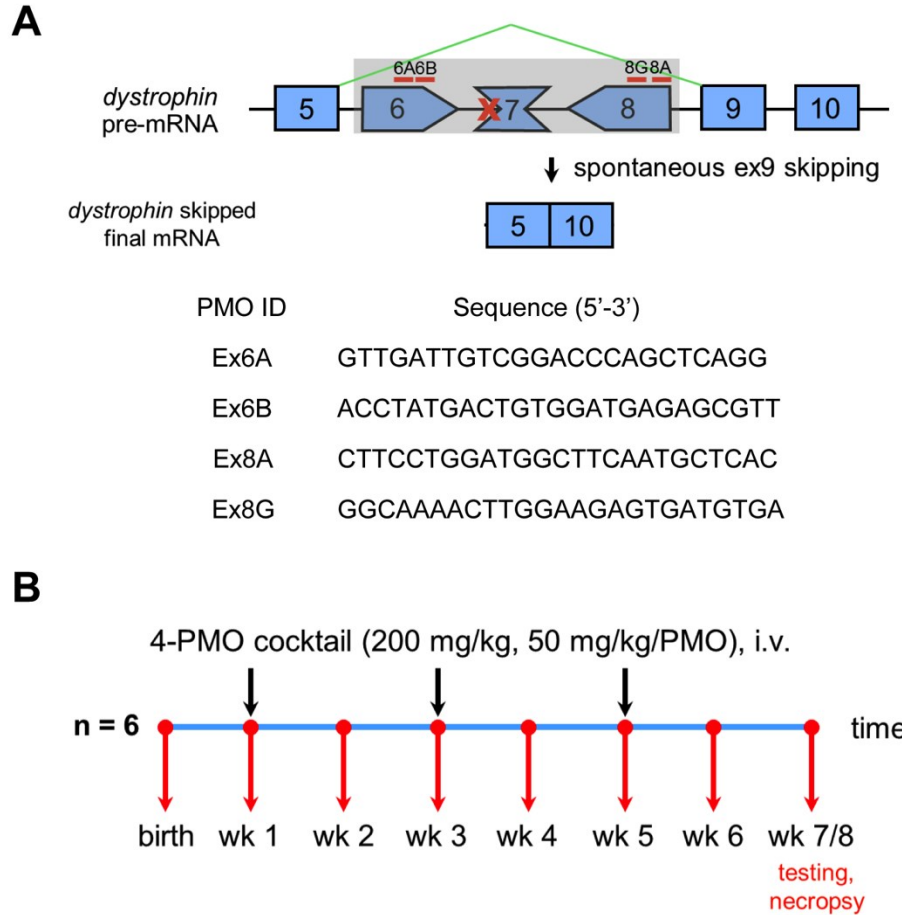


**Figure 4.1. Overview of experimental design.** (A) Approximate locations of the four PMOs used in the study, and the skipped *dystrophin* mRNA after treatment. The sequences of the PMOs are shown below. (B) Treatment schedule for the study; black arrows indicate injection times; red arrows indicate blood collection.

**Table 4.1. Comprehensive list of dogs used in the study.**

Dog ID*	Treatment group	Functional testing				Molecular analyses**		Histology	ELISA (serum, tissues)	Blood tests
		Grading	15m run	Standing time	Open-mouth width	Skeletal muscles	Cardiac muscles			
8603MA	Treated		X			X	X	X	X	X
9202MA	Treated	X	X	X	X	X		X	X	X
10504MA	Treated	X	X	X	X	X		X	X	X
12301MA	Treated	X	X	X	X	X	X	X	X	X
12303MA	Treated	X	X	X	X	X	X	X	X	X
12502MA	Treated	X	X	X	X	X	X	X	X	X
8609MA	Non-treated		X					X		X
9201MA§	Non-treated									X
12305MA	Non-treated	X	X	X	X	X	X	X		X
12501MA	Non-treated	X	X	X	X	X	X	X		X
11403MA	Non-treated	X	X	X						
402MA	Non-treated					X		X		
2301MA	Non-treated							X		
3701MA	Non-treated			X	X					
5301FA	Non-treated			X	X					
5302FA	Non-treated			X	X					
5303MA	Non-treated			X	X					
5306MA	Non-treated			X	X					
5308FA	Non-treated			X	X					
8106MA	Non-treated			X	X					
11303MA	Non-treated			X	X					
14804MA	Non-treated									X
15001MA	Non-treated									X
15002MA	Non-treated									X
8601MN	Wild-type		X							X
9203MN	Wild-type		X	X	X					
10502MN	Wild-type	X	X	X	X	X	X	X		
12302MN	Wild-type	X	X	X	X	X		X		
12304MN	Wild-type					X		X		
12104MN	Wild-type	X	X	X						
601MN	Wild-type							X		
E09MN	Wild-type							X		
2303MN	Wild-type						X	X		
14003MN	Wild-type									X
14103MN	Wild-type									X
14104MN	Wild-type									X
14304MN	Wild-type									X
14402MN	Wild-type									X
14502MN	Wild-type									X
14504MN	Wild-type									X
14603MN	Wild-type									X
14701MN	Wild-type									X
14702MN	Wild-type									X
14703MN	Wild-type									X
14803MN	Wild-type									X

\*the two letters at the end of each ID: the first indicates sex (M/F), the second indicates genotype (N = normal, A = affected, with CXMD<sub>J</sub> mutation), \*\*molecular analyses include: RT-PCR, Western blotting, immunohistochemistry, §died prior to endpoint.

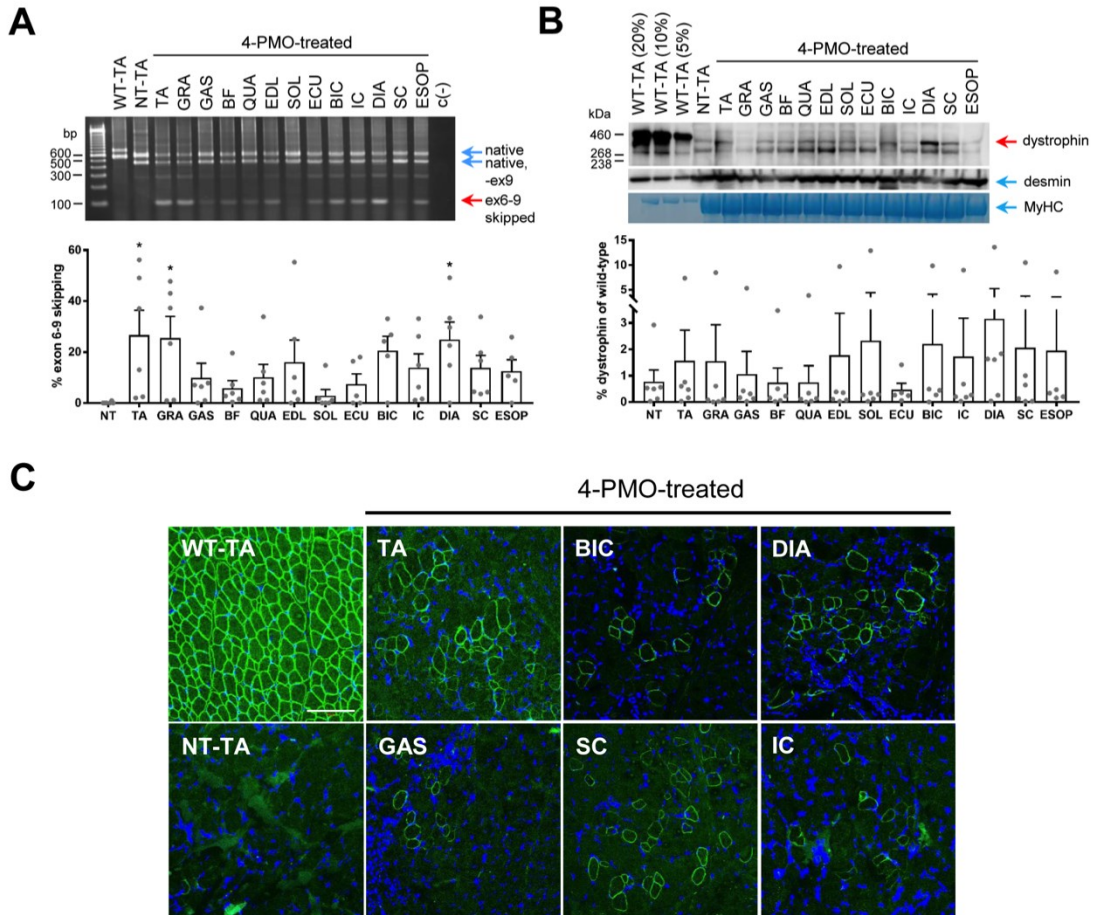


**Figure 4.2. Effects of early exon skipping treatment on dystrophin production in CXMD<sub>J</sub> skeletal muscles.** (A) Representative RT-PCR image showing exons 6-9 skipped bands across skeletal muscles after PMO treatment. For non-treated (NT) and treated samples, native (exon 5-6-8-9-10) and skipped (exon 5-10) bands are indicated, the rest are intermediate skipping products; specifically for NT, the band below the native band is due to spontaneous exon 9 skipping. For wild-type (WT), the topmost band is the native (exon 5-6-7-8-9-10) band, while the lower band has exon 9 spontaneously skipped. Calculated exon skipping efficiencies are shown below. Error bars: S.E.M., \* $p \leq 0.05$  versus NT, one-way ANOVA, Dunnett's multiple comparisons test. Dots represent individual dogs. (B) Representative Western blot showing dystrophin rescue in treated CXMD<sub>J</sub> skeletal muscles (12303MA). For non-treated and treated muscle samples, 40  $\mu$ g of protein was loaded. Dystrophin was detected using DYS1; desmin and myosin heavy chain (MyHC) serve as loading controls. Dystrophin rescue was quantified relative to 5% WT levels. The band observed below the rescued dystrophin band is likely due to the high amount of total protein loaded. Dots represent individual dogs. Error bars: S.E.M. (C) Representative immunohistochemistry images show restored dystrophin (green, DYS1) in PMO-treated skeletal muscles localizing correctly to the sarcolemma; blue: nuclei. Total magnification: 200x; scale bar: 100  $\mu$ m. For all panels,  $n = 5-6$  (PMO-treated dogs). Abbreviations: TA, tibialis anterior; GRA, gracilis major; GAS, gastrocnemius; BF, biceps femoris; QUA, quadriceps; EDL, extensor digitorum longus; SOL, soleus; ECU, extensor carpi ulnaris; BIC, biceps brachii; IC, intercostal muscles; DIA, diaphragm; SC, sternocleidomastoid; ESOP, esophagus.

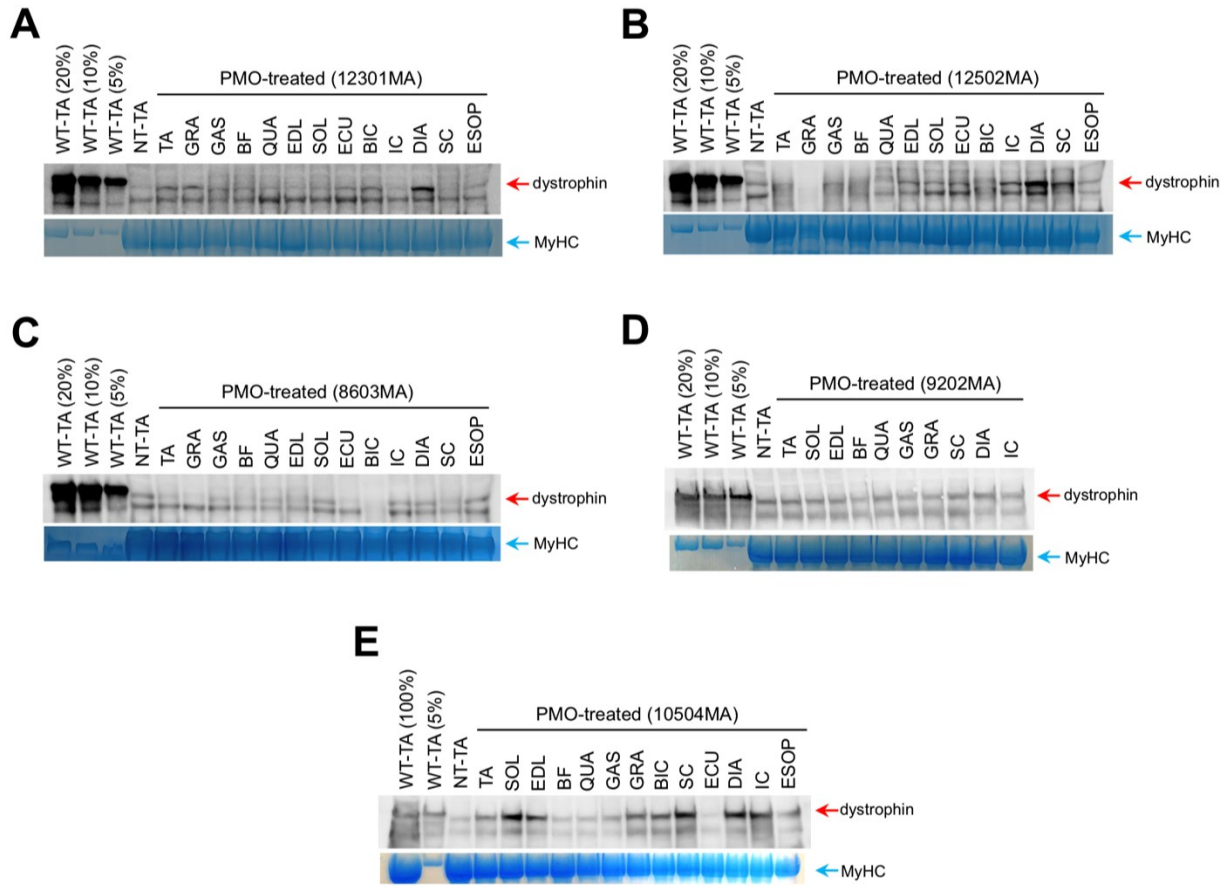


**Figure 4.3. Dystrophin Western blot results for other treated CXMD<sub>j</sub> neonatal dogs.** Images showing dystrophin protein rescue in (A) 12301MA, (B) 12502MA, (C) 8603MA, (D) 9202MA, and (E) 10504MA. Myosin heavy chain (MyHC) is shown as a loading control. For (A) to (C), 40  $\mu$ g protein was loaded for non-treated (NT) and treated muscles; for (D) and (E), 60  $\mu$ g was loaded instead. Wild-type (WT) samples were loaded at the indicated levels, as percentages of the amounts loaded for the treated muscles. Abbreviations: TA, tibialis anterior; GRA, gracilis major; GAS, gastrocnemius; BF, biceps femoris; QUA, quadriceps; EDL, extensor digitorum longus; SOL, soleus; ECU, extensor carpi ulnaris; BIC, biceps brachii; IC, intercostal muscles; DIA, diaphragm; SC, sternocleidomastoid; ESOP, esophagus.

Immunohistochemistry with the same antibody also showed dystrophin protein restoration in all skeletal muscles tested as well as proper sarcolemmal localization (**Figure 4.2c**), indicating the restored dystrophin is potentially functional. Dystrophin-positive fibers were observed in a patched distribution across muscle sections, similar to results from other studies. The number of dystrophin-positive fibers varied across treated dogs, for instance with 8603MA showing a higher abundance of these than others (**Figure 4.4**).

The skeletal muscles of treated CXMD<sub>J</sub> dogs generally exhibited less degeneration, fibrosis, and necrosis than non-treated dystrophic dogs (**Figures 4.5a,b**). The fibrotic/necrotic area was significantly decreased in the diaphragm of treated dogs (**Figure 4.5b**). We also quantified the percentage of CNFs in HE-stained muscle sections; CNF counts serve as an index of the amount of regeneration that has occurred in a certain muscle. Overall, fewer CNFs were observed in the skeletal muscles of dogs treated with the 4-PMO exon skipping cocktail (**Figure 4.5c**). The reduction in CNF count was significant in the diaphragm and intercostal muscles. This can be because the other skeletal muscles (e.g. tibialis anterior) did not display as severe a dystrophic pathology as that in the diaphragm or intercostal muscles of neonatal dogs (**Figure 4.5**).

PMO-treated (8603MA)

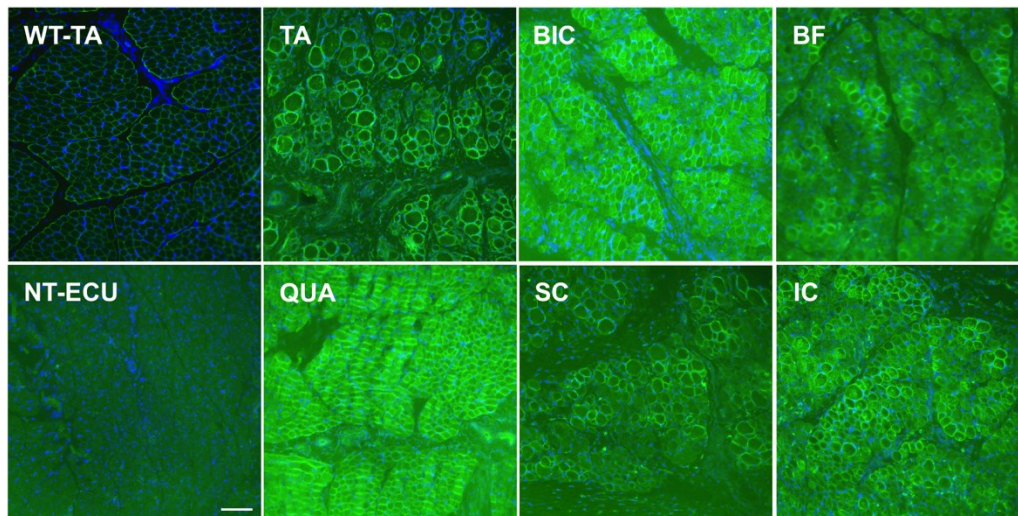


**Figure 4.4. Representative immunohistochemistry images of skeletal muscles from 8603MA, stained using DYS1.** Numerous dystrophin-positive fibers (green) can be observed in various skeletal muscles upon treatment; blue: nuclei. Total magnification: 200x; scale bar: 100  $\mu$ m. Abbreviations: TA, tibialis anterior; ECU, extensor carpi ulnaris; BIC, biceps brachii; BF, biceps femoris; QUA, quadriceps; SC, sternocleidomastoid; IC, intercostal muscles.

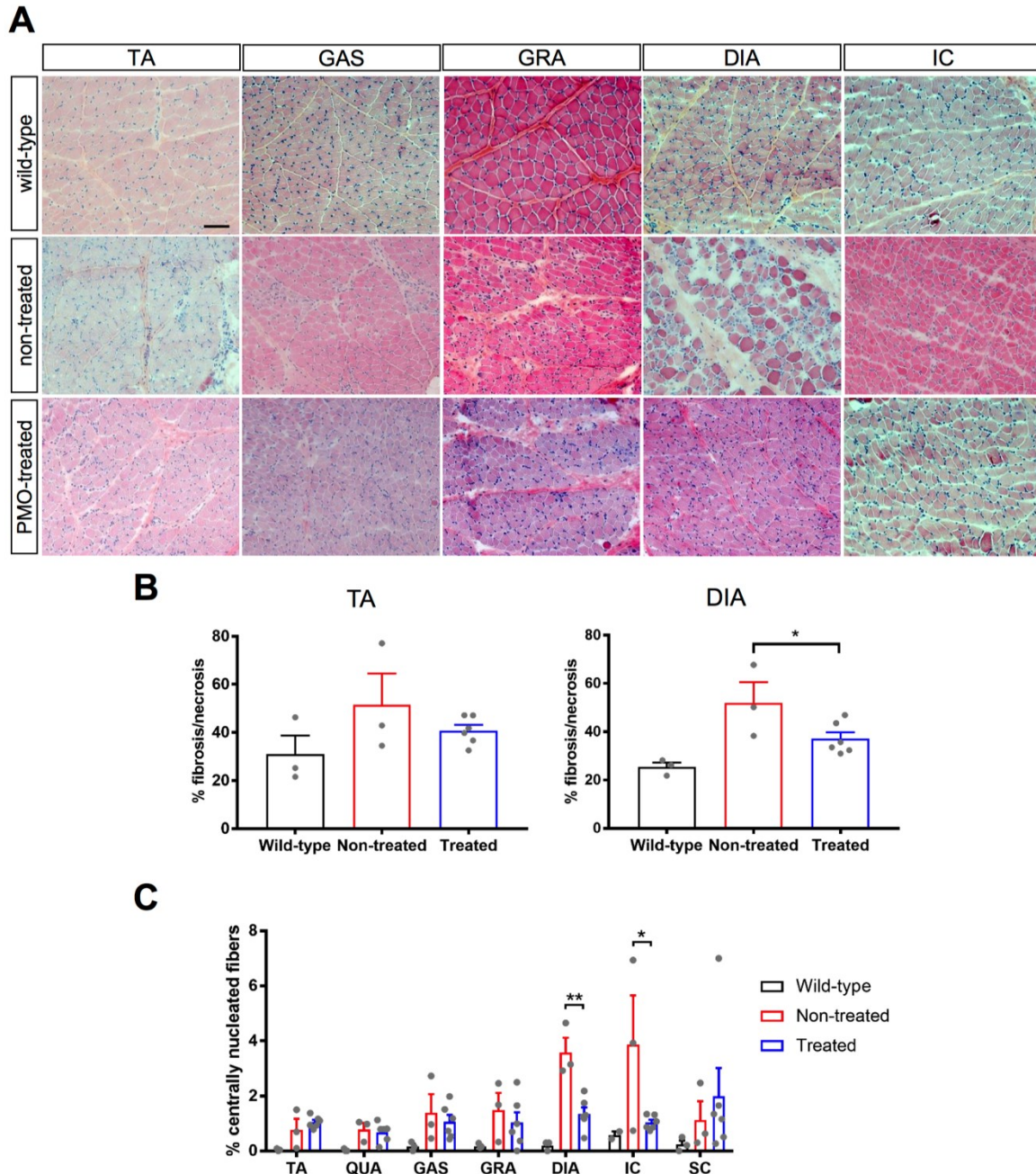


**Figure 4.5. Histopathological improvements in PMO-treated neonatal CXMD<sub>J</sub> skeletal muscles.** (A) Representative hematoxylin and eosin (HE)-stained sections of various skeletal muscles from PMO-treated CXMD<sub>J</sub> dogs, as well as age-matched non-treated CXMD<sub>J</sub> and wild-type dogs. Scale bar: 100  $\mu$ m. (B) Fibrosis/necrosis quantification from HE-stained sections of the tibialis anterior (TA) and diaphragm (DIA). n = 3, wild-type and non-treated; n = 6, treated. Error bars: S.E.M., \*p  $\leq$  0.05, one-tailed Student's t-test. (C) Centrally nucleated fiber count quantification from HE-stained sections of various skeletal muscles. n = 2-3, wild-type; n = 3, non-treated; n = 6, treated. Error bars: S.E.M., \*p  $\leq$  0.05, \*\*p  $\leq$  0.01, one-tailed Student's t-test. For all plots, dots represent individual dogs. Abbreviations: QUA, quadriceps; GAS, gastrocnemius; GRA, gracilis major; IC, intercostal muscles; SC, sternocleidomastoid.

### **4.3.2. Treatment-related dystrophin rescue is not detectable in cardiac muscle regardless of early-age PMO administration**

Early treatment of CXMD<sub>J</sub> dogs with the 4-PMO cocktail did not lead to appreciable exon skipping in various cardiac muscles. All examined regions of the heart in treated dogs exhibited exon 6-9 skipping efficiencies up to 4% (**Figure 4.6a**). However, no appreciable increase of dystrophin expression was detected by Western blotting with the DYS1 antibody; all cardiac regions examined had around 1% dystrophin of wild-type levels, which non-treated dystrophic cardiac muscle similarly possessed (**Figure 4.6b**).

Contrary to expectation, immunohistochemistry with DYS1 showed an absence of dystrophin in the myocardium or Purkinje fiber regions of various cardiac muscles in treated dogs (**Figure 4.6c**). Immunostaining with DYS2, specific for the C-terminal domain, confirmed the absence of dystrophin isoforms in the myocardium; staining was observed in the Purkinje fiber region, indicating the presence of a non-full-length dystrophin isoform (e.g. Dp71) in these structures, consistent with the previous study of Urasawa et al. (2008)<sup>292</sup> (**Figure 4.7**). Thus, the dystrophin protein detected in cardiac muscles via Western blotting could either be due to revertant fibers or the presence of putative heart-specific dystrophin isoforms.

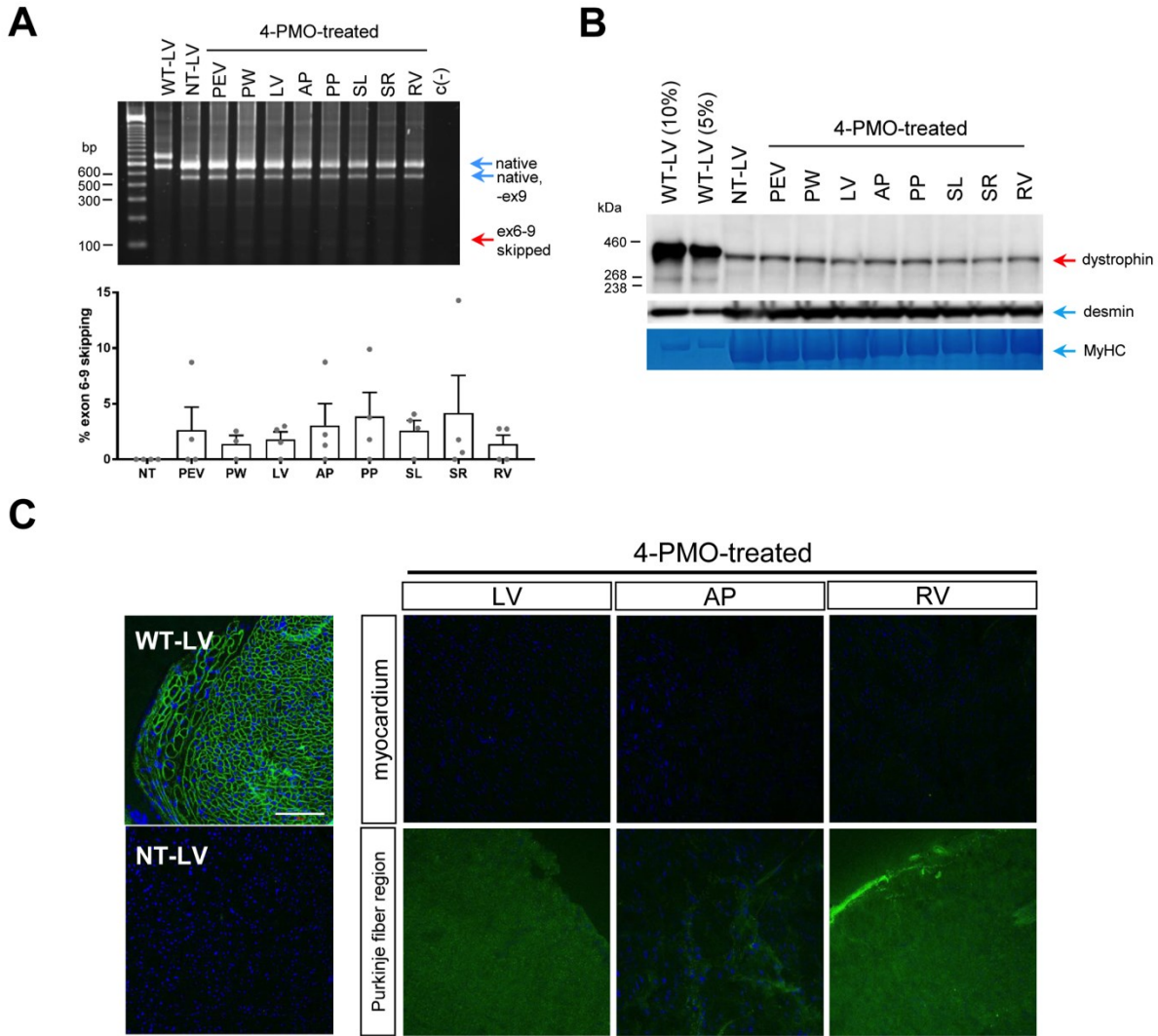


**Figure 4.6. Effects of early exon skipping treatment on dystrophin production in CXMD<sub>J</sub> cardiac muscles.** (A) Representative RT-PCR image showing exon 6-9 skipping across different regions of the heart after treatment with the 4-PMO cocktail. Native, intermediate, and exon skipped bands for wild-type (WT), non-treated (NT), and treated samples are indicated as in Figure 2. Exon skipping efficiencies were quantified, as shown below. Error bars: S.E.M. Dots represent individual dogs. (B) Representative Western blot detecting for dystrophin in various cardiac muscles using DYS1. Desmin and myosin heavy chain (MyHC) were used as loading controls. (C) Representative immunohistochemistry images showing an absence of DYS1 dystrophin signal (green) in treated cardiac muscles, either in the myocardium or the Purkinje fiber region; blue: nuclei. Total magnification: 200x; scale bar: 100  $\mu$ m. For all panels, n = 4 (PMO-treated dogs). Abbreviations: PEV, posterior external left ventricle region; PW, posterior wall of the left ventricle; LV, left ventricle; AP, anterior papillary muscle; PP, posterior papillary muscle; SL, left side of the interventricular septum; SR, right side of the interventricular septum; RV, right ventricle.

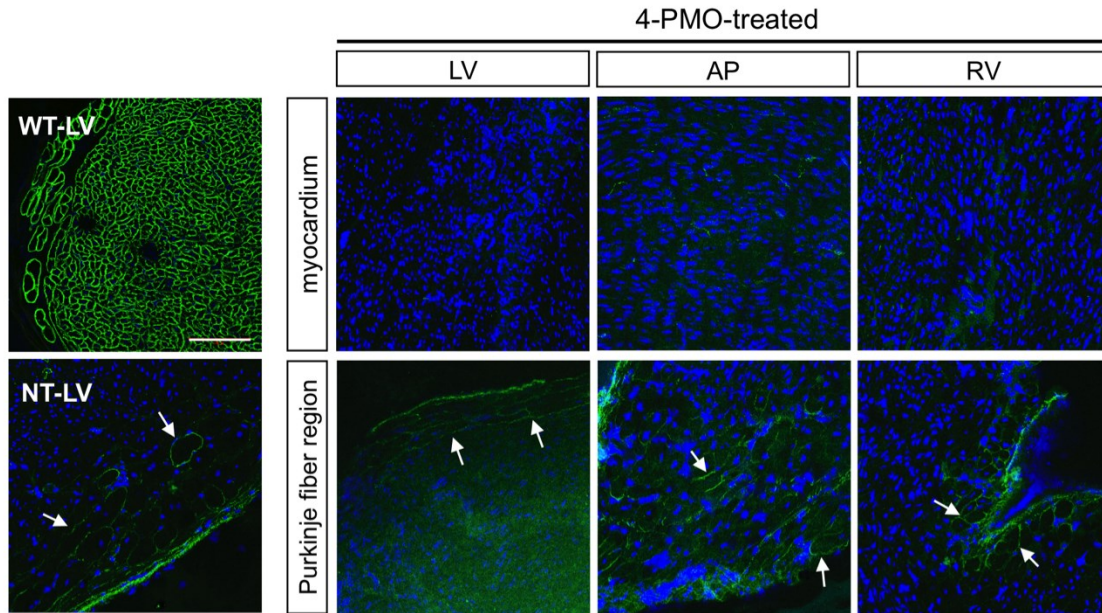


**Figure 4.7. Representative immunohistochemistry images of cardiac muscles detected with DYS2.** DYS2 is specific for the C-terminal domain of dystrophin. Dystrophin (green) can be detected in Purkinje fibers, as indicated by the white arrows, but not in the myocardium of treated CXMD<sub>J</sub> dog cardiac muscles; blue: nuclei. Total magnification: 200x; scale bar: 100 μm. n = 4 (PMO-treated dogs). Abbreviations: WT, wild-type; NT, non-treated; LV, left ventricle; AP, anterior papillary muscle; RV, right ventricle.

### 4.3.3. PMO serum clearance and muscle uptake in treated neonatal dystrophic dogs

ELISA-based detection of PMOs in the sera of treated dogs showed that all four PMOs in the administered cocktail were rapidly cleared from circulation within a week after an injection; serum samples showed little (generally  $\leq 3$  nM) to no PMOs between injections as well as during the last weeks of the study (**Figure 4.8a**). Noticeably higher concentrations of each PMO were detected in sera collected a day post-injection versus those collected two days post-injection, indicative of the short half-life associated with PMOs *in vivo*.

All four PMOs in the systemically administered cocktail had good distribution, with certain levels of accumulation observed in body-wide muscles including cardiac muscle (**Figure 4.8b**). PMO uptake in muscles was variable across the treated neonatal CXMD<sub>J</sub> dogs and across skeletal muscles within individual dogs. Relatively high PMO concentrations were observed in the diaphragm and sternocleidomastoid. Surprisingly, PMO uptake was considerably increased in cardiac muscle across dogs, with PMO concentrations comparable to other skeletal muscles.

In both sera and muscles, strikingly higher concentrations of Ex8G were observed compared to Ex6A, Ex6B, or Ex8A. This is likely due to the tendency of Ex8G to aggregate in solution, despite its low GC content compared to other PMOs in the cocktail. The aggregation of Ex8G may have physiologically increased its retention in the sera and muscles.

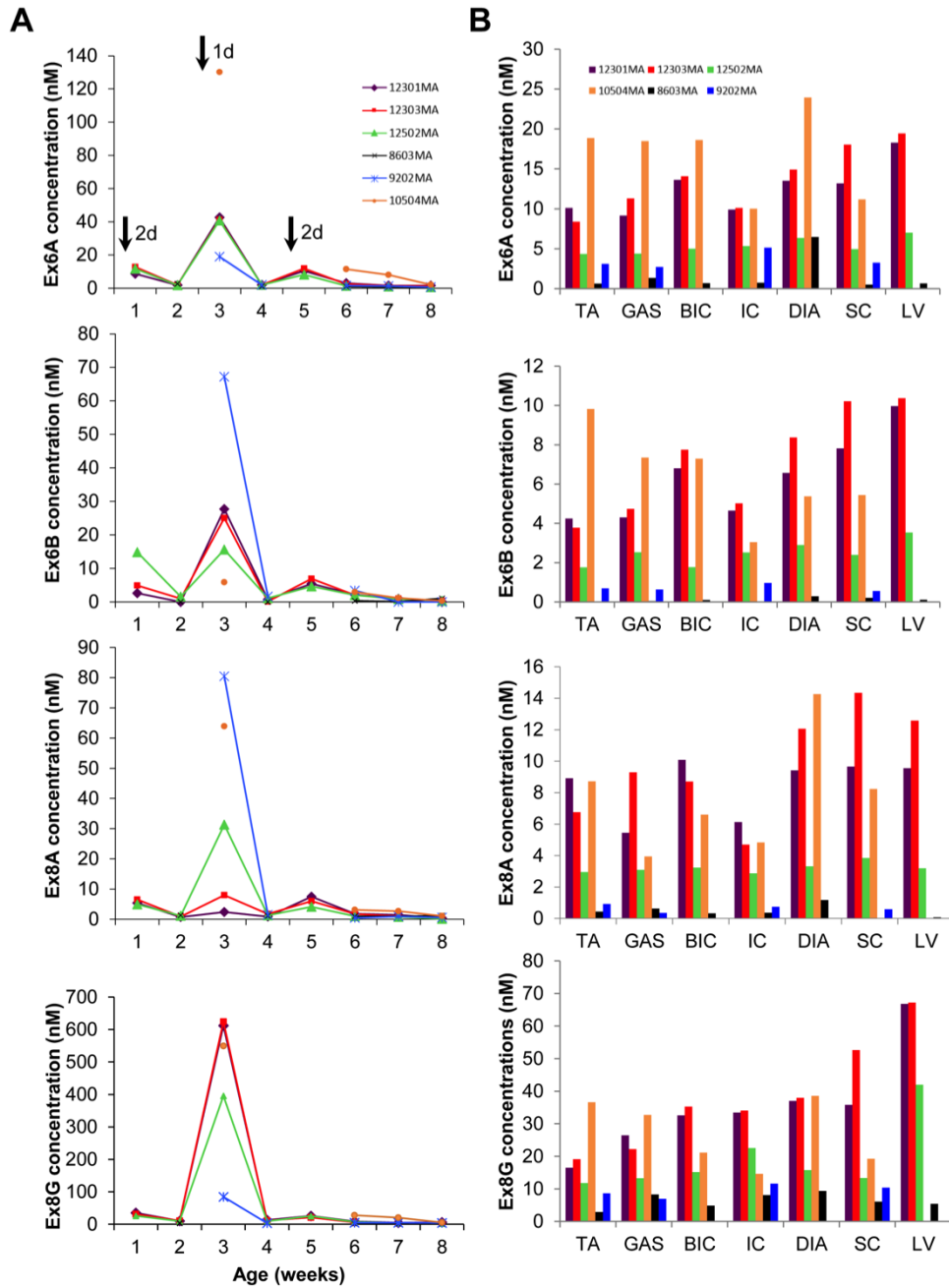


**Figure 4.8. ELISA-based quantification of PMOs in serum and muscle.** (A) Plots show the concentrations of each PMO in the cocktail found in weekly serum samples from treated CXMD<sub>J</sub> dogs. Different colors indicate individual dogs. Black arrows in the topmost plot represent times of injection; numbers beside the arrows indicate how many days post-injection sample collection was done. (B) The concentrations of each of the four PMOs in various muscles are shown. Muscles were collected 2-3 weeks after the final injection. Different colors indicate individual dogs. For 10504MA, data for the left ventricle (LV) is not available, while for 9202MA, data for the biceps brachii (BIC), diaphragm (DIA), and LV are not available. For both (A) and (B), n = 4-6 (PMO-treated). Abbreviations: TA, tibialis anterior; GAS, gastrocnemius; IC, intercostal muscles; DIA, diaphragm; SC, sternocleidomastoid.

#### **4.3.4. Functional testing of treated neonatal CXMD<sub>J</sub> dogs**

Four different tests were performed to analyze muscle function in 7- or 8-week old treated (2 or 3 weeks after the final injection) and non-treated neonatal CXMD<sub>J</sub> dogs, as well as in corresponding wild-type controls (**Figure 4.9**). Of the functional tests performed, treated neonatal CXMD<sub>J</sub> dogs only showed significant improvement in the standing test compared to non-treated controls (**Figure 4.9c**).

#### **4.3.5. Early treatment with exon skipping PMOs is not associated with detectable toxicity in blood tests**

Serum biomarkers for muscle, kidney, liver, and general toxicity were analyzed in weekly blood samples from non-treated and PMO-treated dystrophic neonatal dogs throughout the course of the study. Corresponding wild-type samples were analyzed to provide reference values. CK levels increased with age in both non-treated and treated dystrophic dogs; CK values, however, did not vary widely between the two across all ages. Wild-type CK levels were low at all ages (**Figure 4.10a**). Nephrotoxicity was not detected, as BUN and CRE levels were similar across all groups, regardless of age (**Figure 4.10b**). Hepatotoxicity was also not detectable (**Figure 4.10c**). AST and ALT levels, while elevated compared to wild-type values, were similar between non-treated and treated dystrophic dogs in all time points. GGT, TBIL, and ALB levels did not differ among all groups throughout the study. Levels of other clinical markers (i.e., TP, LDH, ALP, ion levels) also did not show changes between wild-type, non-treated, and treated dogs (**Figure 4.10d**). Based on these, PMO treatment in neonatal CXMD<sub>J</sub> dogs did not induce any adverse side effects.

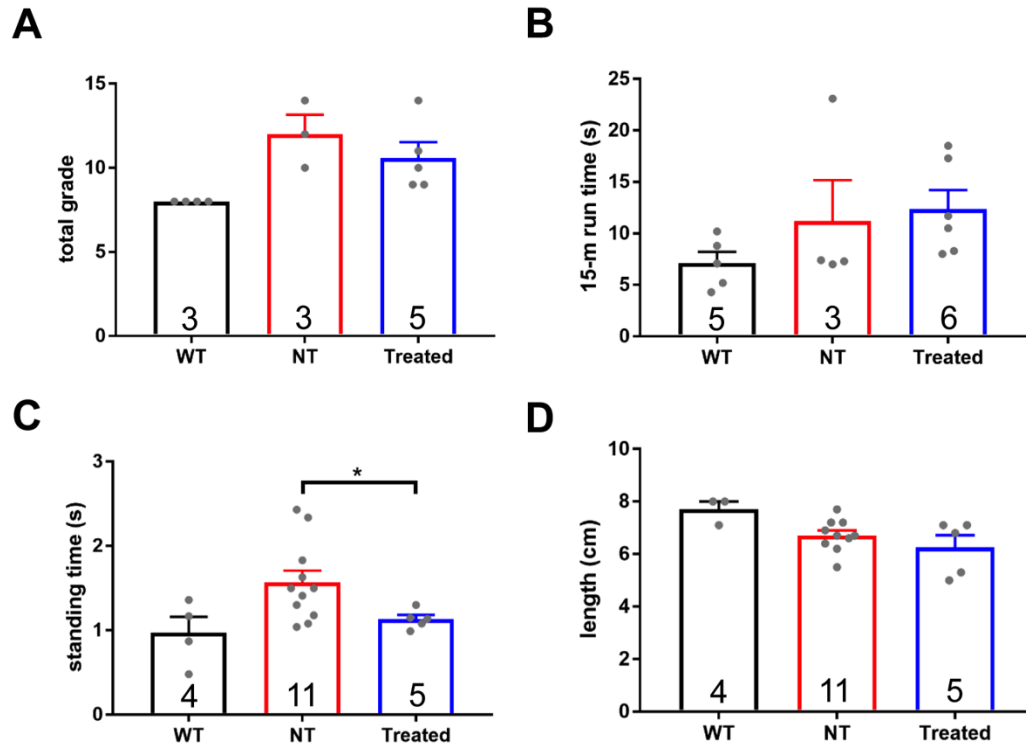


**Figure 4.9. Functional testing of CXMD<sub>J</sub> dogs.** PMO-treated CXMD<sub>J</sub> dogs, together with age-matched non-treated (NT) CXMD<sub>J</sub> and wild-type (WT) dogs, were subjected to four different functional tests, (A) clinical grading, (B) the 15-m run test, (C) the standing test, and (D) the aperture test. Results for each of these tests are shown. Sample sizes are indicated within the bars. Dots represent individual dogs. Error bars: S.E.M., \* $p < 0.05$ , one-tailed Welch t-test.

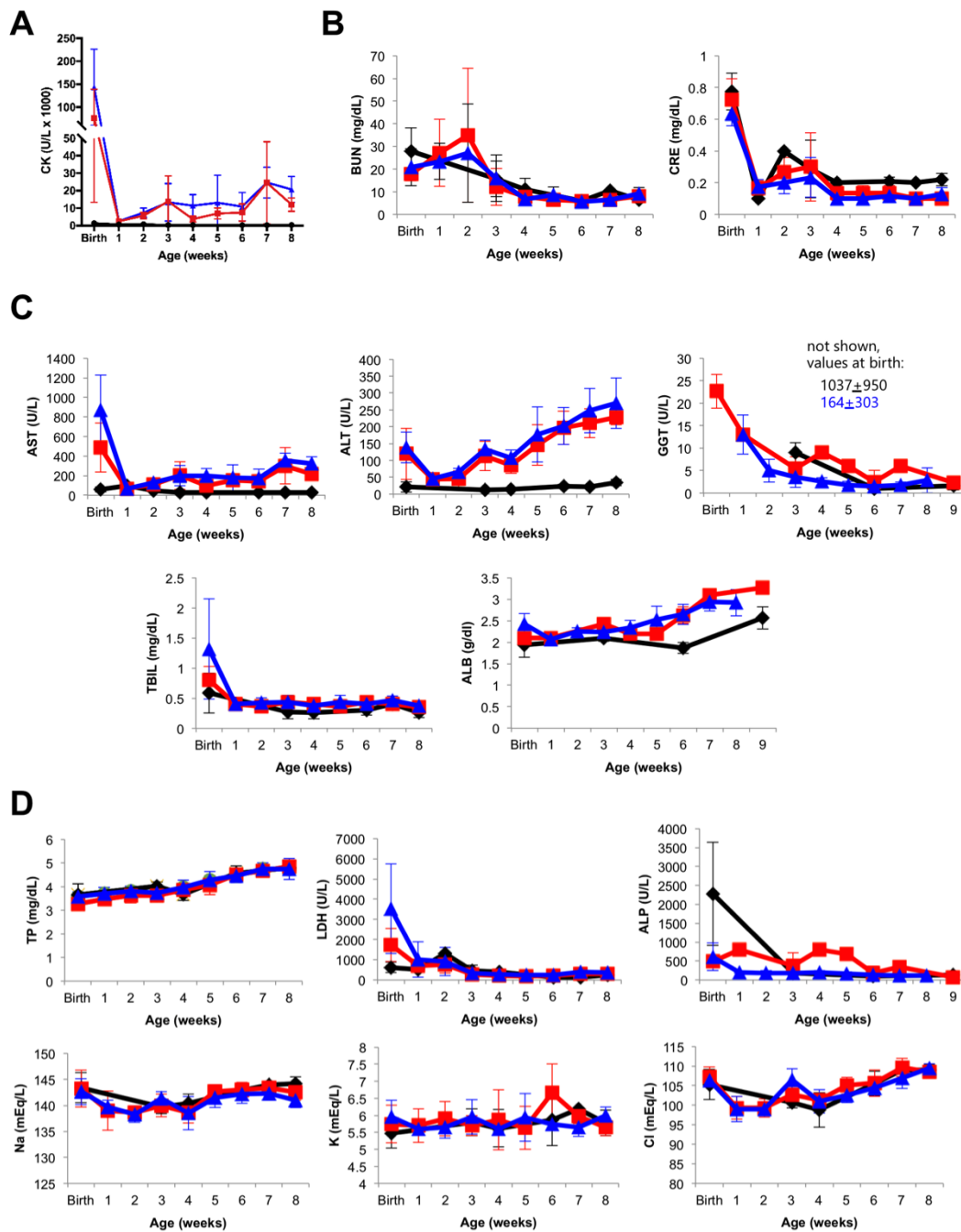


**Figure 4.10. Analysis of serum biomarkers from weekly blood tests in neonatal dogs.** The levels of various serum biomarkers were analyzed in weekly samples collected from wild-type (black), non-treated CXMD<sub>j</sub> (red), and PMO-treated CXMD<sub>j</sub> (blue) dogs. (A) Creatine kinase (CK) levels. (B) Kidney damage marker levels: blood urea nitrogen (BUN), serum creatinine (CRE). (C) Liver damage marker levels: aspartate aminotransferase (AST), alanine aminotransferase (ALT), gamma-glutamyl transferase (GGT), total bilirubin (TBIL), serum albumin (ALB). (D) General marker levels: total protein (TP), lactate dehydrogenase (LDH), alkaline phosphatase (ALP), sodium (Na), potassium (K), chloride (Cl). Error bars: S.D. n = 1-12, wild-type; n = 3-4, non-treated; n = 4-6, treated.

#### 4.4. Discussion

The childhood onset of DMD and its progressive nature form a strong rationale for its early treatment. Younger patients are not typically exposed to increased rates of muscular deterioration and to various organ-related complications, presenting better opportunities for preventative treatment. As well, DMD is characterized by the progressive replacement of muscle with fat and connective tissue.<sup>293</sup> Exon skipping can only rescue and protect existing muscle fibers and therapeutic outcome depends on the levels of muscle preservation, therefore earlier treatment provides higher therapeutic value to DMD patients. Here, we sought to determine the advantages, if any, of early exon skipping treatment *in vivo*. This is the first demonstration in the neonatal CXMD<sub>J</sub> model of the efficacy of early treatment with a multi-exon skipping PMO cocktail. This is also the first statistically powered investigation of exon skipping therapy in this model, providing strong insight into the efficacy and safety of exon skipping in a large animal system.

Early exon skipping treatment restored dystrophin at varying levels across both muscles and individual dogs; certain muscles only had trace amounts of dystrophin post-treatment (**Figures 4.2b, 4.3**). This variability has been reported in other studies in mice,<sup>294</sup> including our previous study in adult dogs<sup>198</sup> where some muscles did not respond well to the PMO treatment even at high doses and extended treatments. The factors influencing this are unknown.<sup>294</sup> Skeletal muscle type does not appear to strongly impact exon skipping outcome; however, the success of PMO delivery into each muscle may have an effect. Interestingly, there seems to be a disparity between Western blotting and immunohistochemistry results (**Figures 4.2b, 4.4**). This might be because the truncated dystrophin with exons 6-9 skipped is less stable than full-length dystrophin and more susceptible to degradation during preparation for Western blot.

Alternatively, dystrophin rescue along a muscle is typically variable and patchy;<sup>294</sup> it may simply be fortuitous that a high density of dystrophin-positive fibers was observed for 8603MA in the examined sections (**Figure 4.4**) than others (**Figure 4.2c**).

Early treatment with the 4-PMO cocktail was most beneficial for the diaphragm, which showed the highest levels of dystrophin rescue and the greatest amelioration of histopathology among muscles (**Figures 4.2b, 4.5**). As the diaphragm is one of the first, most severely affected muscles in neonatal dystrophic dogs,<sup>295</sup> the finding that it responded well suggests that early exon skipping can oppose the initial stages of muscular deterioration, should it occur (not all skeletal muscles examined in neonatal CXMD<sub>J</sub> dogs showed signs of severe degeneration; **Figure 4.5**). Further testing will determine if treatment improves respiratory function. Given the central role of the diaphragm in respiration, early treatment with exon skipping PMOs could be considered for preventing or delaying pulmonary malfunction, one of the leading causes of death in patients.<sup>112,296</sup>

In adult CXMD<sub>J</sub> dogs, intravenous treatment with a 3-PMO cocktail (Ex6A, Ex6B, Ex8A) restored >25% dystrophin of wild-type levels in skeletal muscles such as the triceps brachii and diaphragm; other muscles did not respond as highly.<sup>198</sup> The levels of dystrophin rescue observed here were not as high as those in treated adult dogs—this was likely due to differences in experimental design between the two studies, e.g. treatment frequency and length, and/or due to differences in PMO uptake efficiency or behavior between neonatal and adult dog muscles. Dystrophin restoration accumulates with longer and more frequent exon skipping treatment.<sup>194</sup> Potentially higher levels of rescue can be obtained with increased injection frequencies over an extended period of time, as previously reported in the eteplirsen clinical trials.<sup>18</sup> Additionally, this delayed accumulation of dystrophin could explain why the rescue

levels observed were not as high as the exon skipping efficiencies obtained in each muscle. PMOs also have a dose-dependent effect extensively observed in pre-clinical studies; increasing the dose could have been another option. Given these, it is highly encouraging that even with the amounts of dystrophin rescue obtained, treated neonatal dystrophic dogs still showed significant improvements in histology and a test of muscle function, i.e., the standing test. Indeed, this calls into question what amount of dystrophin rescue can be considered as being “clinically beneficial”. While 10% dystrophin of healthy levels is usually the least amount thought to be of clinical benefit based on BMD patient reference values,<sup>211</sup> a study using transgenic mice suggests as low as ~3% of healthy levels can be beneficial.<sup>297</sup> Additionally, some amount of therapeutic benefit, though not considerable, was observed with eteplirsen use despite the drug only rescuing <1% dystrophin of normal levels after 180 weeks.<sup>18</sup> The validity of dystrophin as a biomarker for functional improvement will therefore have to be investigated carefully, especially given the many inherent sources of variability associated with its quantification.<sup>294</sup>

The mechanisms underlying PMO delivery into dystrophic muscle are an area of active research. It was believed that the compromised permeability of dystrophic muscle was responsible for enhancing PMO entry into tissues.<sup>298</sup> Recent evidence, however, suggests that PMO entry is largely influenced by the regenerative/inflammatory state of muscle. Increased PMO uptake was observed in muscle cells undergoing differentiation, as one would observe in actively regenerating muscle, compared to when they were proliferating.<sup>299,300</sup> It was also discovered that macrophages act as PMO reservoirs, taking up large amounts of PMOs and gradually releasing them into their surroundings, increasing the duration these PMOs are available to the muscle.<sup>300</sup> The clustered, patchy distribution of dystrophin-positive fibers in treated muscle (**Figure 4.2c**) supports the above models, as distinct centers of regeneration and

inflammation can be found along the length of the dystrophic muscle. Since the majority of skeletal muscles in CXMD<sub>J</sub> dogs are not yet in a state of severe dystrophic pathology at an early age (**Figure 4.5**), this may have resulted in sub-optimal PMO uptake into tissues. This may be one issue to consider should exon skipping AOs be administered to young DMD patients. However, early exon skipping treatment would theoretically be capable of acting on the pathology as soon as it begins, since the AOs could gain entry at the earliest signs of muscular degeneration.

The PMO uptake observed in cardiac muscle remains a curious observation (**Figure 4.8b**). The levels of cardiac PMO uptake (and even skeletal muscle uptake) we found here were similar to those observed in our previous study in CXMD<sub>J</sub> dogs, where we administered peptide-conjugated PMOs (PPMOs) (3-PPMO cocktail, 4 mg/kg/PPMO) instead, a chemistry that exhibits enhanced cardiac uptake.<sup>301</sup> PMOs have historically been known to have poor uptake in the heart,<sup>302</sup> hence the low to nonexistent exon skipping activity observed. From a previous study of CXMD<sub>J</sub> dog hearts, abnormalities, as detected by electrocardiography, echocardiography, and histology, were detectable by 2, 6-7, and 21 months of age, respectively.<sup>303</sup> Hence, the increase in uptake cannot be explained by heightened regeneration or inflammation in the heart of neonatal dystrophic dogs. We hypothesize that the conflicting observation of both high PMO uptake and the absence of dystrophin rescue in the heart is due to the increased endosomal trapping of PMOs in cardiac muscle cells. PMOs and most other AOs enter cells via receptor-mediated endocytosis.<sup>304</sup> Once internalized, AOs must escape from endosomes to reach their target in the nucleus. AOs have a greater propensity to be trapped in these endosomes in cardiomyocytes than in myotubes in vitro.<sup>305</sup> The conjugation of cell-penetrating peptides to PMOs (i.e., PPMOs) is thought to facilitate endosomal escape, hence the increased activity of

PPMOs compared to PMOs.<sup>306,307</sup> Of course, intracellular mechanisms other than endosomal trapping could have resulted in a similar phenomenon of PMO retention. Thus, in-depth studies of PMO intracellular trafficking in cardiac muscle cells is recommended to better understand PMO uptake in the heart. Findings from these should inform us on how we can better target cardiac muscle with exon skipping AOs, for instance, by informing a more rational design of cell-penetrating peptides and other AO chemistries.

The present study shows that early treatment with multi-exon skipping PMOs is safe, as assessed using serum biomarker analysis (**Figure 4.10**). There was also no accumulation of the four PMOs in the sera of treated dogs throughout the study (**Figure 4.8a**). This implies that early treatment with exon skipping PMOs should be safe regardless of age, indicating the possibility of applying this strategy to young DMD patients in the clinic. This should also support the inclusion of younger patients in clinical trials for exon skipping therapies, which would help increase the sample sizes for these trials. On a related note, Sarepta is currently recruiting for a phase II clinical trial that aims to determine the efficacy of eteplirsen treatment in boys with early-stage DMD, aged 4-6 years old.<sup>203</sup> Results from this trial should shed more light on how useful early exon skipping treatment is for patients.

In conclusion, early treatment of neonatal CXMD<sub>J</sub> dogs with a multi-exon skipping PMO cocktail led to body-wide exon skipping and dystrophin rescue, as well as the amelioration of dystrophic histopathology, in skeletal muscles with no evidence of toxicity. Early exon skipping treatment was most beneficial for the diaphragm, with implications for preventing respiratory failure in young DMD patients. The treatment also resulted in some amount of functional improvement. While the efficacy in cardiac muscles was low, there was a surprisingly high uptake of PMOs in the dog heart, an observation that warrants further investigation. A more

extended study is recommended to determine the efficacy of early exon skipping treatment in the long run. Though not many, a certain population of patients with point, duplication, and deletion mutations amenable to exon 6-8/9 skipping have been enrolled in DMD mutation databases (UMD-DMD and LOVD). We have previously demonstrated in vitro translation of the 4-PMO cocktail for the dog model to a patient with an exon 7 deletion.<sup>28</sup> The in vivo finding shown here further confirms the therapeutic potential of exon 6-8/9 skipping to such patients. Finally, as the technology for facilitating DMD diagnosis continues to advance, safe and effective therapies can be provided at an earlier time to patients. This enables us to act on the disease before it even manifests, potentially generating more improved health outcomes for patients with DMD.

## **4.5. Methods**

### **4.5.1. Animals**

Animals were housed at the National Center for Neurology and Psychiatry (NCNP) in Tokyo, Japan following guidelines by their Ethics Committee for the Treatment of Laboratory Middle-sized Animals. All procedures were reviewed and approved by the respective Institutional Animal Experiment Committees at NCNP. A listing of animals used, with information on respective experimental groups and the procedures conducted for each, is provided in **Table 4.1**. Genotyping confirmed the presence of the CXMD<sub>J</sub> mutation.

### **4.5.2. Intravenous PMO treatment and sample collection**

PMO sequences and target regions are in **Figure 4.1a**; sequences were based on our previous work.<sup>198,289</sup> A cocktail consisting of Ex6A, Ex6B, Ex8A, and Ex8G, each synthesized by Gene Tools, was prepared in saline with 50 mg/kg/PMO (total 200 mg/kg). Intravenous

injection of the cocktail into CXMD<sub>J</sub> dogs via the saphenous vein was performed as described.<sup>308</sup> Injections were done every other week, at 1, 3, and 5 weeks of age (**Figure 4.1b**). Weekly blood samples were collected for toxicity testing. At 2-3 weeks after the final injection, dogs were subjected to functional testing and then euthanized by exsanguination while under general anesthesia. Muscle samples were collected as previously described.<sup>309</sup> Corresponding muscles were also collected from age-matched non-treated CXMD<sub>J</sub> and wild-type dogs.

#### **4.5.3. Functional assessment**

Four functional tests were done: clinical grading, 15-m run, standing, and maximum open-mouth width determination. Clinical grading was done as previously described.<sup>310</sup> to assess overall condition/phenotype using standardized 5-point scales. In the 15-m run test, the time it took to traverse a 15-m distance was recorded. For the standing test, dogs were laid in a lateral recumbent position and the time for each dog to stand back up was recorded. The 15-m run and standing tests were repeated up to 5 times per dog; the average across all trials was obtained. Finally, the maximum open-mouth distance for each dog was measured to evaluate jaw joint contracture. All tests were performed by handlers (led by, and including, M.K.) blinded to the treatment allocation.

#### **4.5.4. Exon skipping efficiency determination**

Exon skipping efficiencies were determined as previously described,<sup>309</sup> with modifications below. cDNA was synthesized from 1000 ng of total RNA using SuperScript IV reverse transcriptase (Invitrogen), with 2.5  $\mu$ M random hexamers (Invitrogen) and a final volume of 20  $\mu$ l; a reaction containing nuclease-free water instead of RNA served as a negative control.

PCR was performed with 8  $\mu$ l of cDNA or negative control using GoTaq (Promega). To detect skipping, a forward exon 5 primer (5'-CTGACTCTTGGTTTGATTTGGA-3') and a reverse exon 10 primer (5'-TGCTTCGGTCTCTGTCAATG-3') were used at final concentrations of 0.3  $\mu$ M. The following program was used: 1) 95°C, 2 min, 2) 40 cycles of 95°C, 30 s; 60°C, 30 s; 72°C, 42 s, 3) 72°C, 5 min, 4) 4°C, hold. PCR products were run on an agarose gel and band intensities were quantified using Image J (NIH). Exon skipping efficiency was calculated using: [(skipped band intensity)/(total intensity of native, intermediate, and skipped bands)]  $\times$  100 (%). Identities of skipped products were confirmed by sequencing.

#### **4.5.5. Western blot analysis of dystrophin rescue**

For protein extraction, 100  $\mu$ l of a high SDS lysis buffer (10% SDS, 70 mM Tris-HCl at pH 6.7, 5 mM EDTA at pH 8.0, 5%  $\beta$ -mercaptoethanol in water) with proteinase inhibitor cocktail (Roche) was added to 20- $\mu$ m frozen muscle sections. This was mixed, incubated at 37°C for 5 min, and spun at max speed for 30 min at 16°C to collect the protein-containing supernatant. Protein was quantified using the Pierce<sup>TM</sup> Coomassie (Bradford) Protein Assay kit (Thermo Fisher). Protein was prepared by adding NuPAGE<sup>TM</sup> LDS Sample Buffer (Thermo Fisher) and NuPAGE<sup>TM</sup> Sample Reducing Agent (Thermo Fisher) at 1 $\times$  final concentrations into the samples, and then incubating at 70°C for 10 min. Western blotting was performed as described previously.<sup>309</sup> For non-treated and treated CXMD<sub>J</sub> dogs, 40 or 60  $\mu$ g protein was used; 100%, 20%, 10%, or 5% of this was used for wild-type samples. The primary antibodies used, diluted using 2% Amersham ECL Prime blocking reagent (GE Healthcare) in phosphate buffered saline with 0.05% Tween 20 (PBST), were: NCL-DYS1 (1:200, Leica Biosystems) for the dystrophin rod domain and desmin (1:4000, Abcam) as a loading control. Appropriate HRP-

conjugated secondary antibodies (anti-mouse IgG2a for DYS1, anti-rabbit IgG H+L for desmin; Bio-Rad) were used at a 1:10000 dilution in PBST. Post-transfer, the gel was stained with PageBlue<sup>TM</sup> Protein Staining Solution (Thermo Fisher) for 1 hr at room temperature to visualize myosin heavy chain (MyHC), as another loading control. Dystrophin levels were quantified from DYS1 band intensities, relative to the intensity of the wild-type band with 5% protein.

#### **4.5.6. Immunohistochemistry**

Frozen muscles from wild-type, non-treated CXMD<sub>J</sub>, and treated CXMD<sub>J</sub> dogs were sectioned with 7- $\mu$ m thickness and placed on poly-L-lysine-coated slides. Sections were air-dried for at least 30 min at room temperature. These were then incubated in NCL-DYS1 (1:50) or NCL-DYS2 (1:50, Leica Biosystems; targets the dystrophin C-terminal domain), diluted in PBS with 0.1% Triton X-100 (PBSTX), for 1 hr at room temperature. Following three 5-min PBS washes, sections were incubated with AlexaFluor 594-conjugated secondary antibodies (anti-mouse IgG2a for DYS1, anti-mouse IgG1 for DYS2; Thermo Fisher) at a 1:1000 dilution in PBSTX for 1 hr at room temperature. After three 5-min PBS washes, samples were mounted with VECTASHIELD HardSet Antifade Mounting Medium with DAPI (Vector Laboratories). Samples were visualized in a blinded manner at a total magnification of 200 $\times$  using the Zeiss LSM 710 confocal microscopy system or the Olympus FluoView<sup>TM</sup> laser-scanning microscope.

#### **4.5.7. Histology**

Samples were prepared as in the *Immunohistochemistry* section. Sections were stained using Mayer's hematoxylin and eosin Y (Electron Microscopy Sciences), following standard procedure. Samples were visualized at 200 $\times$  magnification, using a Nikon Eclipse TE2000-U

microscope. Images were taken in at least three random fields of view per sample. Centrally nucleated fibers (CNFs) were quantified using Image J, with:  $[(\# \text{ CNFs}) / (\text{total } \# \text{ fibers})] \times 100$  (%). Around 200 to 2,800 of total myofibers were counted per muscle sample for CNF analysis. Fibrosis/necrosis was quantified following TREAT-NMD SOP DMD\_M.1.2.007 v.1.0 and van Putten et al. (2010).<sup>311</sup> Image J with the color deconvolution plugin (G. Landini, free from <http://www.mecourse.com/landinig/software/cdeconv/cdeconv.html>) was used. The following was used for fibrosis/necrosis quantification:  $[(\text{fibrotic or necrotic area}) / (\text{total image area})] \times 100$  (%). Values obtained across all fields of view were averaged for each sample. Image acquisition and both CNF and fibrosis/necrosis quantification were done blinded.

#### **4.5.8. Blood tests**

Serum was obtained from weekly blood samples of treated CXMD<sub>J</sub> dogs and used for determining the levels of: CK, blood urea nitrogen (BUN), serum creatinine (CRE), aspartate aminotransferase (AST), alanine aminotransferase (ALT), serum albumin (ALB), total bilirubin (TBIL), gamma-glutamyl transferase (GGT), total protein (TP), lactate dehydrogenase (LDH), alkaline phosphatase (ALP), sodium (Na<sup>+</sup>), potassium (K<sup>+</sup>), and chloride (Cl<sup>-</sup>). These were also analyzed in sera from non-treated CXMD<sub>J</sub> and wild-type dogs at various ages, to provide reference values. NCNP performed tests for all biomarkers, with additional tests by C-Path (Comparative Clinical Pathology Services, LLC, Columbia, MO) for ALB, ALP, and GGT.

#### **4.5.9. ELISA**

ELISA was performed based on the method by Burki et al. (2015)<sup>312</sup> and in our previous study.<sup>301</sup> PMOs in the blood were quantified using sera from weekly blood samples of treated

CXMD<sub>J</sub> dogs, or from age-matched samples of non-treated CXMD<sub>J</sub> and wild-type dogs. For PMO uptake quantification, protein was extracted from 20- $\mu$ m frozen muscle sections using RIPA buffer (Thermo Fisher) with proteinase inhibitor cocktail (Roche). Lysates were incubated overnight at 55°C, and then spun at maximum speed for 15 min to collect the protein-containing supernatant. Protein was quantified using the Pierce<sup>TM</sup> BCA Protein Assay kit (Thermo Fisher). Probes with complementary sequences to the PMOs used were synthesized (IDT) and modified at the 5' and 3' ends with digoxigenin and biotin, respectively; the first and last seven nucleotides were fully phosphorothioated.<sup>301</sup> PMO amounts were calculated in reference to a standard curve constructed from fluorescence values given by the respective PMO standards. We thank Dyanna Melo and Quynh Nguyen (Yokota lab, University of Alberta) for their technical assistance and support with this experiment.

#### **4.5.10. Statistical analysis**

Statistical analysis was conducted using GraphPad Prism 7 (GraphPad Software, Inc.). As appropriate, one-way ANOVA with Tukey's post hoc test or Dunnett's multiple comparisons test, a one-tailed Student's t-test or Welch t-test was conducted to determine statistical significance.

## **Chapter 5 Development of DG9 Peptide-Conjugated Single- and Multi-exon Skipping Antisense Oligonucleotides for the Treatment of Duchenne Muscular Dystrophy**

Chapter 5 was derived from the following article being prepared for submission:

Lim, K. R. Q., Woo, S., Melo, D., Huang, Y., Dzierlega, K., Aslesh, T., Roshmi, R. R., Shah, M. N. A., Echigoya, Y., Maruyama, R., Moulton, H. & Yokota, T. Development of a minimized, peptide-conjugated exons 45-55 skipping therapy for Duchenne muscular dystrophy.

## 5.1. Abstract

Duchenne muscular dystrophy (DMD) is primarily caused by out-of-frame deletions in the dystrophin gene. Exon skipping using phosphorodiamidate morpholino oligomers (PMOs) converts out-of-frame to in-frame mutations, producing partially functional dystrophin. Four single-exon skipping PMOs are approved for DMD, but treat only 8-14% of patients each and some exhibit poor efficacy. Alternatively, exons 45-55 skipping could treat 40-47% of all patients and is associated with improved clinical outcomes. Here, we report the development of peptide-conjugated PMOs for exons 45-55 skipping. Experiments with immortalized patient myotubes revealed that exons 45-55 could be skipped by targeting as few as 5 exons. We also found that conjugating DG9, a cell-penetrating peptide, to PMOs improved single-exon 51 skipping, dystrophin restoration, and muscle function in hDMDdel52;*mdx* mice. Local administration of a minimized exons 45-55-skipping DG9-PMO cocktail restored dystrophin production. This study provides proof-of-concept towards development of a more economical and effective exons 45-55 skipping DMD therapy.

## 5.2. Introduction

Duchenne muscular dystrophy (DMD) is a fatal, X-linked recessive disorder caused by mutations in the *DMD* gene that lead to absence of dystrophin in muscle. Dystrophin stabilizes the sarcolemma by bridging cytoskeletal actin to the extracellular matrix, via the formation of a membrane-associated glycoprotein complex.<sup>109,118</sup> Dystrophin loss results in progressive body-wide muscle degeneration, loss of ambulation before the teens, and cardiorespiratory malfunction during the twenties that typically leads to death.<sup>112,120</sup> DMD affects 1:3,500-5,000

male births and is considered the most common inherited neuromuscular disorder in the world.<sup>110,111</sup>

There is still no effective cure for DMD, but exon skipping is emerging as a promising therapeutic approach. The majority of patients (~70%) have large out-of-frame deletions in *DMD*.<sup>167</sup> Exon skipping is based on the observation that, at least ~90% of the time, in-frame mutations in *DMD* give rise to milder phenotypes, as found in patients with Becker muscular dystrophy.<sup>165,167</sup> By excluding out-of-frame exons from the final *DMD* transcript using antisense oligonucleotides, exon skipping converts out-of-frame into in-frame mutations, allowing for the production of truncated but partially functional dystrophin protein.<sup>73</sup> Four exon skipping therapies have been approved by the U.S. Food and Drug Administration: eteplirsen/Exondys 51 (Sarepta),<sup>203</sup> golodirsen/Vyondys 53 (Sarepta),<sup>313</sup> viltolarsen/Viltepso (NS Pharma),<sup>314</sup> and casimersen/Amondys45 (Sarepta).<sup>315</sup> Eteplirsen skips *DMD* exon 51, golodirsen and viltolarsen skip exon 53, and casimersen skips exon 45. All are antisense oligonucleotides with the phosphorodiamidate morpholino oligomer (PMO) chemistry.

The applicability of single-exon skipping therapies is, however, inherently limited due to their mutation-specific nature. The therapies above could each treat at most only 8-13% of all patients.<sup>130</sup> Multi-exon skipping overcomes this issue, particularly skipping *DMD* exons 45-55. Exons 45-55 is a mutation hotspot in the *DMD* gene. It harbors 66% of all large ( $\geq 1$  exon) deletions and 15% of all large duplications found in patients according to a study of the global TREAT-NMD database,<sup>167</sup> a finding corroborated by other databases.<sup>168,316</sup> Exons 45-55 skipping could thus theoretically treat 40-47% of all DMD patients.<sup>317-319</sup> An exons 45-55 deletion is also commonly associated with asymptomatic to mild phenotypes in patients. The

deletion leads to BMD in 90% of cases, supporting the potential therapeutic benefit of skipping the region.<sup>320</sup>

The development of effective exons 45-55 skipping cocktails has been challenging, since at most 10 exons have to be skipped simultaneously. Previous works from our group focused on targeting each exon in the region for skipping, as this is the most direct approach. Using *in silico* tools to minimize detrimental interactions between PMOs, we developed an exons 45-55 skipping cocktails that restored dystrophin synthesis in the muscles of a dystrophic mouse model.<sup>321</sup> More importantly, using similar approaches we have also developed a PMO cocktail that induced human *DMD* exons 45-55 skipping in immortalized patient myotubes and in humanized DMD mice.<sup>320</sup> Average skipping efficacies of 27-61% and 15-22% were observed, respectively, and treatment produced up to 14% dystrophin of normal levels *in vitro*. However, this cocktail uses one PMO for each exon (except for exon 48, which required two) to skip exons 45-55. As all cocktail PMOs have to be present in the same nuclei at the same time to induce exon skipping, it may be beneficial to use less PMOs to improve efficacy. There is also a lower risk of off-target effects when less PMOs are used. Moreover, using a large number of PMOs is not economically favorable as a therapy given how expensive it is to synthesize each PMO. We aim to reduce the number of PMOs required to skip exons 45-55 in this study. This objective is also inspired by previous observations, where skipping a target exon sometimes leads to the skipping of an adjacent non-target exon, e.g. when skipping dystrophin exons 6-8, we tend to see the spontaneous skipping of exon 9.<sup>301,322</sup>

Another issue associated with exon skipping therapies is their efficacy. In the case of PMOs, this is largely tied to their rapid clearance from the bloodstream, poor uptake into muscle, and the inability to escape from endosomes once internalized.<sup>305,323</sup> As a result, PMOs display

reduced skipping efficiencies *in vivo* to the extent that they are incapable of even inducing exon skipping in the heart.<sup>324</sup> Eteplirsen for instance, though approved, only restored 0.93% dystrophin of normal levels in patients after 180 weeks of treatment with a 30 or 50 mg/kg/week dose.<sup>203</sup> One solution to this efficacy problem is the conjugation of cell-penetrating peptides to PMOs.<sup>323,325</sup> By enhancing PMO uptake *in vivo*, these peptides have been widely documented to improve exon skipping efficiencies and treatment outcomes in pre-clinical trials. It has been quite successful that a peptide-conjugated exon 51-skipping PMO by Sarepta (SRP-5051) is currently being tested in phase II human clinical trials, with reportedly positive results.<sup>326</sup>

Using a zebrafish reporter system, we have identified DG9 as a promising, novel PMO peptide conjugate that induced strong exon skipping in skeletal muscle and even higher skipping levels the heart.<sup>327</sup> In this work, we test the therapeutic efficacy of DG9-conjugated exon skipping PMOs (DG9-PMOs) in humanized dystrophic hDMDdel52;*mdx* mice. These mice have a stably integrated human *DMD* transgene in chromosome 5, with an out-of-frame partial deletion of exon 52.<sup>328-330</sup> These mice also have the *mdx* mutation, a nonsense point mutation in exon 23 of the mouse *Dmd* gene,<sup>176</sup> and so do not have detectable levels of both human and mouse dystrophin protein. This genetic configuration makes the hDMDdel52;*mdx* mouse an excellent model for testing the therapeutic efficacy of human sequence-specific exon skipping PMOs *in vivo*. We first evaluate the efficacy of systemic DG9-PMO treatment in this model using a single-exon (exon 51) skipping approach. We then apply DG9 to the minimized exons 45-55 skipping cocktail developed in this study, and determine its potential as a multi-exon skipping therapy for DMD.

## 5.3. Results

### 5.3.1. Minimizing the exons 45-55 skipping cocktail

We sought to minimize the number of PMOs needed to skip human *DMD* exons 45-55 using two strategies. First, we took our previously developed exons 45-55 skipping cocktail<sup>320</sup> (**Table 5.1**) and prepared derivatives where we each removed a PMO (or PMOs) that targeted an exon in the region. We refer to the full cocktail, which has PMOs targeting all exons within exons 45-55, as the “all” cocktail from this point onward (**Figure 5.1a**). Upon transfecting the “all” cocktail and its derivatives into healthy KM155 myotubes (**Figure 5.1b**), the resulting exons 45-55 skipping efficiencies were examined. Only the “all” cocktail skipped exons 45-55 significantly higher than the mock control ( $p<0.005$ ) (**Figure 5.2a**). PMOs whose absence led to a considerable drop in skipping efficiency were kept as part of the minimized cocktail, i.e., those targeting exons 45, 47, and 53. We also decided to retain PMOs targeting exons 49, 51, and 55 based on their position, to presumably keep the cocktail working at an appreciable efficiency. This minimized cocktail was called the “base” cocktail, which was subjected to another round of minimization in exon 52-deleted KM571 myotubes similar to what we did before. The “base” cocktail showed significant exons 45-55 skipping ( $p<0.05$ ) compared to the mock control, as well as its derivatives where exons 47 ( $p<0.05$ ) or 51 ( $p<0.05$ ) were not targeted (**Figure 5.2a**). We decided to move forward with the “base” and “base -51” cocktail since these were the minimized cocktails that showed the highest skipping efficiency in this batch (**Figure 5.1a**).

**Table 5.1. List of PMO sequences used for exons 45-55 skipping.**

<b>ID*</b>	<b>Sequence, 5' to 3'</b>
Ex45_Ac9	GACAACAGTTTGCCGCTGCCCAATGCCATC
Ex46_Ac93	AGTTGCTGCTCTTTTCCAGGTTCAAGTGGG
Ex47_Ac13	GTTTGAGAATCCCTGGCGCAGGGGCAACT
Ex48_Ac7	CAATTTCTCCTTGTTTCTCAGGTAAAGCTC
Ex48_Ac78	CAGATGATTTAACTGCTCTTCAAGGTCTTC
Ex49_Ac17	ATCTCTTCCACATCCGGTTGTTTAGCTTGA
Ex50_Ac19	GTAAACGGTTTACCGCCTTCCACTCAGAGC
Ex51_Ac0	GTGTCACCAGAGTAACAGTCTGAGTAGGAG
Ex52_Ac24	GGTAATGAGTTCTTCCAACCTGGGGACGCCT
Ex53_Ac26	CCTCCGGTTCTGAAGGTGTTCTTGTACTTC
Ex54_Ac42	GAGAAGTTTCAGGGCCAAGTCATTTGCCAC
Ex55_Ac0	TCTTCCAAAGCAGCCTCTCGCTCACTCACC

\*represented as: exon target\_distance from target exon acceptor site

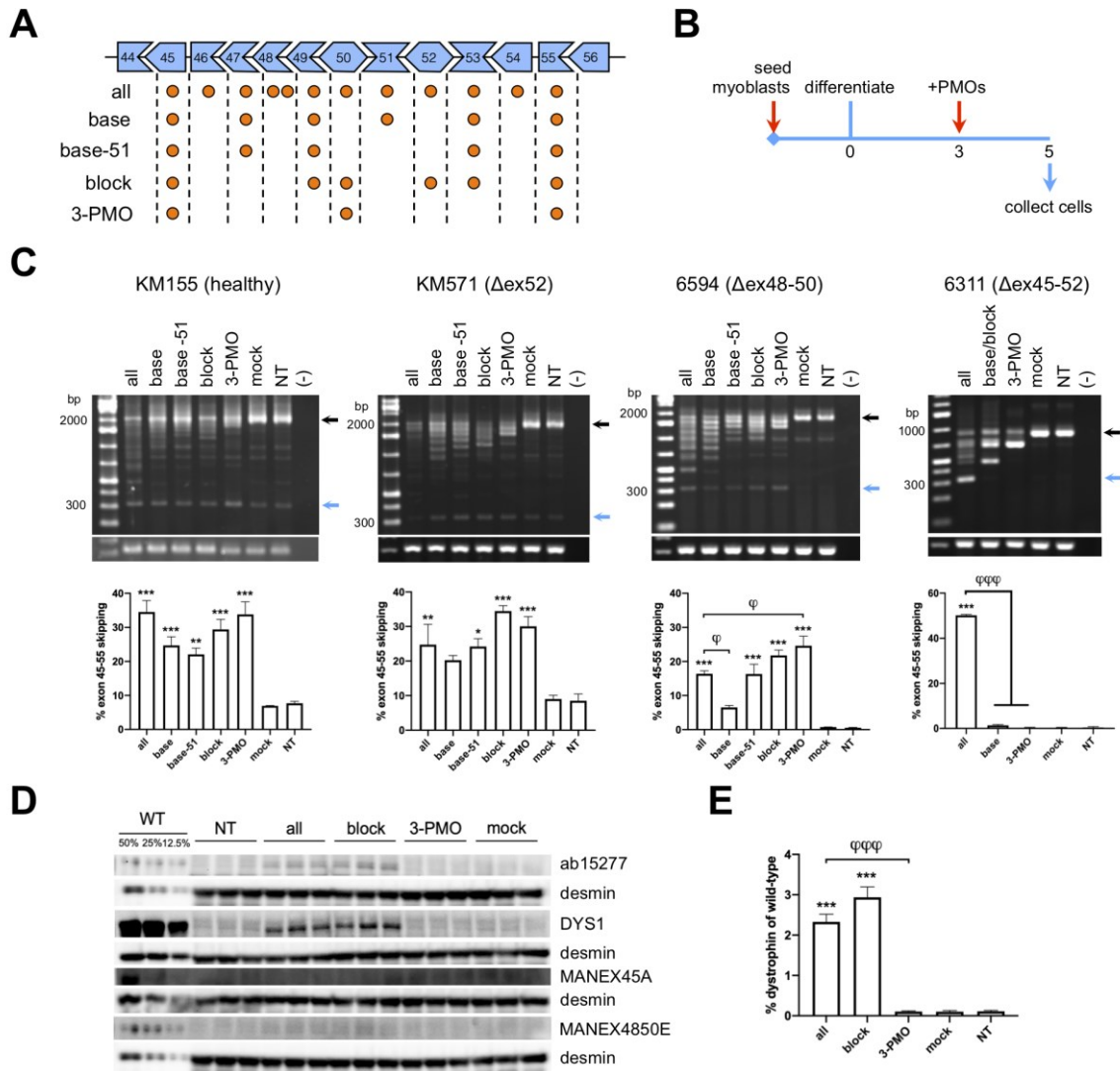


**Figure 5.1. Testing minimized exons 45-55 skipping cocktails in immortalized patient myotubes.** (A) *DMD* exons 45-55 are shown at the top, and exons targeted by the “all” cocktail and its minimized derivatives are indicated by orange circles. (B) Culture scheme used for PMO cocktail transfection in immortalized patient myotubes. (C) RT-PCR *DMD* exons 45-55 skipping efficiency results upon transfection of the “all” and minimized PMO cocktails in KM155, KM571, 6594, and 6311 myotubes. Black arrows indicate native, unskipped bands while blue arrows indicate exons 45-55-skipped bands. *GAPDH* is shown as a control. Quantification is shown at the bottom of each representative gel image. (D) Western blot detection for dystrophin in PMO-treated and non-treated (NT) KM571 myotubes using various antibodies (ab15277, DYS1, MANEX45A, MANEX4850E). Protein extracts were loaded at 40  $\mu$ g for treated and NT samples, and at indicated percentages of this for wild-type KM155 samples (WT). Desmin was detected as a loading control for each dystrophin antibody. (E) Quantification of DYS1 signals shown in (D), with values shown relative to the intensity of the 12.5% WT band. (n=3 for C-E) Error bars: S.E.M. \* $p$ <0.05, \*\* $p$ <0.005, \*\*\* $p$ <0.001 one-way ANOVA with Dunnett’s test versus mock,  $\varphi p$ <0.05,  $\varphi\varphi\varphi p$ <0.001 one-way ANOVA with Dunnett’s test versus “all”.

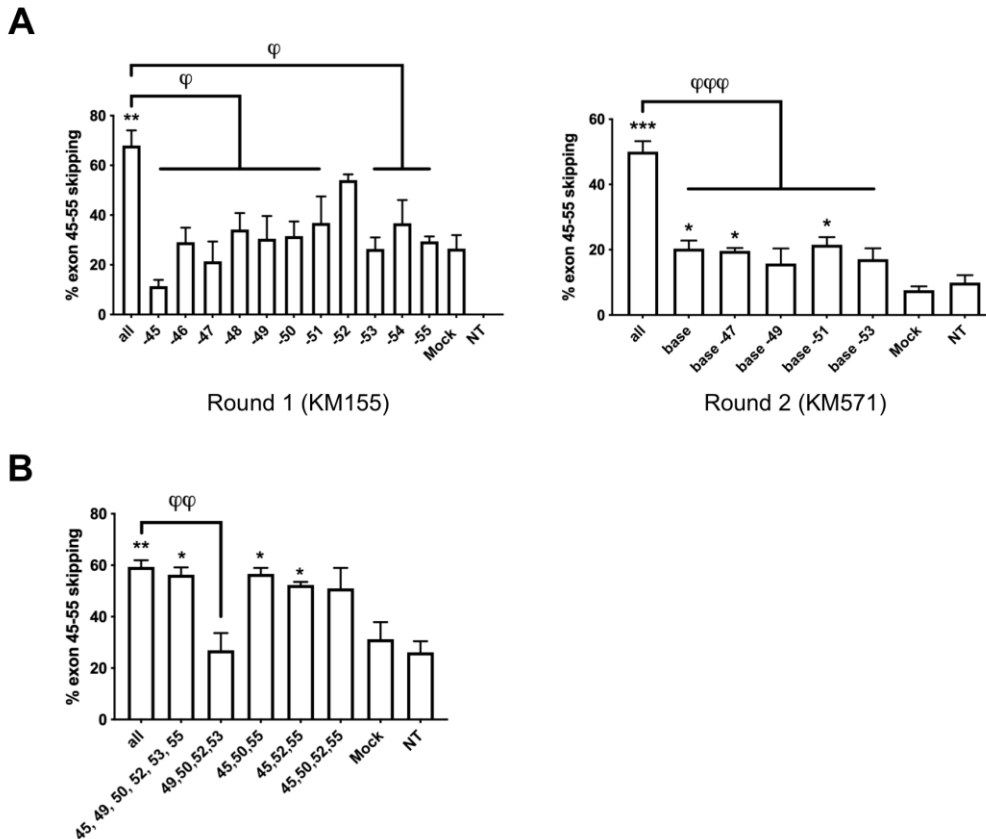


**Figure 5.2. Preliminary testing of minimized exons 45-55 skipping cocktails.** Minimized derivatives of the “all” exons 45-55 skipping PMO cocktail were generated and tested in immortalized myotubes. (A) Strategy #1 for minimization involved two rounds of sequential removal of individual PMOs from the “all” cocktail. (B) Strategy #2 involved preparing “all” cocktail derivatives based on the endogenous splicing of the exons 45-55 region in humans. RT-PCR exons 45-55 skipping efficiency results are shown in both (A) and (B). (n=3) Error bars: S.E.M. \* $p < 0.05$ , \*\* $p < 0.005$ , \*\*\* $p < 0.001$  one-way ANOVA with Dunnett’s test versus mock,  $\phi p < 0.05$ ,  $\phi\phi p < 0.005$ ,  $\phi\phi\phi p < 0.001$  one-way ANOVA with Dunnett’s test versus “all”. NT, non-treated.

For the second strategy, we prepared minimized cocktails based on the endogenous splicing pattern of human *DMD* exons 45-55. The region is hypothesized to be spliced in groups, with certain splicing events occurring faster than others. A model proposes that exons 45-49, 50-52, and 53-55 are spliced together first, after which these groups are spliced together to complete the exons 45-55 region.<sup>331</sup> We designed derivative exons 45-55 skipping cocktails from the “all” cocktail with PMOs targeting the terminal exons of these three groups. Transfection into healthy KM155 myotubes revealed three derivative cocktails to skip exons 45-55 significantly higher than the mock ( $p<0.05$ ) (**Figure 5.2b**). These produced skipping efficiencies that were not significantly different from the “all” cocktail. Based on this result, we selected the cocktails targeting exons 45, 49, 50, 52, 53, and 55 (“block” cocktail) as well as targeting exons 45, 50, and 55 (“3-PMO” cocktail) for further experiments (**Figure 5.1a**).

### **5.3.2. Minimized exon skipping cocktails effectively skip exons 45-55 in various patient cells**

The “all”, “base”, “base -51”, “block”, and “3-PMO” exons 45-55 skipping cocktails were subsequently tested in the following immortalized muscle cell lines: KM155 (healthy), KM571 ( $\Delta$ ex52), 6594 ( $\Delta$ ex48-50), and 6311 ( $\Delta$ ex45-52) (**Figure 5.1a**). Mutation-tailored versions of the cocktails were used for each cell line, with unnecessary PMOs removed. Upon transfection into myotubes (**Figure 5.1b**) and RT-PCR analysis, the “all” cocktail significantly skipped exons 45-55 in all lines compared to the mock ( $p<0.005$  or  $p<0.001$ ) (**Figure 5.1c**). Considering the minimized cocktails, the “base -51”, “block”, and “3-PMO” cocktails induced significant exons 45-55 skipping in KM155, KM571, and 6594 myotubes compared to the mock (at least  $p<0.05$ ); the “base” cocktail only showed significant skipping in KM155 cells ( $p<0.001$ ). In 6594 myotubes, the “3-PMO” cocktail induced significantly higher skipping than

the “all” cocktail. Intriguingly, none of the minimized cocktails showed any exons 45-55 skipping in 6311 myotubes.

We then evaluated the dystrophin restoration capabilities of the “block” and “3-PMO” cocktails in KM571 myotubes, since these cocktails induced the highest levels of exons 45-55 skipping in this line. Western blot using antibodies against the rod (DYS1, corresponding to exons 26-30) and C-terminal domains (ab15277) of dystrophin successfully detected dystrophin protein upon treatment with the “all” and “block” cocktails, but not with the “3-PMO” cocktail (**Figure 5.1d**). Quantification of the DYS1 signal showed that “block” cocktail treatment restored an average 2.94% dystrophin of wild-type levels, which was slightly higher than the average 2.33% dystrophin restored by the “all” cocktail and considerably elevated compared to the 0.10% dystrophin level in the mock ( $p<0.001$ ) (**Figure 5.1e**). Western blot with the MANEX45A (corresponding to exons 45-46) and MANEX4850E (corresponding to exons 48-50) anti-dystrophin antibodies failed to detect dystrophin in treated myotubes (**Figure 5.1d**), suggesting that the dystrophin induced post-treatment likely came from exons 45-55-skipped transcripts.

### **5.3.3. Single intravenous treatment with DG9-PMO induces higher dystrophin production than unconjugated PMO in the skeletal muscles and the heart**

To evaluate DG9 as a peptide conjugate for our minimized exons 45-55 skipping cocktail, we decided to first test its efficacy *in vivo* as applied to single-exon skipping. DG9 was conjugated to Ex51\_Ac0, an exon 51-skipping PMO that is part of the “all” cocktail and which we have demonstrated to be up to 7 times more effective than eteplirsen in restoring dystrophin production *in vitro*.<sup>320,332</sup> hDMDdel52;*mdx* mice at 3 months were given a single retro-orbital

injection of either saline, 50 mg/kg unconjugated PMO, or 64 mg/kg DG9-PMO (equimolar to the PMO dose) and assessed a week post-treatment (**Figure 5.3a**). RT-PCR clearly showed that DG9-PMO-treated mice had significantly higher levels of exon 51 skipping than the saline- or PMO-treated groups across various skeletal muscles (at least  $p<0.05$ ) and the heart ( $p<0.001$ ) (**Figure 5.3b**). In particular, the DG9-PMO induced 2.2 to 12.3-fold higher skipping in the skeletal muscles and 14.4-fold higher skipping in the heart on average compared to unconjugated PMO. A similar situation was seen when dystrophin protein was detected in muscle samples by Western blot. DG9-PMO treatment significantly restored dystrophin production compared to the saline ( $p<0.005$ ) and PMO ( $p<0.05$ ) treatments in the gastrocnemius and quadriceps, reaching up to 3% of wild-type levels (**Figure 5.3c**). In the heart, DG9-PMO restored an average 2.5% dystrophin of wild-type levels, significantly higher than that observed in the saline or PMO groups ( $p<0.05$ ). Compared to PMO-treated mice, mice that received DG9-PMO displayed 1.5 to 3.4-fold and 4.5-fold higher dystrophin protein levels on average in the skeletal muscles and heart, respectively.

Widespread dystrophin-positive fibers were observed in the tibialis anterior, diaphragm, and heart of DG9-PMO-treated mice by immunofluorescence, and very few to none in that of saline- or PMO-treated mice (**Figure 5.3d**). However, histological analysis revealed no reductions in the percentage of centrally-nucleated fibers (CNFs, a marker of cumulative muscle regeneration) in the tibialis anterior and diaphragm (**Figures 5.4a,b**), nor any improvements in muscle fiber size (**Figures 5.4a,c,d**) after PMO or DG9-PMO treatment.

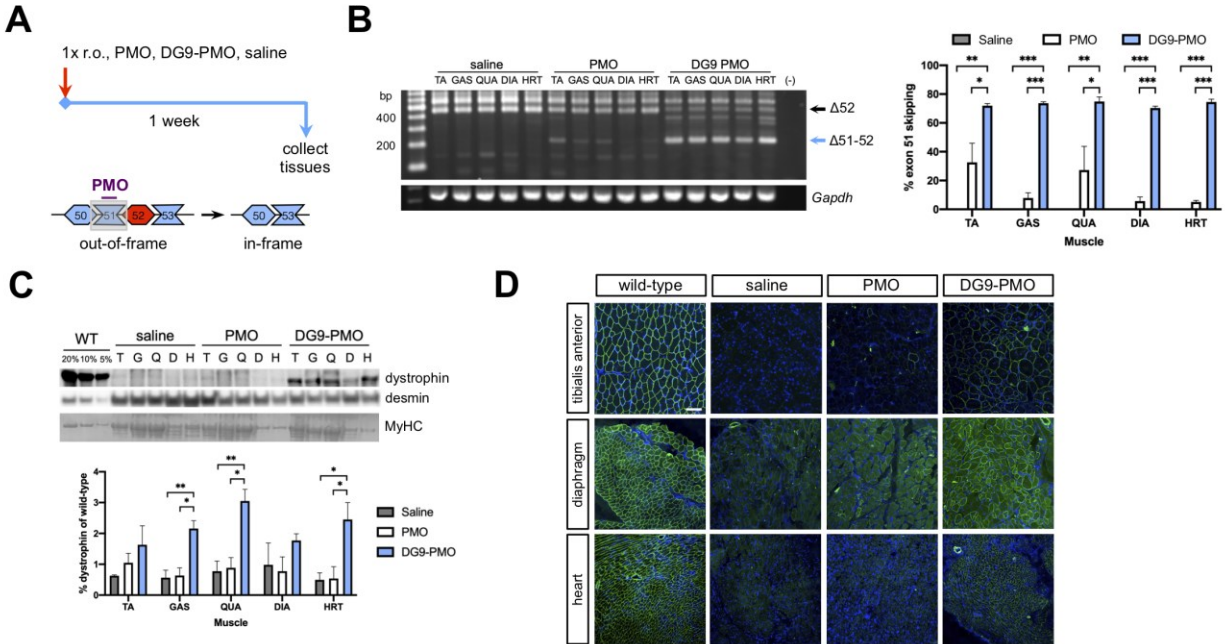


**Figure 5.3. Single-dose exon 51 skipping treatment with DG9-PMO.** (A) Male, 3-month-old hDMD<sup>del52</sup>;mdx mice were given a single retro-orbital injection (1× r.o.) of saline, 50 mg/kg PMO, or equimolar 64 mg/kg DG9-PMO for exon 51 skipping. Tissues were collected 1 week later for assessment. (B) RT-PCR *DMD* exon 51 skipping efficiency results post-treatment in various muscles, with quantification shown on the right. *Gapdh* is shown as a control. (C) Western blot detection for dystrophin (DYS1), with wild-type (WT) shown for reference. Protein extracts were loaded at 40 μg for saline-injected and treated muscles, and at indicated percentages of this for WT tibialis anterior samples. Desmin and myosin heavy chain (MyHC) serve as loading controls. Quantification of dystrophin signals are shown relative to the intensity of the 5% WT band. (D) Representative immunofluorescence images for dystrophin (DYS1, green) and nuclei (DAPI, blue) in various muscles and treatment conditions. Scale bar: 100 μm. (n=3/group for B-D) Error bars: S.E.M. \**p*<0.05, \*\**p*<0.005, \*\*\**p*<0.001 one-way ANOVA with Tukey's test. TA/T, tibialis anterior; GAS/G, gastrocnemius; QUA/Q, quadriceps; DIA/D, diaphragm; HRT/H, heart.

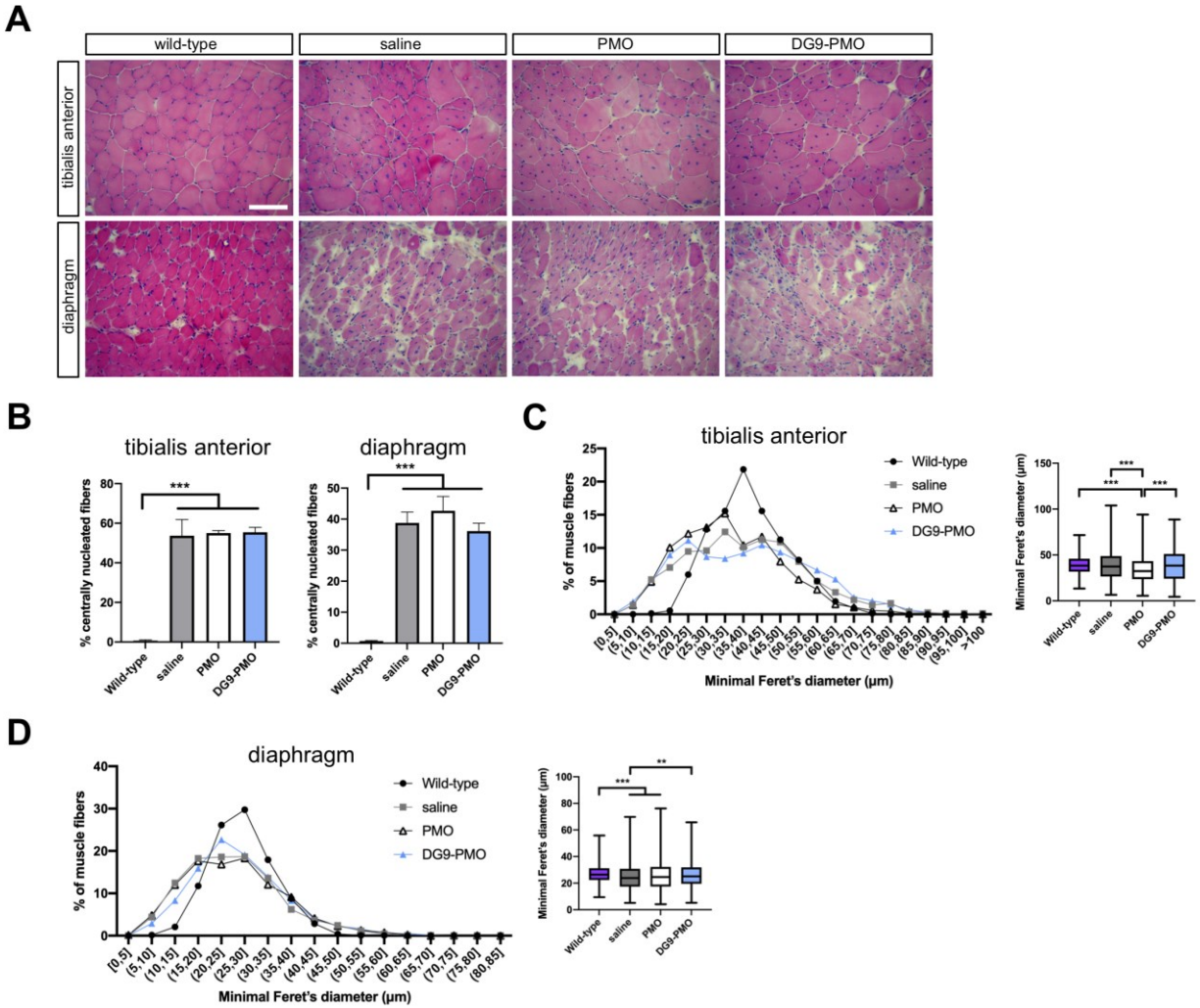


**Figure 5.4. Histological data from single-dose exon 51 skipping treatment with DG9-PMO.** Male, 3-month-old *hDMDel52;mdx* mice were injected once retro-orbitally with saline, 50 mg/kg PMO, or equimolar 64 mg/kg DG9-PMO for exon 51 skipping. Tissues were collected 1 week later for assessment, sectioned, and stained using hematoxylin and eosin (HE). (A) Representative HE images of the tibialis anterior and diaphragm from wild-type, saline-, PMO-, and DG9-PMO-treated mice. Scale bar: 100 μm (B) Centrally nucleated fiber (CNF) quantification from HE images. Error bars: S.E.M. (C) Minimal Feret's diameter quantification from HE images for the tibialis anterior and (D) diaphragm. The frequency distribution is shown on the left, while quantification of individual fibers are shown on the right. Box edges, 25<sup>th</sup> and 75<sup>th</sup> percentiles; central line, median; whiskers, range. (n=3/group for A-D, 719-854 fibers counted for the tibialis anterior and 962-1,479 for the diaphragm per group) \*\* $p < 0.005$ , \*\*\* $p < 0.001$  one-way ANOVA with Tukey's test.

#### **5.3.4. Repeated intravenous treatment with DG9-PMO improves dystrophin production, muscle function, and fiber size in dystrophic mice**

A repeated-dose treatment study was then performed to provide more insight into the efficacy of DG9-PMO exon skipping therapy with regard to ameliorating dystrophic symptoms. hDMDdel152;*mdx* mice at 2 months were systemically injected thrice with either saline or 30 mg/kg of DG9-PMO, once weekly for 3 weeks. Functional assessments were done at baseline and at 2 weeks following the last injection, after which tissues were collected for analysis (**Figure 5.5a**). Once again, DG9-PMO treatment significantly induced exon 51 skipping at high levels across skeletal muscles and the heart (55-71% on average) compared to the saline control ( $p < 0.001$ ) (**Figure 5.5b**). This resulted in significant dystrophin production in various skeletal muscles ranging at an average 2.8-3.9% compared to 0.1-0.3% in saline-treated mice (at least  $p < 0.05$ ) (**Figure 5.5c**), as well as in the heart at an average of 7.7% versus 0.5% in the saline group ( $p < 0.001$ ) (**Figure 5.5d**). Immunofluorescence confirmed presence of widespread dystrophin-positive fibers in the tibialis anterior, diaphragm, and heart (**Figure 5.5e**).

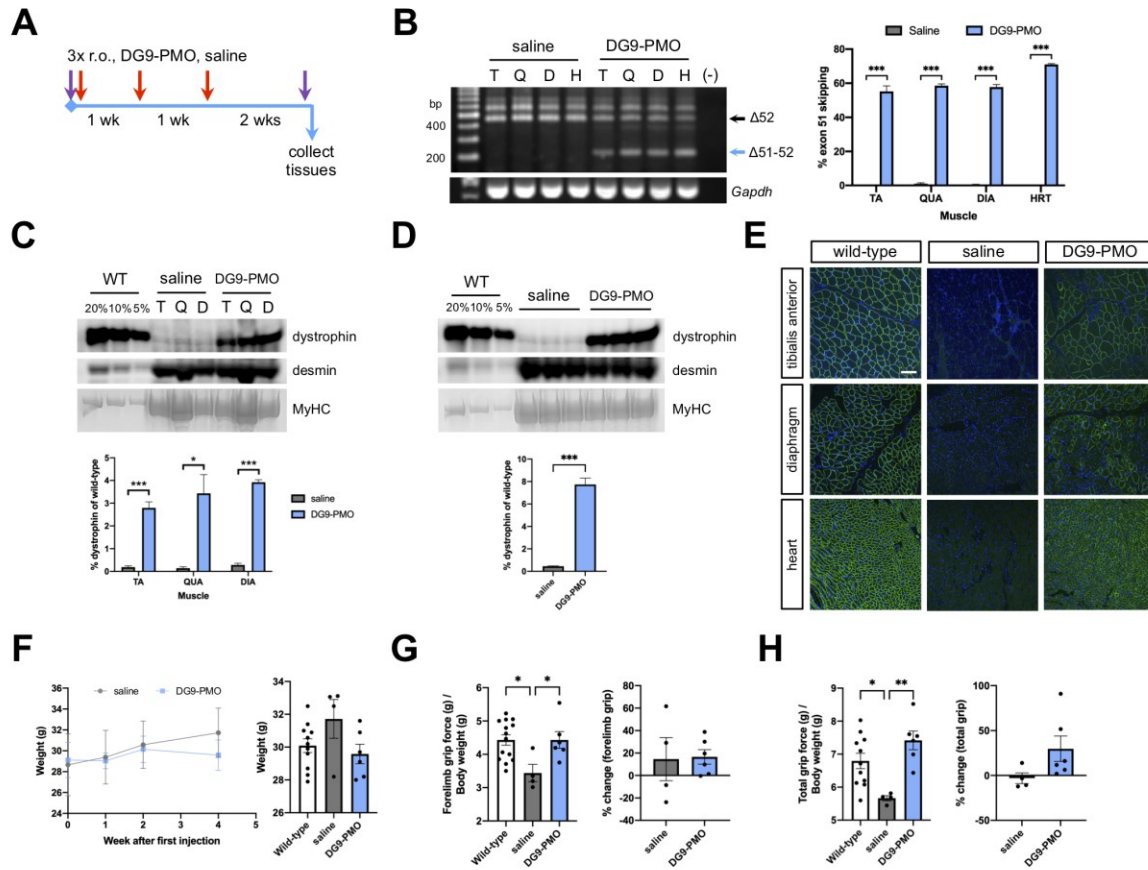


**Figure 5.5. Repeated-dose exon 51 skipping treatment with DG9-PMO.** (A) Male, 2-month-old hDMDdel52;*mdx* mice were given three retro-orbital injections (3× r.o.) of saline or 30 mg/kg DG9-PMO for exon 51 skipping, once a week for 3 weeks. Purple arrows indicate times when functional testing was performed. Tissues were collected 2 week later for assessment. (B) RT-PCR *DMD* exon 51 skipping efficiency results post-treatment in various muscles, with quantification shown on the right. *Gapdh* is shown as a control. (C) Western blot detection for dystrophin (DYS1) in various skeletal muscles or (D) in the heart, with wild-type (WT) samples from either the tibialis anterior or heart used for reference. Protein extracts were loaded at 40  $\mu$ g for saline-injected and treated muscles, and at indicated percentages of this for WT. Desmin and myosin heavy chain (MyHC) serve as loading controls. Quantification of dystrophin signals are shown relative to the intensity of the 5% WT band. (n=3/group for B-D) Error bars: S.E.M. \* $p$ <0.05, \*\*\* $p$ <0.001 unpaired two-tailed *t*-test for (B) to (D). (E) Representative immunofluorescence images for dystrophin (DYS1, green) and nuclei (DAPI, blue) in various muscles and conditions. Scale bar: 100  $\mu$ m. (n=3/group) (F) Body weights of saline- and DG9-PMO-treated mice over the course of the experiment. (G) Forelimb grip strength results for saline- and DG9-PMO-treated mice, normalized to body weight. The % change from baseline is shown on the right. (n= (H) Similar to (G), but for total limb grip strength. (n=11-14 WT; n=4, saline; n=6, DG9-PMO for F-H) Error bars: S.E.M. \* $p$ <0.05, \*\* $p$ <0.005 one-way ANOVA with Tukey's test for (G) to (H). TA/T, tibialis anterior; QUA/Q, quadriceps; DIA/D, diaphragm; HRT/H, heart.

The body weights of the saline and DG9-PMO groups did not significantly differ in the course of treatment (**Figure 5.5f**). However, there was an observable decrease in body weight in the DG9-PMO-treated mice compared to the saline controls, approaching wild-type levels. Most impressively, repeated DG9-PMO treatment significantly improved forelimb ( $p<0.05$ ) (**Figure 5.5g**) and total limb ( $p<0.005$ ) (**Figure 5.5h**) grip strength in *hDMDdel52;mdx* mice, such that they were not significantly different from values seen in matched wild-type mice. Nearly all mice showed an improvement of forelimb and total limb grip strength from baseline, except one which showed a -0.3% difference in forelimb grip strength post-treatment. This is in contrast to the saline control mice, which either showed no discernible direction of change (**Figure 5.5g**) or displayed no observable change from baseline (**Figure 5.5h**). Rotarod and treadmill tests showed similar improvements (**Figures 5.6a,b**).

Histological analysis still did not show any significant reductions in the percentage of observed CNFs in the tibialis anterior and diaphragm (**Figures 5.6c,d**). However, we did observe a significant increase in fiber size with DG9-PMO treatment ( $p<0.001$ ), as evaluated by measuring the minimum Feret's diameter of individual fibers in the tibialis anterior and diaphragm (**Figures 5.6e,f**). Examining the frequency distribution curves for this parameter showed that there was a rightward shift in the curves of DG9-PMO-treated mice, with most fibers having a minimum Feret's diameter of 45-50  $\mu\text{m}$  in the tibialis anterior and 25-30  $\mu\text{m}$  in the diaphragm. This is in contrast to most fibers having diameters of 30-35  $\mu\text{m}$  and 20-25  $\mu\text{m}$  in these muscles, respectively. We also performed a qualitative histological analysis of the liver and kidney in both single- and repeated-dose treatment mice, but found no observable evidence of toxicity as a result of PMO or DG9-PMO treatment (**Figures 5.7a,b**).

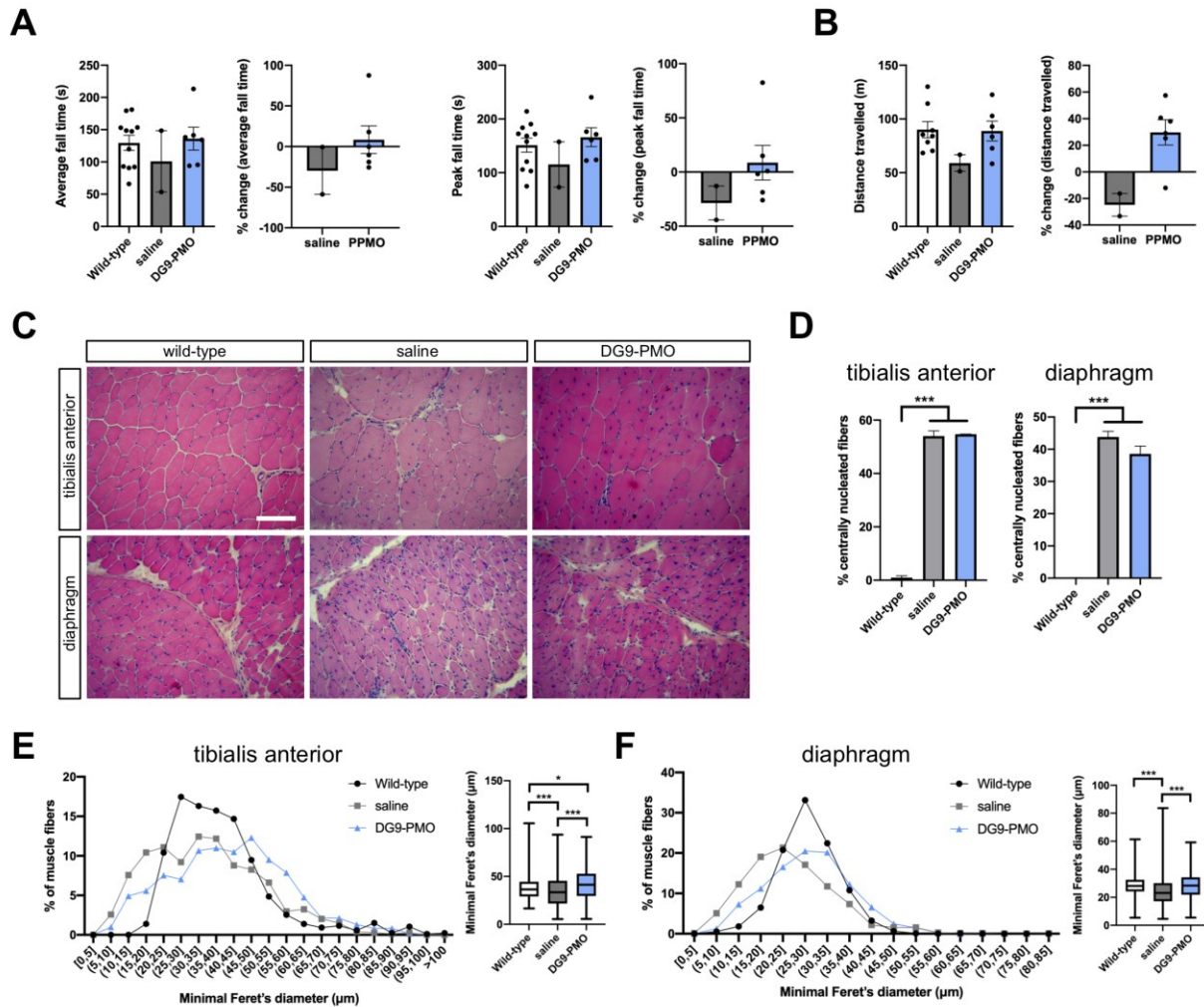


**Figure 5.6. Functional and histological data from repeated-dose exon 51 skipping treatment with DG9-PMO.** Male, 2-month-old hMDMDel52;*mdx* mice were injected thrice retro-orbitally with saline or 30 mg/kg DG9-PMO for exon 51 skipping, once a week for 3 weeks. Functional testing was done at baseline and at 2 weeks after the final injection. (A) Rotarod test results showing average and peak fall times, as well as their respective % change values from baseline. (B) Run-to-exhaustion test results showing total distance travelled on the treadmill, with the % change from baseline on the right. (n=8-11 wild-type; n=2, saline; n=6, DG9-PMO) Error bars: S.E.M. (C) Tissues were collected after post-treatment functional testing and stained using hematoxylin and eosin (HE). Representative HE images of the tibialis anterior and diaphragm from wild-type, saline-, and DG9-PMO-treated mice are shown. Scale bar: 100 µm (D) Centrally nucleated fiber (CNF) quantification from HE images. Error bars: S.E.M. (E) Minimal Feret's diameter quantification for the tibialis anterior and (F) diaphragm, presented as in Supplementary Fig. 2. (n=3/group for C-F, 610-865 fibers counted for the tibialis anterior and 1,167-1,412 for the diaphragm per group) \*\* $p < 0.005$ , \*\*\* $p < 0.001$  one-way ANOVA with Tukey's test.

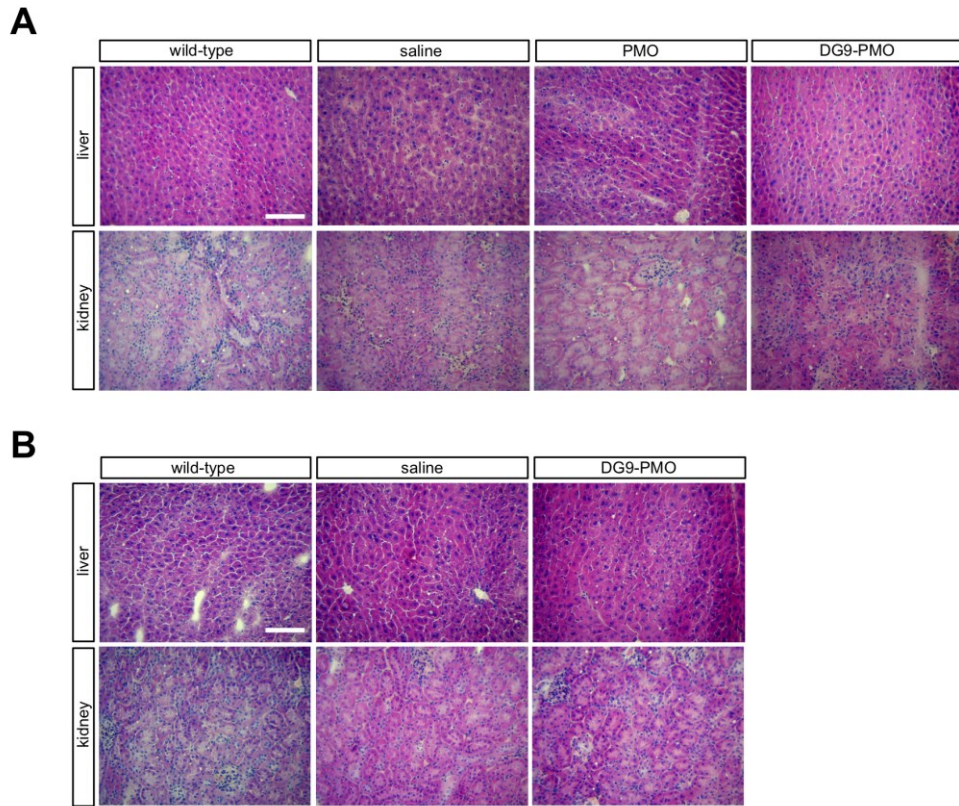


**Figure 5.7. Liver and kidney histology from single- and repeated-dose exon 51 skipping treatment studies.** Representative hematoxylin and eosin-stained images of wild-type and hDMDdel52;*mdx* liver and kidney from the (A) single-dose and (B) repeated-dose experiments are shown. Scale bar: 100  $\mu$ m. (n=3/group)

### **5.3.5. Local treatment with the DG9-conjugated minimized exons 45-55 skipping cocktail induces successful skipping and dystrophin production**

Having observed its success with single-exon skipping, we proceeded to conjugate DG9 to each PMO of the minimized “block” exons 45-55 skipping cocktail for *in vivo* testing. The “block” cocktail was chosen because it induced high levels of both exons 45-55 skipping and dystrophin protein restoration in KM571 myotubes (**Figures 5.1c-e**). Thus, 5- to 6-month-old hDMDdel52;*mdx* mice were intramuscularly injected in the tibialis anterior with either saline or the mutation-tailored DG9-PMO “block” cocktail (5 µg/DG9-PMO), and assessed a week later (**Figure 5.8a**). Significant exons 45-55 skipping was observed compared to the saline control ( $p<0.001$ ) (**Figure 5.8b**). Western blot revealed dystrophin restoration in DG9-PMO-treated muscles at 0.76% of wild-type levels on average, which was significantly higher than that seen in saline-treated muscles at 0.46% ( $p<0.05$ ) (**Figure 5.8c**). As the same mouse received DG9-PMO in one leg and saline in the contralateral leg, we included protein from a completely non-treated mouse to account for possible leakage between legs. We found that non-treated tibialis anterior muscles had 0.12% dystrophin of wild-type levels, which was lower than the level found in the saline control. A few scattered dystrophin-positive fibers in DG9-PMO-treated muscles were observed by immunofluorescence and very few to none in the saline controls, confirming dystrophin restoration (**Figure 5.8d**).

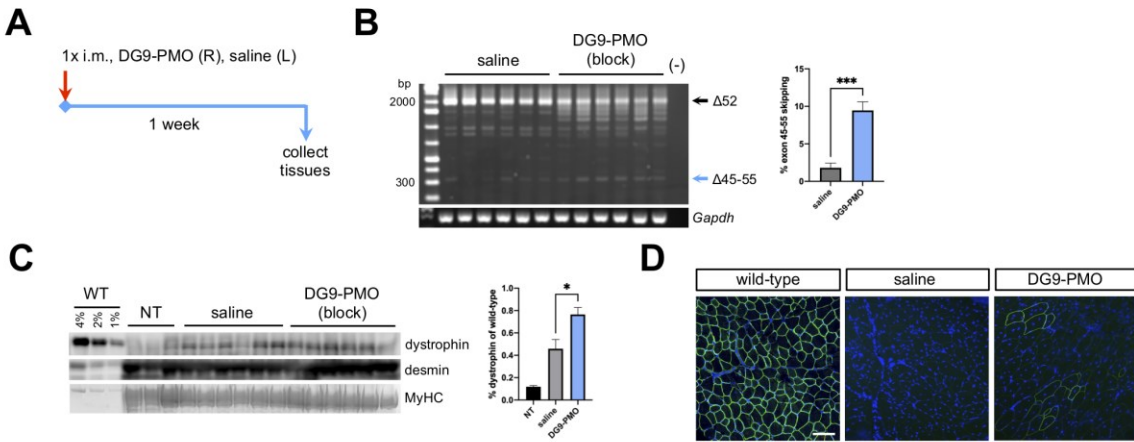


**Figure 5.8. Local treatment with the minimized “block” DG9-PMO exons 45-55 skipping cocktail.** (A) Male, 5-6-month-old hDMDdel52;*mdx* mice were intramuscularly injected with the DG9-PMO “block” cocktail at 5  $\mu$ g/PMO in the right tibialis anterior (R), and saline in the left (L). Tissues were collected 1 week later for assessment. (B) RT-PCR *DMD* exons 45-55 skipping efficiency results post-treatment, with quantification shown on the right. *Gapdh* is shown as a control. (C) Western blot detection for dystrophin (DYS1), with wild-type (WT) and non-treated (NT) tibialis anterior samples used for reference. Protein extracts were loaded at 40  $\mu$ g for NT, saline- and DG9-PMO-treated muscles, and at indicated percentages of this for WT. Desmin and myosin heavy chain (MyHC) serve as loading controls. Quantification of dystrophin signals are shown relative to the intensity of the 1% WT band. (D) Representative immunofluorescence images for dystrophin (DYS1, green) and nuclei (DAPI, blue). Scale bar: 100  $\mu$ m. (n=3 wild-type; n=6, saline; n=6 DG9-PMO) Error bars: S.E.M. \* $p$ <0.05, \*\*\* $p$ <0.001 unpaired two-tailed  $t$ -test.

## 5.4. Discussion

We have successfully developed a minimized exons 45-55 skipping cocktail that induces significant dystrophin restoration in immortalized patient cells and dystrophic hDMDdel52;*mdx* mice. In the case of exon 52-deleted *DMD* transcripts, the number of PMOs used for exons 45-55 skipping was reduced from 11 in the “all” cocktail to 5 in the “block” cocktail (**Figure 5.1a**), more than a 50% decrease in PMO content. The “block” and “3-PMO” cocktails performed the best out of all minimized cocktails in skipping exons 45-55 *in vitro* (**Figure 5.1c**), indicating that a solid understanding of how the *DMD* pre-mRNA is endogenously skipped would be beneficial to designing future multi-exon skipping approaches. Most of the minimized cocktails significantly skipped exons 45-55 in KM571 ( $\Delta$ ex52) and 6594 ( $\Delta$ ex48-50) myotubes. However, apparently all remaining exons have to be targeted in 6311 myotubes ( $\Delta$ ex45-52). The endogenous splicing of human *DMD* exons 45-55 is likely altered by different mutations. Since we only have an idea of endogenous exons 45-55 splicing in normal *DMD* transcripts,<sup>331</sup> studies on how this occurs in mutant transcripts are warranted. In the meantime, any minimized exons 45-55 skipping cocktail should be tested in the context of various mutations, to confirm applicability across patients.

The “block” cocktail was identified as a promising candidate for *in vivo* study, which restored dystrophin production to approximately 3% of wild-type levels, near the amount seen with the “all” cocktail (**Figure 5.1e**). To achieve similar results with a considerably smaller cocktail strengthens our rationale for minimization. Intriguingly, despite showing strong exons 45-55 skipping at the transcript level, treatment with the “3-PMO” cocktail did not restore dystrophin in KM571 myotubes (**Figures 5.1d,e**). We do not know the reason behind this, but it is possible that the exons 45-55 skipped transcript produced by the “3-PMO” cocktail was either

unstable or may not have been the predominant skipping product. In the latter scenario, splicing in the region may have been perturbed such that adjacent exons outside of exons 45-55 were skipped out as well. Further experiments will be done to elucidate the reasons behind this result.

We were likewise successful in demonstrating the therapeutic efficacy of conjugating DG9 to PMOs in single- and multi-exon skipping applications. DG9 is a cell-penetrating peptide based on the protein transduction domain of the human Hph-1 transcription factor. It has been shown that fusion proteins containing this Hph-1 domain have improved delivery in a wide variety of tissues, including the heart;<sup>333</sup> DG9 is comprised of two such Hph-1 domains. Treatment with DG9-PMO clearly resulted in higher single-exon skipping and dystrophin restoration levels *in vivo* compared to unconjugated PMO (**Figures 5.3b-d**), similar to what has been extensively observed for other cell-penetrating peptides.<sup>323,325</sup> Repeated treatment resulted in greater dystrophin restoration in all examined tissues especially the heart, from 2.5% to 7.7% of wild-type levels (**Figures 5.3c, 5.5d**).

Although the dystrophin restoration levels observed here were generally lower than that achieved by other peptide-conjugated PMOs (reaching >50% in some cases),<sup>302,323</sup> the advantage of DG9 is in its potentially better toxicity profile compared to other peptides. Peptide-conjugated PMOs have reportedly induced dose-dependent toxic effects in pre-clinical studies, including lethargy, weight loss, and elevated kidney damage marker levels in rats,<sup>245</sup> as well as tubular degeneration in the kidneys of monkeys.<sup>302,323</sup> This is thought to be linked to the membrane-disruptive properties of cell-penetrating peptides, which in turn is largely influenced by their amino acid compositions.<sup>302,323,334</sup> Certain L-arginine residues in DG9 were converted to D-arginine, as this switch has been shown to improve the viability of peptide-conjugated PMO-treated cells *in vitro*.<sup>335</sup> DG9 also does not contain any 6-aminohexanoic acid residues (often

represented by “X” in peptide sequences), which have been associated with increased toxicity.<sup>335</sup> Even though such modifications decrease the antisense activity of peptide-conjugated PMOs, it comes with the benefit of increased safety for therapeutic application. A balance must be struck between efficacy and safety for peptide-conjugated PMOs, as too frequent or too high doses have been seen to increase toxicity.<sup>302,323</sup> In this study, we did not find any obvious evidence of toxicity caused by DG9-PMO on the liver and kidney, in both single and repeated treatment conditions (**Figure 5.7**). We understand that this is only a preliminary result, and plan to undertake a more extensive study of the pharmacokinetics and safety profile of DG9 versus other published antisense oligonucleotide peptide conjugates.

Despite its relatively reduced activity, we nevertheless and encouragingly observed functional improvement in mice given repeated doses of DG9-PMO (**Figures 5.5g,h, 5.6a,b**). Treated hDMDdel52;*mdx* mice had average dystrophin restoration levels at 2.8-3.9% of wild-type in the skeletal muscles (**Figure 5.5c**). This was accompanied by improvements in fiber size, as seen in the tibialis anterior and diaphragm (**Figures 5.6c,e,f**). Our finding supports the notion that not much dystrophin may be needed to achieve functional benefit *in vivo*. Indeed, previous studies in *mdx* mice with non-random X-chromosome inactivation (*mdx-Xist<sup>Δhs</sup>*) have shown that as little as 3-14% dystrophin of normal levels were sufficient to significantly improve performance in hanging wire and grip strength tests to a degree that was approaching or even equivalent to wild-type mice.<sup>212</sup> Moreover, at least 4% dystrophin of normal levels in the heart have been suggested to ameliorate cardiac dysfunction, with these *mdx-Xist<sup>Δhs</sup>* mice having wild-type-like ejection fraction values in both ventricles.<sup>336</sup> Since hDMDdel52;*mdx* mice do not exhibit overt cardiac phenotypes at younger ages, we were unable to evaluate the effects of repeated DG9-PMO therapy on cardiac function in this study. Future work will require the use of

hDMDdel52;*mdx* mice either at advanced ages or under stressed conditions for dystrophic cardiac symptoms to be observed and therapeutically targeted. Humanizing DMD models with stronger cardiac phenotypes such as utrophin/dystrophin double-knockout mice<sup>337,338</sup> is also a possibility, but technically challenging.

In terms of multi-exon skipping, it was promising that the DG9-conjugated version of our minimized “block” cocktail successfully skipped exons 45-55 at 9.5% efficiency and restored dystrophin production in hDMDdel52;*mdx* mice at nearly 0.8% of wild-type levels, on average (**Figures 5.8b,c**). The “all” cocktail was previously shown to induce 15% exons 45-55 skipping efficiency upon intramuscular treatment of a different humanized DMD mouse model, at a dose of 1.67 µg/PMO.<sup>320</sup> Unlike what we saw *in vitro*, a higher dose of the “block” cocktail is apparently needed to induce comparable skipping levels to the “all” cocktail *in vivo*. Understanding how DG9 affects PMO interactions in a multi-exon skipping cocktail may be necessary, similar to the *in silico* work we did to minimize self- and cross-annealing between PMOs in the “all” cocktail.<sup>320</sup> Machine learning has already been applied to the development of novel and more effective cell-penetrating peptides for PMOs, albeit focused more on improving the activity of individual PMOs.<sup>339</sup> Perhaps the same approach could be used for PMOs administered as a group. Aside from conducting an *in silico* analysis of DG9/PMO interactions, we will investigate how the efficacy of our minimized multi-exon skipping cocktail could be increased by varying treatment doses, frequencies and regimens. The possibility of systemic treatment would also be explored. In summary, we have shown proof-of-concept that a minimized, more economical antisense oligonucleotide cocktail for skipping human *DMD* exons 45-55 could be developed. Exons 45-55 skipping is applicable to nearly half of the DMD patient population, with evidence supporting favorable clinical outcomes for such therapy. We have also

identified DG9 to be a promising, effective cell-penetrating peptide for PMO conjugation not only for multi-exon skipping, but also for single-exon skipping approaches.

## **5.5. Methods**

### **5.5.1. Cell culture**

All immortalized human muscle cells were kindly provided by the MRC Center for Neuromuscular Diseases Biobank (NHS Research Ethics Committee reference 06/Q0406/33, HTA license number 12198), through Dr. Francesco Muntoni. Experiments with these cells were approved by the University of Alberta Health Research Ethics Board, under study ID Pr00079871. The following immortalized myoblast cell lines were used: KM155 (healthy), KM571 (*DMD*  $\Delta$ ex52), 6594 (*DMD*  $\Delta$ ex48-50), and 6311 (*DMD*  $\Delta$ ex45-52). Myoblasts were grown in DMEM/F12 medium (with HEPES; Gibco) containing 20% fetal bovine serum (Sigma), 1 vial of skeletal muscle growth supplement mix (Promocell), 50 U/mL penicillin, and 50  $\mu$ g/mL streptomycin. Myoblasts were then seeded into collagen type 1-coated 12-well plates, at a density of  $0.53 \times 10^5$  cells/cm<sup>2</sup>. Once 90% confluent, myoblasts were differentiated into myotubes by replacing the growth medium with differentiation medium (DMEM/F12 containing 2% horse serum [GE Healthcare], 1 $\times$  ITS solution [Sigma], 50 U/mL penicillin, and 50  $\mu$ g/mL streptomycin). All cells were incubated at 37°C, 5% CO<sub>2</sub>.

### **5.5.2. PMO transfection**

The PMOs used are summarized in **Table 5.1** and were derived from cocktail set no. 3 in our previous publication.<sup>320</sup> Prior to transfection, PMOs (Gene Tools) were heated at 65°C for 15 min to remove aggregates. PMOs were then transfected into muscle fibers at 3 days post-

differentiation using 6  $\mu$ M Endoportor reagent (Gene Tools) in differentiation medium. Each PMO in a cocktail was transfected at a final 5  $\mu$ M concentration for all experiments. Cells were incubated in PMOs for 2 days, after which they were harvested for RNA and protein (**Figure 5.1a**). Random control 25-N (Gene Tools) was used for mock treatment. For non-treated samples, transfection was done as described with Endoportor, only without any PMO.

### 5.5.3. Animals and treatments

Mice were housed and cared for at the University of Alberta Health Sciences Laboratory Animal Services facility. All experiments were reviewed and approved by the Animal Care and Use Committee at the University of Alberta Research Ethics Office, under study ID AUP00000365. Dr. Annemieke Aartsma-Rus (Leiden University Medical Center) provided the hDMDdel52;*mdx* mice we used to start our colony. Only male hDMDdel52;*mdx* mice (C57BL/6J background)<sup>328,330</sup> heterozygous for the hDMDdel52 transgene were used in this study.

For single-exon skipping studies, DG9 (sequence N-YArVRRrGPRGYArVRRrGPRr-C; uppercase: L-amino acids, lowercase: D-amino acids) was conjugated to the 3' end of Ex51\_Ac0 (**Table 5.1**), a human *DMD* exon 51-skipping PMO we previously developed.<sup>320,332</sup> We performed two experiments: single-dose and repeated-dose treatment. For single-dose treatment, 3-month-old hDMDdel52;*mdx* mice were retro-orbitally injected with either phosphate-buffered saline (PBS), PMO (50 mg/kg, unconjugated Ex51\_Ac0), or DG9-PMO (64 mg/kg, equimolar to 50 mg/kg PMO) and then euthanized a week later for tissue collection. For repeated-dose treatment, 2-month-old hDMDdel52;*mdx* mice were given three retro-orbital injections of either PBS or DG9-PMO (30 mg/kg) once a week for 3 weeks. Body weights were recorded throughout

the course of treatment, and mice were subjected to muscle function tests before the first injection and 2 weeks after the last injection as described in *Functional testing*. Mice were euthanized after the post-function tests for tissue collection. Upon dissection, tissues were mounted in tragacanth gum on corks and snap-frozen in liquid nitrogen-cooled isopentane.

For multi-exon skipping, DG9 was conjugated to each PMO of the minimized “block” exons 45-55 skipping cocktail (**Figure 5.1a**). This DG9-PMO cocktail (5  $\mu$ g per DG9-PMO, total dose of 25  $\mu$ g) was then administered intramuscularly into the tibialis anterior of 5- to 6-month-old hDMDdel152;*mdx* mice; the contralateral leg was injected with PBS. Mice were euthanized a week later for tissue collection as described above. All injections, retro-orbital and intramuscular, were conducted under isoflurane anesthesia. Tissues from age-matched wild-type male C57BL/6J mice were collected as controls.

#### **5.5.4. Functional testing**

Forelimb and total limb grip tests were conducted by blinded personnel according to TREAT-NMD SOP DMD\_M.2.2.001 using the Chatillon DFE II grip strength meter (Columbus Instruments). The average of the three most consistent readings was used per mouse, and results were normalized to body weight. The rotarod test was performed using the AccuRotor 4-channel rotarod (Omnitech Electronics, Inc.). Mice were first placed on a rod rotating at a steady speed of 5 rpm. Once all mice were in place, rotation was accelerated from 5 to 45 rpm over a span of 300 s.<sup>340</sup> Fall times were automatically recorded by the software. Three trials were conducted, spaced 15 min apart, and the average or peak fall time from these trials was used for analysis. The run-to-exhaustion test was performed using the Exer 3/6 animal treadmill (Columbus Instruments), according to TREAT-NMD SOP DMD\_M.2.1.003. Mice were run on the treadmill with the

following program: 5 m/min for 5 min, and then speed is increased by 1 m/min every minute until exhaustion. Exhaustion is considered as the point when the mouse does not get back on the treadmill within 10 s following repeated, gentle nudges. The maximum test duration was set at 15 min. All tests were performed at baseline (prior to receiving treatment) and at 2 weeks after receiving final treatment. Age-matched wild-type male C57BL/6J mice were used as controls.

### 5.5.5. RT-PCR and exon skipping evaluation

Total RNA was extracted from cells and 20- $\mu$ m tissue sections using Trizol (Invitrogen), following manufacturer's instructions. For exons 45-55 skipping analysis, SuperScript<sup>TM</sup> III One-Step RT-PCR system with Platinum<sup>TM</sup> *Taq* (Invitrogen) was used. Briefly, 200 ng of total RNA was used as template in a 25- $\mu$ L solution containing 1 $\times$  reaction mix, 0.2  $\mu$ M each of forward and reverse primers for *DMD* or *GAPDH/Gapdh* (**Table 5.2**), and 1  $\mu$ L of SuperScript III RT/Platinum *Taq*. The reaction was run under the following conditions: 1) 50°C, 5 min, 2) 94°C, 2 min, 3) 35 cycles of 94°C, 15 s; 60°C, 30 s; 68°C, 33-118 s, 4) 68°C, 5 min, 5) 4°C, hold.

**Table 5.2. List of primers and sequences used in this study.**

Target	Sequence, 5' to 3'	Product size/s, bp
<i>hDMD</i> (ex45-55)	F: GACAAGGGCGATTTGACAG (ex43/44) R: TCCGAAGTTCCTCCACTTG (ex56)	2088 (wild-type), 1970 ( $\Delta$ ex52), 1691 ( $\Delta$ ex48-50), 866 ( $\Delta$ ex45-52), 309 ( $\Delta$ ex45-55)
<i>hDMD</i> (ex51)	F: CAGCCAGTGAAGAGGAAGTTAG (ex49/50) R: CCAGCCATTGTGTTGAATCC (ex53)	453 ( $\Delta$ ex52), 220 ( $\Delta$ ex51-52)
<i>hGAPDH</i>	F: TCCCTGAGCTGAACGGGAAG R: GGAGGAGTGGGTGTCGCTGT	218
<i>mGapdh</i>	F: CAACTTTGGCATTGTGGAAGG R: GAAGAGTGGGAGTTGCTGTT	381

For exon 51 skipping analysis, cDNA was synthesized from 750-1000 ng of total RNA using SuperScript™ IV Reverse Transcriptase (Invitrogen) with 2.5 μM random hexamers (Invitrogen) in a 20-μL reaction following manufacturer's instructions. From this, 8 μL of cDNA was used for PCR with 1× GoTaq® Green Master Mix (Promega) and 0.3 μM each of forward and reverse primers for *DMD* or *Gapdh* (**Table 5.2**) in a 25-μL reaction. The reaction was run as follows: 1) 95°C, 2 min, 2) 40 cycles of 95°C, 30 s; 60°C, 30 s; 72°C, 35 s, 3) 72°C, 5 min, and 4) 4°C, hold. All PCR products (exons 45-55 or exon 51 skipping) were run in 1.5% agarose gels in 1× tris-borate-EDTA buffer, and band intensities were quantified by Image J (NIH). The % of successful exon skipping was calculated using the following formula: (intensity of desired skipped band / total intensity of unskipped, intermediate, and desired skipped bands) × 100.

#### **5.5.6. Western blot**

Total protein was extracted from cells using RIPA buffer (Sigma) supplemented with cOmplete, Mini, EDTA-free protease inhibitor cocktail (Roche), according to our previously published protocol.<sup>341</sup> On the other hand, total protein was extracted from 20-μm tissue sections using a high-SDS lysis buffer containing 10% SDS, 70 mM Tris-HCl (pH 6.7), 5 mM EDTA (pH 8.0), 5% β-mercaptoethanol, and cOmplete protease inhibitor cocktail in water, also according to a previous protocol.<sup>309</sup> Proteins were quantified using the Pierce™ BCA kit (Thermo Scientific) or the Pierce™ Coomassie (Bradford) kit (Thermo Fisher), respectively.

In preparation for Western blot, proteins were mixed with NuPAGE™ LDS Sample Buffer (Invitrogen; 1× final concentration) and NuPAGE™ Sample Reducing Agent (Invitrogen; 1× final concentration), then heated at 70°C for 10 min. SDS-PAGE was performed using pre-cast NuPAGE™ 3-8% Tris-Acetate Midi gels (Invitrogen), run at 150 V for 75 min. Proteins

were then transferred onto a PVDF membrane (Millipore) using a semi-dry blotting system at 20 V for 70 min. Membranes were blocked overnight in 2% ECL Prime Blocking Agent (GE Healthcare) while shaking at 4°C; the post-transfer gel was stained with PageBlue Protein Staining solution (Thermo Scientific) for 1 hr at room temperature to detect myosin heavy chain bands. After blocking, membranes were cut and incubated in one of the following primary antibodies for 1 hr at room temperature: 1:200 NCL-DYS1 (Leica), 1:2,500 anti-dystrophin C-terminal (Abcam, ab15277), 1:100 MANEX45A (Developmental Studies Hybridoma Bank; DSHB),<sup>342</sup> 1:100 MANEX4850E (MDA Monoclonal Antibody Resource, Wolfson Centre for Inherited Neuromuscular Disease),<sup>342</sup> or 1:4,000 anti-desmin (Abcam, ab8592) in blocking agent. The membranes were then washed thrice for 10 min each with PBS containing 0.05% Tween 20 (PBST), before incubating in either anti-mouse IgG2a, anti-mouse IgG1, or anti-rabbit IgG (H+L) horseradish peroxidase-conjugated secondary antibodies (Invitrogen) as appropriate, all 1:10,000 in PBST. Membranes were then similarly washed in PBST, and detected with ECL Select Detection Reagent (GE Healthcare). DYS1 band intensities were quantified using Image Lab<sup>TM</sup> software, v.6.0.1 (Bio-Rad), and dystrophin levels were expressed relative to the intensity of the least concentrated wild-type sample in a series.

### **5.5.7. Dystrophin immunofluorescence**

Frozen muscle and heart samples were sectioned at 7- $\mu$ m thickness and placed on poly-L-lysine-coated slides. After thawing at room temperature for 30 min, sections were blocked for 2 hr in PBS with 10% goat serum and 0.1% Triton X-100 at room temperature. Sections were then incubated with 1:50 NCL-DYS1 in the blocking agent overnight at 4°C. The following day, sections were washed thrice with PBS for 5 min each and subsequently incubated with Alexa

488-conjugated goat anti-mouse IgG2a secondary antibody (Life Technologies) for 30 min at room temperature. Sections were washed again with PBS, and mounted with Vectashield HardSet Antifade Mounting Medium with DAPI (Vector Laboratories). Samples were visualized for dystrophin and DAPI using a Zeiss LSM 710 confocal microscope at 200× magnification, by personnel blinded to the treatment condition.

### 5.5.8. Histology

Frozen muscles were sectioned at 7- $\mu$ m and placed on poly-L-lysine-coated slides. After thawing at room temperature for 30 min, slides were stained with Mayer's hematoxylin (Electron Microscopy Sciences) for 15 min, washed with running tap water for 15 min, and then stained with eosin Y (Electron Microscopy Sciences) for 10 min. Sections were then dehydrated with an ethanol series (70%-90%-99%), cleared with a xylene substitute, and mounted with Permount™ (Fisher Scientific). Blinded personnel visualized the samples under brightfield using the Optika B-290TB microscope at 200× magnification, taking three randomly chosen fields of view per sample. CNF percentage was calculated by  $(\# \text{ CNFs} / \text{total} \# \text{ fibers}) \times 100$ , with fibers counted manually using Image J. The average CNF percentage from all fields of view was taken per sample. Minimal Feret's diameters were quantified by blinded personnel in two steps. First, images were semi-automatically measured using an in-house developed Image J macro based on Open-CSAM.<sup>343</sup> As Open-CSAM was initially developed for immunofluorescence images, we had to extensively modify it for compatibility with hematoxylin and eosin-stained images, which required use of the Colour Deconvolution 2 plugin.<sup>344,345</sup> Second, images that passed semi-automatic measurement were manually curated to correct fiber boundaries. Individual fiber

measurements across samples were considered for analysis. For both CNF and minimal Feret's diameter quantification, fibers that touched the edges of an image were not considered.

### **5.5.9. Statistical Analysis**

All statistical tests were performed using Prism v.9.0.1 (GraphPad Software). Unpaired two-tailed t-test, or one-way ANOVA with post-hoc Tukey's or Dunnett's multiple comparisons test were conducted as appropriate. P-values < 0.05 were considered statistically significant.

## **Chapter 6 Conclusions and future directions**

## 6.1. Developing an antisense therapy for FSHD

The discovery of aberrant *DUX4* expression as the defining feature of FSHD pathology has enabled the creation of targeted genetic therapies for the disorder. There are now various strategies available to inhibit DUX4-mediated toxicity, targeting DUX4 at the DNA, RNA, and protein levels.<sup>346</sup> In this thesis, we developed LNA and 2'-MOE gapmers that effectively reduced *DUX4* transcript expression *in vitro* and *in vivo*. While both induced near-complete knockdown of *DUX4* in immortalized patient-derived myotubes at the highest transfected dose (100 nM), experiments at lower doses showed that LNA gapmers were more potent than 2'-MOE gapmers. This is similarly reflected by qPCR data on DUX4 downstream target expression, as well as our more comprehensive RNA sequencing results. Previous studies suggest that LNA gapmers have considerably higher binding affinity to their target transcripts than 2'-MOE gapmers, which may explain the observed differences in efficacy.<sup>347,348</sup> Despite this, both LNA and 2'-MOE gapmers improved muscle fusion and fiber size at a low transfected dose (10 nM). This implies that it is possible to ameliorate FSHD-associated cellular phenotypes even with reduced transfected amounts of either gapmer.

It is important to note that this increased potency of LNA gapmers comes with an increased risk of toxicity. One study found that LNA gapmer treatment in mice was associated with weight loss, strongly elevated alanine and aspartate aminotransferase levels in the serum, and liver damage in a dose-dependent, target-independent manner.<sup>348</sup> In the same study, 2'-MOE gapmers administered under similar conditions did not show any signs of toxicity. It appears that gapmer toxicity may be attributed to an increased tendency to bind cellular proteins.<sup>349,350</sup> Fortunately, chemical modification of toxic gapmers can significantly reduce this protein-binding ability and, consequently, avoid *in vivo* hepatotoxicity. Such alterations can be as simple

as substituting one base in the central DNA gap to a different chemistry, e.g. 2'-*O*-methyl.<sup>350</sup> Other important safety considerations for antisense therapies would be their off-target and damaging on-target effects. We observed minimal off-targeting from our LNA and 2'-MOE gapmers *in vitro*. However, for this assay we only considered transcripts with sequences closely matching those of our gapmers', and so a more in-depth exploration of off-target effects would be recommended in the next stages of pre-clinical development. In terms of damaging on-target effects, we refer to the fact that non-pathogenic *DUX4* isoforms are expressed in healthy tissues.<sup>18,19</sup> This should not be an issue for our gapmers, as they target an exon specific to the muscle-specific pathogenic isoform, but should be kept as a consideration for the design of future AOs. Also, while we demonstrated effective *DUX4* knockdown with the use of our gapmers *in vivo*, a limitation in the present work is that we were unable to characterize the safety profiles of our gapmers in treated mice. Systemic treatment studies of our gapmers would be better positioned to evaluate not only their therapeutic efficacy but also their toxicity.

On that note, it would be important to perform systemic treatment on a mouse model that manifests FSHD-like symptoms. Non-induced *FLEXDUX4* mice, while useful for preliminary investigations into the *in vivo* efficacy of our gapmers, do not show FSHD-associated phenotypes due to their very low level of *DUX4* expression.<sup>90</sup> Tunable *DUX4* expression is possible in this model by crossing it with a tamoxifen-inducible Cre driver line, and would permit assessment of the functional benefits of gapmer therapy.<sup>277</sup> One group has recently reported on the outcomes of systemic treatment with *DUX4*-targeting vivo-PMOs using this inducible *FLEXDUX4* model, and revealed generally minimal but significant improvements in muscle mass, function, and histopathology.<sup>351</sup> It would be interesting to determine how our gapmers would compare to the efficacy of steric-blocking AOs in this model. Very few AO therapies for FSHD have been tested

*in vivo*, with only the one report above having performed a systemic treatment study. Further work to evaluate the outcomes of systemic AO therapy will enlighten us on the pharmacological behavior of AOs in the context of FSHD, and identify any vital concerns early on (e.g. delivery).

The RNA sequencing data produced in our work can also be used for other purposes. Our usage of this data focused entirely on determining if gapmer-mediated *DUX4* knockdown could restore the pathological transcriptomic landscape in patient-derived cells towards a healthy state. This analysis was highly specific, as we only examined the expression of FSHD signature genes derived from comparisons with transcriptomic data from one or two other studies. Our RNA sequencing results could be used a step further, to determine the molecular pathways or networks affected by gapmer treatment and whether these differ depending on the AO chemistry used. Since we also have data from healthy and FSHD-affected muscle cells, our data could be used towards better understanding the biology of FSHD itself. Together with RNA sequencing results from other groups, meta-analyses can be done to identify biomarkers robustly associated with FSHD. Transcriptomic differences between samples obtained from patient biopsies or patient-derived cells may likewise be helpful in untangling aspects of *DUX4*-mediated toxicity that have not been appreciated before. There is still much we do not know about FSHD, e.g. why it presents asymmetrically, or how rare *DUX4* expression can affect an entire tissue. Gaining a more complete understanding of the disease should aid the design and development of genetic therapies and, more importantly, their transition into the clinic.

## **6.2. Developing an antisense therapy for DMD**

There are many factors that influence the success of exon skipping therapies, which can generally be summarized into those that relate to the AO employed, the treatment design, or the

model used for therapeutic evaluation. In this thesis, we focused on exon skipping AOs with the PMO chemistry in the context of DMD therapy. Systemic treatment of neonatal dystrophic dogs with a 4-PMO cocktail led to variable dystrophin restoration across skeletal muscles, histopathological improvement in respiratory muscles, and some amount of functional benefit. ELISA results indicate that the PMOs were rapidly cleared from circulation shortly after injections, suggesting that therapeutic outcomes could have been further improved with better PMO retention in the system. Although PMO uptake was comparable between cardiac and skeletal muscles, dystrophin levels in the heart did not increase beyond amounts in non-treated dogs. In dystrophic mice, DG9 conjugation considerably improved PMO single-exon skipping across skeletal muscles and in the heart, with corresponding improvements in skeletal muscle function. The conjugation of cell-penetrating peptides provides a viable solution towards enhancing the systemic efficacy of treatment with single PMOs, as has been thoroughly demonstrated in the literature.<sup>323,325</sup> However, application to multi-exon skipping would require more study as to how peptide conjugation affects interactions between PMOs and whether this will have any negative impact on their pharmacological properties. The toxicity of such cell-penetrating peptides should be duly considered in future pre-clinical trials as well.

Using both dystrophic dog and mouse models, we showed that multi-exon skipping is feasible *in vivo*, and leads to dystrophin restoration and functional improvement. Based on our experience here with exons 45-55 skipping in mice, there was a stark reduction in efficacy *in vivo* compared to what was observed *in vitro*. As previously mentioned, this could be due to our poor understanding of how peptide conjugation influences PMO interactions. Reducing the number of exons targeted in the exons 45-55 region likely had an effect as well, since our previous work using full exons 45-55 skipping cocktails showed relatively higher skipping

efficiencies upon intramuscular administration.<sup>320,321</sup> The development of multi-exon skipping as a therapeutic approach for DMD is still at a young phase. Research into the endogenous splicing of *DMD* transcripts will provide valuable insight into the rational design of multi-exon skipping strategies, which would positively impact performance in systemic animal treatment studies.

Treatment design likewise plays a large role in demonstrating the efficacy of exon skipping therapies. Human clinical trials and animal studies have shown that increased doses and longer treatment both lead to dystrophin accumulation and improved functional performance. The treatment structures used in this thesis are rather short-term, and involved at most three systemic injections. This regimen is sufficient for proof-of-concept, and serves as a useful foundation for long-term studies. Our work supports the potential of early exon skipping treatment to better ameliorate dystrophic symptoms, particularly in muscles that have experienced more degeneration, and should be considered in the design of future studies.

Finally, a strength of the present work was the use of humanized dystrophic mice for the testing of our exon skipping PMOs. The use of humanized mice for evaluating the efficacy of exon skipping therapies is not new in the field. For instance, previous studies from our group and others have used mice carrying a stably integrated, full-length version of the human *DMD* gene on either the *mdx* or dystrophin-null background for exon skipping evaluation.<sup>320,332,352–355</sup> However, these models do not present any dystrophic symptoms and are only suitable for confirming the exon skipping activity of AOs in an animal system. Through genome editing, mice were created from this initial model that harbored out-of-frame mutations in the human *DMD* transgene.<sup>328,356</sup> This paved the way for evaluating the effects of human sequence-specific exon skipping AOs on dystrophin restoration, muscle histopathology, and muscle function. The

work in this thesis is the first demonstration of functional improvement resulting from systemic exon skipping therapy in one such model, i.e., hDMDdel52;*mdx*.

An important limitation with using hDMDdel52;*mdx* mice, however, is that they have a relatively mild phenotype compared to what is seen in patients and do not show cardiac dysfunction at young ages. This is reminiscent of what is seen in *mdx* mice, where cardiac failure only manifest at advanced ages (>1 yr) or when mice are subjected to physical or chemical stress.<sup>357–360</sup> The expression of genetic modifiers is thought to explain these mild symptoms, as *mdx* mice that are deficient in utrophin,<sup>337,338,361</sup> cytidine monophosphate-sialic acid hydroxylase,<sup>362,363</sup> or the RNA component of telomerase<sup>364</sup> show more severe cardiac phenotypes and dystrophic progression at younger ages. Genetic background is also an important modifier of phenotype, since *mdx* mice on the DBA/2 background show stronger cardiac phenotypes than those on the C57BL/10 background.<sup>365,366</sup> The next challenge in the field would be to create a humanized dystrophic mouse model with phenotypes closer to those observed in patients, particularly those concerning the heart. Heart failure is becoming the leading cause of death among DMD patients,<sup>367</sup> and so it is critical for exon skipping therapies to have demonstrated benefits to the heart. Of course, large animal models such as DMD dogs can be used for these purposes but would require correspondingly larger amounts of AOs, which would be too costly for preliminary pre-clinical study. Testing on engineered heart muscle constructed from human induced pluripotent stem cells is another alternative, and could provide insights into how exon skipping therapies improve cardiac phenotypes in a completely humanized model.<sup>368–370</sup>

In summary, the work in this thesis has not only produced promising exon skipping therapies for further pre-clinical development but has also provided insights into how the efficacy of exon skipping therapies could be further improved.

## Bibliography

1. Mercuri, E., Bönnemann, C. G. & Muntoni, F. Muscular dystrophies. *Lancet* **394**, 2025–2038 (2019).
2. Crisafulli, S. *et al.* Global epidemiology of Duchenne muscular dystrophy: an updated systematic review and meta-analysis. *Orphanet J. Rare Dis.* **15**, 141 (2020).
3. Mah, J. K. *et al.* A systematic review and meta-analysis on the epidemiology of Duchenne and Becker muscular dystrophy. *Neuromuscul. Disord.* **24**, 482–491 (2014).
4. Mah, J. K. *et al.* A Systematic Review and Meta-analysis on the Epidemiology of the Muscular Dystrophies. *Can. J. Neurol. Sci. / J. Can. des Sci. Neurol.* **43**, 163–177 (2016).
5. Wang, L. H. & Tawil, R. Facioscapulohumeral Dystrophy. *Curr. Neurol. Neurosci. Rep.* **16**, 66 (2016).
6. Richards, M., Coppée, F., Thomas, N., Belayew, A. & Upadhyaya, M. Facioscapulohumeral muscular dystrophy (FSHD): an enigma unravelled? *Hum. Genet.* **131**, 325–340 (2012).
7. Lim, K. R. Q. K. R. Q., Nguyen, Q. & Yokota, T. DUX4 Signalling in the Pathogenesis of Facioscapulohumeral Muscular Dystrophy. *Int. J. Mol. Sci.* **21**, 729 (2020).
8. Scully, M. A., Eichinger, K. J., Donlin-Smith, C. M., Tawil, R. & Statland, J. M. Restrictive lung involvement in facioscapulohumeral muscular dystrophy. *Muscle Nerve* **50**, 739–743 (2014).
9. Laforêt, P. *et al.* Cardiac involvement in genetically confirmed facioscapulohumeral muscular dystrophy. *Neurology* **51**, 1454–1456 (1998).
10. Padberg, G. W. *et al.* On the significance of retinal vascular disease and hearing loss in facioscapulohumeral muscular dystrophy. *Muscle Nerve. Suppl.* **2**, S73-80 (1995).

11. Lutz, K. L., Holte, L., Kliethermes, S. A., Stephan, C. & Mathews, K. D. Clinical and genetic features of hearing loss in facioscapulohumeral muscular dystrophy. *Neurology* **81**, 1374–1377 (2013).
12. Fitzsimons, R. B., Gurwin, E. B. & Bird, A. C. Retinal vascular abnormalities in facioscapulohumeral muscular dystrophy. A general association with genetic and therapeutic implications. *Brain* **110**, 631–648 (1987).
13. Tawil, R., van der Maarel, S. M. & Tapscott, S. J. Facioscapulohumeral dystrophy: the path to consensus on pathophysiology. *Skelet. Muscle* **4**, 12 (2014).
14. Klinge, L. *et al.* Severe phenotype in infantile facioscapulohumeral muscular dystrophy. *Neuromuscul. Disord.* **16**, 553–558 (2006).
15. Goselink, R. J. M. *et al.* Early onset facioscapulohumeral dystrophy - a systematic review using individual patient data. *Neuromuscul. Disord.* **27**, 1077–1083 (2017).
16. Hendrickson, P. G. *et al.* Conserved roles of mouse DUX and human DUX4 in activating cleavage-stage genes and MERVL/HERVL retrotransposons. *Nat. Genet.* **49**, 925–934 (2017).
17. De Iaco, A. *et al.* DUX-family transcription factors regulate zygotic genome activation in placental mammals. *Nat. Genet.* **49**, 941–945 (2017).
18. Snider, L. *et al.* Facioscapulohumeral Dystrophy: Incomplete Suppression of a Retrotransposed Gene. *PLoS Genet.* **6**, e1001181 (2010).
19. Das, S. & Chadwick, B. P. Influence of Repressive Histone and DNA Methylation upon D4Z4 Transcription in Non-Myogenic Cells. *PLoS One* **11**, e0160022 (2016).
20. Dixit, M. *et al.* DUX4, a candidate gene of facioscapulohumeral muscular dystrophy, encodes a transcriptional activator of PITX1. *Proc. Natl. Acad. Sci.* **104**, 18157–18162

- (2007).
21. Hamel, J. & Tawil, R. Facioscapulohumeral Muscular Dystrophy: Update on Pathogenesis and Future Treatments. *Neurotherapeutics* **15**, 863–871 (2018).
  22. Le Gall, L., Sidlauskaite, E., Mariot, V. & Dumonceaux, J. Therapeutic Strategies Targeting DUX4 in FSHD. *J. Clin. Med.* **9**, 2886 (2020).
  23. Vilquin, J.-T. *et al.* Normal growth and regenerating ability of myoblasts from unaffected muscles of facioscapulohumeral muscular dystrophy patients. *Gene Ther.* **12**, 1651–1662 (2005).
  24. Morosetti, R. *et al.* Mesoangioblasts from Facioscapulohumeral Muscular Dystrophy Display in Vivo a Variable Myogenic Ability Predictable by their in Vitro Behavior. *Cell Transplant.* **20**, 1299–1313 (2011).
  25. Bao, B., Maruyama, R. & Yokota, T. Targeting mRNA for the treatment of facioscapulohumeral muscular dystrophy. *Intractable rare Dis. Res.* **5**, 168–176 (2016).
  26. Bouwman, L. F., van der Maarel, S. M. & de Greef, J. C. The prospects of targeting DUX4 in facioscapulohumeral muscular dystrophy. *Curr. Opin. Neurol.* **33**, 635–640 (2020).
  27. Cohen, J., DeSimone, A., Lek, M. & Lek, A. Therapeutic Approaches in Facioscapulohumeral Muscular Dystrophy. *Trends Mol. Med.* **27**, 123–137 (2021).
  28. Gabriëls, J. *et al.* Nucleotide sequence of the partially deleted D4Z4 locus in a patient with FSHD identifies a putative gene within each 3.3 kb element. *Gene* **236**, 25–32 (1999).
  29. Lemmers, R. J. L. F. *et al.* A unifying genetic model for facioscapulohumeral muscular dystrophy. *Science* **329**, 1650–1653 (2010).
  30. Deidda, G. *et al.* Physical Mapping Evidence for a Duplicated Region on Chromosome

- 10qter Showing High Homology with the Facioscapulohumeral Muscular Dystrophy Locus on Chromosome 4qter. *Eur. J. Hum. Genet.* **3**, 155–167 (1995).
31. Bakker, E. *et al.* The FSHD-linked locus D4F104S1 (p13E-11) on 4q35 has a homologue on 10qter. *Muscle Nerve. Suppl.* **2**, S39-44 (1995).
  32. Himeda, C. L. & Jones, P. L. The Genetics and Epigenetics of Facioscapulohumeral Muscular Dystrophy. *Annu. Rev. Genomics Hum. Genet.* **20**, 265–291 (2019).
  33. Lemmers, R. J. L. F. *et al.* Facioscapulohumeral muscular dystrophy is uniquely associated with one of the two variants of the 4q subtelomere. *Nat. Genet.* **32**, 235–236 (2002).
  34. Lemmers, R. J. F. L. *et al.* Contractions of D4Z4 on 4qB Subtelomeres Do Not Cause Facioscapulohumeral Muscular Dystrophy. *Am. J. Hum. Genet.* **75**, 1124–1130 (2004).
  35. Hewitt, J. E. *et al.* Analysis of the tandem repeat locus D4Z4 associated with facioscapulohumeral muscular dystrophthy. *Hum. Mol. Genet.* **3**, 1287–1295 (1994).
  36. van Overveld, P. G. M. *et al.* Hypomethylation of D4Z4 in 4q-linked and non-4q-linked facioscapulohumeral muscular dystrophy. *Nat. Genet.* **35**, 315–317 (2003).
  37. Hewitt, J. E. Loss of epigenetic silencing of the DUX4 transcription factor gene in facioscapulohumeral muscular dystrophy: Figure 1. *Hum. Mol. Genet.* **24**, R17-23 (2015).
  38. Lemmers, R. J. L. F. *et al.* Inter-individual differences in CpG methylation at D4Z4 correlate with clinical variability in FSHD1 and FSHD2. *Hum. Mol. Genet.* **24**, 659–669 (2015).
  39. Ricci, G. *et al.* Large scale genotype–phenotype analyses indicate that novel prognostic tools are required for families with facioscapulohumeral muscular dystrophy. *Brain* **136**, 3408–3417 (2013).

40. Van Overveld, P. G. M. *et al.* Variable hypomethylation of D4Z4 in facioscapulohumeral muscular dystrophy. *Ann. Neurol.* **58**, 569–576 (2005).
41. Nikolic, A. *et al.* Clinical expression of facioscapulohumeral muscular dystrophy in carriers of 1–3 D4Z4 reduced alleles: experience of the FSHD Italian National Registry. *BMJ Open* **6**, e007798 (2016).
42. Lunt, P. W. *et al.* Correlation between fragment size at D4F104S1 and age at onset or at wheelchair use, with a possible generational effect, accounts for much phenotypic variation in 4q35-facioscapulohumeral muscular dystrophy (FSHD). *Hum. Mol. Genet.* **4**, 951–958 (1995).
43. de Greef, J. C. *et al.* Clinical features of facioscapulohumeral muscular dystrophy 2. *Neurology* **75**, 1548–1554 (2010).
44. Lemmers, R. J. L. F. *et al.* Digenic inheritance of an SMCHD1 mutation and an FSHD-permissive D4Z4 allele causes facioscapulohumeral muscular dystrophy type 2. *Nat. Genet.* **44**, 1370–1374 (2012).
45. van den Boogaard, M. L. *et al.* Mutations in DNMT3B Modify Epigenetic Repression of the D4Z4 Repeat and the Penetrance of Facioscapulohumeral Dystrophy. *Am. J. Hum. Genet.* **98**, 1020–1029 (2016).
46. Hamanaka, K. *et al.* Homozygous nonsense variant in LRIF1 associated with facioscapulohumeral muscular dystrophy. *Neurology* **94**, e2441–e2447 (2020).
47. de Greef, J. C. *et al.* Smchd1 haploinsufficiency exacerbates the phenotype of a transgenic FSHD1 mouse model. *Hum. Mol. Genet.* **27**, 716–731 (2018).
48. Sacconi, S. *et al.* The FSHD2 Gene SMCHD1 Is a Modifier of Disease Severity in Families Affected by FSHD1. *Am. J. Hum. Genet.* **93**, 744–751 (2013).

49. Sacconi, S. *et al.* FSHD1 and FSHD2 form a disease continuum. *Neurology* **92**, e2273–e2285 (2019).
50. Tassin, A. *et al.* DUX4 expression in FSHD muscle cells: how could such a rare protein cause a myopathy? *J. Cell. Mol. Med.* **17**, 76–89 (2013).
51. Kowaljow, V. *et al.* The DUX4 gene at the FSHD1A locus encodes a pro-apoptotic protein. *Neuromuscul. Disord.* **17**, 611–623 (2007).
52. Wallace, L. M. *et al.* DUX4, a candidate gene for facioscapulohumeral muscular dystrophy, causes p53-dependent myopathy in vivo. *Ann. Neurol.* **69**, 540–552 (2011).
53. Aubrey, B. J., Kelly, G. L., Janic, A., Herold, M. J. & Strasser, A. How does p53 induce apoptosis and how does this relate to p53-mediated tumour suppression? *Cell Death Differ.* **25**, 104–113 (2018).
54. Fridman, J. S. & Lowe, S. W. Control of apoptosis by p53. *Oncogene* **22**, 9030–9040 (2003).
55. Block, G. J. *et al.* Wnt/ $\beta$ -catenin signaling suppresses DUX4 expression and prevents apoptosis of FSHD muscle cells. *Hum. Mol. Genet.* **22**, 4661–4672 (2013).
56. Shadle, S. C. *et al.* DUX4-induced dsRNA and MYC mRNA stabilization activate apoptotic pathways in human cell models of facioscapulohumeral dystrophy. *PLOS Genet.* **13**, e1006658 (2017).
57. Bosnakovski, D. *et al.* An isogenetic myoblast expression screen identifies DUX4-mediated FSHD-associated molecular pathologies. *EMBO J.* **27**, 2766–2779 (2008).
58. Bosnakovski, D. *et al.* p53-independent DUX4 pathology in cell and animal models of facioscapulohumeral muscular dystrophy. *Dis. Model. Mech.* **10**, 1211–1216 (2017).
59. Banerji, C. R. S. *et al.*  $\beta$ -catenin is central to DUX4-driven network rewiring in

- facioscapulohumeral muscular dystrophy. *J. R. Soc. Interface* **12**, 20140797 (2015).
60. Xu, H. *et al.* Dux4 induces cell cycle arrest at G1 phase through upregulation of p21 expression. *Biochem. Biophys. Res. Commun.* **446**, 235–240 (2014).
  61. Bosnakovski, D. *et al.* Low level DUX4 expression disrupts myogenesis through deregulation of myogenic gene expression. *Sci. Rep.* **8**, 16957 (2018).
  62. Knopp, P. *et al.* DUX4 induces a transcriptome more characteristic of a less-differentiated cell state and inhibits myogenesis. *J. Cell Sci.* **129**, 3816–3831 (2016).
  63. Vanderplanck, C. *et al.* The FSHD Atrophic Myotube Phenotype Is Caused by DUX4 Expression. *PLoS One* **6**, e26820 (2011).
  64. Campbell, A. E. *et al.* BET bromodomain inhibitors and agonists of the beta-2 adrenergic receptor identified in screens for compounds that inhibit DUX4 expression in FSHD muscle cells. *Skelet. Muscle* **7**, 16 (2017).
  65. Seko, D., Ogawa, S., Li, T.-S., Taimura, A. & Ono, Y.  $\mu$ -Crystallin controls muscle function through thyroid hormone action. *FASEB J.* **30**, 1733–1740 (2016).
  66. Oshima, A. CRYM mutations cause deafness through thyroid hormone binding properties in the fibrocytes of the cochlea. *J. Med. Genet.* **43**, e25–e25 (2006).
  67. Moyle, L. A. *et al.* Ret function in muscle stem cells points to tyrosine kinase inhibitor therapy for facioscapulohumeral muscular dystrophy. *Elife* **5**, 1–35 (2016).
  68. Anseau, E. *et al.* Homologous Transcription Factors DUX4 and DUX4c Associate with Cytoplasmic Proteins during Muscle Differentiation. *PLoS One* **11**, e0146893 (2016).
  69. Jagannathan, S., Ogata, Y., Gafken, P. R., Tapscott, S. J. & Bradley, R. K. Quantitative proteomics reveals key roles for post-transcriptional gene regulation in the molecular pathology of facioscapulohumeral muscular dystrophy. *Elife* **8**, 1–16 (2019).

70. Rickard, A. M., Petek, L. M. & Miller, D. G. Endogenous DUX4 expression in FSHD myotubes is sufficient to cause cell death and disrupts RNA splicing and cell migration pathways. *Hum. Mol. Genet.* **24**, 5901–5914 (2015).
71. Homma, S., Beermann, M. Lou, Boyce, F. M. & Miller, J. B. Expression of FSHD-related DUX4-FL alters proteostasis and induces TDP-43 aggregation. *Ann. Clin. Transl. Neurol.* **2**, 151–166 (2015).
72. Geng, L. N. *et al.* DUX4 activates germline genes, retroelements and immune-mediators: implications for facioscapulohumeral dystrophy. *Dev. Cell* **22**, 38–51 (2012).
73. Lim, K. R. Q. & Yokota, T. Invention and early history of exon skipping and splice modulation. in *Exon Skipping and Inclusion Therapies: Methods and Protocols* (eds. Yokota, T. & Maruyama, R.) 3–30 (Springer, 2018).
74. Lim, K. R. Q. & Yokota, T. Invention and Early History of Gapmers. in *Gapmers: Methods and Protocols* (eds. Yokota, T. & Maruyama, R.) 3–19 (Springer, 2020).
75. Anseau, E. *et al.* Antisense Oligonucleotides Used to Target the DUX4 mRNA as Therapeutic Approaches in FaciosScapuloHumeral Muscular Dystrophy (FSHD). *Genes (Basel)*. **8**, 93 (2017).
76. Derenne, A. *et al.* Induction of a local muscular dystrophy using electroporation in vivo: an easy tool for screening therapeutics. *Sci. Rep.* **10**, 11301 (2020).
77. Morcos, P. A., Li, Y. & Jiang, S. Vivo-Morpholinos: A non-peptide transporter delivers Morpholinos into a wide array of mouse tissues. *Biotechniques* **45**, 613–623 (2008).
78. Marsollier, A.-C. *et al.* Antisense targeting of 3' end elements involved in DUX4 mRNA processing is an efficient therapeutic strategy for facioscapulohumeral dystrophy: a new gene-silencing approach. *Hum. Mol. Genet.* **25**, 1468–1478 (2016).

79. Chen, J. C. *et al.* Morpholino-mediated Knockdown of DUX4 Toward Facioscapulohumeral Muscular Dystrophy Therapeutics. *Mol. Ther.* **24**, 1405–1411 (2016).
80. Lim, J.-W. *et al.* DICER/AGO-dependent epigenetic silencing of D4Z4 repeats enhanced by exogenous siRNA suggests mechanisms and therapies for FSHD. *Hum. Mol. Genet.* **24**, 4817–4828 (2015).
81. Holoch, D. & Moazed, D. RNA-mediated epigenetic regulation of gene expression. *Nat. Rev. Genet.* **16**, 71–84 (2015).
82. Wallace, L. M. *et al.* RNA Interference Inhibits DUX4-induced Muscle Toxicity In Vivo: Implications for a Targeted FSHD Therapy. *Mol. Ther.* **20**, 1417–1423 (2012).
83. Wallace, L. M. *et al.* Pre-clinical Safety and Off-Target Studies to Support Translation of AAV-Mediated RNAi Therapy for FSHD. *Mol. Ther. - Methods Clin. Dev.* **8**, 121–130 (2018).
84. Mariot, V. *et al.* A Deoxyribonucleic Acid Decoy Trapping DUX4 for the Treatment of Facioscapulohumeral Muscular Dystrophy. *Mol. Ther. - Nucleic Acids* **22**, 1191–1199 (2020).
85. Klingler, C. *et al.* DNA aptamers against the DUX4 protein reveal novel therapeutic implications for FSHD. *FASEB J.* **34**, 4573–4590 (2020).
86. Pandey, S. N. *et al.* Conditional over-expression of PITX1 causes skeletal muscle dystrophy in mice. *Biol. Open* **1**, 629–639 (2012).
87. Pandey, S. N., Lee, Y.-C., Yokota, T. & Chen, Y.-W. Morpholino treatment improves muscle function and pathology of Pitx1 transgenic mice. *Mol. Ther.* **22**, 390–396 (2014).
88. Bortolanza, S. *et al.* AAV6-mediated Systemic shRNA Delivery Reverses Disease in a

- Mouse Model of Facioscapulohumeral Muscular Dystrophy. *Mol. Ther.* **19**, 2055–2064 (2011).
89. Ferri, G., Huichalaf, C. H., Caccia, R. & Gabellini, D. Direct interplay between two candidate genes in FSHD muscular dystrophy. *Hum. Mol. Genet.* **24**, 1256–1266 (2015).
  90. Jones, T. & Jones, P. L. A cre-inducible DUX4 transgenic mouse model for investigating facioscapulohumeral muscular dystrophy. *PLoS One* **13**, e0192657 (2018).
  91. Bosnakovski, D. *et al.* Muscle pathology from stochastic low level DUX4 expression in an FSHD mouse model. *Nat. Commun.* **8**, 550 (2017).
  92. Bosnakovski, D. *et al.* Transcriptional and cytopathological hallmarks of FSHD in chronic DUX4-expressing mice. *J. Clin. Invest.* **130**, 2465–2477 (2020).
  93. Giesige, C. R. *et al.* AAV-mediated follistatin gene therapy improves functional outcomes in the TIC-DUX4 mouse model of FSHD. *JCI Insight* **3**, e123538 (2018).
  94. Jinek, M. *et al.* A programmable dual-RNA-guided DNA endonuclease in adaptive bacterial immunity. *Science* **337**, 816–821 (2012).
  95. Jiang, F. & Doudna, J. A. CRISPR-Cas9 Structures and Mechanisms. *Annu. Rev. Biophys.* **46**, 505–529 (2017).
  96. Mojica, F. J. M., Díez-Villaseñor, C., García-Martínez, J. & Almendros, C. Short motif sequences determine the targets of the prokaryotic CRISPR defence system. *Microbiology* **155**, 733–740 (2009).
  97. O’Connell, M. R. *et al.* Programmable RNA recognition and cleavage by CRISPR/Cas9. *Nature* **516**, 263–266 (2014).
  98. Goossens, R. *et al.* Intronic SMCHD1 variants in FSHD: testing the potential for CRISPR-Cas9 genome editing. *J. Med. Genet.* **56**, 828–837 (2019).

99. Himeda, C. L., Jones, T. I. & Jones, P. L. CRISPR/dCas9-mediated Transcriptional Inhibition Ameliorates the Epigenetic Dysregulation at D4Z4 and Represses DUX4-fl in FSH Muscular Dystrophy. *Mol. Ther.* **24**, 527–535 (2016).
100. Himeda, C. L. *et al.* Identification of Epigenetic Regulators of DUX4-fl for Targeted Therapy of Facioscapulohumeral Muscular Dystrophy. *Mol. Ther.* **26**, 1797–1807 (2018).
101. Lek, A. *et al.* Applying genome-wide CRISPR-Cas9 screens for therapeutic discovery in facioscapulohumeral muscular dystrophy. *Sci. Transl. Med.* **12**, eaay0271 (2020).
102. Dmitriev, P. *et al.* DUX4-induced constitutive DNA damage and oxidative stress contribute to aberrant differentiation of myoblasts from FSHD patients. *Free Radic. Biol. Med.* **99**, 244–258 (2016).
103. Denny, A. P. & Heather, A. K. Are Antioxidants a Potential Therapy for FSHD? A Review of the Literature. *Oxid. Med. Cell. Longev.* **2017**, 1–10 (2017).
104. Mitsuhashi, H. *et al.* Functional domains of the FSHD-associated DUX4 protein. *Biol. Open* **7**, bio033977 (2018).
105. Geng, L. N., Tyler, A. E. & Tapscott, S. J. Immunodetection of Human Double Homeobox 4. *Hybridoma* **30**, 125–130 (2011).
106. Mitsuhashi, H., Mitsuhashi, S., Lynn-Jones, T., Kawahara, G. & Kunkel, L. M. Expression of DUX4 in zebrafish development recapitulates facioscapulohumeral muscular dystrophy. *Hum. Mol. Genet.* **22**, 568–577 (2013).
107. Bosnakovski, D. *et al.* The DUX4 homeodomains mediate inhibition of myogenesis and are functionally exchangeable with the Pax7 homeodomain. *J. Cell Sci.* **130**, 3685–3697 (2017).
108. Rodino-Klapac, L. R. *et al.* Inhibition of myostatin with emphasis on follistatin as a

- therapy for muscle disease. *Muscle Nerve* **39**, 283–296 (2009).
109. Hoffman, E. P., Brown, R. H. & Kunkel, L. M. Dystrophin: the protein product of the Duchenne muscular dystrophy locus. *Cell* **51**, 919–928 (1987).
  110. Emery, A. E. H. Population frequencies of inherited neuromuscular diseases—a world survey. *Neuromuscul. Disord.* **1**, 19–29 (1991).
  111. Mendell, J. R. *et al.* Evidence-based path to newborn screening for Duchenne muscular dystrophy. *Ann. Neurol.* **71**, 304–313 (2012).
  112. Manzur, A., Kinali, M. & Muntoni, F. Update on the management of Duchenne muscular dystrophy. *Arch. Dis. Child.* **93**, 986–990 (2008).
  113. Mah, J. K. Current and emerging treatment strategies for Duchenne muscular dystrophy. *Neuropsychiatr. Dis. Treat.* **12**, 1795–1807 (2016).
  114. Koenig, M., Monaco, A. P. & Kunkel, L. M. The complete sequence of dystrophin predicts a rod-shaped cytoskeletal protein. *Cell* **53**, 219–228 (1988).
  115. Ervasti, J. M. & Campbell, K. P. A role for the dystrophin-glycoprotein complex as a transmembrane linker between laminin and actin. *J. Cell Biol.* **122**, 809–823 (1993).
  116. Ervasti, J. M. & Campbell, K. P. Membrane organization of the dystrophin-glycoprotein complex. *Cell* **66**, 1121–1131 (1991).
  117. Ervasti, J. M. Dystrophin, its interactions with other proteins, and implications for muscular dystrophy. *Biochim. Biophys. Acta* **1772**, 108–117 (2007).
  118. Petrof, B. J., Shrager, J. B., Stedman, H. H., Kelly, A. M. & Sweeney, H. L. Dystrophin protects the sarcolemma from stresses developed during muscle contraction. *Proc. Natl. Acad. Sci. U. S. A.* **90**, 3710–3714 (1993).
  119. Nichols, B., Takeda, S. & Yokota, T. Nonmechanical Roles of Dystrophin and Associated

- Proteins in Exercise, Neuromuscular Junctions, and Brains. *Brain Sci.* **5**, 275–298 (2015).
120. van Deutekom, J. C. T. & van Ommen, G.-J. B. Advances in Duchenne muscular dystrophy gene therapy. *Nat. Rev. Genet.* **4**, 774–783 (2003).
  121. Koenig, M. *et al.* Complete cloning of the Duchenne muscular dystrophy (DMD) cDNA and preliminary genomic organization of the DMD gene in normal and affected individuals. *Cell* **50**, 509–517 (1987).
  122. Roberts, R. G., Coffey, A. J., Bobrow, M. & Bentley, D. R. Exon structure of the human dystrophin gene. *Genomics* **16**, 536–538 (1993).
  123. Buzin, C. H. *et al.* Mutation rates in the dystrophin gene: a hotspot of mutation at a CpG dinucleotide. *Hum. Mutat.* **25**, 177–188 (2005).
  124. Takeshima, Y. *et al.* Mutation spectrum of the dystrophin gene in 442 Duchenne/Becker muscular dystrophy cases from one Japanese referral center. *J. Hum. Genet.* **55**, 379–388 (2010).
  125. White, S. *et al.* Comprehensive detection of genomic duplications and deletions in the DMD gene, by use of multiplex amplifiable probe hybridization. *Am. J. Hum. Genet.* **71**, 365–374 (2002).
  126. Goto, M. *et al.* Long-term outcomes of steroid therapy for Duchenne muscular dystrophy in Japan. *Brain Dev.* **38**, 785–791 (2016).
  127. Biggar, W. D., Harris, V. A., Eliasoph, L. & Alman, B. Long-term benefits of deflazacort treatment for boys with Duchenne muscular dystrophy in their second decade. *Neuromuscul. Disord.* **16**, 249–255 (2006).
  128. Kole, R. & Krieg, A. M. Exon skipping therapy for Duchenne muscular dystrophy. *Adv. Drug Deliv. Rev.* **87**, 104–107 (2015).

129. Guncay, A. & Yokota, T. Antisense oligonucleotide drugs for Duchenne muscular dystrophy: how far have we come and what does the future hold? *Future Med. Chem.* **7**, 1631–1635 (2015).
130. Aartsma-Rus, A. *et al.* Theoretic applicability of antisense-mediated exon skipping for Duchenne muscular dystrophy mutations. *Hum. Mutat.* **30**, 293–299 (2009).
131. Gao, Q. Q. & McNally, E. M. The Dystrophin Complex: Structure, Function, and Implications for Therapy. *Compr. Physiol.* **5**, 1223–1239 (2015).
132. Way, M., Pope, B., Cross, R. A., Kendrick-Jones, J. & Weeds, A. G. Expression of the N-terminal domain of dystrophin in *E. coli* and demonstration of binding to F-actin. *FEBS Lett.* **301**, 243–245 (1992).
133. Stone, M. R., O’Neill, A., Catino, D. & Bloch, R. J. Specific Interaction of the Actin-binding Domain of Dystrophin with Intermediate Filaments Containing Keratin 19. *Mol. Biol. Cell* **16**, 4280–4293 (2005).
134. Norwood, F. L., Sutherland-Smith, A. J., Keep, N. H. & Kendrick-Jones, J. The structure of the N-terminal actin-binding domain of human dystrophin and how mutations in this domain may cause Duchenne or Becker muscular dystrophy. *Structure* **8**, 481–491 (2000).
135. Koenig, M. & Kunkel, L. M. Detailed analysis of the repeat domain of dystrophin reveals four potential hinge segments that may confer flexibility. *J. Biol. Chem.* **265**, 4560–4566 (1990).
136. Amann, K. J., Renley, B. A. & Ervasti, J. M. A Cluster of Basic Repeats in the Dystrophin Rod Domain Binds F-actin through an Electrostatic Interaction. *J. Biol. Chem.* **273**, 28419–28423 (1998).
137. Bhosle, R. C., Michele, D. E., Campbell, K. P., Li, Z. & Robson, R. M. Interactions of

- intermediate filament protein synemin with dystrophin and utrophin. *Biochem. Biophys. Res. Commun.* **346**, 768–777 (2006).
138. Belanto, J. J. *et al.* Microtubule binding distinguishes dystrophin from utrophin. *Proc. Natl. Acad. Sci.* **111**, 5723–5728 (2014).
139. Zhao, J. *et al.* Dystrophin contains multiple independent membrane-binding domains. *Hum. Mol. Genet.* **25**, 3647–3653 (2016).
140. Legardinier, S. *et al.* Mapping of the Lipid-Binding and Stability Properties of the Central Rod Domain of Human Dystrophin. *J. Mol. Biol.* **389**, 546–558 (2009).
141. Le Rumeur, E. *et al.* Interaction of Dystrophin Rod Domain with Membrane Phospholipids. *J. Biol. Chem.* **278**, 5993–6001 (2003).
142. Lai, Y. *et al.* Dystrophins carrying spectrin-like repeats 16 and 17 anchor nNOS to the sarcolemma and enhance exercise performance in a mouse model of muscular dystrophy. *J. Clin. Invest.* **119**, 624–635 (2009).
143. Adams, M. E., Odom, G. L., Kim, M. J., Chamberlain, J. S. & Froehner, S. C. Syntrophin binds directly to multiple spectrin-like repeats in dystrophin and mediates binding of nNOS to repeats 16–17. *Hum. Mol. Genet.* **27**, 2978–2985 (2018).
144. Rentschler, S. *et al.* The WW Domain of Dystrophin Requires EF-Hands Region to Interact with  $\beta$ -Dystroglycan. *Biol. Chem.* **380**, 431–442 (1999).
145. Ponting, C. P., Blake, D. J., Davies, K. E., Kendrick-Jones, J. & Winder, S. J. ZZ and TAZ: new putative zinc fingers in dystrophin and other proteins. *Trends Biochem. Sci.* **21**, 11–13 (1996).
146. Hijikata, T., Murakami, T., Ishikawa, H. & Yorifuji, H. Plectin tethers desmin intermediate filaments onto subsarcolemmal dense plaques containing dystrophin and

- vinculin. *Histochem. Cell Biol.* **119**, 109–123 (2003).
147. Ayalon, G., Davis, J. Q., Scotland, P. B. & Bennett, V. An Ankyrin-Based Mechanism for Functional Organization of Dystrophin and Dystroglycan. *Cell* **135**, 1189–1200 (2008).
  148. Jung, D., Yang, B., Meyer, J., Chamberlain, J. S. & Campbell, K. P. Identification and Characterization of the Dystrophin Anchoring Site on  $\beta$ -Dystroglycan. *J. Biol. Chem.* **270**, 27305–27310 (1995).
  149. Ishikawa-Sakurai, M. ZZ domain is essentially required for the physiological binding of dystrophin and utrophin to -dystroglycan. *Hum. Mol. Genet.* **13**, 693–702 (2004).
  150. Kawasaki, H. & Kretsinger, R. H. Structural and functional diversity of EF-hand proteins: Evolutionary perspectives. *Protein Sci.* **26**, 1898–1920 (2017).
  151. Sadoulet-Puccio, H. M., Rajala, M. & Kunkel, L. M. Dystrobrevin and dystrophin: An interaction through coiled-coil motifs. *Proc. Natl. Acad. Sci.* **94**, 12413–12418 (1997).
  152. Newey, S., Benson, M. A., Ponting, C. P., Davies, K. E. & Blake, D. J. Alternative splicing of dystrobrevin regulates the stoichiometry of syntrophin binding to the dystrophin protein complex. *Curr. Biol.* **10**, 1295–1298 (2000).
  153. Constantin, B. Dystrophin complex functions as a scaffold for signalling proteins. *Biochim. Biophys. Acta - Biomembr.* **1838**, 635–642 (2014).
  154. Adams, M. E., Mueller, H. A. & Froehner, S. C. In vivo requirement of the  $\alpha$ -syntrophin PDZ domain for the sarcolemmal localization of nNOS and aquaporin-4. *J. Cell Biol.* **155**, 113–122 (2001).
  155. Yoshida, M. Biochemical evidence for association of dystrobrevin with the sarcoglycan-sarcospan complex as a basis for understanding sarcoglycanopathy. *Hum. Mol. Genet.* **9**, 1033–1040 (2000).

156. Acharyya, S. *et al.* Dystrophin glycoprotein complex dysfunction: A regulatory link between muscular dystrophy and cancer cachexia. *Cancer Cell* **8**, 421–432 (2005).
157. Nudel, U. *et al.* Duchenne muscular dystrophy gene product is not identical in muscle and brain. *Nature* **337**, 76–78 (1989).
158. Górecki, D. C. *et al.* Expression of four alternative dystrophin transcripts in brain regions regulated by different promoters. *Hum. Mol. Genet.* **1**, 505–510 (1992).
159. D'Souza, V. N. *et al.* A novel dystrophin isoform is required for normal retinal electrophysiology. *Hum. Mol. Genet.* **4**, 837–842 (1995).
160. Lidov, H. G. W., Selig, S. & Kunkel, L. M. Dp140: a novel 140 kDa CNS transcript from the dystrophin locus. *Hum. Mol. Genet.* **4**, 329–335 (1995).
161. Byers, T. J., Lidov, H. G. W. & Kunkel, L. M. An alternative dystrophin transcript specific to peripheral nerve. *Nat. Genet.* **4**, 77–81 (1993).
162. Tinsley, J. M., Blake, D. J. & Davies, K. E. Apo-dystrophin-3: a 2.2kb transcript from the DMD locus encoding the dystrophin glycoprotein binding site. *Hum. Mol. Genet.* **2**, 521–524 (1993).
163. Feener, C. A., Koenig, M. & Kunkel, L. M. Alternative splicing of human dystrophin mRNA generates isoforms at the carboxy terminus. *Nature* **338**, 509–511 (1989).
164. Rapaport, D. *et al.* Characterization and cell type distribution of a novel, major transcript of the Duchenne Muscular Dystrophy gene. *Differentiation* **49**, 187–193 (1992).
165. Monaco, A. P., Bertelson, C. J., Liechti-Gallati, S., Moser, H. & Kunkel, L. M. An explanation for the phenotypic differences between patients bearing partial deletions of the DMD locus. *Genomics* **2**, 90–95 (1988).
166. Koenig, M. *et al.* The molecular basis for Duchenne versus Becker muscular dystrophy:

- correlation of severity with type of deletion. *Am. J. Hum. Genet.* **45**, 498–506 (1989).
167. Bladen, C. L. *et al.* The TREAT-NMD DMD Global Database: Analysis of More than 7,000 Duchenne Muscular Dystrophy Mutations. *Hum. Mutat.* **36**, 395–402 (2015).
168. Lim, K. R. Q., Nguyen, Q. & Yokota, T. Genotype–Phenotype Correlations in Duchenne and Becker Muscular Dystrophy Patients from the Canadian Neuromuscular Disease Registry. *J. Pers. Med.* **10**, 241 (2020).
169. Lee, J. J. A. & Yokota, T. Antisense therapy in neurology. *J. Pers. Med.* **3**, 144–176 (2013).
170. Nicholson, L. V. B. *et al.* Dystrophin in skeletal muscle II. Immunoreactivity in patients with Xp21 muscular dystrophy. *J. Neurol. Sci.* **94**, 137–146 (1989).
171. Hoffman, E. P., Morgan, J. E., Watkins, S. C. & Partridge, T. A. Somatic reversion/suppression of the mouse mdx phenotype in vivo. *J. Neurol. Sci.* **99**, 9–25 (1990).
172. Klein, C. J. *et al.* Somatic reversion/suppression in Duchenne muscular dystrophy (DMD): evidence supporting a frame-restoring mechanism in rare dystrophin-positive fibers. *Am. J. Hum. Genet.* **50**, 950–959 (1992).
173. Thanh, L. T., Nguyen, T. M., Helliwell, T. R. & Morris, G. E. Characterization of revertant muscle fibers in Duchenne muscular dystrophy, using exon-specific monoclonal antibodies against dystrophin. *Am. J. Hum. Genet.* **56**, 725–731 (1995).
174. Echigoya, Y. *et al.* Mutation Types and Aging Differently Affect Revertant Fiber Expansion in Dystrophic Mdx and Mdx52 Mice. *PLoS One* **8**, e69194 (2013).
175. Rodrigues, M. *et al.* Impaired regenerative capacity and lower revertant fibre expansion in dystrophin-deficient mdx muscles on DBA/2 background. *Sci. Rep.* **6**, 38371 (2016).

176. Sicinski, P. *et al.* The molecular basis of muscular dystrophy in the mdx mouse: a point mutation. *Science* **244**, 1578–1580 (1989).
177. Duncckley, M. G., Manoharan, M., Villiet, P., Eperon, I. C. & Dickson, G. Modification of splicing in the dystrophin gene in cultured mdx muscle cells by antisense oligoribonucleotides. *Hum. Mol. Genet.* **7**, 1083–1090 (1998).
178. Wilton, S. D. *et al.* Specific removal of the nonsense mutation from the mdx dystrophin mRNA using antisense oligonucleotides. *Neuromuscul. Disord.* **9**, 330–338 (1999).
179. van Deutekom, J. C. *et al.* Antisense-induced exon skipping restores dystrophin expression in DMD patient derived muscle cells. *Hum. Mol. Genet.* **10**, 1547–1554 (2001).
180. Takeshima, Y. *et al.* Oligonucleotides against a splicing enhancer sequence led to dystrophin production in muscle cells from a Duchenne muscular dystrophy patient. *Brain Dev.* **23**, 788–790 (2001).
181. Aartsma-Rus, A. *et al.* Therapeutic antisense-induced exon skipping in cultured muscle cells from six different DMD patients. *Hum. Mol. Genet.* **12**, 907–914 (2003).
182. Aartsma-Rus, A. *et al.* Antisense-induced multiexon skipping for Duchenne muscular dystrophy makes more sense. *Am. J. Hum. Genet.* **74**, 83–92 (2004).
183. Aartsma-Rus, A. *et al.* Comparative analysis of antisense oligonucleotide analogs for targeted DMD exon 46 skipping in muscle cells. *Gene Ther.* **11**, 1391–1398 (2004).
184. Surono, A. *et al.* Chimeric RNA/ethylene-bridged nucleic acids promote dystrophin expression in myocytes of duchenne muscular dystrophy by inducing skipping of the nonsense mutation-encoding exon. *Hum. Gene Ther.* **15**, 749–757 (2004).
185. Aartsma-Rus, A., Janson, A. A. M., van Ommen, G.-J. B. & van Deutekom, J. C. T.

- Antisense-induced exon skipping for duplications in Duchenne muscular dystrophy. *BMC Med. Genet.* **8**, 43 (2007).
186. Mann, C. J. *et al.* Antisense-induced exon skipping and synthesis of dystrophin in the mdx mouse. *Proc. Natl. Acad. Sci. U. S. A.* **98**, 42–47 (2001).
187. Lu, Q. L. *et al.* Functional amounts of dystrophin produced by skipping the mutated exon in the mdx dystrophic mouse. *Nat. Med.* **9**, 1009–1014 (2003).
188. Summerton, J. E. Invention and Early History of Morpholinos: From Pipe Dream to Practical Products. *Methods Mol. Biol.* **1565**, 1–15 (2017).
189. Summerton, J. & Weller, D. Morpholino antisense oligomers: design, preparation, and properties. *Antisense Nucleic Acid Drug Dev.* **7**, 187–195 (1997).
190. Moulton, J. D. Guide for morpholino users: toward therapeutics. *J. Drug Discov. Dev. Deliv.* **3**, 1023 (2016).
191. Gebiski, B. L., Mann, C. J., Fletcher, S. & Wilton, S. D. Morpholino antisense oligonucleotide induced dystrophin exon 23 skipping in mdx mouse muscle. *Hum. Mol. Genet.* **12**, 1801–1811 (2003).
192. Wells, K. E., Fletcher, S., Mann, C. J., Wilton, S. D. & Wells, D. J. Enhanced in vivo delivery of antisense oligonucleotides to restore dystrophin expression in adult mdx mouse muscle. *FEBS Lett.* **552**, 145–149 (2003).
193. Graham, I. R., Hill, V. J., Manoharan, M., Inamati, G. B. & Dickson, G. Towards a therapeutic inhibition of dystrophin exon 23 splicing in mdx mouse muscle induced by antisense oligoribonucleotides (splicomers): target sequence optimisation using oligonucleotide arrays. *J. Gene Med.* **6**, 1149–1158 (2004).
194. Lu, Q. L. *et al.* Systemic delivery of antisense oligoribonucleotide restores dystrophin

- expression in body-wide skeletal muscles. *Proc. Natl. Acad. Sci. U. S. A.* **102**, 198–203 (2005).
195. Alter, J. *et al.* Systemic delivery of morpholino oligonucleotide restores dystrophin expression bodywide and improves dystrophic pathology. *Nat. Med.* **12**, 175–177 (2006).
  196. Yu, X., Bao, B., Echigoya, Y. & Yokota, T. Dystrophin-deficient large animal models: translational research and exon skipping. *Am. J. Transl. Res.* **7**, 1314–1331 (2015).
  197. Shimatsu, Y. *et al.* Canine X-linked muscular dystrophy in Japan (CXMDJ). *Exp. Anim.* **52**, 93–97 (2003).
  198. Yokota, T. *et al.* Efficacy of systemic morpholino exon-skipping in Duchenne dystrophy dogs. *Ann. Neurol.* **65**, 667–676 (2009).
  199. McClorey, G., Moulton, H. M., Iversen, P. L., Fletcher, S. & Wilton, S. D. Antisense oligonucleotide-induced exon skipping restores dystrophin expression in vitro in a canine model of DMD. *Gene Ther.* **13**, 1373–1381 (2006).
  200. Takeshima, Y. *et al.* Intravenous infusion of an antisense oligonucleotide results in exon skipping in muscle dystrophin mRNA of Duchenne muscular dystrophy. *Pediatr. Res.* **59**, 690–694 (2006).
  201. van Deutekom, J. C. *et al.* Local dystrophin restoration with antisense oligonucleotide PRO051. *N. Engl. J. Med.* **357**, 2677–2686 (2007).
  202. Kesselheim, A. S. & Avorn, J. Approving a Problematic Muscular Dystrophy Drug: Implications for FDA Policy. *JAMA* **316**, 2357–2358 (2016).
  203. Lim, K. R. Q. K. R. Q., Maruyama, R. & Yokota, T. Eteplirsen in the treatment of Duchenne muscular dystrophy. *Drug Des. Devel. Ther.* **11**, 533–545 (2017).
  204. U.S. Food and Drug Administration. FDA grants accelerated approval to first drug for

- Duchenne muscular dystrophy. (2016). Available at:  
<http://www.fda.gov/NewsEvents/Newsroom/PressAnnouncements/ucm521263.htm>.  
(Accessed: 30th August 2017)
205. U.S. Food and Drug Administration: Center for Drug Evaluation and Research. Summary review, application number: 206488Orig1s000. (2016). Available at:  
[http://www.accessdata.fda.gov/drugsatfda\\_docs/nda/2016/206488\\_summary review\\_Redacted.pdf](http://www.accessdata.fda.gov/drugsatfda_docs/nda/2016/206488_summary_review_Redacted.pdf). (Accessed: 30th August 2017)
206. Mendell, J. R. *et al.* Eteplirsen for the treatment of Duchenne muscular dystrophy. *Ann. Neurol.* **74**, 637–647 (2013).
207. Frank, D. E. *et al.* Increased dystrophin production with golodirsen in patients with Duchenne muscular dystrophy. *Neurology* **94**, e2270–e2282 (2020).
208. Komaki, H. *et al.* Viltolarsen in Japanese Duchenne muscular dystrophy patients: A phase 1/2 study. *Ann. Clin. Transl. Neurol.* **7**, 2393–2408 (2020).
209. Clemens, P. R. *et al.* Safety, Tolerability, and Efficacy of Viltolarsen in Boys With Duchenne Muscular Dystrophy Amenable to Exon 53 Skipping. *JAMA Neurol.* **77**, 982 (2020).
210. Wagner, K. R. *et al.* Casimersen Treatment in Patients With Duchenne Muscular Dystrophy: Safety, Tolerability, and Pharmacokinetics Over 144 Weeks of Treatment. (2020). Available at: <https://investorrelations.sarepta.com/static-files/4fd181c5-73ec-4c89-ba29-e25ea2b7c776>. (Accessed: 29th April 2021)
211. van den Bergen, J. C. *et al.* Dystrophin levels and clinical severity in Becker muscular dystrophy patients. *J. Neurol. Neurosurg. Psychiatry* **85**, 747–753 (2014).
212. van Putten, M. *et al.* The Effects of Low Levels of Dystrophin on Mouse Muscle Function

- and Pathology. *PLoS One* **7**, e31937 (2012).
213. Finkel, R. S. Read-Through Strategies for Suppression of Nonsense Mutations in Duchenne/ Becker Muscular Dystrophy: Aminoglycosides and Ataluren (PTC124). *J. Child Neurol.* **25**, 1158–1164 (2010).
214. Finkel, R. S. *et al.* Phase 2a Study of Ataluren-Mediated Dystrophin Production in Patients with Nonsense Mutation Duchenne Muscular Dystrophy. *PLoS One* **8**, e81302 (2013).
215. Bushby, K. *et al.* Ataluren treatment of patients with nonsense mutation dystrophinopathy. *Muscle Nerve* **50**, 477–487 (2014).
216. McDonald, C. M. *et al.* Ataluren in patients with nonsense mutation Duchenne muscular dystrophy (ACT DMD): a multicentre, randomised, double-blind, placebo-controlled, phase 3 trial. *Lancet* **390**, 1489–1498 (2017).
217. Borgatti, M., Altamura, E., Salvatori, F., D’Aversa, E. & Altamura, N. Screening Readthrough Compounds to Suppress Nonsense Mutations: Possible Application to  $\beta$ -Thalassemia. *J. Clin. Med.* **9**, 289 (2020).
218. Khurana, T. S. *et al.* Immunolocalization and developmental expression of dystrophin related protein in skeletal muscle. *Neuromuscul. Disord.* **1**, 185–194 (1991).
219. Ohlendieck, K. *et al.* Dystrophin-related protein is localized to neuromuscular junctions of adult skeletal muscle. *Neuron* **7**, 499–508 (1991).
220. Clerk, A., Morris, G. E., Dubowitz, V., Davies, K. E. & Sewry, C. A. Dystrophin-related protein, utrophin, in normal and dystrophic human fetal skeletal muscle. *Histochem. J.* **25**, 554–561 (1993).
221. Miura, P. & Jasmin, B. J. Utrophin upregulation for treating Duchenne or Becker

- muscular dystrophy: how close are we? *Trends Mol. Med.* **12**, 122–129 (2006).
222. Lim, K. R. Q., Yoon, C. & Yokota, T. Applications of CRISPR/Cas9 for the Treatment of Duchenne Muscular Dystrophy. *J. Pers. Med.* **8**, 38 (2018).
223. Nguyen *et al.* Genome Editing for the Understanding and Treatment of Inherited Cardiomyopathies. *Int. J. Mol. Sci.* **21**, 733 (2020).
224. Duan, D. Systemic AAV Micro-dystrophin Gene Therapy for Duchenne Muscular Dystrophy. *Mol. Ther.* **26**, 2337–2356 (2018).
225. Chamberlain, J. R. & Chamberlain, J. S. Progress toward Gene Therapy for Duchenne Muscular Dystrophy. *Mol. Ther.* **25**, 1125–1131 (2017).
226. Gonzalez, P. SGT-001 Microdystrophin Gene Therapy for Duchenne Muscular Dystrophy. (2020). Available at: [https://s3.us-east-2.amazonaws.com/solid-bio-assets.investeddigital.com/pubs/Gonzalez\\_ASGCT\\_2020\\_11May2020.pdf](https://s3.us-east-2.amazonaws.com/solid-bio-assets.investeddigital.com/pubs/Gonzalez_ASGCT_2020_11May2020.pdf). (Accessed: 29th April 2021)
227. Pfizer. Pfizer doses first participant in phase 3 study for Duchenne muscular dystrophy investigational gene therapy. (2021). Available at: <https://www.pfizer.com/news/press-release/press-release-detail/pfizer-doses-first-participant-phase-3-study-duchenne>. (Accessed: 25th April 2021)
228. Pfizer. Pfizer’s new phase 1B results of gene therapy in ambulatory boys with Duchenne muscular dystrophy (DMD) support advancement into pivotal phase 3 study. (2020). Available at: <https://www.pfizer.com/news/press-release/press-release-detail/pfizers-new-phase-1b-results-gene-therapy-ambulatory-boys>. (Accessed: 25th April 2021)
229. Sarepta. Sarepta Therapeutics Announces Top-line Results for Part 1 of Study 102 Evaluating SRP-9001, its Investigational Gene Therapy for the Treatment of Duchenne

- Muscular Dystrophy. (2021). Available at: <https://investorrelations.sarepta.com/news-releases/news-release-details/sarepta-therapeutics-announces-top-line-results-part-1-study-102>. (Accessed: 25th April 2021)
230. Genethon. Genethon announces First Patient dosed in Clinical Trial of Investigational Gene therapy GNT 0004 for Duchenne Muscular Dystrophy. (2021). Available at: [https://www.genethon.fr/wp-content/uploads/2021/04/PR\\_GENETHON\\_DMD-1.pdf](https://www.genethon.fr/wp-content/uploads/2021/04/PR_GENETHON_DMD-1.pdf). (Accessed: 25th April 2021)
231. Banks, G. B., Chamberlain, J. S. & Odom, G. L. Microutrophin expression in dystrophic mice displays myofiber type differences in therapeutic effects. *PLoS Genet.* **16**, e1009179 (2020).
232. Odom, G. L., Gregorevic, P., Allen, J. M., Finn, E. & Chamberlain, J. S. Microutrophin Delivery Through rAAV6 Increases Lifespan and Improves Muscle Function in Dystrophic Dystrophin/Utrophin-deficient Mice. *Mol. Ther.* **16**, 1539–1545 (2008).
233. Durko, M., Allen, C., Nalbantoglu, J. & Karpati, G. CT-GalNAc transferase overexpression in adult mice is associated with extrasynaptic utrophin in skeletal muscle fibres. *J. Muscle Res. Cell Motil.* **31**, 181–193 (2010).
234. Mendell, J. R. *et al.* A Phase 1/2a Follistatin Gene Therapy Trial for Becker Muscular Dystrophy. *Mol. Ther.* **23**, 192–201 (2015).
235. Wasala, N. B. *et al.* Single SERCA2a Therapy Ameliorated Dilated Cardiomyopathy for 18 Months in a Mouse Model of Duchenne Muscular Dystrophy. *Mol. Ther.* **28**, 845–854 (2020).
236. Wijmenga, C. *et al.* Chromosome 4q DNA rearrangements associated with facioscapulohumeral muscular dystrophy. *Nat. Genet.* **2**, 26–30 (1992).

237. Barro, M. *et al.* Myoblasts from affected and non-affected FSHD muscles exhibit morphological differentiation defects. *J. Cell. Mol. Med.* **14**, 275–289 (2010).
238. Dandapat, A. *et al.* Dominant Lethal Pathologies in Male Mice Engineered to Contain an X-Linked DUX4 Transgene. *Cell Rep.* **8**, 1484–1496 (2014).
239. Pandey, S. N., Khawaja, H. & Chen, Y.-W. Culture Conditions Affect Expression of DUX4 in FSHD Myoblasts. *Molecules* **20**, 8304–8315 (2015).
240. Banerji, C. R. S. *et al.* Dynamic transcriptomic analysis reveals suppression of PGC1  $\alpha$  /ERR  $\alpha$  drives perturbed myogenesis in facioscapulohumeral muscular dystrophy. *Hum. Mol. Genet.* **28**, 1244–1259 (2019).
241. Shen, X. & Corey, D. R. Chemistry, mechanism and clinical status of antisense oligonucleotides and duplex RNAs. *Nucleic Acids Res.* **46**, 1584–1600 (2018).
242. Hair, P., Cameron, F. & McKeage, K. Mipomersen sodium: first global approval. *Drugs* **73**, 487–493 (2013).
243. Keam, S. J. Inotersen: First Global Approval. *Drugs* **78**, 1371–1376 (2018).
244. Moreno, P. M. D. & Pêgo, A. P. Therapeutic antisense oligonucleotides against cancer: hurdling to the clinic. *Front. Chem.* **2**, 87 (2014).
245. Amantana, A. *et al.* Pharmacokinetics, biodistribution, stability and toxicity of a cell-penetrating peptide - Morpholino oligomer conjugate. *Bioconjug. Chem.* **18**, 1325–1331 (2007).
246. Kurreck, J., Wyszko, E., Gillen, C. & Erdmann, V. A. Design of antisense oligonucleotides stabilized by locked nucleic acids. *Nucleic Acids Res.* **30**, 1911–1918 (2002).
247. Crooke, S. T., Wang, S., Vickers, T. A., Shen, W. & Liang, X. Cellular uptake and

- trafficking of antisense oligonucleotides. *Nat. Biotechnol.* **35**, 230–237 (2017).
248. Oszolak, F. *et al.* Comprehensive Polyadenylation Site Maps in Yeast and Human Reveal Pervasive Alternative Polyadenylation. *Cell* **143**, 1018–1029 (2010).
249. Echigoya, Y., Mouly, V., Garcia, L., Yokota, T. & Duddy, W. In Silico Screening Based on Predictive Algorithms as a Design Tool for Exon Skipping Oligonucleotides in Duchenne Muscular Dystrophy. *PLoS One* **10**, e0120058 (2015).
250. Yip, D. J. & Picketts, D. J. Increasing D4Z4 repeat copy number compromises C2C12 myoblast differentiation. *FEBS Lett.* **537**, 133–138 (2003).
251. Stadler, G. *et al.* Establishment of clonal myogenic cell lines from severely affected dystrophic muscles - CDK4 maintains the myogenic population. *Skelet. Muscle* **1**, 12 (2011).
252. Dobin, A. *et al.* STAR: ultrafast universal RNA-seq aligner. *Bioinformatics* **29**, 15–21 (2013).
253. Liao, Y., Smyth, G. K. & Shi, W. featureCounts: an efficient general purpose program for assigning sequence reads to genomic features. *Bioinformatics* **30**, 923–930 (2014).
254. Love, M. I., Huber, W. & Anders, S. Moderated estimation of fold change and dispersion for RNA-seq data with DESeq2. *Genome Biol.* **15**, 550 (2014).
255. Yoshida, T. *et al.* Estimated number of off-target candidate sites for antisense oligonucleotides in human mRNA sequences. *Genes to Cells* **23**, 448–455 (2018).
256. Sharma, V., Harafuji, N., Belayew, A. & Chen, Y.-W. DUX4 Differentially Regulates Transcriptomes of Human Rhabdomyosarcoma and Mouse C2C12 Cells. *PLoS One* **8**, e64691 (2013).
257. Zuker, M. Mfold web server for nucleic acid folding and hybridization prediction. *Nucleic*

- Acids Res.* **31**, 3406–3415 (2003).
258. Deenen, J. C. W. *et al.* Population-based incidence and prevalence of facioscapulohumeral dystrophy. *Neurology* **83**, 1056–1059 (2014).
259. Brouwer, O. F., Padberg, G. W., Wijmenga, C. & Frants, R. R. Facioscapulohumeral muscular dystrophy in early childhood. *Arch. Neurol.* **51**, 387–394 (1994).
260. Lu, J. *et al.* Management strategies in facioscapulohumeral muscular dystrophy. *Intractable Rare Dis. Res.* **8**, 9–13 (2019).
261. Scoles, D. R., Minikel, E. V. & Pulst, S. M. Antisense oligonucleotides. *Neurol. Genet.* **5**, e323 (2019).
262. Paik, J. & Duggan, S. Volanesorsen: First Global Approval. *Drugs* **79**, 1349–1354 (2019).
263. Khvorova, A. & Watts, J. K. The chemical evolution of oligonucleotide therapies of clinical utility. *Nat. Biotechnol.* **35**, 238–248 (2017).
264. Garay, M., Gaarde, W., Monia, B. P., Nero, P. & Cioffi, C. L. Inhibition of hypoxia/reoxygenation-induced apoptosis by an antisense oligonucleotide targeted to JNK1 in human kidney cells. *Biochem. Pharmacol.* **59**, 1033–1043 (2000).
265. Levesque, L., Dean, N. M., Sasmor, H. & Crooke, S. T. Antisense oligonucleotides targeting human protein kinase C- $\alpha$  inhibit phorbol ester-induced reduction of bradykinin-evoked calcium mobilization in A549 cells. *Mol. Pharmacol.* **51**, 209–216 (1997).
266. Geary, R. S., Baker, B. F. & Crooke, S. T. Clinical and Preclinical Pharmacokinetics and Pharmacodynamics of Mipomersen (Kynamro®): A Second-Generation Antisense Oligonucleotide Inhibitor of Apolipoprotein B. *Clin. Pharmacokinet.* **54**, 133–146 (2015).
267. Goodkey, K., Aslesh, T., Maruyama, R. & Yokota, T. Nusinersen in the Treatment of

- Spinal Muscular Atrophy. in *Exon Skipping and Inclusion Therapies: Methods and Protocols* (eds. Yokota, T. & Maruyama, R.) 69–76 (Springer, 2018).
268. Meijboom, K. E. K. E., Wood, M. J. A. A. & McClorey, G. Splice-Switching Therapy for Spinal Muscular Atrophy. *Genes (Basel)*. **8**, 161 (2017).
269. Crooke, S. T. *et al.* Integrated Safety Assessment of 2'-O-Methoxyethyl Chimeric Antisense Oligonucleotides in NonHuman Primates and Healthy Human Volunteers. *Mol. Ther.* **24**, 1771–1782 (2016).
270. Crooke, S. T. *et al.* Integrated Assessment of the Clinical Performance of GalNAc 3 - Conjugated 2'- O -Methoxyethyl Chimeric Antisense Oligonucleotides: I. Human Volunteer Experience. *Nucleic Acid Ther.* **29**, 16–32 (2019).
271. Margalit, A., Brachner, A., Gotzmann, J., Foisner, R. & Gruenbaum, Y. Barrier-to-autointegration factor – a BAFfling little protein. *Trends Cell Biol.* **17**, 202–208 (2007).
272. Cox, J. L. *et al.* Banfl1 is required to maintain the self-renewal of both mouse and human embryonic stem cells. *J. Cell Sci.* **124**, 2654–2665 (2011).
273. Geng, L. N. *et al.* DUX4 Activates Germline Genes, Retroelements, and Immune Mediators: Implications for Facioscapulohumeral Dystrophy. *Dev. Cell* **22**, 38–51 (2012).
274. Yao, Z. *et al.* DUX4-induced gene expression is the major molecular signature in FSHD skeletal muscle. *Hum. Mol. Genet.* **23**, 5342–5352 (2014).
275. Banerji, C. R. S. *et al.* PAX7 target genes are globally repressed in facioscapulohumeral muscular dystrophy skeletal muscle. *Nat. Commun.* **8**, 2152 (2017).
276. Mueller, A. L. *et al.* Muscle xenografts reproduce key molecular features of facioscapulohumeral muscular dystrophy. *Exp. Neurol.* **320**, 113011 (2019).
277. Jones, T. I. *et al.* Transgenic mice expressing tunable levels of DUX4 develop

- characteristic facioscapulohumeral muscular dystrophy-like pathophysiology ranging in severity. *Skelet. Muscle* **10**, 8 (2020).
278. Bray, N. L., Pimentel, H., Melsted, P. & Pachter, L. Near-optimal probabilistic RNA-seq quantification. *Nat. Biotechnol.* **34**, 525–527 (2016).
279. Bushby, K. *et al.* Diagnosis and management of Duchenne muscular dystrophy, part 1: diagnosis, and pharmacological and psychosocial management. *Lancet Neurol.* **9**, 77–93 (2010).
280. Yokota, T., Duddy, W. & Partridge, T. Optimizing exon skipping therapies for DMD. *Acta Myol.* **26**, 179–184 (2007).
281. Echigoya, Y. & Yokota, T. Skipping multiple exons of dystrophin transcripts using cocktail antisense oligonucleotides. *Nucleic Acid Ther.* **24**, 57–68 (2014).
282. Aartsma-Rus, A. & Krieg, A. M. FDA Approves Eteplirsen for Duchenne Muscular Dystrophy: The Next Chapter in the Eteplirsen Saga. *Nucleic Acid Ther.* **27**, 1–3 (2017).
283. Sarepta Therapeutics. Sarepta Therapeutics Announces Positive Results in Its Study Evaluating Gene Expression, Dystrophin Production, and Dystrophin Localization in Patients with Duchenne Muscular Dystrophy (DMD) Amenable to Skipping Exon 53 Treated with Golodirsen (SRP-4053). (2017). Available at: <https://globenewswire.com/news-release/2017/09/06/1108211/0/en/Sarepta-Therapeutics-Announces-Positive-Results-in-Its-Study-Evaluating-Gene-Expression-Dystrophin-Production-and-Dystrophin-Localization-in-Patients-with-Duchenne-Muscular-Dystrop.html>. (Accessed: 8th September 2017)
284. Aoki, Y. *et al.* In-frame dystrophin following exon 51-skipping improves muscle pathology and function in the exon 52-deficient mdx mouse. *Mol. Ther.* **18**, 1995–2005

- (2010).
285. Merlini, L. *et al.* Early prednisone treatment in Duchenne muscular dystrophy. *Muscle Nerve* **27**, 222–227 (2003).
  286. Merlini, L. *et al.* Early corticosteroid treatment in 4 duchenne muscular dystrophy patients: 14-year follow-up. *Muscle Nerve* **45**, 796–802 (2012).
  287. Raman, S. V *et al.* Eplerenone for early cardiomyopathy in Duchenne muscular dystrophy: a randomised, double-blind, placebo-controlled trial. *Lancet Neurol.* **14**, 153–161 (2015).
  288. Rafael-Fortney, J. A. *et al.* Early Treatment With Lisinopril and Spironolactone Preserves Cardiac and Skeletal Muscle in Duchenne Muscular Dystrophy Mice. *Circulation* **124**, 582–588 (2011).
  289. Saito, T. *et al.* Antisense PMO Found in Dystrophic Dog Model Was Effective in Cells from Exon 7-Deleted DMD Patient. *PLoS One* **5**, e12239 (2010).
  290. Yokota, T. *et al.* Extensive and prolonged restoration of dystrophin expression with vivo-morpholino-mediated multiple exon skipping in dystrophic dogs. *Nucleic Acid Ther.* **22**, 306–315 (2012).
  291. Gazzoli, I. *et al.* Non-sequential and multi-step splicing of the dystrophin transcript. *RNA Biol.* **13**, 290–305 (2016).
  292. Urasawa, N. *et al.* Selective Vacuolar Degeneration in Dystrophin-Deficient Canine Purkinje Fibers Despite Preservation of Dystrophin-Associated Proteins With Overexpression of Dp71. *Circulation* **117**, 2437–2448 (2008).
  293. Klingler, W., Jurkat-Rott, K., Lehmann-Horn, F. & Schleip, R. The role of fibrosis in Duchenne muscular dystrophy. *Acta Myol.* **31**, 184–195 (2012).

294. Vila, M. C. *et al.* Elusive sources of variability of dystrophin rescue by exon skipping. *Skelet. Muscle* **5**, 44 (2015).
295. Nakamura, A. *et al.* Initial pulmonary respiration causes massive diaphragm damage and hyper-CKemia in Duchenne muscular dystrophy dog. *Sci. Rep.* **3**, 2183 (2013).
296. LoMauro, A., D'Angelo, M. G. & Aliverti, A. Assessment and management of respiratory function in patients with Duchenne muscular dystrophy: current and emerging options. *Ther. Clin. Risk Manag.* **11**, 1475–1488 (2015).
297. van Putten, M. *et al.* Low dystrophin levels increase survival and improve muscle pathology and function in dystrophin/utrophin double-knockout mice. *FASEB J.* **27**, 2484–2495 (2013).
298. Yokota, T. *et al.* A renaissance for antisense oligonucleotide drugs in neurology: exon skipping breaks new ground. *Arch. Neurol.* **66**, 32–38 (2009).
299. Aoki, Y. *et al.* Highly efficient in vivo delivery of PMO into regenerating myotubes and rescue in laminin- $\alpha$ 2 chain-null congenital muscular dystrophy mice. *Hum. Mol. Genet.* **22**, 4914–4928 (2013).
300. Novak, J. S. *et al.* Myoblasts and macrophages are required for therapeutic morpholino antisense oligonucleotide delivery to dystrophic muscle. *Nat. Commun.* **8**, 941 (2017).
301. Echigoya, Y. *et al.* Effects of systemic multiexon skipping with peptide-conjugated morpholinos in the heart of a dog model of Duchenne muscular dystrophy. *Proc. Natl. Acad. Sci.* **114**, 4213–4218 (2017).
302. Moulton, H. M. & Moulton, J. D. Morpholinos and their peptide conjugates: Therapeutic promise and challenge for Duchenne muscular dystrophy. *Biochim. Biophys. Acta - Biomembr.* **1798**, 2296–2303 (2010).

303. Yugeta, N. *et al.* Cardiac involvement in Beagle-based canine X-linked muscular dystrophy in Japan (CXMDJ): electrocardiographic, echocardiographic, and morphologic studies. *BMC Cardiovasc. Disord.* **6**, 47 (2006).
304. Juliano, R. L. The delivery of therapeutic oligonucleotides. *Nucleic Acids Res.* **44**, 6518–6548 (2016).
305. Lehto, T. *et al.* Cellular trafficking determines the exon skipping activity of Pip6a-PMO in mdx skeletal and cardiac muscle cells. *Nucleic Acids Res.* **42**, 3207–3217 (2014).
306. Youngblood, D. S., Hatlevig, S. A., Hassinger, J. N., Iversen, P. L. & Moulton, H. M. Stability of cell-penetrating peptide-morpholino oligomer conjugates in human serum and in cells. *Bioconjug. Chem.* **18**, 50–60 (2007).
307. Järver, P. *et al.* Peptide-mediated Cell and In Vivo Delivery of Antisense Oligonucleotides and siRNA. *Mol. Ther. Nucleic Acids* **1**, e27 (2012).
308. Miskew Nichols, B. *et al.* Multi-exon Skipping Using Cocktail Antisense Oligonucleotides in the Canine X-linked Muscular Dystrophy. *J. Vis. Exp.* 1–15 (2016). doi:10.3791/53776
309. Maruyama, R. *et al.* Systemic Delivery of Morpholinos to Skip Multiple Exons in a Dog Model of Duchenne Muscular Dystrophy. *Methods Mol. Biol.* **1565**, 201–213 (2017).
310. Shimatsu, Y. *et al.* Major clinical and histopathological characteristics of canine X-linked muscular dystrophy in Japan, CXMDJ. *Acta Myol.* **24**, 145–154 (2005).
311. van Putten, M. *et al.* A 3 months mild functional test regime does not affect disease parameters in young mdx mice. *Neuromuscul. Disord.* **20**, 273–280 (2010).
312. Burki, U. *et al.* Development and Application of an Ultrasensitive Hybridization-Based ELISA Method for the Determination of Peptide-Conjugated Phosphorodiamidate

- Morpholino Oligonucleotides. *Nucleic Acid Ther.* **25**, 275–284 (2015).
313. Anwar, S. & Yokota, T. Golodirsen for Duchenne muscular dystrophy. *Drugs of Today* **56**, 491–504 (2020).
314. Roshmi, R. R., Yokota, T., Roshmi, R. R. & Yokota, T. Viltolarsen for the treatment of Duchenne muscular dystrophy. *Drugs of Today* **55**, 627–639 (2019).
315. Shirley, M. Casimersen: First Approval. *Drugs* (2021). doi:10.1007/s40265-021-01512-2
316. Echigoya, Y., Lim, K. R. Q., Nakamura, A. & Yokota, T. Multiple Exon Skipping in the Duchenne Muscular Dystrophy Hot Spots: Prospects and Challenges. *J. Pers. Med.* **8**, 41 (2018).
317. Aoki, Y., Yokota, T. & Wood, M. J. A. Development of multiexon skipping antisense oligonucleotide therapy for Duchenne muscular dystrophy. *Biomed Res. Int.* **2013**, 402369 (2013).
318. Bérout, C. *et al.* Multiexon skipping leading to an artificial DMD protein lacking amino acids from exons 45 through 55 could rescue up to 63% of patients with Duchenne muscular dystrophy. *Hum. Mutat.* **28**, 196–202 (2007).
319. Nakamura, A. *et al.* Comparison of the phenotypes of patients harboring in-frame deletions starting at exon 45 in the Duchenne muscular dystrophy gene indicates potential for the development of exon skipping therapy. *J. Hum. Genet.* **62**, 459–463 (2017).
320. Echigoya, Y. *et al.* Exons 45–55 Skipping Using Mutation-Tailored Cocktails of Antisense Morpholinos in the DMD Gene. *Mol. Ther.* **27**, 2005–2017 (2019).
321. Aoki, Y. *et al.* Bodywide skipping of exons 45–55 in dystrophic mdx52 mice by systemic antisense delivery. *Proc. Natl. Acad. Sci. U. S. A.* **109**, 13763–13768 (2012).
322. Lim, K. R. Q. *et al.* Efficacy of Multi-exon Skipping Treatment in Duchenne Muscular

- Dystrophy Dog Model Neonates. *Mol. Ther.* **27**, 76–86 (2019).
323. Tsumpra, M. K. *et al.* Peptide-conjugate antisense based splice-correction for Duchenne muscular dystrophy and other neuromuscular diseases. *EBioMedicine* **45**, 630–645 (2019).
324. Nguyen, Q. & Yokota, T. Antisense oligonucleotides for the treatment of cardiomyopathy in Duchenne muscular dystrophy. *Am. J. Transl. Res.* **11**, 1202–1218 (2019).
325. Lehto, T., Ezzat, K., Wood, M. J. A. & El Andaloussi, S. Peptides for nucleic acid delivery. *Adv. Drug Deliv. Rev.* **106**, 172–182 (2016).
326. Sarepta Therapeutics. Sarepta Therapeutics Announces Positive Clinical Results from MOMENTUM, a Phase 2 Clinical Trial of SRP-5051 in Patients with Duchenne Muscular Dystrophy Amenable to Skipping Exon 51. (2020). Available at: <https://investorrelations.sarepta.com/news-releases/news-release-details/sarepta-therapeutics-announces-positive-clinical-results>. (Accessed: 20th April 2021)
327. Kim, J., Clark, K., Barton, C., Tanguay, R. & Moulton, H. A Novel Zebrafish Model for Assessing In Vivo Delivery of Morpholino Oligomers. in 293–306 (2018).  
doi:10.1007/978-1-4939-8651-4\_18
328. Veltrop, M. *et al.* A dystrophic Duchenne mouse model for testing human antisense oligonucleotides. *PLoS One* **13**, e0193289 (2018).
329. 't Hoen, P. A. C. *et al.* Generation and characterization of transgenic mice with the full-length human DMD gene. *J. Biol. Chem.* **283**, 5899–5907 (2008).
330. Yavas, A. *et al.* Detailed genetic and functional analysis of the hDMDdel52/mdx mouse model. *PLoS One* **15**, e0244215 (2020).
331. Suzuki, H. *et al.* Endogenous Multiple Exon Skipping and Back-Splicing at the DMD Mutation Hotspot. *Int. J. Mol. Sci.* **17**, 1722 (2016).

332. Echigoya, Y. *et al.* Quantitative Antisense Screening and Optimization for Exon 51 Skipping in Duchenne Muscular Dystrophy. *Mol. Ther.* **25**, 2561–2572 (2017).
333. Choi, J.-M. *et al.* Intranasal delivery of the cytoplasmic domain of CTLA-4 using a novel protein transduction domain prevents allergic inflammation. *Nat. Med.* **12**, 574–579 (2006).
334. Saar, K. *et al.* Cell-penetrating peptides: A comparative membrane toxicity study. *Anal. Biochem.* **345**, 55–65 (2005).
335. Wu, R. P. *et al.* Cell-penetrating peptides as transporters for morpholino oligomers: effects of amino acid composition on intracellular delivery and cytotoxicity. *Nucleic Acids Res.* **35**, 5182–5191 (2007).
336. van Putten, M. *et al.* Low dystrophin levels in heart can delay heart failure in mdx mice. *J. Mol. Cell. Cardiol.* **69**, 17–23 (2014).
337. Deconinck, A. E. *et al.* Utrophin-Dystrophin-Deficient Mice as a Model for Duchenne Muscular Dystrophy. *Cell* **90**, 717–727 (1997).
338. Grady, R. M. *et al.* Skeletal and Cardiac Myopathies in Mice Lacking Utrophin and Dystrophin: A Model for Duchenne Muscular Dystrophy. *Cell* **90**, 729–738 (1997).
339. Wolfe, J. M. *et al.* Machine Learning To Predict Cell-Penetrating Peptides for Antisense Delivery. *ACS Cent. Sci.* **4**, 512–520 (2018).
340. Aartsma-Rus, A. & van Putten, M. Assessing Functional Performance in the Mdx Mouse Model. *J. Vis. Exp.* 51303 (2014). doi:10.3791/51303
341. Lim, K. R. Q. & Yokota, T. Quantitative evaluation of exon skipping in immortalized muscle cells in vitro. in *Exon Skipping and Inclusion Therapies: Methods and Protocols* (eds. Yokota, T. & Maruyama, R.) 127–140 (Springer, 2018).

342. Thanh, L. T. *et al.* Characterization of genetic deletions in becker muscular dystrophy using monoclonal antibodies against a deletion-prone region of dystrophin. *Am. J. Med. Genet.* **58**, 177–186 (1995).
343. Desgeorges, T. *et al.* Open-CSAM, a new tool for semi-automated analysis of myofiber cross-sectional area in regenerating adult skeletal muscle. *Skelet. Muscle* **9**, 2 (2019).
344. Landini, G., Martinelli, G. & Piccinini, F. Colour deconvolution: stain unmixing in histological imaging. *Bioinformatics* btaa847 (2020). doi:10.1093/bioinformatics/btaa847
345. Ruifrok, A. C. & Johnston, D. A. Quantification of histochemical staining by color deconvolution. *Anal. Quant. Cytol. Histol.* **23**, 291–299 (2001).
346. Lim, K. R. Q. & Yokota, T. Genetic Approaches for the Treatment of Facioscapulohumeral Muscular Dystrophy. *Front. Pharmacol.* **12**, 642858 (2021).
347. Hagedorn, P. H. *et al.* Locked nucleic acid: modality, diversity, and drug discovery. *Drug Discov. Today* **23**, 101–114 (2018).
348. Swayze, E. E. *et al.* Antisense oligonucleotides containing locked nucleic acid improve potency but cause significant hepatotoxicity in animals. *Nucleic Acids Res.* **35**, 687–700 (2007).
349. Burdick, A. D. *et al.* Sequence motifs associated with hepatotoxicity of locked nucleic acid—modified antisense oligonucleotides. *Nucleic Acids Res.* **42**, 4882–4891 (2014).
350. Shen, W. *et al.* Chemical modification of PS-ASO therapeutics reduces cellular protein-binding and improves the therapeutic index. *Nat. Biotechnol.* **37**, 640–650 (2019).
351. Lu-Nguyen, N. B., Malerba, A., Dickson, G. & Popplewell, L. Systemic antisense therapeutics inhibiting DUX4 expression improves muscle function in an FSHD mouse model. *bioRxiv* (2021). doi:10.1101/2021.01.14.426659

352. Bremmer-Bout, M. *et al.* Targeted Exon Skipping in Transgenic hDMD Mice: A Model for Direct Preclinical Screening of Human-Specific Antisense Oligonucleotides. *Mol. Ther.* **10**, 232–240 (2004).
353. Arechavala-Gomez, V. *et al.* Comparative Analysis of Antisense Oligonucleotide Sequences for Targeted Skipping of Exon 51 During Dystrophin Pre-mRNA Splicing in Human Muscle. *Hum. Gene Ther.* **18**, 798–810 (2007).
354. Popplewell, L. J. *et al.* Comparative analysis of antisense oligonucleotide sequences targeting exon 53 of the human DMD gene: Implications for future clinical trials. *Neuromuscul. Disord.* **20**, 102–110 (2010).
355. Heemskerk, H. A. *et al.* In vivo comparison of 2'- O -methyl phosphorothioate and morpholino antisense oligonucleotides for Duchenne muscular dystrophy exon skipping. *J. Gene Med.* **11**, 257–266 (2009).
356. Young, C. S., Mokhonova, E., Quinonez, M., Pyle, A. D. & Spencer, M. J. Creation of a Novel Humanized Dystrophic Mouse Model of Duchenne Muscular Dystrophy and Application of a CRISPR/Cas9 Gene Editing Therapy. *J. Neuromuscul. Dis.* **4**, 139–145 (2017).
357. Van Erp, C., Loch, D., Laws, N., Trebbin, A. & Hoey, A. J. Timeline of cardiac dystrophy in 3-18-month-old MDX mice. *Muscle Nerve* **42**, 504–513 (2010).
358. Yue, Y. Full-length dystrophin expression in half of the heart cells ameliorates - isoproterenol-induced cardiomyopathy in mdx mice. *Hum. Mol. Genet.* **13**, 1669–1675 (2004).
359. Spurney, C. F. *et al.* Membrane Sealant Poloxamer P188 Protects Against Isoproterenol Induced Cardiomyopathy in Dystrophin Deficient Mice. *BMC Cardiovasc. Disord.* **11**, 20

- (2011).
360. Betts, C. A. *et al.* Prevention of exercised induced cardiomyopathy following Pip-PMO treatment in dystrophic mdx mice. *Sci. Rep.* **5**, 8986 (2015).
  361. Janssen, P. M. L., Hiranandani, N., Mays, T. A. & Rafael-Fortney, J. A. Utrophin deficiency worsens cardiac contractile dysfunction present in dystrophin-deficient mdx mice. *Am. J. Physiol. Circ. Physiol.* **289**, H2373–H2378 (2005).
  362. Betts, C. A. *et al.* Cmah-dystrophin deficient mdx mice display an accelerated cardiac phenotype that is improved following peptide-PMO exon skipping treatment. *Hum. Mol. Genet.* **28**, 396–406 (2019).
  363. Chandrasekharan, K. *et al.* A Human-Specific Deletion in Mouse Cmah Increases Disease Severity in the mdx Model of Duchenne Muscular Dystrophy. *Sci. Transl. Med.* **2**, 42ra54 (2010).
  364. Mourkioti, F. *et al.* Role of telomere dysfunction in cardiac failure in Duchenne muscular dystrophy. *Nat. Cell Biol.* **15**, 895–904 (2013).
  365. Coley, W. D. *et al.* Effect of genetic background on the dystrophic phenotype in mdx mice. *Hum. Mol. Genet.* **25**, 130–145 (2016).
  366. van Putten, M. *et al.* Natural disease history of the D2-mdx mouse model for Duchenne muscular dystrophy. *FASEB J.* **33**, 8110–8124 (2019).
  367. Passamano, L. *et al.* Improvement of survival in Duchenne Muscular Dystrophy: retrospective analysis of 835 patients. *Acta Myol. myopathies cardiomyopathies Off. J. Mediterr. Soc. Myol.* **31**, 121–5 (2012).
  368. Tiburcy, M. *et al.* Defined Engineered Human Myocardium With Advanced Maturation for Applications in Heart Failure Modeling and Repair. *Circulation* **135**, 1832–1847

(2017).

369. Long, C. *et al.* Correction of diverse muscular dystrophy mutations in human engineered heart muscle by single-site genome editing. *Sci. Adv.* **4**, eaap9004 (2018).
370. Kyrychenko, V. *et al.* Functional correction of dystrophin actin binding domain mutations by genome editing. *JCI Insight* **2**, e95918 (2017).